Hybrid Integrator-Gain Systems

Hybrid Integrator-Gain Systems

Analysis, Design, and Applications

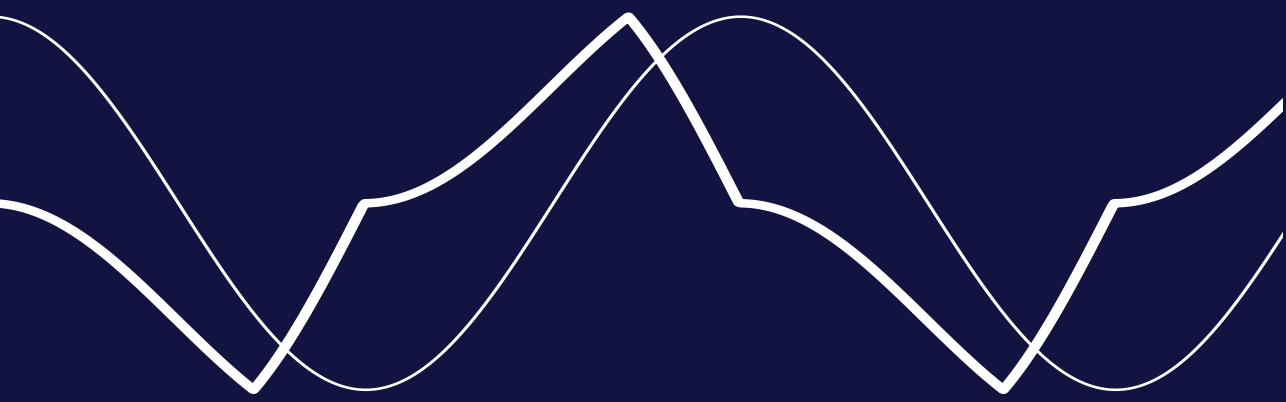

Sebastiaan van den Eijnden

Hybrid Integrator-Gain Systems

Analysis, Design, and Applications

Sebastiaan van den Eijnden

The author has successfully completed the educational program of the Graduate School of the Dutch Institute of Systems and Control (DISC).

The work described in this thesis has been carried out at the Eindhoven University of Technology, and was financially supported by ASML, Veldhoven, The Netherlands.

A catalogue record is available from the Eindhoven University of Technology Library.
ISBN: 978-90-386-5506-2

Typeset using LaTeX.

Reproduction: Ipskamp Printing, Enschede, the Netherlands
Cover design: Sebastiaan van den Eijnden

Hybrid Integrator-Gain Systems

Analysis, Design, and Applications

PROEFSCHRIFT

ter verkrijging van de graad van doctor aan de
Technische Universiteit Eindhoven, op gezag van de
rector magnificus prof.dr.ir. F.P.T. Baaijens, voor een
commissie aangewezen door het College voor
Promoties, in het openbaar te verdedigen
op vrijdag 3 juni 2022 om 11:00 uur

door

Sebastiaan Johannes Anna Maria van den Eijnden

geboren te Eindhoven

Dit proefschrift is goedgekeurd door de promotoren en de samenstelling van de promotiecommissie is als volgt:

voorzitter:	prof.dr. L.P.H. de Goey
1^{e} promotor:	prof.dr. H. Nijmeijer
2^{e} promotor:	prof.dr.ir. M.F. Heertjes
co-promotor:	prof.dr.ir. W.P.M.H. Heemels
leden:	dr.ir. R. Tóth
	prof.dr. J.S. Freudenberg (University of Michigan)
	prof.dr. M.K. Çamlıbel (Rijksuniversiteit Groningen)
	prof.dr. L. Zaccarian (LAAS-CNRS and University of Trento)

Het onderzoek dat in dit proefschrift wordt beschreven is uitgevoerd in overeenstemming met de TU/e Gedragscode Wetenschapsbeoefening.

voor mijn ouders

Summary

Hybrid Integrator-Gain Systems
Analysis, Design, and Applications

Fundamental limitations of linear time-invariant (LTI) control for LTI systems pose a serious challenge for meeting the ever increasing demands on accuracy, speed, and reliability of high-precision positioning systems such as wafer scanners. As a potential means for overcoming these limitations, and realize performance beyond what is achievable with LTI control, this thesis studies the use of a hybrid control solution known as the *hybrid integrator-gain system* (HIGS). The working principle underlying HIGS is inspired by reset integrators, and offers phase advantages over LTI integrators that suggest the possibility for overcoming limitations imposed by, *e.g.*, Bode's gain-phase relationship. In achieving these phase advantages, HIGS avoids the need for hard state resets and generates continuous (non-smooth) control signals. The latter may provide a distinct benefit over reset control both from a practical as well as a system-theoretic perspective. This thesis contributes to the development of (practically) effective tools for the design and analysis of HIGS-based controllers aiming toward performance improvements of LTI systems, and is structured in three parts.

In the first part of this thesis, HIGS is formally presented, and the fundamental question if (and how) HIGS-based control can enable genuine performance advantages over LTI control is addressed. A positive answer to this question is provided in the form of a numerical example that explicitly demonstrates the possibility for overcoming inherent time-domain performance limitations of LTI control. Key in these results is the careful interplay between the linear filters and HIGS as a consequence of their sequence in the controller. The obtained insights provide valuable guidelines for a general control design with HIGS.

Despite its potential, the hybrid nature of HIGS makes a closed-loop stability and performance analysis far from trivial. In addressing this issue, the second part of this thesis develops rigorous tools for analysing (robust) stability and performance of the feedback interconnection of an LTI system and HIGS.

Regarding stability analysis, two approaches are considered. The first approach leads to novel frequency-domain conditions for robust stability that can be verified graphically using (measured) frequency response data, something which is highly valued by control engineers in practice. However, ease-of-use may come at the expense of increased conservatism in the conditions. As an alternative, the second approach presents seemingly less conservative, but more involved time-domain (Lyapunov-based) conditions for stability that make use of piecewise quadratic (PWQ) functions, and are formulated in terms of numerically tractable linear matrix inequalities (LMIs). For performance analysis, the LMI conditions are extended toward computation of the $\mathcal{H}_2$-norm and $\mathcal{L}_2$-gain. The generality of these measures, however, may not always reflect the actual performance objective of the system under study, concerning, for instance, specific steady-state response characteristics in the presence of specific inputs. To accommodate such situations, another approach toward performance analysis is pursued that exploits the notion of convergent systems. Such systems enjoy the property of having for each bounded (time-varying) input, a unique and bounded steady-state response, thereby allowing for accurate performance characterizations. By exploiting incremental properties of HIGS, time-domain conditions for convergence of HIGS-based control systems are formulated in terms of LMIs. A frequency-domain interpretation of these LMIs is provided as well, resulting in graphically verifiable conditions for convergence. The conditions are extended for estimating the accuracy of a performance analysis using describing functions.

The third part of this thesis addresses (practical) design aspects and experimental evaluation of HIGS-based controllers for LTI systems. In particular, a design procedure is proposed that exploits describing functions within a robust loop-shaping framework, and complies with the current industrial practice. The procedure guides a HIGS-based PID controller design for a wafer-stage system of an industrial wafer scanner. Compared to a linear equivalent design, the phase advantages associated with a HIGS-based design enable a substantial increase in proportional gain and controller bandwidth. Wafer-stage measurement results demonstrate a significant improvement in low-frequency disturbance rejection without excessive transmission of high-frequency noise. The results support the potential of HIGS-based control for industrial high-precision systems.

This thesis contributes to the design and analysis of HIGS-based controllers for LTI systems. With a suitable design, HIGS-based controllers have the ability to outperform any LTI controller, thereby opening up unique possibilities to push the performance of high-tech systems to new heights.

Contents

Summary **i**

1 Introduction **1**
1.1 Control of high-precision motion systems 1
1.2 Trade-offs in linear control design 2
1.3 Hybrid control as a possible solution? 3
1.3.1 Reset control 4
1.3.2 Split-path nonlinear (SPAN) filters 5
1.3.3 Hybrid integrator-gain systems (HIGS) 7
1.4 Research objectives and contributions 8
1.4.1 Objective statement 8
1.4.2 Contributions 9
1.5 Outline of the thesis 11

I Fundamentals of HIGS **13**

2 Formalization and Basic Results **15**
2.1 Introduction 15
2.2 Open-loop system representation 16
2.2.1 State-space description of HIGS 16
2.2.2 Time-domain properties 20
2.2.3 Describing function analysis 21
2.2.4 HIGS and projected dynamical systems 25
2.3 Closed-loop system representation 27
2.3.1 Closed-loop system description 28
2.3.2 Solution concept and well-posedness 29
2.3.3 Stability and performance: Preliminaries 29
2.3.4 Robustness aspects 32

2.4 Summary . . . 33
2.A Proofs and technical results . . . 34
2.A.1 Proof of Theorem 2.2.3 . . . 34
2.A.2 Proof of Theorem 2.2.4 . . . 34

3 A Remedy for Performance Limitations in LTI Control? 37
3.1 Introduction . . . 37
3.2 Limitations of LTI control . . . 38
3.3 Nonlinear control context . . . 40
3.4 Plant with a real unstable pole . . . 42
3.4.1 LTI control . . . 43
3.4.2 HIGS-based control . . . 43
3.4.3 Simulation results . . . 45
3.4.4 Robust non-overshoot performance . . . 46
3.5 Design considerations and non-overshoot . . . 47
3.5.1 Controller configuration . . . 47
3.5.2 Non-overshoot mechanism . . . 48
3.6 Summary . . . 50
3.A Additional details and numerical results . . . 51
3.A.1 State-space derivation . . . 51
3.A.2 Numerical solutions to the matrix inequalities . . . 52

II Stability and Performance 53

4 Frequency-Domain Tools for Robust Stability Analysis 55
4.1 Introduction . . . 55
4.1.1 Notation . . . 57
4.2 System setting and problem formulation . . . 57
4.2.1 Closed-loop system description . . . 57
4.2.2 Problem formulation . . . 59
4.3 Frequency-domain conditions for ISS . . . 61
4.3.1 Existing results . . . 61
4.3.2 Main results . . . 65
4.3.3 Verifying the frequency-domain conditions . . . 68
4.3.4 Example: Mass-spring-damper system . . . 71
4.4 Robustifying the conditions . . . 74
4.4.1 Stability criteria for plants with multiplicative uncertainty 74
4.4.2 Example: Rotating beam . . . 76
4.5 Application to a motor-load motion system . . . 79
4.5.1 Controller design . . . 80
4.6 Summary . . . 83
4.A Proofs and technical results . . . 84
4.A.1 Preliminaries . . . 84

4.A.2 Summary of relevant matrices 85
4.A.3 Proof of Theorem 4.3.1 86
4.A.4 Proof of Theorem 4.3.2 88
4.A.5 Proof of Theorem 4.3.3 90
4.A.6 Proof of Proposition 4.4.1 92
4.B Numerical results for the rotating beam example 94

5 Time-Domain Tools for Stability and Performance Analysis: An LMI Approach 97
5.1 Introduction 97
5.1.1 Notation 99
5.2 System setting and problem formulation 99
5.2.1 Closed-loop system description 99
5.2.2 Problem formulation 101
5.3 Partition strategy, PWQ functions, and constraint matrices . . 102
5.3.1 Simplicial partitioning of $\mathcal{F}$ 103
5.3.2 PWQ function parametrization and constraint matrices 106
5.4 LMI conditions for stability and performance 110
5.4.1 Main results 110
5.4.2 On (in)feasibility of the LMI conditions 112
5.5 Numerical examples 115
5.5.1 Mass-spring-damper system revisited 115
5.5.2 Fourth-order motion system 118
5.6 Summary 124
5.A Proofs and technical results 125
5.A.1 Proof of Proposition 5.3.5 125
5.A.2 Proof of Proposition 5.3.6 126
5.A.3 Proof of Proposition 5.3.8 126
5.A.4 Proof of Theorem 5.4.1 130
5.A.5 Proof of Proposition 5.4.5 131

6 Steady-State Performance Analysis: A Convergent Dynamics Approach 135
6.1 Introduction 135
6.1.1 Notations 137
6.2 System setting and problem formulation 137
6.2.1 An extended hybrid integrator design 138
6.2.2 Closed-loop system formulation 139
6.2.3 Incremental stability, convergence, and problem formulation 141
6.3 Incremental form and system properties 144
6.3.1 Incremental dynamics 144
6.3.2 Properties 144

6.4 Time-domain conditions for ISC . . . 145
6.4.1 A small-gain condition . . . 145
6.4.2 Lyapunov-based conditions . . . 147
6.5 Frequency-domain conditions for ISC . . . 151
6.6 Steady-state performance estimation . . . 153
6.6.1 Linear approximation of steady-state solutions . . . 153
6.6.2 Accuracy of the harmonic linearization . . . 154
6.7 A numerical case-study . . . 157
6.7.1 Convergence . . . 158
6.7.2 Steady-state performance estimation . . . 160
6.8 Summary . . . 163
6.A Proofs and technical results . . . 164
6.A.1 Proof of Property 6.3.1 . . . 164
6.A.2 Proof of Theorem 6.4.2 . . . 166
6.A.3 Proof of Theorem 6.4.5 . . . 167
6.A.4 Proof of Theorem 6.5.1 . . . 171
6.A.5 Proof of Corollary 6.5.2 . . . 174
6.B Describing function for HIGS with an additional pole . . . 176

III Design and Applications 179

7 HIGS-Based Controller Design 181
7.1 Introduction . . . 181
7.2 System description and problem formulation . . . 182
7.2.1 General system description . . . 182
7.2.2 Problem formulation . . . 183
7.2.3 Toward HIGS-based controller design . . . 184
7.3 Synthesis using matrix inequalities . . . 185
7.3.1 System setting . . . 185
7.3.2 From analysis to synthesis . . . 187
7.3.3 Controller synthesis algorithm . . . 191
7.3.4 Example . . . 192
7.4 Robust loop-shaping design . . . 193
7.4.1 A conceptual loop-shaping idea . . . 195
7.4.2 Characterizing Δ_Ψ . . . 197
7.4.3 Design procedure . . . 203
7.5 Summary . . . 207

8 Case-Study on an Industrial Wafer Scanner 209
8.1 Introduction . . . 209
8.2 Wafer scanning principles . . . 210
8.2.1 Scanning procedure and setpoint definition . . . 210
8.2.2 Scanning performance measures . . . 214

8.3 Wafer-stage dynamics and control 214
8.3.1 Control problem formulation 215
8.3.2 Feedforward control 216
8.3.3 Feedback control 217
8.4 HIGS in a PID architecture 218
8.4.1 HIGS-based integrator and low-pass filter design 218
8.4.2 HIGS-based PID scheme 220
8.4.3 Frequency-domain approximation 222
8.5 Closed-loop design aspects 223
8.5.1 Modelling uncertainty 223
8.5.2 Design and tuning of the pre- and post-filters 226
8.6 Comparative design and performance evaluation 230
8.6.1 Design for performance 230
8.6.2 Time-domain measurement results 233
8.6.3 Frequency-domain measurement results 233
8.7 Summary 236

IV Closing **239**

9 Conclusions and Recommendations **241**
9.1 Conclusions 241
9.1.1 Overcoming fundamental limitations of LTI control . . . 242
9.1.2 Stability and performance analysis 242
9.1.3 Design and experimental validation 243
9.2 Recommendations 244
9.3 Final thoughts 246

Bibliography **249**

List of publications **265**

Dankwoord **269**

About the author **273**

Chapter 1

Introduction

1.1 Control of high-precision motion systems

Over the last decades, progress in science and technology has been a major determining factor for economic growth and social welfare (Coccia, 2019; Mokyr, 2018; Solarin and Yuen, 2016). A fundamental mechanism for driving scientific and technological innovations is an increase in precision with which it is possible to observe and interact with the physical world. A prominent example is found in the semiconductor industry, where increased precision in complex lithography machines such as wafer scanners enables a continued exponential growth in available computing power, greatly impacting all aspects of science and technology as well as everyday life (Moore, 1998; van Schoot et al., 2017). Other examples illustrating the impact of increased precision include electron microscopy for molecular research (Callaway, 2015), pick-and-place equipment in the manufacturing industry (Huang and Wey, 2010), and laser interferometry used, for example, in the detection of gravitational waves (Abbott et al., 2016).

To meet the extreme requirements on precision, as well as the increasing demands on operating speed, stability, and reliability, high-precision systems heavily depend on the control solutions being used. Control of high-precision systems is often simplified by a stiff mechanical design combined with strategically placed actuators and sensors. The electro-mechanical system components such as motors, bearings, and transmissions are optimized as to achieve a functional behaviour that is highly deterministic, predictable, and reproducible (Munnig Schmidt et al., 2014). Consequently, the plant dynamics can be modelled accurately according to the linear paradigm. A decoupling strategy is typically applied for reducing multivariable design aspects to multi-loop single-input single-output (SISO) design, see, *e.g.*, Butler, 2011. Given this practice,

the class of SISO linear time-invariant (LTI) plants is of particular relevance in the high-precision industry, and will be of primary scope in this thesis.

The specific class of (to-be-controlled) SISO LTI plants allows for the application of well-developed LTI feedback control methods such as proportional-integral-derivative (PID) control (Åström and Hägglund, 2001) that can be designed using intuitive techniques such as loop-shaping (Franklin et al., 2005; Steinbuch and Norg, 1998), and more advanced methods including H_∞-optimal design and μ-synthesis (Skogestad and Postlethwaite, 2010; van de Wal et al., 2002). The sense and simplicity of an LTI control design in meeting performance requirements makes it a widely adopted method in practice that often sets the industrial standard (Samad et al., 2020).

1.2 Trade-offs in linear control design

Despite the clear advantages, restricting the applied control solutions to the linear time-invariant domain only is not without drawbacks. No matter the variety of LTI control structures or the method used to design the controllers, all LTI designs are bound to fundamental limitations in both time- and frequency-domain, leading to inevitable design trade-offs (Freudenberg et al., 2000; Middleton, 1991; Seron et al., 1997). These trade-offs are generally encountered in high-precision positioning systems where an increase in precision and speed often require enhanced low-frequency disturbance suppression and increased controller bandwidths (Heertjes et al., 2020; Lamnabhi-Lagarrigue et al., 2017). However, improving low-frequency disturbance rejection properties of linear systems, *e.g.*, by increasing the bandwidth or adding integral action to the controller, directly comes at the cost of increased sensitivity to high-frequency noise. This is an inevitable consequence of the Bode sensitivity integral, often referred to as the "waterbed effect" (Freudenberg and Looze, 1985; Freudenberg et al., 2000). Simply stated: a change in controller design to achieve sensitivity reduction in some frequency interval necessarily comes at the expense of a sensitivity increase in another frequency interval.

Even if a desired shape on the sensitivity is determined that yields an acceptable trade-off between low-frequency disturbance suppression and high-frequency noise amplification, it may still be possible that no robustly stabilizing LTI controller exists that achieves such a shape. This is due to a limitation known as Bode's gain-phase relationship, which states that the phase of the frequency response of a linear system is completely determined by its magnitude characteristics and vice versa. Hence the two parameters - gain and phase - that describe a complex function yield only one degree of freedom in design (Freudenberg et al., 2000). As a consequence, attempts to specify certain design requirements in one frequency range may compromise those in other frequency ranges. An example is given by the use of low-pass filters in the controller design with the

aim to provide high-frequency roll-off. As prescribed by Bode's gain-phase relationship, this roll-off comes at the expense of phase lag that may compromise robust stability margins and limits the achievable bandwidth, see Åström, 2000.

Besides suffering from limitations in the frequency-domain, time-domain limitations also pose restrictions on linear time-invariant feedback designs. For example, it is well-known (Seron et al., 1997) that a stable closed-loop LTI system having at least two open-loop integrators must necessarily exhibit overshoot in its step-response. Typical high-precision positioning systems often contain a free-moving mass (or inertia) and therefore generally satisfy this limitation. Moreover, adding integral action in the controller for the purpose of counteracting static disturbances and improving low-frequency disturbance rejection properties may come at the expense of overshoot, which can compromise settling time, resulting in loss of system throughput.

The fact that modern linear techniques such as H_∞-design and μ-synthesis (Skogestad and Postlethwaite, 2010) cannot overcome the fundamental design trade-offs in LTI control systems poses a serious challenge for meeting the ever tightening performance requirements for high-precision positioning systems.

1.3 Hybrid control as a possible solution?

Part of the limitations discussed above are a consequence of the LTI structure imposed on the feedback controller. This naturally raises the question whether these limitations can be overcome by using nonlinear/hybrid feedback control strategies. Being aware of the complexity normally associated with nonlinear systems, at first sight it may appear counter-intuitive to intentionally de-linearise an otherwise linear system. However, in some cases there may be good reason for doing so. Nonlinear/hybrid systems generally do not obey the same rules as LTI systems, and thus may potentially offer the necessary design freedom to break away from the fundamental limitations imposed by classical LTI control. Over the years, many different nonlinear/hybrid control strategies that specifically aim at overcoming the limitations of LTI control have been proposed. Examples include variable-gain control (Armstrong et al., 1996; Armstrong et al., 2006; Heertjes et al., 2009; Heertjes and Steinbuch, 2004; Heertjes and Verstappen, 2014; Hunnekens et al., 2016), sliding-mode control (Abidi and Sabanovic, 2007; Sam et al., 2004; Utkin, 1993), switching control (Deenen et al., 2021; Feuer et al., 1997; Heertjes et al., 2019; Hespanha and Morse, 2002; Lau and Middleton, 2003; Liberzon, 2003; Sharif et al., 2021b), and reset control (Aangenent et al., 2010; Beker et al., 2001; Clegg, 1958; Heertjes et al., 2013; Horowitz and Rosenbaum, 1975; Nešić et al., 2011; Zaccarian et al., 2011). Some of these strategies have, in fact, explicitly been shown to be able to outperform LTI feedback control for LTI plants, see, for instance, the works in Beker et al., 2001; Hunnekens et al., 2016; Stoorvogel, 1995; Zhao et al., 2019.

In this thesis, the focus is explicitly on dealing with the unavoidable phase lag involved with LTI filters that limits the increase of bandwidth and may compromise time-domain performance properties. Within this scope, several hybrid control concepts are of particular interest. Hybrid controllers consist of a dynamical system with interacting continuous and discrete (or non-smooth) components (Goebel et al., 2009). Three prominent "classical" examples of hybrid control strategies dedicated to overcoming fundamental limitations of LTI control are given by reset control, split-path nonlinear filters, and hybrid integrator-gain systems.

1.3.1 Reset control

Reset control emerged with the introduction of the Clegg integrator (Clegg, 1958), being an integrator that resets its state to zero upon a zero crossing of its input. Compared to an LTI integrator, the resetting mechanism in the Clegg integrator forces the sign of the integrator output to be equivalent to the sign of its input at all times. A typical response of the classical Clegg integrator when subjected to a sinusoidal input is shown in Figure 1.1 (in black), together with the response of an LTI integrator (in grey).

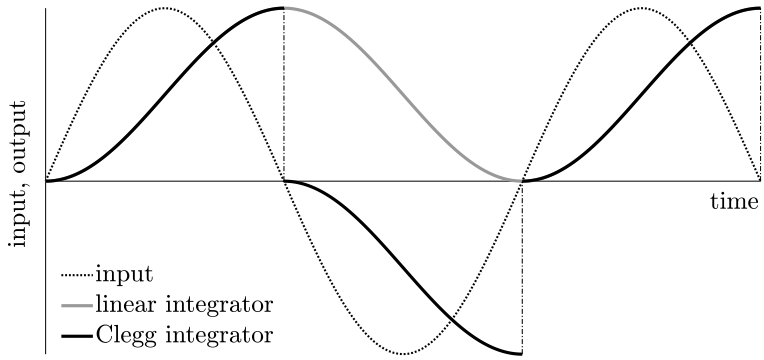

Figure 1.1. Typical time response of a linear integrator (grey) and the Clegg integrator (black) when subject to a sinusoidal input signal (dotted).

A desirable feature of the resetting mechanism in the Clegg integrator is characterized by its describing function, which relates amplitude and phase properties of the driving sinusoidal input to amplitude and phase properties of the first harmonic in the corresponding steady-state response (Gelb and Vander Velde, 1968). The describing function of the Clegg integrator exhibits a 20 dB/decade amplitude decay similar to that of a linear integrator, but with an induced

phase lag of only 38.15 degrees as opposed to 90 degrees for the linear integrator (Chait and Hollot, 2002). Clearly, such favourable phase behaviour hints toward improved performance of LTI systems by designing a compensator capable of supplying the required bandwidth with less gain at high frequencies. The development of reset control involved various generalizations such as the first-order reset element (Beker et al., 2004; Chait and Hollot, 2002; Horowitz and Rosenbaum, 1975; Zhao et al., 2019), second-order reset element (Hazeleger et al., 2016), generalized fractional order reset elements (HosseinNia et al., 2013), and conditional reset integrators (Gruntjens et al., 2019) to name but a few. Extensive research on reset control systems has led to various fruitful results regarding stability and performance analysis (Aangenent et al., 2010; Baños and Barreiro, 2012; Beerens et al., 2019; Beker et al., 2004; Carrasco et al., 2010; Loquen et al., 2010; Nešić et al., 2008; Zaccarian et al., 2011; Zhao et al., 2013; Zhao and Wang, 2016), hybrid formulations (Zaccarian et al., 2005), and experimental demonstrations of reset control systems achieving improved performance (Beerens et al., 2022; Gruntjens et al., 2019; HosseinNia et al., 2014; Panni et al., 2014; Saikumar et al., 2019; Zheng et al., 2000). To date, reset control is one of the few nonlinear strategies that has been shown to overcome fundamental time-domain limitations of LTI control (Beker et al., 2001; Zhao et al., 2019).

1.3.2 Split-path nonlinear (SPAN) filters

Related strategies that specifically challenge Bode's gain-phase relationship, but have received considerably less attention than reset control are given by the driven limiter (Bailey, 1963) and split-path nonlinear (SPAN) filter (Aangenent et al., 2005; Fong and Szeto, 1980; Foster et al., 1966; Karybakas, 1977). The main design philosophy of these strategies is to "split" the magnitude and phase characteristics of a filter as to design these separately, thereby facilitating an additional degree-of-freedom for controller design. Variants of the SPAN filter that include integral action have recently been proposed in Sharif et al., 2021b; van der Maas et al., 2017; van Loon et al., 2016. These so-called SPAN integrators (SPANI) aim for an improved integrator design, with all the benefits of a linear integrator in terms of achieving zero steady-state tracking error, but without introducing the usual 90 degrees phase lag. For achieving this, the output of the SPAN integrator is composed as the product of the absolute value (magnitude) of the integrator state, and the sign (phase) of the input signal. A typical response of a SPAN integrator subject to a sinusoidal input is shown in Figure 1.2 in black, along with the response of an LTI integrator in grey. In terms of its describing function, the SPAN integrator exhibits similar magnitude characteristics as an LTI integrator, but with zero phase lag (Sharif et al., 2021b). The absence of phase lag is attributed to the fact that the output of the SPAN filter shows a certain symmetry after the switching instance.

Regarding its design philosophy, the SPAN(I) filter exhibits some interesting

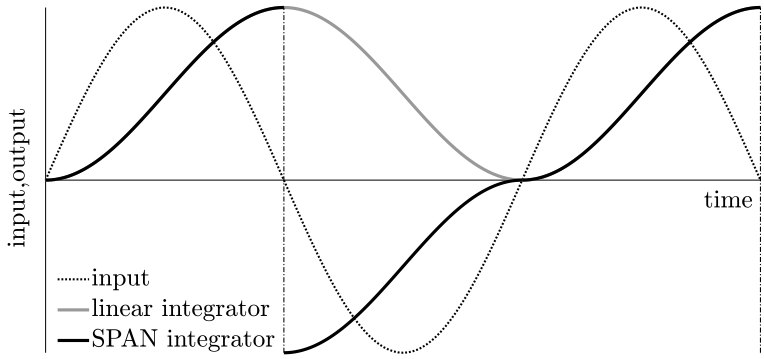

Figure 1.2. Typical time response of a linear integrator (grey) and the SPAN integrator (black) when subject to a sinusoidal input signal (dotted).

analogies with the previously discussed reset control strategy. Both strategies adopt "close-to-linear" thinking in their design. That is, the designs adopt the structure of basic LTI filters such as an integrator to which certain modifications are made in order to provide additional functionality. In particular, SPAN(I) filters and reset strategies use a switching surface to trigger changes in the control signal, leading to the injection of *discontinuous* control signals into an otherwise smooth (linear) feedback system.

Although promising, the aforementioned control structures were only partially successful. The reasons vary from lack of appealing for broad adoption in industrial applications or complications in establishing essential system-theoretic results. For instance, the hard resets in the Clegg integrator as in Figure 1.1, and the discontinuous control signals of the SPAN filter as shown in Figure 1.2 increase the risk of exciting higher-order modes in the controlled plant (Armstrong et al., 2006). In particular, such signals may distribute low-frequency input energy over a broad frequency interval, including the high-frequency range in which the controlled system may contain multiple lightly-damped resonances. As a result the controlled system is usually more sensitive in the high-frequency range. This may lead to unwanted behaviour that generally deteriorates performance and may even lead to system failure or damage. Moreover, the need for taking into account discontinuities in the state trajectories may hamper the formal derivation of key properties such as incremental stability (Angeli, 2002; Biemond et al., 2018) and convergence (Pavlov et al., 2006b), as well as the development of easy-to-use (frequency-domain) tools for controller design and analysis (Kamenetskiy, 2017). These aspects are instrumental to set up comprehensive design and analysis frameworks that adhere to the "close-to-linear" way

of thinking, something which is highly valued by control engineers in industry and which could expedite the acceptance in industry.

1.3.3 Hybrid integrator-gain systems (HIGS)

As an alternative to discontinuous control strategies, a nonlinear integrator referred to as the hybrid integrator-gain system (HIGS) has been proposed recently by Deenen et al., 2017, see also Deenen et al., 2021. The underlying philosophy of HIGS is inspired by the Clegg integrator, *i.e.*, keeping the sign of the integrator's output equal to that of the input at all times, thereby inheriting the hinted phase advantages of reset control. However, HIGS avoids hard resets of the integrator state, and instead exploits mode switching between an integrator-mode and a gain-mode (hence the terminology hybrid integrator-gain system) to enforce sign-equivalence. Switching is done in a manner that results in a *continuous* output signal as opposed to the *discontinuous* signals generated by reset control or as generated by SPAN(I) filters. A typical response of HIGS subject to a sinusoidal input is shown in Figure 1.3. The describing function characteristics of HIGS demonstrate an amplitude decay comparable to that of an LTI integrator, but with an induced phase lag of at most 38.15 degrees.

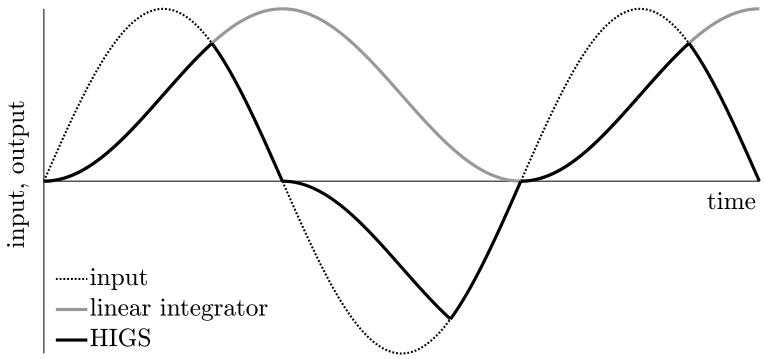

Figure 1.3. Typical time response of a linear integrator (grey) and HIGS (black) when subject to a sinusoidal input signal (dotted).

Given the previous discussion on the possible difficulties arising from the use of discontinuous control signals with reset control and SPAN(I) filters, continuous control with HIGS offers comparable performance benefits as the previous strategies, for example in terms of reduced phase lag, but may provide different opportunities in both application-based as well as system-theoretic directions. In particular, due to their continuous nature, HIGS-based controllers may be easier to construct, analyse, employ, and adopt than their discontinuous counterparts.

Finally, within the context of continuous control with HIGS, the related line of research on so-called "soft-reset" control systems that has emerged recently in Le and Teel, 2021 and Teel, 2022 should be mentioned. This strategy aims at approximating hard reset controllers via a differential inclusion, resulting in continuous states/outputs, which is also the objective with HIGS. As discussed in Teel, 2022, however, within a closed-loop setting this approach may not always bear much resemblance to reset control, thereby potentially loosing the intuitive and desirable features of a reset control strategy.

1.4 Research objectives and contributions

1.4.1 Objective statement

This thesis is devoted to studying the potential of hybrid integrator-gain systems (HIGS) within the control design. The general objective pursued in this thesis can be stated as follows:

Explore the possibilities of HIGS as a viable hybrid control strategy for enabling performance improvements for continuous time SISO LTI motion systems, and develop comprehensive and useful tools for the design and analysis of HIGS-controlled systems.

In view of this research objective, this thesis contributes to the development of the theory and practice concerning the relatively new concept of HIGS. In order for any nonlinear/hybrid control strategy to be accepted as a viable extension to the well-developed class of linear control methods, two key aspects should be addressed. First, performance advantages in comparison to linear control should be evident. Second, techniques for design and analysis should be accurate, systematic, and easy-to-use, the latter possibly conflicting with the former requirements. Taking this into account, the general objective of this thesis can be refined in terms of the following research objectives:

(i) *Establish rigorous performance advantages of HIGS-based control in comparison to well-accepted linear control strategies.* (Chapter 3)

(ii) *Develop novel techniques for accurately analysing stability and performance of HIGS-controlled systems, preferably by exploiting "easy-to-use" frequency-domain tools accommodating relevant performance measures.* (Chapter 4-6)

(iii) *Develop practically relevant and systematic guidelines for the performance-based design of HIGS-controlled systems.* (Chapter 7)

(iv) *Demonstrate by experiment the performance improving potential of HIGS-based control on an industrial high-tech application.* (Chapter 8)

The next section discusses the main contributions of this thesis.

1.4.2 Contributions

This thesis presents five main contributions that directly address the four research objectives such as discussed above.

Contribution 1. The first main contribution of this thesis, addressing the first research objective and presented in Chapter 3, establishes the possibility of overcoming a fundamental time-domain limitation of LTI control for LTI systems by carefully embedding HIGS into an otherwise linear feedback control structure. The fundamental limitation that is shown to be overcome is the unavoidable presence of overshoot in the step-response of a closed-loop controlled single-input single-output (SISO) LTI plant having a real unstable open-loop pole. It is shown that with a HIGS-based controller design, overshoot can be completely avoided. In addition, it is demonstrated that the trade-off between overshoot and zero steady-state error in the presence of constant input disturbances that typically arises when using integral control can be alleviated with HIGS-based control. Key for alleviating the overshoot limitations is the sequence in which the linear filters in the controller appear with respect to the HIGS component(s). This insight provides a valuable guideline for controller design with HIGS to enable genuine performance advantages over LTI controller designs. The main results in Chapter 3 are based on van den Eijnden et al., 2020a. Related results can be found in Dinther et al., 2021.

Contribution 2. The second main contribution, addressing the second research objective and presented in Chapters 4-5, is the development of techniques for stability analysis of HIGS-controlled systems. Two directions are pursued: a direction developing frequency-domain based conditions for stability, and a direction that presents time-domain conditions in the form of numerically tractable linear matrix inequalities (LMIs) (Boyd et al., 1994). The former frequency-domain approach allows for easy-to-verify conditions based on measured plant data, but possibly at the cost of increased conservatism, whereas the latter time-domain approach allows for very tight stability estimates, but possibly at the cost of increased (numerical) complexity in verifying the conditions. The specific contributions in Chapter 4 and Chapter 5 are as follows.

In Chapter 4 novel (sufficient) stability conditions for HIGS-controlled systems based on frequency-response functions are presented. The results are novel in the sense that these guarantee the existence of a quadratic Lyapunov function that is only positive in a subset of the state-space where trajectories of the controlled system can exist. In this way the class of admissible Lyapunov function candidates underlying the frequency-domain conditions is extended and the conservatism in the analysis is generally reduced as compared to existing methods such as the circle-criterion (Khalil, 2002). The presented conditions are easy-to-use on the basis of a graphical Popov-like plot which can be assessed by using non-parametric models such as (measured) frequency-response functions. The

results in Chapter 4 are based on van den Eijnden et al., 2021.

In Chapter 5 the use of piecewise quadratic (PWQ) Lyapunov functions for stability analysis is considered. For constructing such functions, a novel partitioning of the subset determining the active modes of HIGS is considered. Inspired by the seminal work in Johansson and Rantzer, 1998, this partitioning allows for parametrizing the PWQ function in such a manner that the necessary continuity requirements are directly incorporated in the description of the PWQ function, thereby guaranteeing continuity a priori, see also Deenen et al., 2021. On the basis of this strategy, rigorous conditions for stability are formulated as a set of LMIs. The LMI conditions are extended toward performance analysis in terms of the $\mathcal{L}_2$-gain and the $\mathcal{H}_2$-norm, providing quantitative measures for disturbance rejection and transient performance. Additional insight regarding (in)feasibility of the LMI conditions is provided, and highlights the indispensable flexibility offered by PWQ functions over, *e.g.*, quadratic ones. By means of a numerical study, it is shown that the conditions can lead to accurate stability and performance estimates. The main contents in Chapter 5 are based on Van den Eijnden et al., 2019 and van den Eijnden et al., 2022b. Related results are presented in Deenen et al., 2021.

Contribution 3. The third main contribution in this thesis, addressing the second research objective and presented in Chapter 6, is the development of techniques for incremental stability and convergence analysis of HIGS-controlled systems. Convergent systems enjoy the property of possessing for each bounded (time-varying) input, a unique and bounded steady-state response. This property opens up the possibility for characterizing steady-state performance in a more accurate manner as compared to, *e.g.*, the $\mathcal{L}_2$-gain as presented in Chapter 5. Namely, the generality of the $\mathcal{L}_2$-gain may not always reflect the actual performance objective of the system under study, concerning, for instance, specific steady-state response characteristics in the presence of specific inputs. Establishing the desirable property of incremental stability/convergence for hybrid/switched systems is, in general, not an easy task. The thesis contributes to this problem by presenting time- and frequency-domain conditions for verifying incremental stability and convergence of HIGS-controlled systems. Though specifically tailored to these systems, the approaches may open up fruitful directions for analysis of other classes of hybrid/switched systems as well.

The specific contributions in Chapter 6 are as follows. Novel LMI-based conditions for convergence of HIGS-controlled systems are presented. In deriving the conditions, new incremental properties of the vector field of HIGS are exploited. These properties are shown to hold only in subregions of the state-space, thereby motivating the construction of a piecewise quadratic incremental Lyapunov function. The existence of such a function is cast as a verifiable set of LMI conditions. In addition, a frequency-domain interpretation of the LMIs is provided, leading to graphically verifiable conditions for convergence. The

results in Chapter 6 are based on van den Eijnden et al., 2022a.

Contribution 4. The fourth contribution, addressing the third research objective and presented in Chapter 7, is the development of design tools for HIGS-controlled systems. Two distinct approaches are pursued in this chapter. The first approach exploits the conditions presented in Chapter 4. In particular, the frequency-domain conditions presented in this chapter are reformulated as matrix inequalities. Combined with conditions for $\mathcal{L}_2$-performance as derived in Chapter 5, these lead to appropriate (robust) synthesis conditions.

An alternative approach toward HIGS-based controller design exploits a describing function characterization of HIGS within a robust loop-shaping framework. Key in the approach is to express the modelling error induced by the describing function as an uncertainty in the controller. Deriving such an uncertainty is highly specific to the problem at hand. Nevertheless, practically useful guidelines are presented which allow for effective frequency-domain-based controller design. The approach strongly connects to the industrial practice and in that sense may aid further development of HIGS as a nonlinear control solution. Part of the content in Chapter 7 is based on the concepts in van den Eijnden et al., 2018 and Heertjes et al., 2021.

Contribution 5. The fifth contribution, addressing the fourth research objective and which is presented in Chapter 8, is the experimental validation of a HIGS-based PID control strategy on an industrial wafer scanner. Controller design is based on frequency-domain loop-shaping such as outlined in Chapter 7, and which is demonstrated to be valuable in an industrial setting. Compared to the state-of-practice linear control solution, the HIGS-based strategy allows for a significant increase in both controller bandwidth and low-frequency disturbance rejection properties as hinted by a describing function analysis. This is supported by measurements which show a significant improvement in tracking accuracy without strong penalties on high-frequency noise amplification, thereby underlining the potential of HIGS-based control in the industrial practice. Chapter 8 is based on the preliminary results in van den Eijnden et al., 2020b and van den Eijnden et al., 2020c.

1.5 Outline of the thesis

The remainder of this thesis is divided into four parts. Part I consists of Chapters 2 and 3 and provides a mathematical introduction to the concept of HIGS, as well as a demonstration of its performance advantages, covering Contribution 1. Part II consists of Chapters 4-6 and presents the results in this thesis related to (incremental) stability and performance analysis, covering Contributions 2 and 3. Proofs and technical results are provided at the end of each chapter in an

appendix. Part III includes Chapters 7 and 8, which present approaches toward design as well as an experimental case-study, covering Contributions 4 and 5. It should be mentioned that Chapters 3–8 are largely based on research papers such that, besides some prerequisites from Chapter 2, each of these chapters can be read individually. Note that this may introduce some repetition with respect to the introductions and/or system descriptions in the individual chapters. However, the chapters do provide some continuity and relevant information linking them with each other. Finally, Part IV, consisting of Chapter 9 provides a reflection of the obtained results by summarizing the main conclusions of this thesis together with recommendations for future research.

Part I

Fundamentals of HIGS

Chapter 2

Formalization and Basic Results

2.1 Introduction

The hybrid integrator-gain system, abbreviated as HIGS, first appeared in the literature in Deenen et al., 2017 where it was introduced for dealing with the classical trade-offs resulting from the use of linear time-invariant (LTI) integral control. The underlying principle of HIGS is inspired by reset control solutions, see, *e.g.*, Aangenent et al., 2010; Baños and Barreiro, 2012; Beker et al., 2004; Clegg, 1958; Nešić et al., 2008; Van Loon et al., 2017, and can best be understood when considering the step-response of the feedback interconnection of an LTI integrator and a plant. The integrator accumulates its input - the feedback error signal - over time for achieving zero steady-state error. When the error crosses zero for the first time, however, the accumulated past (positive) error signal is still stored in the integrator's state. As a consequence, the integrator produces a positive output and keeps on pushing the system in the direction away from zero error, causing overshoot. To improve upon this aspect, a simple idea is to keep the sign of the integrator's output the same as that of its input, thereby forcing the system toward zero error at all times. Reset integrators achieve this sign-equivalence by instantaneously resetting their buffer (state) to zero upon a sign change of the input. Discontinuities in the generated output signal resulting from the resetting action, however, may increase the risk of exciting structural modes of the plant dynamics, possibly leading to unwanted behaviour that potentially can damage the system. To avoid state resets, but still preserve sign equivalence of the integrator's input and output signals, HIGS exploits switching between integrator dynamics and gain characteristics. In particular, a HIGS element acts as a linear integrator as long as its input-output pair lies within a sector. This mode of operation is referred to as the *integrator-mode*. At moments when the

sector conditions tend to be violated, a switch is enforced to keep trajectories to stay on the boundary of the mentioned sector. This second mode of operation is referred to as the *gain-mode*, explaining the terminology hybrid integrator-gain system. Switching between integrator and gain characteristics is orchestrated in a manner such that the generated output is guaranteed to be continuous. As a result, HIGS inherits the benefits of reset controllers, often expressed in terms of phase advantages, but avoids explicit resets.

To introduce HIGS properly, this chapter presents relevant preliminaries. In particular, a mathematical description of HIGS in an open-loop setting is provided in Section 2.2. To obtain more insights in the working principle of HIGS, and better appreciate its benefits, time- and frequency-domain properties, the latter of which are studied by means of the describing function method, are discussed. In Section 2.3, the formal closed-loop setting with HIGS that will be considered throughout this thesis is presented. Additional preliminaries regarding the upcoming stability and performance analysis are provided as well. The most important findings in this chapter are summarized in Section 2.4.

2.2 Open-loop system representation

In this section, the hybrid integrator-gain system is introduced. In order to develop insights into its working principle, and appreciate the benefits it can offer for control, an open-loop analysis is conducted in both time- and frequency-domain, the latter which is based on the describing function method.

2.2.1 State-space description of HIGS

The hybrid integrator-gain system (HIGS) can mathematically be formulated as a piecewise linear (PWL) system with discontinuous right-hand side, given by

$$\mathcal{H}: \begin{cases} \dot{x}_h(t) = \omega_h z(t), & \text{if } (z(t), u(t), \dot{z}(t)) \in \mathcal{F}_1, \quad (2.1a) \\ x_h(t) = k_h z(t), & \text{if } (z(t), u(t), \dot{z}(t)) \in \mathcal{F}_2, \quad (2.1b) \\ u(t) = x_h(t), & \quad (2.1c) \end{cases}$$

where $x_h(t) \in \mathbb{R}$ denotes the state of the integrator, $z(t) \in \mathbb{R}$ is the input, and $u(t) \in \mathbb{R}$ is the generated output at time $t \in \mathbb{R}_{\geq 0}$. Note that (2.1b) can alternatively be described by $\dot{x}_h(t) = k_h \dot{z}(t)$, indicating the discontinuous nature of the vector field of (2.1). To have well-defined behaviour, it is assumed that the input z is a *continuous* piecewise Bohl (PB) function (see, *e.g.* Heemels et al., 2002, Definition IV.2, and Deenen et al., 2021, Definition 2.2), such that its time-derivative $\dot{z}$ exists for almost all times t. Though in general this assumption is somewhat restrictive, for the purpose of illustrating the working principle of HIGS it is sufficient at this point. In the next section, regularity conditions on the input signals will be discussed and motivated within the closed-loop setting.

The parameters $\omega_h \in (0,\infty)$ and $k_h \in (0,\infty)$ in (2.1) represent the integrator frequency and the proportional gain, respectively. The active mode of HIGS is dictated by the flow sets $\mathcal{F}_1$ and $\mathcal{F}_2$. When (2.1a) is active, HIGS is said to operate in *integrator-mode*, whereas if (2.1b) is active, it is said to be in *gain-mode*. Before specifying the sets $\mathcal{F}_1$ and $\mathcal{F}_2$ in more detail, the design philosophy of HIGS is discussed first.

In its primary mode of operation, HIGS exhibits integrator dynamics (2.1a). To maintain the idea of keeping the sign of the integrator's output u equal to that of its input z at all times, operating in integrator-mode is allowed as long as the input-output pair (z,u) remains inside the $[0,k_h]$-sector defined by

$$\mathcal{F} := \left\{ (z,u,\dot{z}) \in \mathbb{R}^3 \mid zu \geq \frac{1}{k_h} u^2 \right\}. \tag{2.2}$$

However, using integrator dynamics on the boundary $u = k_h z$ of the sector $\mathcal{F}$, may result in the vector-field $(\dot{x}_h, \dot{z}) = (\omega_h z, \dot{z})$ to point outside of the sector $\mathcal{F}$. As a consequence, the corresponding trajectory can escape the sector when sticking to the integrator-mode. Specifically, provided $u = k_h z$, this occurs when $\dot{x}_h > k_h \dot{z}$ for $z > 0$, or when $\dot{x}_h < k_h \dot{z}$ for $z < 0$. Since in integrator-mode one has $\dot{x}_h = \omega_h z$, the inequalities can equivalently be expressed in a quadratic form by $\omega_h z^2 > k_h \dot{z} z$. To prevent a trajectory from escaping the sector, a switch to gain-mode (2.1b) is initiated, thereby enforcing the trajectory to slide continuously over the sector boundary according to the dynamics $\dot{x}_h = k_h \dot{z}$. A transition from gain-mode back to integrator-mode is allowed whenever $\omega_h z^2 \leq k_h z \dot{z}$, *i.e.*, when the vector field $(\dot{x}_h, \dot{z}) = (\omega_h z, \dot{z})$ that results from applying the integrator dynamics, points to the interior of the sector $\mathcal{F}$. Note that on the boundary of $\mathcal{F}$ defined by $u = 0$, enforcing the integrator dynamics $\dot{x}_h = \omega_h z$ will ensure the vector field $(\dot{x}_h, \dot{z}) = (\omega_h z, \dot{z})$ to point toward the interior of the sector.

On the basis of the above reasoning, the sets governing the active dynamics of HIGS are constructed as

$$\mathcal{F}_1 := \left\{ (z,u,\dot{z}) \in \mathbb{R}^3 \mid k_h z u \geq u^2 \wedge (z,u,\dot{z}) \notin \mathcal{F}_2 \right\}, \tag{2.3a}$$

$$\mathcal{F}_2 := \left\{ (z,u,\dot{z}) \in \mathbb{R}^3 \mid u = k_h z \wedge \omega_h z^2 > k_h \dot{z} z \right\}. \tag{2.3b}$$

By construction, it follows that $\mathcal{F} = \mathcal{F}_1 \cup \mathcal{F}_2$. A visualization of the sets in (2.3) is provided in Figure 2.1.

Remark 2.2.1. *Note that the dynamics in* (2.1) *are currently defined for initial values* $(z(0), u(0), \dot{z}(0)) \in \mathcal{F}$*, but can be extended such that these are also defined for* $(z(0), u(0), \dot{z}(0)) \notin \mathcal{F}$*. To account for the latter, additional jump dynamics can be defined as*

$$x_h(t^+) = cz(t), \quad \text{if } (z,u,\dot{z}) \in \mathcal{J}, \tag{2.4}$$

where $c \in [0, k_h]$*, and in which the jump set is defined by*

$$\mathcal{J} := \left\{ (z,u,\dot{z}) \in \mathbb{R}^3 \mid zu < \frac{1}{k_h} u^2 \right\}. \tag{2.5}$$

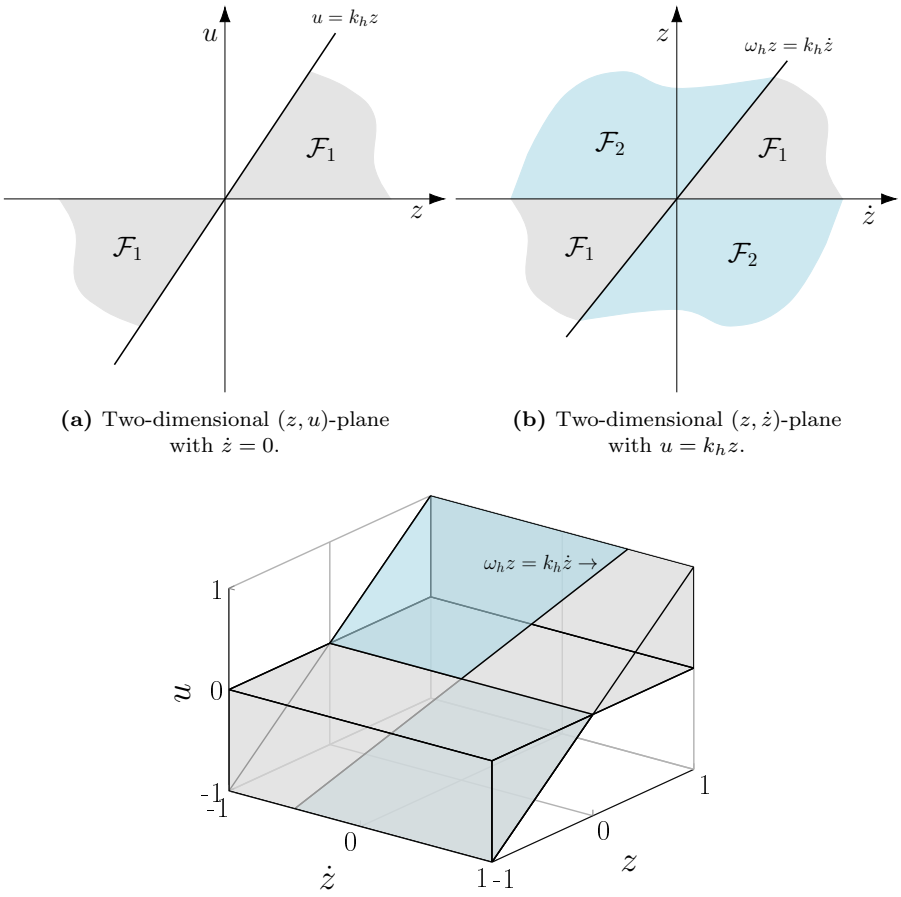

(a) Two-dimensional (z, u)-plane with $\dot{z} = 0$.

(b) Two-dimensional $(z, \dot{z})$-plane with $u = k_h z$.

(c) Three-dimensional region $\mathcal{F} = \mathcal{F}_1 \cup \mathcal{F}_2$.

Figure 2.1. Flow sets $\mathcal{F}_1$ and $\mathcal{F}_2$ as described in (2.3), which determine the active dynamics of HIGS. The integrator mode region $\mathcal{F}_1$ is depicted in gray, and the gain mode region $\mathcal{F}_2$ is depicted in blue.

These dynamics describe an instantaneous reset which, by the choice of $c \in [0, k_h]$*, results in* $(z(t^+), u(t^+), \dot{z}(t^+)) \in \mathcal{F}$*. Note that such reset occurs only at the initial time* $t = 0$ *and not at times* $t > 0$*, as from the previous reasoning (and the fact that* z *is continuous) the specific switching strategy of HIGS would enforce* $(z(t), u(t), \dot{z}(t))$ *to remain within the sector* $\mathcal{F}$ *for all times* $t > 0$*.*

Figure 2.2 illustrates the switching strategy in (2.3) by depicting a simulated response of HIGS in (2.1) to a multi-sine input $z(t) = \sin(t) + 0.5\sin(3t)$, with the parameters set to $k_h = 1.5$, and $\omega_h = 1$ rad/s. When starting in integrator-mode,

the system generates the output u, depicted by the red curve in Figure 2.2. Upon reaching the sector boundary $u = k_h z$, HIGS switches to gain-mode, resulting in the output u as depicted by the blue curve which slides along the sector boundary until the integrator output no longer leads to a violation of the sector constraint. At that point, the gain-mode terminates and HIGS re-enters the integrator-mode. The system continues in integrator-mode, again followed by a switch to gain-mode when necessary, and so on. In this manner, HIGS generates a *continuous* (but non-smooth) output that satisfies the sector constraint in (2.2) at all times. Figure 2.2 additionally shows the two-valued switching sequence (dotted), where the zero values correspond to HIGS being in integrator-mode, and the non-zero values indicate HIGS being in gain-mode.

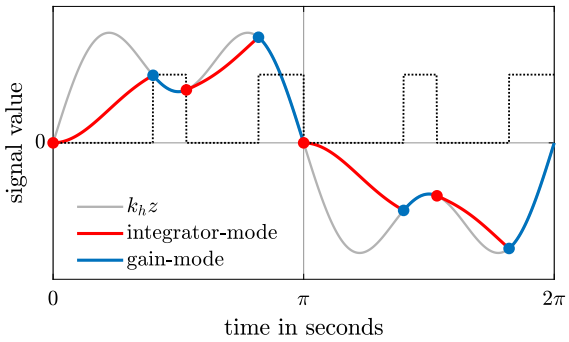

(a) Time-series response of HIGS to a multi-sine input.

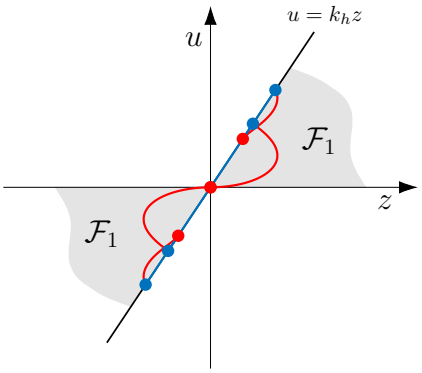

(b) Trajectory in (z, u)-plane.

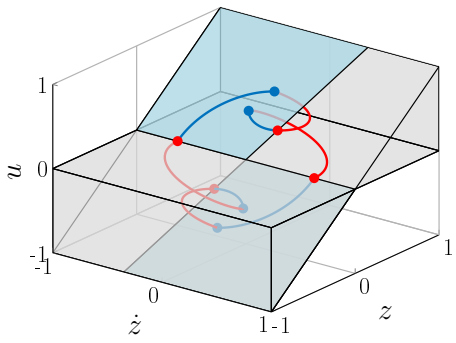

(c) Trajectory in $(z, u, \dot{z})$-space.

Figure 2.2. Time response of HIGS when subjected to a multi-sine input $z(t) = \sin(t) + 0.5\sin(3t)$, $t \in \mathbb{R}_{\geq 0}$ (top figure) and corresponding spatial plots of the input-output trajectories (bottom figures).

2.2.2 Time-domain properties

In this section, useful time-domain properties of HIGS in (2.1) are discussed. Before, going into more detail, however, the adopted solution concept for the discontinuous differential equation in (2.1) is formalized first.

Definition 2.2.2. *Let $\mathbb{T} \subset \mathbb{R}_{\geq 0}$ be an interval of the form $[0, T]$ or $[0, T)$ with $T \in \mathbb{R}_{\geq 0}$ a finite number, or $\mathbb{T} = \mathbb{R}_{\geq 0}$. A locally absolutely continuous (AC) function $x_h : \mathbb{R} \to \mathbb{R}$ is called a solution to the discontinuous differential equation in (2.1) on $\mathbb{T}$ with initial state $x_h(0) = x_{h,0} \in \mathbb{R}$ and locally integrable input $z \in \mathcal{L}_1^{\text{loc}}$, if $(z(t), x_h(t), \dot{z}(t)) \in \mathcal{F}$ for almost all $t \in \mathbb{T}$, and (2.1) holds almost everywhere in $\mathbb{T}$.*

The solutions in Definition 2.2.2 are *Carathéodory*-type of solutions, see, *e.g.*, Cortes, 2008 for more details regarding solution concepts for discontinuous dynamical systems. Under the assumption that the input z is an (absolutely) continuous Piecewise Bohl function, using similar arguments as in Section 4 of Deenen et al., 2021, it can be guaranteed that (2.1) admits at least one solution on $[0, \infty)$, and all maximal solutions are forward complete.

The following result establishes an important and useful input-output (passivity) property of HIGS.

Theorem 2.2.3. *The hybrid integrator-gain system in (2.1) is strictly passive in the sense that there exists a positive definite storage function $V(x_h) = \frac{\lambda}{2} x_h^2$ with $\lambda = k/\omega_h$ and $k \in (0, 1)$ that satisfies*

$$\dot{V} \leq -c x_h^2 + z u, \quad \text{with} \quad c \in (0, k_h), \tag{2.6}$$

along all solutions of (2.1) with continuous $z \in \mathcal{L}_1^{\text{loc}}$ for almost all times $t \in \mathbb{R}_{\geq 0}$.

Proof. The proof can be found in Appendix 2.A.1 and builds on some technical results that will be introduced in Section 2.3. □

Strict passivity (Khalil, 2002; van der Schaft, 2017) is a particularly useful property for stability analysis as it implies that a well-posed feedback interconnection of HIGS with any strictly passive nonlinear plant is passive, see also Khalil, 2002, Theorem 6.1. Under mild detectability conditions, this, in turn, can imply asymptotic stability of the closed-loop system.

The next result establishes useful *incremental* properties of HIGS.

Theorem 2.2.4. *For any input $z \in PB$ that is bounded and continuous, and initial states $x_{h,0}, x'_{h,0} \in \mathbb{R}$ the hybrid integrator-gain system in (2.1) is incrementally asymptotically stable, i.e., it is incrementally stable (in the sense of Lyapunov), and*

$$\|x_h(t, x_{h,0}, z) - x'_h(t, x'_{h,0}, z)\| \to 0 \quad \text{as} \quad t \to \infty. \tag{2.7}$$

Proof. The proof can be found in Appendix 2.A.2. □

Theorem 2.2.5. *The hybrid integrator-gain system in* (2.1) *is homogeneous of degree one in the sense that for any* $\alpha \in \mathbb{R}$*, inputs* $z \in \mathcal{L}_1^{\mathrm{loc}}$*, and initial condition* $x_h(0) \in \mathbb{R}$ *the solutions satisfy*

$$\alpha x_h(t, x_h(0), z(t)) = x_h(t, \alpha x_h(0), \alpha z(t)) \tag{2.8}$$

for all times $t \in \mathbb{R}_{\geq 0}$*.*

Proof. Denote $x_h(t) := x_h(t, x_h(0), z(t))$ and $x_{h,\alpha}(t) := x_h(t, \alpha x_h(0), \alpha z(t))$. Then, one can deduce in a similar manner as in the proof of Theorem 2.2.4 that a Lyapunov function candidate of the form $V(x_h, x_{h,\alpha}) = \frac{1}{2}(\alpha x_h - x_{h,\alpha})^2$ satisfies $\dot{V} \leq 0$ for almost all $t \geq 0$. Since $\alpha x_h(0) = x_{h,\alpha}(0)$ one finds $V(0) = 0$ which implies $V(t) = 0$ for all $t \in \mathbb{R}_{\geq 0}$. □

From Theorem 2.2.4 and Theorem 2.2.5 several important properties of HIGS appear. First, from the result in Theorem 2.2.5 it immediately follows (with $\alpha = 1$) that for an initial state $x_h(0)$ and $z \in \mathcal{L}_1^{\mathrm{loc}}$ the solution to the discontinuous differential equation in (2.1) is unique. Moreover, for all admissible initial conditions $x_{h,1}(0) \neq x_{h,2}(0)$ and $z \in PB$ there is a unique steady-state solution (for $t \to \infty$), and for any periodic input $z(t) = z(t+T)$ with period time T, the corresponding steady-state solution is periodic with the same period, *i.e.*, $x_h(t) = x_h(t+T)$ for all $t \in \mathbb{R}_{\geq 0}$ (Angeli, 2002). For switched systems with discontinuous right-hand sides such as in (2.1), properties such as uniqueness of (steady-state) solutions are far from being trivial (Pavlov et al., 2006b), making this result remarkable. From (2.8) it is also immediate that the output of HIGS scales linearly with input amplitude, hence demonstrating amplitude invariance. Moreover, it is an odd function in the sense that $-x_h(t, x_h(0), z(t)) = x_h(t, -x_h(0), -z(t))$. The discussed properties are instrumental in conducting a describing function analysis in the next section.

Remark 2.2.6. *The above properties do not rely upon the specific class of piecewise Bohl (PB) inputs. Hence, these results still apply when other input classes are considered for which* (2.1) *is well-posed in the sense of having a solution defined on* $[0, \infty)$*, and forward completeness of maximal solutions is established*

2.2.3 Describing function analysis

A cornerstone of the success of LTI control is the fact that industry relies heavily on frequency-domain design techniques. A reason for the latter is that frequency-domain characterizations such as magnitude and phase provide transparent insights in the behaviour of a feedback loop in terms of robust stability and performance. However, the behaviour of nonlinear systems in general, and HIGS in specific, cannot be evaluated in the frequency-domain in the same manner

as is done for LTI systems, the main reasons being: *i*) the absence of the superposition principle, *ii*) the fact that a nonlinear system may possess multiple steady-state solutions to a single (periodic) excitation, and *iii*) the fact that a single-frequency excitation signal typically induces a response that contains harmonic content at multiple frequencies. To deal with these shortcomings, the describing function method is adopted (Gelb and Vander Velde, 1968). In describing function analysis, an approximate frequency-domain characterization of nonlinear systems is determined by relating a sinusoidal input signal to the fundamental harmonic of the system's steady-state response. Higher harmonics that the output signal may contain are usually neglected in the analysis.

In the previous section it has been shown in Theorem 2.2.4 that HIGS in (2.1) has a unique steady-state response to a given input signal. This justifies the use of the describing function approach to study frequency-domain properties of HIGS. For this purpose, consider a sinusoidal input (which is a Bohl function) of the form

$$z(t) = A\sin(\omega t), \tag{2.9}$$

with amplitude $A \in \mathbb{R}$, and frequency $\omega \in \mathbb{R}_{\geq 0}$. Remark that by virtue of Theorem 2.2.5 the steady-state response of HIGS scales linearly with the input amplitude, such that without loss of generality the amplitude of (2.9) can be set to one, *i.e.*, $A = 1$. Moreover, the steady-state response of HIGS to the sinusoidal input in (2.9) is unique, and has a period of $2\pi/\omega$ seconds. The response is found analytically by solving (2.1) for $x_h(0) = 0$ within the time-interval $[0, 2\pi/\omega]$, resulting in

$$u(\tau) = \begin{cases} \frac{\omega_h}{\omega}\left(1 - \cos(\tau)\right), & \text{if } 0 \leq \tau \leq \gamma(\omega), \\ k_h \sin(\tau), & \text{if } \gamma(\omega) \leq \tau \leq \pi, \\ \frac{\omega_h}{\omega}\left(-1 - \cos(\tau)\right), & \text{if } \pi \leq \tau \leq \pi + \gamma(\omega), \\ k_h \sin(\tau), & \text{if } \pi + \gamma(\omega) \leq \tau \leq 2\pi, \end{cases} \tag{2.10}$$

where $\tau = \omega t$ and $\gamma(\omega)$ represents the switching instance, which is specified hereafter. The steady-state response in (2.10) is depicted in Figure 2.3.

An explicit expression for the switching instance $\gamma(\omega)$ is found from equating the generated output in integrator-mode to the output in gain-mode, that is

$$\frac{\omega_h}{\omega}(1 - \cos(\gamma(\omega))) = k_h \sin(\gamma(\omega)). \tag{2.11}$$

Using the standard trigonometric identities $1 - \cos(a) = 2\sin^2(\frac{a}{2})$ and $\sin(a) = 2\sin(\frac{a}{2})\cos(\frac{a}{2})$ this yields

$$\frac{\omega_h}{\omega}\sin\left(\frac{\gamma(\omega)}{2}\right) = k_h \cos\left(\frac{\gamma(\omega)}{2}\right), \tag{2.12}$$

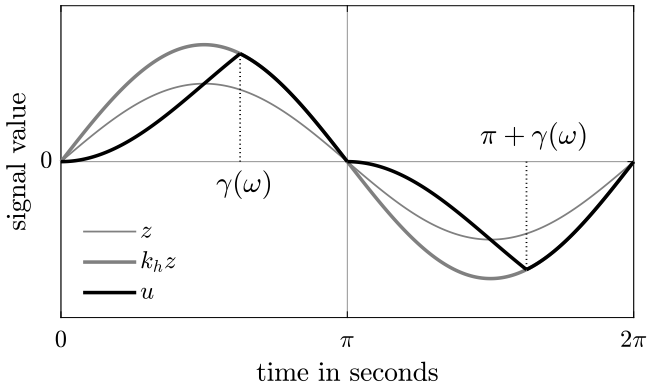

Figure 2.3. Steady-state response of HIGS (black) to a sinusoidal input (thin grey) for $\omega_h = \omega$ and $k_h = 1.5$, alongside the maximum allowable output as given by the sector $[0, k_h]$ (bold grey).

which by $\tan(a) = \frac{\sin(a)}{\cos(a)}$ gives

$$\gamma(\omega) = 2 \arctan\left(\frac{k_h \omega}{\omega_h}\right). \tag{2.13}$$

Given the uniqueness and periodicity of the response in (2.10), it is possible to write $u(\tau)$ in the form of the Fourier series expansion

$$u(\tau) = \frac{a_0}{2} + \sum_{k=1}^{\infty} (a_k(\omega)\cos(k\tau) + b_k(\omega)\sin(k\tau)), \tag{2.14}$$

where the Fourier coefficients are given by

$$a_k(\omega) = \frac{\omega}{\pi} \int_0^{2\pi} u(\tau)\cos(k\tau)d\tau, \tag{2.15a}$$

$$b_k(\omega) = \frac{\omega}{\pi} \int_0^{2\pi} u(\tau)\sin(k\tau)d\tau, \tag{2.15b}$$

with $k \in \mathbb{Z}_{>0}$ a multitude of the input frequency. Since $u(\tau)$ in (2.10) is an odd function, *i.e.*, $u(-\tau) = -u(\tau)$, it follows that $a_0 = 0$ in (2.14). The coefficients for $k = 1$ obtained after some algebra are given by (where for brevity dependency of γ on ω is omitted)

$$a_1(\omega) = \frac{1}{2\pi}\left(\frac{\omega_h}{\omega}\left(4\sin(\gamma) - \sin(2\gamma) - 2\gamma\right) - k_h\left(1 - \cos(2\gamma)\right)\right), \tag{2.16a}$$

$$b_1(\omega) = \frac{1}{2\pi}\left(\frac{\omega_h}{\omega}\left(3 - 4\cos(\gamma) + \cos(2\gamma)\right) + k_h\left(2(\pi - \gamma) + \sin(2\gamma)\right)\right). \tag{2.16b}$$

By neglecting all contributions in (2.14) at $k > 1$, and using Euler's formula, the describing function of HIGS is derived as

$$\begin{aligned}\mathcal{D}(j\omega) &= b_1(\omega) + ja_1(\omega) \\ &= \frac{\omega_h}{j\omega}\left(\frac{\gamma(\omega)}{\pi} + j\frac{e^{-2j\gamma(\omega)} - 4e^{-j\gamma(\omega)} + 3}{2\pi}\right) + k_h\left(\frac{\pi - \gamma(\omega)}{\pi} + j\frac{e^{-2j\gamma(\omega)} - 1}{2\pi}\right).\end{aligned} \tag{2.17}$$

The direct contribution of the integrator dynamics and gain dynamics can be recognized by the combination of the terms $\omega_h/j\omega$ and k_h in the respective ratios $\gamma(\omega)/\pi$ and $(\pi - \gamma(\omega))/\pi$, which correspond to the relative time-intervals in which these dynamics are active, see also Figure 2.3.

A Bode-like plot of the describing function in (2.17) for different values of ω_h and k_h is shown in Figure 2.4.

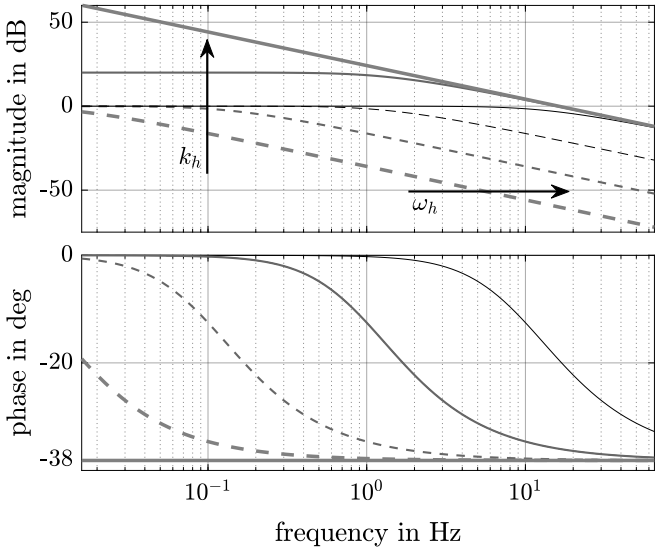

Figure 2.4. Bode-like diagram of the describing function in (2.17) for different values of k_h and ω_h. The cross-over frequency is given by $\omega_c = |1 + 4j/\pi|\frac{\omega_h}{k_h}$.

Two asymptotes appear in this figure:

- For $\omega \to 0$, the describing function (2.17) tends to a static gain, *i.e.*,

$$\lim_{\omega \to 0} \mathcal{D}(j\omega) = k_h, \tag{2.18}$$

  as a result of $\lim_{\omega \to 0} \gamma(\omega) = 0$. This can be explained in the time-domain as for harmonic inputs with $\omega << \omega_h/k_h$, the integrator buffer reaches its

sector-admissible value after a time interval negligible when compared to the input frequency, meaning HIGS effectively reduces to a static gain. In the same spirit, for $\omega_h/k_h \to \infty$ the above asymptote holds for all $\omega \in \mathbb{R}_{\geq 0}$.

- In contrast, for $\omega \to \infty$, the describing function characteristics tend to that of an integrator in terms of the magnitude, but with significantly less phase lag. Given (2.13), (2.17) this is found by $\lim_{\omega\to\infty} \gamma(\omega) = \pi$ yielding

$$\lim_{\omega\to\infty} \mathcal{D}(j\omega) = \frac{\omega_h}{j\omega}\left(1 + \frac{4j}{\pi}\right), \tag{2.19}$$

for which the magnitude and phase characteristics can be computed as

$$\lim_{\omega\to\infty} |\mathcal{D}(j\omega)| = \left|1 + \frac{4j}{\pi}\right| \frac{\omega_h}{\omega} \approx 1.62\frac{\omega_h}{\omega}, \tag{2.20a}$$

$$\lim_{\omega\to\infty} \angle\mathcal{D}(j\omega) = \arctan\left(-\frac{\pi}{4}\right) \approx -38.15^\circ. \tag{2.20b}$$

Interestingly, for $\omega \to \infty$, (2.19) tends to the describing function characteristics of the Clegg (reset) integrator, see Clegg, 1958; Horowitz and Rosenbaum, 1975. A time-domain interpretation is given as follows. For $\omega >> \omega_h/k_h$, the integrator buffer builds up very slowly compared to the time-scale of excitation, making the time interval in which the gain mode is active negligible compared to the interval in which integrator dynamics are active. As sign-equivalence is enforced due to switching, this behaviour somewhat resembles that of the Clegg integrator, though without hard resets. The asymptote is also found for $\omega_h/k_h \to 0$.

From the above reasoning, one may observe the ratio ω_h/k_h as the leading factor that determines whether integrator or gain characteristics dominate the overall behaviour of HIGS both in time- and frequency-domain. This is also seen from the cross-over frequency of the describing function (2.17), which is given by $\omega_c := |1 + 4j/\pi|\frac{\omega_h}{k_h}$ rad/s. Loosely speaking, for $\omega_h/k_h \to \infty$, HIGS behaves as a linear gain k_h, whereas for $\omega_h/k_h \to 0$, HIGS mimics the behaviour of a Clegg (reset) integrator without hard resets. This behaviour can be recognized in time-domain from the simulated time-responses as depicted in Figure 2.5.

2.2.4 HIGS and projected dynamical systems

A strongly related, but seemingly different approach for formalizing the working principle and closed-loop description of HIGS comes from considering a class of systems referred to as projected dynamical systems (PDS), see *e.g.*, Dupuis and Nagurney, 1993; Heemels et al., 2000; Nagurney and Zhang, 1996. Such systems are described by differential equations of which the solutions are restricted to be contained in a constraint set. At moments when the solutions tend to leave this

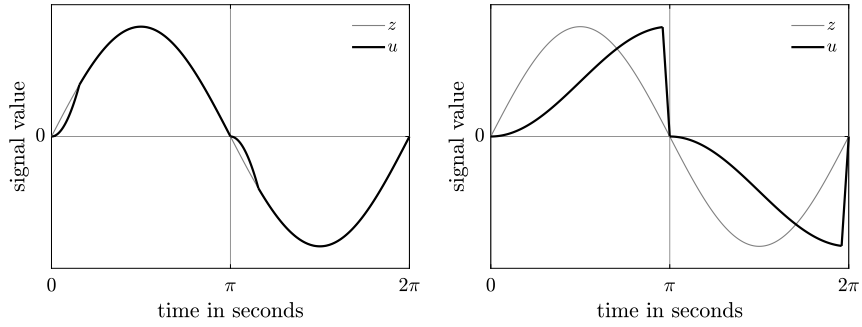

(a) Time-response for $\omega_h/k_h = 6\omega$. **(b)** Time-response for $\omega_h/k_h = \omega/16$.

Figure 2.5. Time-response of HIGS (black) for different ratios of ω_h/k_h. The response in Figure 2.5a resembles that of a linear gain, whereas the response in Figure 2.5b resembles that of the Clegg integrator. Note that in both cases the responses are continuous, but not smooth.

set, the vector field of the system is changed by means of *projection* to ensure that the solutions remain inside the constraint set. Although the PDS philosophy naturally resembles that of HIGS, there are key differences that prevent a direct description of HIGS as a PDS. For instance, the constraint set of HIGS (the sector), does not satisfy certain regularity requirements necessary for the PDS framework to be applicable, see Henry, 1973. Furthermore, in the case of PDS, the complete vector field is projected on the constraint set. In a control context, however, when considering HIGS in feedback with a physical plant as done in the next section, it is only possible to project the dynamics of the controller and not the full dynamics including the plant. For that reason, in Deenen et al., 2021; Sharif et al., 2019 a generalization of PDS, referred to as *extended* projected dynamical systems (ePDS) has been proposed, which deals with these issues in a natural manner, thereby allowing for an alternative and intuitive representation of HIGS. One of the main advantages of formulating a HIGS-controlled system in the ePDS framework is that it may link to other classes of dynamical systems such that system theoretical properties directly transfer from one class to the other, see for instance the results in Heemels et al., 2020; Sharif et al., 2021a. In Deenen et al., 2021, it was shown that in a closed-loop setting, the ePDS formulation can be written equivalently as a piecewise linear (PWL) model. As such, properties established for the former representation are directly inherited by the latter. Moreover, as for classical PDS stability and performance properties are well-established, these may naturally extend to systems with HIGS. In this thesis, however, the PWL formulation that will be introduced in the next section is adopted as it is more convenient for the stability and performance analysis approaches adopted in the subsequent parts. For a thorough exposition of the

ePDS framework in general, and the link with HIGS in particular, the reader is referred to Sharif et al., 2019 and Deenen et al., 2021.

2.3 Closed-loop system representation

Having developed more insight into the working principle and key properties of HIGS, this section formally discusses the closed-loop setting as considered for stability and performance analysis purposes throughout this thesis. The generic setup is depicted in Figure 2.6, and consists of a linear time-invariant (LTI), multi-input multi-output (MIMO) generalized plant G interconnected with a single-input single-output (SISO) HIGS element $\mathcal{H}$. The generalized plant G contains the linear parts of the system, including the physical plant to be controlled and filters related to the LTI part of the feedback controller. In state-space formulation, the plant G is given by

$$G : \begin{cases} \dot{x}_g(t) &= A_g x_g(t) + B_g u(t) + B_w w(t), \\ y(t) &= C_g x_g(t) + D_g u(t) + D_w w(t), \\ q(t) &= C_q x_g(t) + D_q w(t) + D_u u(t), \end{cases} \tag{2.21}$$

with states $x_g(t) \in \mathbb{R}^p$, regulated outputs $q(t) \in \mathbb{R}^r$, and external inputs $w(t) \in \mathbb{R}^m$. The input and output of HIGS are denoted by $z(t) = -y(t) \in \mathbb{R}$, and $u(t) \in \mathbb{R}$, respectively.

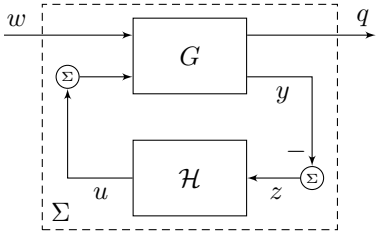

Figure 2.6. Generic feedback interconnection of an LTI system G and HIGS $\mathcal{H}$ with inputs w and outputs q.

The realization (A_g, B_g, C_g, D_g) is assumed to be a minimal realization. For ensuring the closed-loop system in Figure 2.6 to have well-behaved dynamics, the following standing assumption is made throughout this thesis.

Assumption 2.3.1. *The LTI system G given in* (2.21) *and depicted in Figure 2.6 satisfies $D_g = D_w = 0$ and $C_g B_g = C_g B_w = 0$.*

This assumption implies that the transfer functions from u to y and w to y have a relative degree of at least two. It removes the occurrence of an algebraic

loop when HIGS is in gain-mode, ensures the absence of a direct feedthrough from the signals $(w, \dot{w})$ to $(z, \dot{z})$, and guarantees the input to HIGS to be continuous and at least one time continuously differentiable. Note that within the relevant and broad class of motion systems, where plants are typically described by double integrators with additional structural dynamics, the relative degree assumption is often naturally satisfied.

2.3.1 Closed-loop system description

Due to the piecewise linear (PWL) nature of HIGS in (2.1), and under Assumption 2.3.1, the closed-loop system in Figure 2.6 naturally admits the PWL formulation

$$\Sigma : \begin{cases} \dot{x}(t) &= A_i x(t) + Bw(t), \quad \text{if } x(t) \in \mathcal{X}_i,\ i \in \{1,2\} \\ q(t) &= Cx(t) + Dw(t), \end{cases} \tag{2.22}$$

with state $x(t) = \begin{bmatrix} x_g(t)^\top & x_h(t) \end{bmatrix}^\top \in \mathbb{R}^n$, in which x_g and x_h are the states of G and $\mathcal{H}$, respectively, so that $n = p + 1$. The sets $\mathcal{X}_i$, $i \in \{1, 2\}$, are defined as

$$\mathcal{X}_i := \{x \in \mathbb{R}^n \mid Ex \in \mathcal{F}_i\}, \tag{2.23}$$

in which the matrix E extracts those signals from x that determine mode switching of HIGS, *i.e.*, E is such that $Ex := (z\ u\ \dot{z})^\top$, and is, therefore, given by

$$E^\top = \begin{bmatrix} -C_g^\top & 0 & -(C_g A_g)^\top \\ 0 & 1 & 0 \end{bmatrix}. \tag{2.24}$$

Remark that $\mathcal{X}_1 \cup \mathcal{X}_2 = \mathcal{X} := \{x \in \mathbb{R}^n \mid Ex \in \mathcal{F}\}$, with $\mathcal{F}$ the sector defined in (2.2). The mode-dependent system matrices in (2.22) are given by

$$A_1 = \begin{bmatrix} A_g & B_g \\ -\omega_h C_g & 0 \end{bmatrix}, \quad \text{and} \quad A_2 = \begin{bmatrix} A_g & B_g \\ -k_h C_g A_g & 0 \end{bmatrix}, \tag{2.25}$$

and furthermore $B = [B_w^\top, 0]^\top$, $C = [C_q, D_u]$, and $D = D_q$. Note that this formulation results from Assumption 2.3.1 and explicit differentiation of the algebraic constraint $x_h = k_h z$ in (2.1) in gain-mode.

It can be seen that (2.22) describes a *discontinuous* differential equation. This makes proving (global) existence of solutions, given an initial state x_0 and external signal w a difficult problem, since typical continuity properties used for studying differential equations/inclusions (such as upper-semicontinuity of the right-hand side conform Aubin and Cellina, 1984) are not fulfilled, see also Cortes, 2008. The next section briefly revisits some of the results presented in Deenen et al., 2021 regarding well-posedness of the HIGS-controlled system (2.22) in the sense of global existence and forward completeness of solutions.

2.3.2 Solution concept and well-posedness

For the results in Deenen et al., 2021 to be applicable, the class of exogenous signals that are considered here should be of a piecewise Bohl (PB) nature, see Deenen et al., 2021, Definition 2.2. As sines, cosines, exponentials, polynomials, and sums thereof are all Bohl functions, the class of PB functions is considered to be sufficiently rich to accurately describe (deterministic) input signals frequently encountered in practice. In particular, any piecewise constant signal is PB, and thus this class of functions can approximate any measurable function arbitrarily close. The following solution concept, related to Definition 2.2.2 is adopted from Deenen et al., 2021.

Definition 2.3.2. *Let $\mathbb{T} \subset \mathbb{R}_{\geq 0}$ be an interval of the form $[0, T]$ or $[0, T)$ with $T \in \mathbb{R}_{\geq 0}$ a finite number, or $\mathbb{T} = \mathbb{R}_{\geq 0}$. A locally absolutely continuous (AC) function $x : \mathbb{T} \to \mathbb{R}^n$ is called a solution to the HIGS-controlled system in* (2.22) *on $\mathbb{T}$ with initial state $x_0 \in \mathcal{X}$ and $w \in \mathcal{L}_1^{\text{loc}}$, if $x(0) = x_0$, $x(t) \in \mathcal{X}$ for all $t \in \mathbb{T}$, and* (2.22) *holds almost everywhere in $\mathbb{T}$.*

Definition 2.3.3 (Deenen et al., 2021)**.** *Let $\mathbb{T} \subset \mathbb{R}_{\geq 0}$ be an interval of the form $[0, T]$ or $[0, T)$ with $T \in \mathbb{R}_{\geq 0}$ a finite number, or $\mathbb{T} = \mathbb{R}_{\geq 0}$. A solution $x : \mathbb{T} \to \mathbb{R}^n$ to* (2.22) *with $w \in \mathcal{L}_1^{\text{loc}}$ on $\mathbb{T}$ is called maximal if there does not exist a solution $x' : \mathbb{T}' \to \mathbb{R}^n$ with $w \in \mathcal{L}_1^{\text{loc}}$ on $\mathbb{T}'$, where $\mathbb{T}' = [0, T')$ with $T' \in \mathbb{R}_{\geq T}$, that satisfies $x(t) = x'(t)$ for $t \in \mathbb{T}$. A solution $x : \mathbb{T} \to \mathbb{R}^n$ is called forward complete if $\mathbb{T} = \mathbb{R}_{\geq 0}$.*

Theorem 2.3.4. *For all initial states $x_0 \in \mathcal{X}$ and exogenous inputs $w \in PB$ the HIGS-controlled system in* (2.22) *admits at least one solution on $[0, \infty)$, and all maximal solutions for $w \in PB$ are forward complete.*

This result is an immediate consequence of applying Theorem 4.1 and Theorem 4.2 in Deenen et al., 2021, and excludes the existence of Zeno-solutions for PB inputs (Goebel et al., 2009).

Remark 2.3.5. *Since the response of HIGS is amplitude invariant and an odd function (Theorem 2.2.5), it immediately follows that the solutions of the closed-loop interconnection of HIGS and an LTI system as in* (2.22) *scale linearly with the input amplitude as well, i.e., $x(t, \alpha x(0), \alpha w(t)) = \alpha x(t, x(0), w(t))$ for $\alpha \in \mathbb{R}$.*

2.3.3 Stability and performance: Preliminaries

One of the primary objectives in this thesis is to develop tools for verifying stability and performance of the HIGS-controlled system in (2.22). To make the discussions in this thesis precise, preliminary definitions and results heavily used throughout the remainder of this thesis are provided in this section.

To study stability properties of the closed-loop system in (2.22), the notion of input-to-state stability (ISS) is adopted.

Definition 2.3.6 (Sontag and Wang, 1995)**.** *The closed-loop system in* (2.22) *is said to be input-to-state stable (ISS), if there exist a $\mathcal{KL}$-function α and a $\mathcal{K}$-function β such that for any initial condition $x(0) = x_0 \in \mathcal{X}$ and any bounded input signal $w \in \mathcal{L}_1^{\text{loc}}$, all corresponding solutions to* (2.22) *satisfy*

$$\|x(t)\| \leq \alpha(\|x(0)\|, t) + \beta\left(\sup_{0\leq\tau\leq t} \|w(\tau)\|\right), \tag{2.26}$$

for all $t \in \operatorname{dom} x$, where $\operatorname{dom} x$ denotes the projection of a signal $t \mapsto x(t)$ on the time (t) axis.

Remark 2.3.7. *Definition 2.3.6 accounts for the possibility of (maximal) solutions not being forward complete, e.g., solutions of which the domain is not defined for all times $t \in \mathbb{R}_{\geq 0}$. Allowing for this situation separates conditions for forward completeness of solutions from conditions on stability, see also Goebel et al., 2009, Section 3.1 and Van Loon et al., 2017, Remark 5.*

In the study of ISS for discontinuous dynamical systems such as in (2.22), non-smooth Lyapunov functions are often employed, see *e.g.*, Branicky, 1998; Heemels and Weiland, 2008; Rantzer and Johansson, 2000; Shevitz and Paden, 1994. In this context, it is considered useful to revisit some of the machinery used in non-smooth analysis.

Definition 2.3.8 (Clarke, 1983; Shevitz and Paden, 1994)**.** *For a locally Lipschitz function $V : \mathbb{R}^n \to \mathbb{R}$ the generalized gradient of V at x is defined as*

$$\partial V(x) = \overline{\text{co}}\left\{\lim_{i\to\infty} \nabla V(x_i) \mid x_i \to x,\ x_i \notin \Omega_V\right\}, \tag{2.27}$$

where $\overline{\text{co}}$ denotes the closed convex hull, ∇V denotes the gradient of V (at states where it is defined), and Ω_V is the set of measure zero where the gradient of V is not defined.

Theorem 2.3.9. *Let $V : \mathbb{R}^n \to \mathbb{R}_{\geq 0}$ be a locally Lipschitz continuous function and x a locally absolutely continuous solution to $\dot{x}(t) \in F(x(t), w(t))$ for some locally integrable function $w \in \mathcal{L}_1^{\text{loc}}$. Then $t \mapsto V(x(t))$ is locally Lipschitz continuous and*

$$\frac{d}{dt}V(x(t)) \leq \max_{p\in\partial V(x(t))} \max_{f\in F(x(t),w(t))} \langle p, f\rangle \tag{2.28}$$

for almost all times t.

Proof. The proof largely proceeds as the proof of Theorem 3.3 in Heemels and Weiland, 2008. First, observe that since V is locally Lipschitz continuous, and x is locally absolutely continuous, the composite function $t \mapsto V(x(t))$ is locally absolutely continuous and consequently, $t \mapsto V(x(t))$ is differentiable almost everywhere with respect to time t. Suppose that at time t both $\dot{x}(t)$ and

$dV(x(t))/dt$ exist. Note that $\dot{x}(t) = f \in F(x(t), w(t))$. Using the same arguments as in the proof of Theorem 3.3 in Heemels and Weiland, 2008, it can be concluded that

$$\begin{aligned} \frac{d}{dt}V(x(t)) &= \lim_{h\to 0} \frac{V(x(t+h)) - V(x(t))}{h} \\ &= \lim_{h\downarrow 0} \frac{V(x(t)+hf) - V(x(t))}{h}. \end{aligned} \tag{2.29}$$

To evaluate the right-hand side of (2.29) use is made of Lebourg's Lipschitz mean-value theorem (Clarke, 1983, Theorem 2.3.7), which states that for any V that is Lipschitz on an open set containing the closed line segment $[a, b]$, there is a point c in the open line segment (a, b) such that

$$V(a) - V(b) \in \langle a - b, \partial V(c)\rangle. \tag{2.30}$$

Applying this to $V(x(t) + h_i f) - V(x(t))$ for $h_i \downarrow 0$ when $i \to \infty$, one obtains

$$\frac{d}{dt}V(x(t) = \lim_{i\to\infty} \langle p_i, f\rangle, \tag{2.31}$$

where $p_i \in \partial V(x(t) + \alpha_i f)$ with $\alpha_i \in (0, h_i)$. Since V is a locally Lipschitz continuous function, it follows by application of Clarke, 1983, Proposition 2.1.2 and Clarke, 1983, Proposition 2.1.5 that for α_i converging to zero, there is a subsequence $\{p_i\}_{i\in\mathbb{N}}$ converging to p, and one has $p \in \partial V(x)$. It then follows that the right-hand side in (2.29) is equal to

$$\frac{d}{dt}V(x(t)) = \langle p, f\rangle \tag{2.32}$$

for some $p \in \partial V(x)$. Then, an upper-bound on the time-derivative of V immediately follows as

$$\frac{d}{dt}V(x(t)) \leq \max_{p\in\partial V(x(t))} \max_{f\in F(x(t),w(t))} \langle p, f\rangle, \tag{2.33}$$

which holds for almost all times t. □

The above result provides a basis for the definition of an ISS-Lyapunov function for the HIGS-controlled system in (2.22), in line with Heemels and Weiland, 2008; Sontag and Wang, 1995.

Definition 2.3.10. *A locally Lipschitz continuous function $V : \mathbb{R}^n \to \mathbb{R}_{\geq 0}$ is said to be an ISS-Lyapunov function for the system in* (2.22)*, if*

- *there exist $\mathcal{K}_\infty$-functions α_1, α_2 such that for all $x \in \mathbb{R}^n$*

$$\alpha_1(|x|) \leq V(x) \leq \alpha_2(|x|), \tag{2.34}$$

- *there exist $\mathcal{K}$-functions α and β such that for all $x \in \mathbb{R}^n$ and $w \in \mathbb{R}^m$*

$$\max_{p \in \partial V(x)} \max_{f \in F(x,w)} \langle p, f \rangle \leq -\alpha(|x|) + \beta(|w|), \tag{2.35}$$

where

$$F(x,w) = \begin{cases} A_1 x + Bw & \text{if } x \in \mathcal{X}_1, \\ A_2 x + Bw & \text{if } x \in \mathcal{X}_2. \end{cases} \tag{2.36}$$

Theorem 2.3.11. *If there exists an ISS-Lyapunov function for* (2.22) *in the sense of Definition 2.3.10, then system* (2.22) *is ISS for any bounded $w \in \mathcal{L}_1^{\text{loc}}$.*

Proof. The proof is obtained following similar steps as the proof of Heemels and Weiland, 2008, Theorem 3.5. □

In studying different (input-output) performance properties of the closed-loop system in (2.22) the concept of dissipativity will be particularly useful.

Definition 2.3.12 (Willems, 2007)**.** *The closed-loop system in* (2.22) *is said to be dissipative with respect to a supply function $s : \mathbb{R}^n \times \mathbb{R}^r \times \mathbb{R}^m \to \mathbb{R}$, if there exist a positive (semi-)definite continuous function $V : \mathbb{R}^n \to \mathbb{R}_{\geq 0}$, called a storage function, and $\mathcal{K}_\infty$-functions α_1, α_2 such that $\alpha_1(|x|) \leq V(x) \leq \alpha_2(|x|)$ for all $x \in \mathcal{X}$, and*

$$V(x(t)) - V(x(0)) \leq \int_0^t s(w(\tau), q(\tau), x(t)) d\tau, \tag{2.37}$$

for all $t \in \operatorname{dom} x$ and all (x, q, w) with $\operatorname{dom} q \neq \{0\}$ satisfying (2.22) *for almost all times $t \in \operatorname{dom} x$.*

The definition of an ISS-Lyapunov function as given in Definition 2.3.10 can be extended toward a storage function by relaxing condition (2.35) to

$$\max_{p \in \partial V(x)} \max_{f \in F(x,w)} \langle p, f \rangle \leq s(w, q, x). \tag{2.38}$$

Supply functions that are often used to assert performance in terms of, for example, the $\mathcal{L}_2$-gain and $\mathcal{H}_2$-norm are given by $s(w,q,x) = \gamma^2 \|w\|^2 - \|q\|^2$, with $\gamma > 0$, and $s(w,q,x) = -\|q\|^2$, see, *e.g.*, van der Schaft, 2017.

2.3.4 Robustness aspects

Some comments are in order regarding robustness issues that can arise for discontinuous differential equations of the form

$$\dot{x}(t) = f(x(t), w(t)), \quad \text{when } x(t) \in \mathcal{X}, \tag{2.39}$$

with $x(t) \in \mathbb{R}^n$, $w(t) \in \mathbb{R}^m$, and $\mathcal{X} \subseteq \mathbb{R}^n$, just as the closed-loop system in (2.22). As discussed in Goebel et al., 2009, in order to obtain robust stability/performance guarantees (with respect to arbitrary small state perturbations), it is important to consider the so-called Krasovskii regularization (Krasovskii and Subbotin, 1988) of (2.39), which is defined as

$$\dot{x}(t) \in \bigcap_{\delta>0} \overline{\text{co}}(f(\mathbb{B}(x(t),\delta) \cap \mathcal{X}, w(t)), \quad \text{when } x(t) \in \overline{\mathcal{X}}, \tag{2.40}$$

where $\mathbb{B}(x(t),\delta)$ is the open ball of radius δ around $x(t)$ and for a set $\Omega \subseteq \mathbb{R}^n$, $\overline{\text{co}}(\Omega)$ denotes its closed convex hull and $\overline{\Omega}$ denotes the closure. The Krasovskii regularization of (2.22) can be calculated explicitly, giving

$$\dot{x}(t) \in \begin{cases} A_1 x(t) + Bw(t) & \text{if } x(t) \in \mathcal{X} \setminus \overline{\mathcal{X}}_2, \\ \overline{\text{co}}(A_1 x(t), A_2 x(t)) + Bw(t) & \text{if } x(t) \in \overline{\mathcal{X}}_2. \end{cases} \tag{2.41}$$

Solutions to (2.41) are understood in the sense of Krasovskii, see, *e.g.*, Sanfelice et al., 2008. In the remainder it will be shown that for specific choices of V, the conditions in Definition 2.3.10 guarantee ISS/dissipativity of the Krasovskii regularization in (2.41) as well, and thus stronger stability and performance guarantees for (2.22) can be obtained including state perturbations.

The definitions and results as discussed in this chapter will be instrumental in deriving verifiable conditions for asserting (robust) stability and performance properties of the feedback interconnection of the closed-loop system as in (2.22), and are heavily exploited in Chapters 4–6.

2.4 Summary

In this chapter, the hybrid integrator-gain system, abbreviated with HIGS, is formally presented. It is shown that specific switching between integrator and gain characteristics ensures the generated output of the hybrid integrator to have a sign that is equivalent to the sign of the input at all times, thereby adhering to the traditional philosophy of the Clegg (reset) integrator. Different from reset integrators, however, HIGS avoids hard resets, and generates continuous (non-smooth) outputs which may provide benefits. Both time- and frequency-domain properties of HIGS are studied, the latter in an approximate sense through its describing function which reveals magnitude characteristics that correspond to a (weak) integrator, but with an induced phase lag of only 38.15 degrees.

In the next chapter, the properties of HIGS are exploited for constructing nonlinear controllers that are able to overcome some of the fundamental performance limitations of linear time-invariant control.

2.A Proofs and technical results

2.A.1 Proof of Theorem 2.2.3

The proof exploits some of the machinery introduced in Section 2.3. Consider the quadratic storage function candidate $V(x_h) = \frac{\lambda}{2}x_h^2$ with $\lambda = k/\omega_h$ and $k \in (0,1)$. This function is Lipschitz continuous and positive definite. Since x_h is a locally absolutely continuous solution to $\dot{x}_h(t) \in \{\omega_h z(t), k_h \dot{z}(t)\}$ for some continuous $z \in \mathcal{L}_1^{\text{loc}}$, it follows from Theorem 2.3.9 that in integrator-mode

$$\dot{V} = \nabla V(x_h)\omega_h z = kzx_h. \tag{2.42}$$

On the other hand, in gain-mode one finds

$$\dot{V} = \nabla V(x_h)k_h\dot{z} = \lambda k_h x_h \dot{z} < kzx_h, \tag{2.43}$$

where for the inequality use is made of the fact that in gain-mode one has $x_h = k_h z$ and $\omega_h z^2 > k_h z\dot{z}$, see also the definition of the gain-mode set in (2.3b). As such, one finds as a common upper-bound $\dot{V} \leq kzx_h = kzu$, which shows that HIGS is passive. To show *strict* passivity, observe that

$$\dot{V} \leq -(1-k)zx_h + zu \leq -k_h(1-k)x_h^2 + zu, \tag{2.44}$$

where for obtaining the second inequality use is made of the sector condition $x_h^2 \leq k_h z x_h$. Denote $c = k_h(1-k)$ and observe that since $k \in (0,1)$, one finds $c \in (0, k_h)$. This completes the proof.

2.A.2 Proof of Theorem 2.2.4

Consider the difference between two solutions starting from different initial conditions as $\delta x_h(t) := x_h(t, x_h(0), z(t)) - x_h(t, x_h'(0), z(t))$ and define an incremental Lyapunov function candidate as

$$V(\delta x_h) = \frac{1}{2}(\delta x_h)^2. \tag{2.45}$$

Clearly, (2.45) is positive definite. Moreover, since solutions to HIGS in (2.1) are locally absolutely continuous functions, $t \mapsto V(\delta x_h(t))$ is a locally absolutely continuous function as well, and thus $dV(\delta x_h(t))/dt$ exists almost everywhere.

Suppose two trajectories starting at different initial conditions are both in integrator-mode. In this case, one finds the time-derivative along the solutions of (2.1) to satisfy $\dot{V} = 0$, such that V itself remains constant. A similar observation can be made when both trajectories are in gain-mode, in which case it holds that $\dot{V} = 0$ and $V = 0$. Note that the latter case implies $\delta x_h = 0$.

Next, consider the case where both trajectories are in different modes, for which one finds

$$\dot{V} = \begin{cases} (x_h(t) - k_h z(t))(\omega_h z(t) - k_h \dot{z}(t)), & \text{if } (x_h(t), x_h'(t)) \in \mathcal{F}_1 \times \mathcal{F}_2, \\ (k_h z(t) - x_h'(t))(k_h \dot{z}(t) - \omega_h z(t)), & \text{if } (x_h(t), x_h'(t)) \in \mathcal{F}_2 \times \mathcal{F}_1, \end{cases} \tag{2.46}$$

where $x_h(t) = x_h(t, x_h(0), z(t))$ and $x_h'(t) = x_h(t, x_h'(0), z(t))$. In the remainder, dependency on time is omitted for brevity. Suppose x_h' resides in gain-mode. In that case, it holds that $\omega_h z^2 > k_h \dot{z} z$ (see the definition of the gain-mode set $\mathcal{F}_2$ in (2.3b)). Moreover, since $z \neq 0$ and $k_h z - x_h \neq 0$ (x_h cannot be on the sector-boundary otherwise it must be in gain-mode from the fact that $\omega_h z^2 > k_h \dot{z} z$), it follows that $(k_h z - x_h) z > 0$. Hence, $x_h - k_h z$ and $\omega_h z - k_h \dot{z}$ have opposite signs and are both non-zero, such that $\dot{V} < 0$. A similar reasoning applies for the case when x_h is in gain mode. At this point, it is known that $\dot{V} \leq 0$, which implies that i) HIGS in (2.1) is incrementally uniformly stable, and ii) solutions to HIGS are unique. However, this does not yet imply the attractivity property in (2.7). For showing (2.7), first note that there are three "trouble-making" situations in which $\dot{V} = 0$, and thus $V \neq 0$ can get stuck after some time $t \geq T$ with $T \geq 0$:

1. The dynamics governing x_h and x_h' both remain in integrator-mode for all $t \geq T$;
2. The dynamics governing x_h and x_h' both remain in gain-mode for all $t \geq T$;
3. The dynamics governing x_h and x_h' synchronously switch between integrator-mode and gain-mode for all $t \geq T$;

The last two situations can be easily ruled out. Namely, when both dynamics switch to gain-mode at some finite time instance $t^* \geq 0$, one finds $x_h(t^*) = x_h'(t^*) = k_h z(t^*)$. Since $\dot{V} \leq 0$ one finds $V(\delta x_h(t^*)) = 0$ and thus $x_h(t^*) = x_h'(t^*)$ for all $t \geq t^*$. Hence, this leaves the case that both dynamics get stuck in integrator-mode and remain therein forever. However, due to the assumption that z is bounded this cannot happen as will be shown next. First observe that in integrator-mode one has

$$x_h^2(t) - k_h^2 z^2(t) = \left(\int_{t_k}^{t} \omega_h z(\tau) d\tau + x_h(t_k) \right)^2 - k_h^2 z^2(t), \tag{2.47}$$

where $t_k \geq 0$ denotes the time from which solutions evolve according to the integrator-mode. A lower-bound for (2.47) is given by

$$\left(\int_{t_k}^{t} \omega_h z(\tau) d\tau + x_h(t_k) \right)^2 - k_h^2 z^2(t) \geq \left(\int_{t_k}^{t} \omega_h z(\tau) d\tau \right)^2 - k_h^2 z^2(t), \tag{2.48}$$

in which it is used that $x_h(t_k) \int_{t_k}^{t} z(\tau) d\tau \geq 0$ due to the sector-condition. Next, suppose that $z(t)$ has no zero-crossings in finite time. This is the relevant case to

consider, because a zero-crossing $z(t) = 0$ at $t = t^*$ implies $x_h(t^*) = x'_h(t^*) = 0$ due to the sector condition, and, in turn, this implies $V(\delta x_h(t^*)) = 0$. Since $\dot{V} \leq 0$ this implies $V(\delta x_h(t)) = 0$ for all $t \geq t^*$. In the absence of zero-crossings in z and thus $z(t) \neq 0$ for all $t \geq 0$, because of continuity and boundedness of z one finds $0 < c_1 \leq |z| \leq c_2$ such that

$$x_h^2(t) - k_h z^2(t) \geq \left(\int_{t_k}^{t} \omega_h z(\tau) d\tau \right)^2 - k_h^2 z^2(t) \geq (\omega_h c_1 (t - t_k))^2 - (k_h c_2)^2. \tag{2.49}$$

When $t - t_k > T(c_1, c_2) := (k_h c_2)/(\omega_h c_1)$, it follows that $x_h^2 - k_h z^2 > 0$, which violates the sector-condition in integrator-mode and thus a switch to gain-mode must have occurred at a time $t < t_k + T(c_1, c_2)$. As such, $T(c_1, c_2) < \infty$ provides a finite upper-bound on the time-interval in which trajectories can both reside in integrator-mode and thus $\dot{V} = 0$. It remains to be shown that V cannot converge to a non-zero constant. Hereto, the following claim is proven first.

Claim: In the absence of zero crossings, *i.e.*, $z(t) \neq 0$ for all time $t \geq 0$, there exists a time $\tau \leq T(c_1, c_2)$ such that $x_h(\tau) = x'_h(\tau)$.

Proof of the claim: First note that without zero crossings, z retains a similar sign for all $t \geq 0$. It is sufficient to consider the case $z > 0$ (the case $z < 0$ follows analogously). Without loss of generality, suppose $x_h(0) \geq x'_h(0)$, and assume that x'_h starts in integrator-mode (starting in gain-mode leads to a trivial situation). As shown before, x'_h must switch to gain-mode after some finite time $\tau \leq T(c_1, c_2)$. Suppose that $x_h(t) \geq x'_h(t)$ for all $t \leq \tau$. This is the relevant case to consider, because when $x_h(t) \leq x'_h(t)$ there must have been a time $\tau^* \leq \tau$ for which $x_h(\tau^*) = x'_h(\tau^*)$ (since initially $x_h(0) \geq x'_h(0)$). Since $z > 0$, it holds that $k_h z(t) \geq x_h(t)$ for all time $t \geq 0$. Then, at time $t = \tau$ one finds $k_h z(\tau) \geq x_h(\tau) \geq x'_h(\tau) = k_h z(\tau)$, which implies $x_h(\tau) = x'_h(\tau)$, thereby proving the claim.

Given the previous claim, it follows that at some time $\tau \leq T(c_1, c_2)$ one has $V(\delta x_h(\tau)) = 0$. In turn, since $\dot{V} \leq 0$, it follows that $V(\delta x_h(t)) = 0$ for all $t \geq \tau$. Thus, one finds $V(\delta x_h(t)) \leq V(\delta x_h(0))$ for $0 \leq t \leq \tau$, and $V(\delta x_h(t)) = 0$ for $t \geq \tau$. Based on this knowledge, one can construct the upper-bound

$$V(\delta x_h(t)) \leq e^{-(t - T^*)} V(\delta x_h(0)), \tag{2.50}$$

in which $T^* = \min\{T_0, T(c_1, c_2)\} \geq \tau$, and where T_0 denotes the time at which the first zero crossing of z occurs. In the absence of zero crossings, one finds $T_0 = \infty$. Based on the bound in (2.50), one finds $\|\delta x_h(t)\| \to 0$ for $t \to \infty$, thereby demonstrating the attractivity property. Combined with incremental stability (in the sense of Lyapunov) this implies incremental asymptotic stability.

Chapter 3

A Remedy for Performance Limitations in LTI Control?

3.1 Introduction

Fundamental limitations of linear time-invariant (LTI) feedback control design imposed by Bode's gain-phase relationship (Middleton, 1991; Seron et al., 1997; Skogestad and Postlethwaite, 2010) form an excellent motivation for the use of hybrid controllers in general (Feuer et al., 1997; Lau and Middleton, 2003), and hybrid integrator-gain systems (HIGS) in particular. As discussed in the previous chapter, the switching functionality of HIGS gives access to (weak) integrator characteristics with a phase lag of only 38.15 degrees as observed from its describing function. Although the concept of phase is generally defined for linear systems only, these apparent characteristics hint toward the possibility to break free from classical design trade-offs and thus may allow for increased bandwidths and enhanced closed-loop disturbance rejection on the one hand, and desired transient response and robust stability properties on the other hand.

Despite these potential benefits, the fundamental question if (and how) closed-loop LTI systems can truly benefit from feedback control with HIGS in particular in the sense of overcoming LTI performance limitations remains open. One of the objectives in this chapter is to provide a positive answer to this question. To this end, an LTI example is studied that suffers from inherent time-domain performance limitations. In particular, a third-order single-input single-output (SISO) LTI plant containing a real unstable open-loop pole, of which the presence inevitably leads to overshoot in the step-response for *any* stabilizing LTI feedback controller is considered. By exploiting HIGS in combination with specifically designed LTI filters, it is shown for the example that

overshoot in the step-response can be avoided altogether. The results are accompanied by key design considerations, which form important elements in a general design philosophy for control systems including HIGS elements. Systematic design of reset/hybrid controllers so that the performance limitations of LTI controllers can be overcome is acknowledged to be an open research problem, see Zhao et al., 2013.

Within the context of this chapter, it must be mentioned that other results are known in the literature that explicitly demonstrate the ability of nonlinear control strategies to meet certain transient time-domain performance specifications that are unattainable with LTI control. For instance, in Beker et al., 2001; Feuer et al., 1997; Zhao et al., 2019; Zhao et al., 2013, examples are given of hybrid and reset control strategies that can meet transient performance specifications in terms of overshoot and rise time, which cannot be achieved with any LTI controller. Also, in Hunnekens et al., 2016 it is shown by a numerical example that overshoot requirements unattainable by any LTI controller can be met using phase-based variable-gain control, see also Armstrong et al., 2006. Interestingly, these examples all employ a nonlinear element that produces discontinuous outputs, while the example with HIGS in this chapter uses continuous (non-smooth) signals. Other recent examples in which HIGS is shown to be able to overcome inherent performance limitations of LTI controllers can be found in Dinther et al., 2021.

This chapter is organized as follows. In Section 3.2, fundamental time-domain limitations of LTI systems linking the presence of real unstable, and simple open-loop poles to the occurrence of overshoot and performance trade-offs are revisited. The nonlinear control context is discussed in Section 3.3 and a numerical example that illustrates the ability of HIGS to overcome this limitation is presented in Section 3.4. Important design considerations and insights are provided in Section 3.5. The main conclusions of this chapter are summarized in Section 3.6.

3.2 Limitations of LTI control

The example in this chapter involves the class of SISO LTI feedback control systems, depicted in Figure 3.1. Here, an LTI plant given by the transfer function $P(s), s \in \mathbb{C}$, is placed in feedback interconnection with an LTI controller $C(s)$. The input to the plant consists of the control signal $u(t) \in \mathbb{R}$ and an input disturbance $d(t) \in \mathbb{R}$, both applied at time $t \geq 0$. The plant output $y(t) \in \mathbb{R}$ is subtracted from the setpoint $r(t) \in \mathbb{R}$ to form the feedback error $e := r - y$.

A third-order SISO LTI plant $P(s)$ that has a real open-loop pole at $s = p$ is considered. For $p > 0$, *i.e.*, in case of an open-loop unstable pole, when placing this plant in feedback interconnection with *any* internally stabilizing LTI controller $C(s)$, a fundamental time-domain limitation exists between the rise time

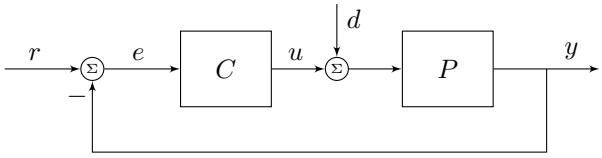

Figure 3.1. Closed-loop system configuration with SISO LTI plant $P(s)$ and SISO LTI feedback controller $C(s)$.

and the amount of overshoot of the closed-loop system's step-response when subject to a unit-step input $r(t) = 1$ for $t \geq 0$, and $r(t) = 0$ otherwise. For $p = 0$, *i.e.*, in case of a simple integrator, an inherent design trade-off exists between overshoot in the step-response and zero steady-state error in the presence of constant input disturbances. Before explicitly stating these limitations, necessary definitions for internal stability, rise time, overshoot, and steady-state error are introduced.

Definition 3.2.1 (Seron et al., 1997)**.** *Let the open-loop system in Figure 3.1 be given by $L(s) = P(s)C(s)$. The closed-loop system is said to be internally stable, if all poles of the transfer function $S(s) = (1 + L(s))^{-1}$ lie in the open left-half complex plane, and there are no unstable pole-zero cancellations in $L(s)$.*

Definition 3.2.2 (Seron et al., 1997)**.** *The rise time of a closed-loop system's step response y, when subject to a unit-step input $r(t) = 1$ for $t \geq 0$, and $r(t) = 0$ otherwise, and for zero initial conditions, is defined as*

$$t_r := \sup_{T>0} \left\{ T : y(t) \leq \frac{t}{T} \text{ for all } t \in [0, T] \right\}. \tag{3.1}$$

Definition 3.2.3 (Seron et al., 1997)**.** *The overshoot of a closed-loop system's step response y when subject to a unit-step input $r(t) = 1$ for $t \geq 0$, and $r(t) = 0$ otherwise, and for zero initial conditions is defined as*

$$y_{os} := \sup_{t \geq 0} \left(y(t) - r(t) \right), \tag{3.2}$$

that is, the maximum value by which the step response exceeds the final set-point value.

Definition 3.2.4 (Zhao et al., 2019)**.** *The steady-state error of the closed-loop system in Figure 3.1, when subject to a reference r and an input disturbance d, is defined as the difference between the reference r and the output y as $t \to \infty$, that is*

$$e_{ss} = \lim_{t \to \infty} (r(t) - y(t)). \tag{3.3}$$

Proposition 3.2.5 (Seron et al., 1997)**.** *Suppose that the plant $P(s)$ in Figure 3.1 has a real pole at $s = p$ with $p > 0$. If the closed-loop system is internally stabilized by any LTI controller $C(s)$, then the step response y resulting from a unit-step input $r(t) = 1$ for $t \geq 0$, and $r(t) = 0$ otherwise, exhibits overshoot, which satisfies the lower-bound*

$$y_{os} \geq \frac{(pt_r - 1)\exp(pt_r) + 1}{pt_r} \geq \frac{pt_r}{2}. \tag{3.4}$$

Proof. The proof can be found in Seron et al., 1997, Section 1.3. □

Proposition 3.2.6. *Suppose that the plant $P(s)$ in Figure 3.1 contains at least one pole at $s = p$ with $p = 0$. Then, for any stabilizing LTI controller $C(s)$ at least one of the following holds:*

- *The closed-loop system has non-zero steady-state error $|e_{ss}| > 0$ in the presence of a constant disturbance $d(t) = c$ for all values of $c \in \mathbb{R} \setminus \{0\}$.*
- *The closed-loop system has overshoot in its step response y resulting from a unit-step input $r(t) = 1$ for $t \geq 0$, and $r(t) = 0$ otherwise.*

Proof. By virtue of the internal model principle (Skogestad and Postlethwaite, 2010), zero steady-state error in the presence of a constant input disturbance requires the use of integral action in the controller. When using integral control, however, the open-loop system $C(s)P(s)$ has at least two poles at $s = 0$ such that, by virtue of Seron et al., 1997, Theorem 1.3.2, the closed-loop system necessarily has overshoot in its step-response. Hence, at least one of the conditions stated in the proposition must hold. □

Although both Proposition 3.2.5 and Proposition 3.2.6 address the presence of overshoot in the step-response when using LTI control, there is an essential difference. Namely, whereas *no* internally stabilizing LTI controller exists that leads to non-overshoot in case the plant has an unstable real open-loop pole, for plants containing multiple integrators, one can actually find LTI controllers that lead to no overshoot, but at the cost of not meeting other requirements such as zero steady-state error. Hence, while in the first case one has to accept overshoot, in the second case there is a possibility to balance objectives in a somewhat more desirable, but still limited, manner if one restricts oneself to LTI control. In this context, HIGS can offer more favourable results as will be shown in the upcoming parts.

3.3 Nonlinear control context

The nonlinear control configuration considered in the numerical examples that demonstrates the ability of HIGS-based control to overcome the limitations

stated in Proposition 3.2.5, and Proposition 3.2.6, is depicted in Figure 3.2.

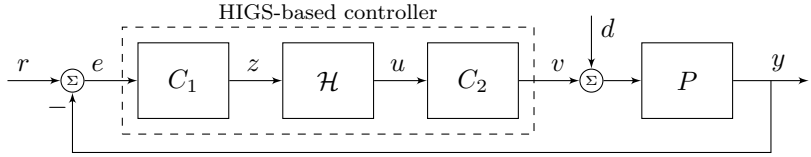

Figure 3.2. Closed-loop system configuration with SISO LTI plant $P(s)$ and HIGS-based controller as considered in the numerical examples.

In this figure, $P(s)$ is an LTI plant, $C_1(s), C_2(s)$ are LTI weighting filters, which are to be specified later, and $\mathcal{H}$ represents HIGS, which has been defined in Chapter 2, Section 2.2 and for convenience is repeated here as

$$\mathcal{H}: \begin{cases} \dot{x}_h(t) = \omega_h z(t), & \text{if } (z(t), u(t), \dot{z}(t)) \in \mathcal{F}_1, \quad (3.5a) \\ x_h(t) = k_h z(t), & \text{if } (z(t), u(t), \dot{z}(t)) \in \mathcal{F}_2, \quad (3.5b) \\ u(t) = x_h(t), & \quad (3.5c) \end{cases}$$

with state $x_h(t) \in \mathbb{R}$, input $z(t) \in \mathbb{R}$, time-derivative $\dot{z}$ (provided it exists), output $u(t) \in \mathbb{R}$ at all times $t \in \mathbb{R}_{\geq 0}$, and

$$\mathcal{F}_1 = \left\{(z, u, \dot{z}) \in \mathbb{R}^3 \mid k_h z u \geq u^2 \wedge (z, u, \dot{z}) \notin \mathcal{F}_2\right\}, \quad (3.6a)$$

$$\mathcal{F}_2 = \left\{(z, u, \dot{z}) \in \mathbb{R}^3 \mid u = k_h z \wedge \omega_h z^2 > k_h \dot{z} z\right\}. \quad (3.6b)$$

As discussed in the previous chapter, the feedback interconnection of HIGS in (3.5) with an LTI system admits the piecewise linear (PWL) state-space representation

$$\Sigma: \begin{cases} \dot{x}(t) = A_i x(t) + B_i w(t), & \text{if } (x(t), w(t)) \in \mathcal{X}_i, \quad i = \{1, 2\}, \\ y(t) = Cx(t) + Dw(t), \end{cases} \quad (3.7)$$

where $x(t) = [x_p^\top(t), x_{c_2}^\top(t), x_h(t), x_{c_1}^\top(t)]^\top \in \mathbb{R}^m$ collects the states $x_p(t)$ of the plant $P(s)$, the states $x_{c_1}(t), x_{c_2}(t)$ of the LTI filters $C_1(s)$, $C_2(s)$, and the state $x_h(t)$ of HIGS, respectively, $w(t) \in \mathbb{R}^w$ is the vector of exogenous input signals, and $y(t) \in \mathbb{R}$ is the relevant performance output at time $t \in \mathbb{R}_{\geq 0}$. Furthermore, the sets $\mathcal{X}_i$, $i = \{1, 2\}$, are given by

$$\mathcal{X}_i = \left\{(x, w) \in \mathbb{R}^{m+w} \mid Ex + Fw \in \mathcal{F}_i\right\}, \quad (3.8)$$

in which the matrices $E \in \mathbb{R}^{3\times m}$ and $F \in \mathbb{R}^{3\times w}$ satisfy $Ex + Fw = [z, u, \dot{z}]^\top$. An explicit derivation of the relevant system matrices in (3.7) and (3.8) can be found in Appendix 3.A. For further details on closed-loop system aspects regarding solution concepts and properties the reader is referred to Chapter 2.

Before presenting the example in more detail, closed-loop stability of the nonlinear system in Figure 3.2 is discussed. Although stability is not the main topic in this chapter, it is a prerequisite for performance, and forms an integral part in the limitations stated above. Therefore, it should be addressed here for making a fair comparison between linear and nonlinear control strategies. In this context, the notion of input-to-state stability (ISS) introduced in Chapter 2 in Definition 2.3.6 is adopted, as it links to the concept of internal stability given in Definition 3.2.1.

Theorem 3.3.1. *Consider the closed-loop system in* (3.7)*. Suppose there exist a symmetric $m \times m$ matrix $P \succ 0$ and a number $\mu \in \mathbb{R}$ that satisfy the matrix inequalities*

$$A_1^\top P + P A_1 \prec 0, \quad \text{and} \quad (A_2 + \mu b H)^\top P + P(A_2 + \mu b H) \prec 0 \tag{3.9}$$

with $b = [0, 1, 0]^\top$ and $H = [k_h, -1, 0]E$. Then, the closed-loop system (3.7) *is input-to-state stable in the sense of Definition 2.3.6.*

The proof of Theorem 3.3.1 largely proceeds along standard steps that can be found in published works on stability of switched and hybrid systems, see *e.g.*, Johansson, 2002; Kamenetskiy, 2017; Liberzon, 2003. Key in the proof is the use of Finsler's lemma (Boyd et al., 1994) for the second inequality in (3.9) via the gain-mode constraint $Hx = k_h z - u = 0$ for $w = 0$. Different (possibly less conservative) conditions for stability are extensively discussed in Chapters 4–5, and the result presented in Theorem 3.3.1 forms a special case of these more general results. Therefore, the proof is omitted here.

3.4 Plant with a real unstable pole

In this section, a numerical example is presented that illustrates the possibility to overcome the fundamental overshoot limitation in Proposition 3.2.5. Consider the LTI plant

$$P(s) = \frac{(s+q)\omega^2}{(s-p)(s^2 + 2\zeta\omega s + \omega^2)}, \tag{3.10}$$

which has a real unstable pole located at $s = p$, with $p = 1$, two stable poles at $s = -\omega(\zeta \pm \sqrt{\zeta^2 - 1})$, where $\omega = 5 \cdot 2\pi$ rad/s and $\zeta = 1.5$, and a zero at $s = -q$ with $q = 3$. Third-order characteristics with a real unstable pole such as in (3.10) may appear for instance in active magnetic bearings (Maslen et al., 2005; Thibeault and Smith, 2002). As a control objective, a feedback controller must be designed that i) *internally stabilizes* the closed-loop system, and ii) achieves a *zero steady-state tracking error* when the system is subject to a unit-step input r *without overshoot.*

3.4.1 LTI control

When considering an LTI controller $C(s)$, the requirement for internal stability of the closed-loop system removes the possibility for $C(s)$ to introduce an unstable pole-zero cancellation, whereas the objective of having zero steady-state tracking error necessitates integral action in the controller $C(s)$ by virtue of the internal model principle (see, *e.g.*, Skogestad and Postlethwaite, 2010). A controller $C(s)$ suitable for this purpose is designed on the basis of the Nyquist stability criterion (Franklin et al., 2005, Section 6.3), resulting in

$$C(s) = \frac{\omega_i}{s} \tag{3.11}$$

with integrator frequency $\omega_i = 10$ rad/s. Note that for achieving the given control objectives, other types of LTI controllers can be considered as well (although all would result in overshoot by virtue of Proposition 3.2.5). To keep the exposition simple and preserve insights in the effects of the controller on the transient response, the choice for an integrator in (3.11) is made.

According to Proposition 3.2.5, the closed-loop system with plant (3.10), and LTI controller (3.11) must exhibit overshoot in its step-response (with $d(t) = 0$), so that the objective regarding overshoot cannot be met. In this specific example, an aspect that additionally contributes to the presence of overshoot is the necessity for integral control. This can be understood as follows. Assuming zero initial conditions, the error initially satisfies $e(t) > 0$, such that the integrator in (3.11) 'sums' the error over time to provide a positive input $u(t) > 0$ for driving the system toward the setpoint. For achieving zero steady-state error, it follows from the final value theorem (Middleton, 1991) that

$$\lim_{t\to\infty} u(t) = \lim_{s\to 0} \frac{sC(s)}{1 + C(s)P(s)} \cdot \frac{1}{s} = -\frac{p}{q} < 0. \tag{3.12}$$

Hence, a negative steady-state input is needed for achieving zero steady-state error. This implies a sign change of u, which can only be achieved if e changes sign, thus requiring overshoot. In case $P(s)$ only has stable poles, and thus $p < 0$, the steady-state input should be positive, and overshoot does not necessarily occur.

3.4.2 HIGS-based control

Given the previous observations, a HIGS-based integrator is proposed that adopts the functionality of a linear integrator for achieving zero steady-state error, but aims at reducing/eliminating overshoot. Hereto, HIGS in (3.5) is appended with LTI filters $C_1(s)$ and $C_2(s)$ in a manner as depicted in Figure 3.2. The filters are specifically chosen as

$$C_1(s) = \left(\frac{s}{\omega_c} + 1\right), \quad \text{and} \quad C_2(s) = \frac{\omega_i}{s} \tag{3.13}$$

with $\omega_c = |1 + 4j/\pi|\frac{\omega_h}{k_h}$ rad/s. This particular choice is motivated by using describing function reasoning. The describing function of HIGS, which has been derived in Chapter 2, and which is repeated here as

$$\mathcal{D}(j\omega) = \frac{\omega_h}{j\omega}\left(\frac{\gamma}{\pi} + j\frac{e^{-2j\gamma} - 4e^{-j\gamma} + 3}{2\pi}\right) + k_h\left(\frac{\pi - \gamma}{\pi} + j\frac{e^{-2j\gamma} - 1}{2\pi}\right) \quad (3.14)$$

with $\gamma(\omega) = 2\arctan(k_h\omega/\omega_h)$, implies first-order low-pass magnitude characteristics with cross-over frequency $\omega_c = |1 + 4j/\pi|\frac{\omega_h}{k_h}$ rad/s, accompanied by a phase lag that does not exceed 38.15 degrees. The filter $C_1(s)$ 'compensates' the magnitude characteristics of $\mathcal{D}(j\omega)$, and provides additional phase lead up to 90 degrees. As a result, for all $\omega \in (0, \infty)$ it follows that $\|C_1(j\omega)\mathcal{D}(j\omega)\| \approx 1$, and $\angle(C_1(j\omega)\mathcal{D}(j\omega)) \in (0, 51.85)$ degrees. The describing function characteristics of the HIGS-based integrator, which also includes $C_2(s) = \omega_i/s$, is given by

$$\mathcal{C}_i(j\omega) = C_1(j\omega)\mathcal{D}(j\omega)C_2(j\omega), \quad (3.15)$$

and demonstrates the characteristic 20 dB/decade magnitude decay similar to the linear integrator in (3.11), but with a phase lag that can be reduced up to 38.15 degrees as shown in Figure 3.3, *i.e.*, $\angle(\mathcal{C}_i(j\omega)) \in (-90, -38.15)$ degrees. A useful feature of this design is that the parameter ω_h (with $k_h = 1$) can be used to vary the phase lag reduction independent from the magnitude, which provides extra freedom in dealing with inherent design limitations. The apparent phase advantage hints toward the possibility for reducing overshoot. Comparable strategies that combine LTI filters with nonlinear elements such as reset integrators (Clegg, 1958) or split-path filters (Sharif et al., 2021b; van Loon et al., 2016) for creating new elements with favourable gain and phase properties can be found in the literature, see for instance Karybakas, 1977; Li et al., 2011; Palanikumar et al., 2018; Zheng et al., 2000.

Remark 3.4.1. *For a practical implementation of the non-proper filter $C_1(s)$ in* (3.13)*, the following adaptations can be made:*

$$C_1(s) = \left(\frac{s}{\omega_c} + 1\right) \cdot \frac{1}{(\tau s + 1)}, \quad \text{and} \quad C_2(s) = \frac{\omega_i}{s} \cdot (\tau s + 1),$$

where $\tau > 0$ is chosen sufficiently small. Both $C_1(s)$ and $C_2(s)$ are proper filters. Note that the describing function characteristics in (3.15) *remain unchanged by these transformations.*

Remark 3.4.2. *It is interesting to mention that for $\omega_h \to 0$ the describing function characteristics of the HIGS-based integrator as depicted in Figure 3.3 are equivalent to that of the Clegg integrator (Clegg, 1958; Horowitz and Rosenbaum, 1975). However, there is an essential difference between the HIGS-based integrator and the Clegg integrator. Namely, due to the additional state in $C_2(s)$, the*

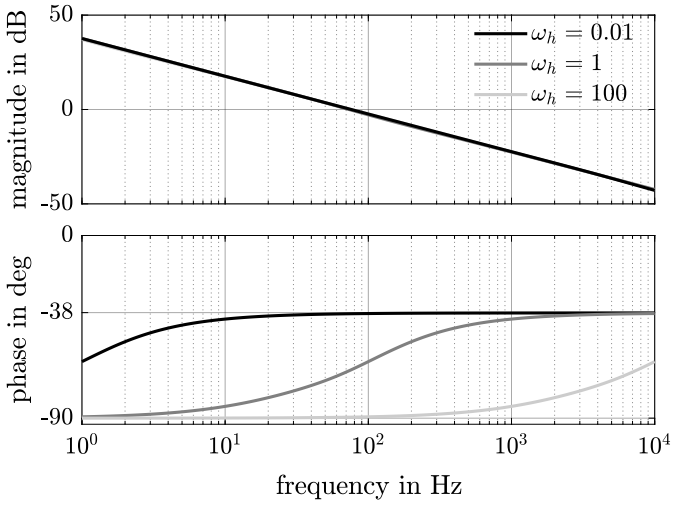

Figure 3.3. Bode-like representation of a HIGS-based integrator (3.15) for different values of HIGS' integrator frequency ω_h (with $k_h = 1$).

HIGS-based integrator is able to preserve a buffer when $e(t) = 0$ to compensate for constant disturbances. The Clegg integrator, however, is not able to preserve such buffer since due to the resetting mechanism the output of the integrator is reset to zero as soon as $e(t) = 0$, such that a constant disturbance is no longer compensated for by the integrator, see also Zhao et al., 2019, Remark 8.

3.4.3 Simulation results

The step-response of the plant (3.10) in feedback with the HIGS-based controller, the latter being the series interconnection of the filters $C_1(s)$, and $C_2(s)$ with $\tau = 10^{-4}$ conform Remark 3.4.1, and HIGS with $k_h = 1$, $\omega_h = 0.8$ rad/s, is shown in Figure 3.4 (in black), along with the generated control output u. In addition, the step-response and control output with the linear controller (3.11) are shown in grey. Overshoot is clearly present for the linear closed-loop system, whereas for the HIGS-based control system there is no overshoot under fairly limited control effort. Note that in both cases the output of the controller attains the steady-state value $u(\infty) = -p/q = -1/3$ that appears necessary for achieving zero steady-state tracking error. It is emphasized that for the linear control system, the overshoot in Figure 3.4 may be influenced by a different choice of LTI filters, *e.g.*, PID-filters, but overshoot cannot be avoided as a consequence of the fundamental limitation stated in Proposition 3.2.5. Moreover, given the rise time $t_r = 0.95$ seconds of the HIGS-controlled system, any linear

controller resulting in a similar (or larger) rise time yields an overshoot of at least $y_{os} = \frac{pt_r}{2} = 0.475$ according to the lower-bound in (3.4). These results highlight the distinct advantage of the HIGS-based controller over any LTI controller in achieving performance without overshoot.

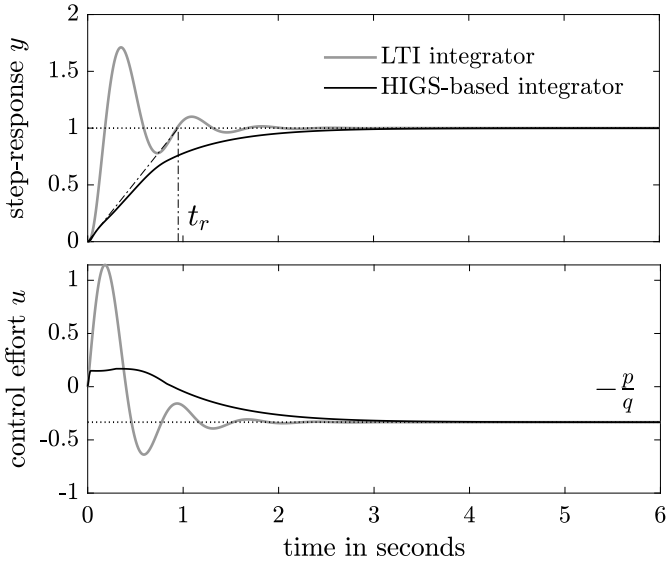

Figure 3.4. Step-response y (top) and control output u (bottom) of the linear (grey) and non-linear (black) closed-loop system.

Before arriving at the final conclusion that for the example discussed, the fundamental limitation in Proposition 3.2.5 is truly overcome with HIGS, it remains to be shown formally that the corresponding closed-loop system is ISS. Hereto, the matrix conditions in Theorem 3.3.1 are solved numerically for which the result is given in Appendix 3.A. Given feasibility of the matrix inequalities in (3.9), together with the time-series simulation result in Figure 3.4, it is concluded that the fundamental limitation presented in Proposition 3.2.5 is truly overcome with the proposed HIGS-based control strategy for the example discussed.

3.4.4 Robust non-overshoot performance

In order to study robust non-overshoot performance properties of the presented approach in the presence of plant uncertainties, the location of the pole p in (3.10) is varied in the range $p \in [-5, 10]$. The amount of overshoot as a function of the pole location is shown in Figure 3.5. Because the plant is different, the amount of overshoot, rise-time, and fundamental lower-bound are different. However, for a range of unstable open-loop poles, the qualitative closed-loop system behaviour

appears the same, in the sense that overshoot is avoided, thereby indicating a certain amount of robustness to plant uncertainties. Stability of the closed-loop system with HIGS has been formally verified by means of the matrix conditions in Theorem 3.3.1 for all $p \in [-5, 1.8]$. However, a stable step-response is observed in simulations up to $p = 7.8$. Note that for the LTI case, internal stability is guaranteed for all $p \leq 4.5$. These observations hint toward improved robust stability properties with HIGS-based control. One could argue that increased robustness is enabled by the alleged reduction in phase lag by the HIGS-based integrator, as opposed to its linear counterpart (see Figure 3.3 in this regard).

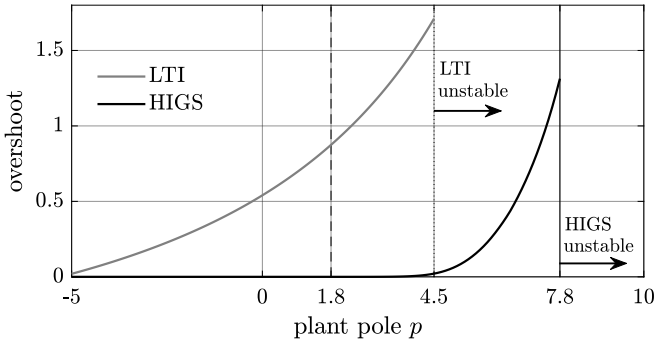

Figure 3.5. Overshoot as a function of the open-loop pole p for the closed-loop system with an LTI integrator (grey) and a HIGS-based integrator (black).

From Figure 3.5 zero overshoot is obtained also for $s = p$ with $p = 0$. In case of LTI integral control, the open-loop contains two integrators which inherently leads to overshoot. When using no integrator in the controller, overshoot can be avoided (for instance with $C(s) = 1$) but at the cost of non-zero steady-state error in the presence of non-zero constant input disturbances. This is stated formally in Proposition 3.2.6. With the considered HIGS-based integrator, however, both constant disturbance rejection as well as non-overshoot in the step-response are achieved. This demonstrates that the fundamental trade-off in Proposition 3.2.6 is overcome for this example, and indicates the additional design flexibility that is offered with HIGS-based control.

3.5 Design considerations and non-overshoot

3.5.1 Controller configuration

The nonlinear control strategy applied to the previous example is initially based on HIGS' describing function characteristics. From a quasi-linear perspective, the particular sequence in which the filters in the HIGS-based controller appear,

is interchangeable. However, from a time-domain perspective this is not the case as switching of HIGS is directly determined by its input z, and, therefore, by the choice for the filter $C_1(s)$ in Figure 3.2. The effect of filter sequence on time-domain performance has also been pointed out in Cai et al., 2020. The rationale behind the proposed configuration in Figure 3.2 for reducing overshoot and alleviating performance trade-offs can be explained as follows.

- By using the output of HIGS directly as an input to the filter $C_2(s)$ which contains the integrator buffer in the HIGS-based controller, a control mode-switching mechanism is provided for filling/depleting this buffer at a variable rate, hence, $C_2(s)$ containing the integrator is located directly after HIGS. Despite the integrator-mode, HIGS itself cannot maintain a buffer necessary for achieving zero steady-state error due to its sector-boundedness, underlining the necessity for including a pure integrator in the designs.

- Due to the previous choice, the output of HIGS should have zero crossings for allowing a sign change of the linear integrator's output; recall the earlier discussions regarding LTI control designs. Sign equivalence of HIGS input and output signals then necessitates the input of HIGS to have zero crossings. For achieving non-overshoot performance, by definition, a sign-change of e must be avoided. Hence, e cannot be used directly as an input to HIGS. Rather, $C_1(s)$ as in (3.13) is used for realizing a filtered version of e, *i.e.*, $z = \frac{\dot{e}}{\omega_c} + e$. The weighted combination of e and $\dot{e}$ creates the possibility for z to have zero crossings without e crossing zero, *i.e.*, without inducing overshoot.

3.5.2 Non-overshoot mechanism

From the previous rationale, in particular the second point, it is clear that the parameter ω_h largely determines whether switching primarily occurs on the basis of the error e or its time-derivative $\dot{e}$, and thus directly influences the interplay between HIGS and the integrator buffer contained in the filter $C_2(s)$. To illustrate the effect of ω_h on such interplay, consider again the example presented in Section 3.4 with $p = 1$. Figure 3.6 depicts the time-response of the HIGS state x_h, and the state x_i of the linear integrator in $C_2(s)$ when subject to a step-input for the values $\omega_h = \{0.08, 0.8, 80\}$ rad/s.

The choice $\omega_h = 80$ rad/s (bottom figure) leads to overshoot. This can be explained from the fact that for $\omega_h \to \infty$ the path composed of $C_1(s)$ and HIGS (see Figure 3.2) effectively reduces to a linear gain. The characteristics of the nonlinear controller tend to that of its linear counterpart, *i.e.*, inherently having overshoot. Hence, choosing ω_h too large results in overshoot. On the other hand, both the choices $\omega_h = 0.08$ rad/s (top figure) and $\omega_h = 0.8$ rad/s (middle figure) result in the absence of overshoot. To understand the underlying

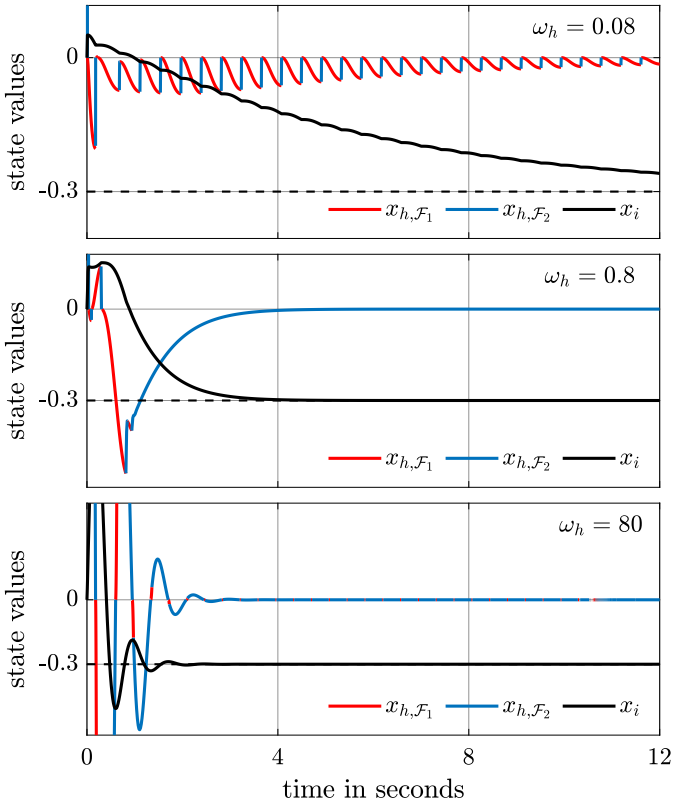

Figure 3.6. HIGS-state $x_h(t)$ (red: integrator-mode, blue: gain-mode) and integrator state $x_i(t) = \int_0^t x_h(\tau)d\tau$ as a function of time for $\omega_h = 0.08$ rad/s (top figure), $\omega_h = 0.8$ rad/s (middle figure), and $\omega_h = 80$ rad/s (bottom figure). The final value of the integrator state for attaining zero steady-state error is indicated by the dashed black line and corresponds to $-p/q = -1/3$.

mechanism leading to non-overshoot, first note that according to the discussion in Chapter 2, for $\omega_h \to 0$ the characteristics of HIGS tend to that of the Clegg integrator, leading to an arbitrarily fast reduction to zero of the HIGS state x_h whenever z crosses zero. When considering a step-response, one initially finds $e(0) > 0$ and $\dot{e}(0) = 0$, such that $z(0) > 0$. In that case, the linear integrator placed behind HIGS starts building up a positive buffer and pushes the system in the direction toward zero error. However, as e is decreasing, at some point the magnitude of $e > 0$ is relatively small compared to the (weighted) magnitude of $\dot{e} < 0$, which results in a sign-change of z. Physically, this means that, relative to the distance toward the set-point, the system is moving fast in the direction of

this set-point. To avoid overshoot, the system must rapidly 'slow down'. This is achieved through HIGS by enforcing Clegg-like switching that either limits the linear integrator buffer build-up or starts depleting it. Such characteristics are particularly visible for $\omega_h = 0.08$ rad/s in Figure 3.6 (top). Note, however, that with ω_h small, even a small change in $\dot{e}$ may already induce a sign change in z. Consequently, the Clegg-like mechanism is triggered in a high-frequent manner, which impedes the integrator build-up and can lead to an extremely slow step-response. This is also observed in Figure 3.6 (top) as the integrator state x_i slowly converges to its steady-state value. When choosing $\omega_h = 0.8$ rad/s, non-overshoot is still achieved, but the integrator attains its steady-state value at a much faster rate as can be seen in Figure 3.6 (middle). In turn, this results in a faster step-response. For an additional discussion on the non-overshoot mechanism see also Dinther et al., 2021; van den Eijnden et al., 2020a.

From the above observations, the parameter ω_h appears as a tuning knob for adjusting the overshoot and settling time. As such, a simple tuning guideline for a HIGS-based integrator design can be derived. One may start with $\omega_h = \infty$, and tune all remaining parameters (ω_i in the example) by means of linear design techniques, *e.g.*, via loop-shaping. Subsequently, one can adjust ω_h to balance the level of overshoot and settling time according to specifications. Note, however, that during such a design process stability of the feedback system needs to be guaranteed. Stability aspects are discussed in more detail in the upcoming chapters.

3.6 Summary

In this chapter, an example is discussed in which HIGS-based control is able to overcome fundamental performance limitations inherent to LTI systems. The example addresses an overshoot performance limitation resulting from the presence of a real unstable or simple open-loop pole in the plant. By interconnecting HIGS in series with well-crafted linear filters, overshoot is avoided, and the limitations are alleviated. Key in the approach is the sequence in which the linear filters appear with respect to HIGS. The obtained insights provide valuable elements for a general control design framework based on HIGS.

Although briefly discussed in this chapter, guaranteeing stability of the closed-loop system remains an issue to be dealt with, particularly in terms of providing easy-to-check and non-conservative conditions. To address this issue, in the next chapter frequency-domain conditions for stability of HIGS-based control systems are presented. Not only are these conditions less conservative than the ones proposed in this chapter, they also provide direction for control design.

3.A Additional details and numerical results

In this appendix, some additional details and numerical results for the example presented in this chapter are discussed. This includes the explicit derivation of the relevant closed-loop system matrices, and numerical solutions to the matrix conditions in Theorem 3.3.1.

3.A.1 State-space derivation

Consider the feedback control system with HIGS as depicted in Figure 3.2 and recall that the closed-loop system dynamics can be written as a switched linear system of the form

$$\Sigma : \begin{cases} \dot{x}(t) = A_i x(t) + B_i w(t), & \text{if } (x(t), w(t)) \in \mathcal{X}_i, \quad i = \{1, 2\}, \\ y(t) = Cx(t) + Dw(t), \end{cases} \tag{3.16}$$

with state vector $x(r) = [x_p^\top(t), x_{c_2}^\top(t), x_h(t), x_{c_1}^\top(t)]^\top$, where $x_p(t) \in \mathbb{R}^p$ denotes the states of the plant $P(s)$, $x_{c_1}(t) \in \mathbb{R}^m$ and $x_{c_2}(t) \in \mathbb{R}^n$ denote the state of the LTI filters $C_1(s)$ and $C_2(s)$, respectively, and $x_h(t) \in \mathbb{R}$ denotes the state of HIGS. The exogenous inputs are denoted by $w(t) \in \mathbb{R}^w$, and $y(t) \in \mathbb{R}$ is the relevant performance output. For the considered set-up, the closed-loop system matrices A_1 and A_2 are given by

$$A_1 = \begin{bmatrix} A_p & B_p C_{c_2} & B_p D_{c_2} & 0 \\ 0 & A_{c_2} & B_{c_2} & 0 \\ -\omega_h D_{c_1} C_p & 0 & 0 & \omega_h C_{c_1} \\ -B_{c_1} C_p & 0 & 0 & A_{c1} \end{bmatrix}, \tag{3.17a}$$

$$A_2 = \begin{bmatrix} A_p & B_p C_{c_2} & B_p D_{c_2} & 0 \\ 0 & A_{c_2} & B_{c_2} & 0 \\ -k_h(C_{c_1} B_{c_1} C_p + D_{c_1} C_p A_p) & 0 & 0 & k_h C_{c_1} A_{c_1} \\ -B_{c_1} C_p & 0 & 0 & A_{c1} \end{bmatrix}, \tag{3.17b}$$

in which the matrices (A_p, B_p, C_p, D_p) describe the plant $P(s)$, *i.e.*,

$$P(s) = C_p(sI - A_p)^{-1} B_p + D_p,$$

and the matrices $(A_{c_1}, B_{c_1}, C_{c_1}, D_{c_1})$, and $(A_{c_2}, B_{c_2}, C_{c_2}, D_{c_2})$ describe the filters $C_1(s)$ and $C_2(s)$, respectively, such that

$$C_1(s) = C_{c_1}(sI - A_{c_1})^{-1} B_{c_1} + D_{c_1},$$
$$C_2(s) = C_{c_2}(sI - A_{c_2})^{-1} B_{c_2} + D_{c_2}.$$

For the considered configuration, the relevant input vector is given by $w = [r, \dot{r}, d]^\top \in \mathbb{R}^3$, and the performance channel y is defined as the output of the

plant, such that the input matrices B_1, B_2 are given by

$$B_1 = \begin{bmatrix} 0 & 0 & \omega_h D_{c_1} & B_{c_1} \\ 0 & 0 & 0 & 0 \\ B_p & 0 & 0 & 0 \end{bmatrix}^\top, \quad B_2 = \begin{bmatrix} 0 & 0 & k_h C_{c_1} B_{c_1} & B_{c_1} \\ 0 & 0 & k_h D_{c_1} & 0 \\ B_p & 0 & 0 & 0 \end{bmatrix}^\top, \tag{3.18}$$

and with output matrices $C = \begin{bmatrix} C_p & 0 & 0 & 0 \end{bmatrix}$, and $D = \begin{bmatrix} 0 & 0 & B_p \end{bmatrix}$. Finally, the matrices E and F in the sets $\mathcal{X}_i$, $i = \{1, 2\}$ defined in (3.8) are given by

$$E = \begin{bmatrix} -D_{c_1} C_p & 0 & 0 & C_{c_1} \\ 0 & 0 & 1 & 0 \\ -C_{c_1} B_{c_1} C_p - D_{c_1} C_p A_p & -D_{c_1} C_p B_p & 0 & C_{c_1} A_{c_1} \end{bmatrix}, \tag{3.19a}$$

$$F = \begin{bmatrix} D_{c_1} & 0 & 0 \\ 0 & 0 & 0 \\ C_{c_1} B_{c_1} & D_{c_1} & 0 \end{bmatrix}. \tag{3.19b}$$

3.A.2 Numerical solutions to the matrix inequalities

Recall the example of Section 3.4 with LTI plant (3.10) and LTI filters (3.13). The respective matrices are given by

$$\left[\begin{array}{c|c} A_p & B_p \\ \hline C_p & D_p \end{array}\right] = \left[\begin{array}{ccc|c} 0 & 1 & 0 & 0 \\ 0 & 0 & 1 & 0 \\ p\omega^2 & \omega(2p\zeta - \omega) & p - 2\zeta\omega & \omega^2 \\ \hline q & 1 & 0 & 0 \end{array}\right],$$

$$\left[\begin{array}{c|c} A_{c_1} & B_{c_1} \\ \hline C_{c_1} & D_{c_1} \end{array}\right] = \left[\begin{array}{c|c} -\frac{1}{\tau} & \frac{1}{\tau} \\ \hline 1 - \frac{1}{\tau\omega_c} & \frac{1}{\tau\omega_c} \end{array}\right], \quad \text{and} \quad \left[\begin{array}{c|c} A_{c_2} & B_{c_2} \\ \hline C_{c_2} & D_{c_2} \end{array}\right] = \left[\begin{array}{c|c} 0 & \omega_i \\ \hline 1 & \omega_i \tau \end{array}\right],$$

with parameters $\omega = 5 \cdot 2\pi$ rad/s, $\zeta = 1.5$, $p = 1$, $q = 3$, $\omega_i = 10$ rad/s, $k_h = 1$, $\omega_h = 0.8$ rad/s, $\omega_c = 1.29$ rad/s, and $\tau = 10^{-4}$. Using the matrices A_1 and A_2 in (3.17), the matrix inequalities in (3.9) are iteratively solved by means of the Matlab toolbox `Yalmip` (Löfberg, 2004) together with the external solver `MOSEK` (Andersen et al., 2003). The resulting matrix P is found to be

$$P = \begin{bmatrix} 5268896.19 & 1756629.55 & -1384.5403 & -4474.1597 & 61.1298 & 1757783.13 \\ 1756629.55 & 585690.381 & -459.0564 & -1521.3239 & 20.6351 & 586047.961 \\ -1384.5403 & -459.0564 & 0.5415 & -0.87052 & 0.00006012 & -461.2236 \\ -4474.1597 & -1521.3239 & -0.87052 & 27.6577 & -0.2525 & -1500.5993 \\ 61.1298 & 20.6351 & 0.00006012 & -0.2525 & 0.005326 & 20.4599 \\ 1757783.13 & 586047.961 & -461.2236 & -1500.5993 & 20.4599 & 586425.592 \end{bmatrix},$$

with corresponding eigenvalues

$$\lambda(P) = \begin{bmatrix} 6440982.17 & 58.1617 & 0.01999 & 0.009841 & 0.003120 & 0.0007173 \end{bmatrix}$$

showing P to be positive definite, and $\mu = 1.5$.

Part II

Stability and Performance

Chapter 4

Frequency-Domain Tools for Robust Stability Analysis

4.1 Introduction

The potential of hybrid integrator gain-systems (HIGS) for overcoming fundamental performance limitations of linear time-invariant (LTI) control systems has been shown in the previous chapter. Unfortunately, performance enhancing benefits often do not come without a cost. While linear systems lend themselves well for robust stability and performance analysis using frequency-domain tools such as the Nyquist stability criterion and Bode plots (Skogestad and Postlethwaite, 2010), the nonlinear/hybrid nature of a control system featuring HIGS renders many of such tools inapplicable. As the current control practice highly exploits frequency-domain methods, lack of appropriate tooling may compromise broad adoption of nonlinear and hybrid control strategies like HIGS in industry.

To accommodate for this situation, frequency-domain tools for stability analysis and design of switched/hybrid systems in general have been recently proposed in, *e.g.*, Arcak et al., 2003; Beker et al., 2004; Dastjerdi et al., 2020; Deenen et al., 2017; Griggs et al., 2010; Kamenetskiy, 2017; Kamenetskiy, 2019; King et al., 2011; Kunze et al., 2008; Shorten et al., 2009; Van Loon et al., 2017. Underlying these tools is the well-known Kalman-Yakubovich-Popov lemma (Khalil, 2002; Yakubovich, 1962), which allows for establishing the equivalence between certain frequency-domain conditions and the existence of a common quadratic Lyapunov function for switched systems, the latter being posed in the time-domain. In principle, these frequency-domain conditions can be verified using *measured* frequency-response function data of the plant to be controlled, thereby making them useful in practical situations, where accurate parametric models

of the plant are often difficult, if not impossible, to obtain.

Although valuable from a practical perspective, existing frequency-domain conditions that are applicable to the class of HIGS-based control systems, such as the ones presented in, *e.g.*, Deenen et al., 2021; Kamenetskiy, 2017; King et al., 2011; Kunze et al., 2008; Van Loon et al., 2017 often render a rather conservative estimate on closed-loop stability. To some extent, this conservatism is caused by the fact that the conditions do not sufficiently take into account the particular switching characteristics of HIGS, thereby leading to overly restrictive formulations. For example, the results in Kamenetskiy, 2017; Kunze et al., 2008, are limited to systems with arbitrary switching, which is too restrictive for HIGS as it adopts a specific state-dependent switching strategy. In King et al., 2011, this result is extended by including state-dependent constraints, leading to improved conditions. Such constraints are also considered in Deenen et al., 2021; Van Loon et al., 2017, but at the same time HIGS is regarded as a generic sector-bounded nonlinearity, thereby ignoring its underlying internal dynamic behaviour. It is interesting to remark that in all mentioned works, the quadratic Lyapunov function that results from satisfying the conditions is guaranteed to be positive within the full state-space. This may be restrictive too because trajectories of a closed-loop system with HIGS are confined to a subset of the state-space only.

The main contribution in this chapter is the presentation of a novel frequency-domain condition for stability analysis of the feedback interconnection of an LTI system and HIGS. The conditions are novel in the sense that, if satisfied, these guarantee the existence of a quadratic Lyapunov function that is not necessarily positive within the full state-space, but rather in a subset of the state-space where HIGS is active. The same holds true for negative definiteness of its corresponding time-derivative. In this way, the class of admissible Lyapunov function candidates is extended and the conservatism in the analysis is generally reduced compared to existing methods. Frequency-domain conditions for guaranteeing the existence of such class of Lyapunov functions have not been established in the literature before. It is shown that the conditions can be verified graphically in a manner that is comparable with the classical Popov plot (Khalil, 2002). The results are further extended toward robust stability analysis. In particular, the presented frequency-domain conditions are reformulated in a manner that takes into account multiplicative uncertainties in the LTI part of the feedback control system. The approach is inspired by the results in Impram and Munro, 2001; Tsypkin and Polyak, 1992, which present robustified versions of classical circle- and Popov criteria that allow for a graphical verification of robust stability, something which is well appreciated in an industrial setting where plant uncertainty is highly relevant.

This chapter is organized as follows. In Section 4.2 the control system setting is discussed, and the problem formulation is given. In Section 4.3, the main results of this chapter are presented in the form of a theorem that sets forth

graphically verifiable frequency-domain stability conditions. The conditions are compared to existing results in a numerical example. An extension toward a robust stability analysis is discussed in Section 4.4. Application of the presented results is demonstrated on an experimental motion control set-up in Section 4.5. A summary of this chapter is provided in Section 4.6.

4.1.1 Notation

Throughout this chapter, use is made of the following notation. A single-input single-output (SISO) transfer function is said to be stable if all its poles are located in the open left-half complex plane. The space of proper and real rational stable SISO transfer functions is denoted by $\mathcal{RH}_\infty$. The real and imaginary parts of a frequency response function $W(j\omega) \in \mathbb{C}$, $\omega \in \mathbb{R}$, are denoted by $\mathrm{Re}\{W(j\omega)\}$ and $\mathrm{Im}\{W(j\omega)\}$, respectively, and the complex conjugate is indicated by $W^*(j\omega) = W(-j\omega)$. The set of real symmetric matrices in $\mathbb{R}^{n\times n}$ is denoted by $\mathbb{S}^{n\times n}$. A symmetric matrix $M \in \mathbb{S}^{n\times n}$ is positive (negative) definite, denoted by $M \succ 0$ ($M \prec 0$), if $x^\top Mx > 0$ ($x^\top Mx < 0$) for all $x \in \mathbb{R}^n \setminus \{0\}$. The inequality symbols $>, \geq, <, \leq$ for vectors are understood componentwise.

4.2 System setting and problem formulation

4.2.1 Closed-loop system description

In this section, the generic closed-loop system setting with HIGS as discussed in detail in Chapter 2 is briefly repeated here for convenience. Hereto, the single-input single-output (SISO) configuration as depicted in Figure 4.1 is considered.

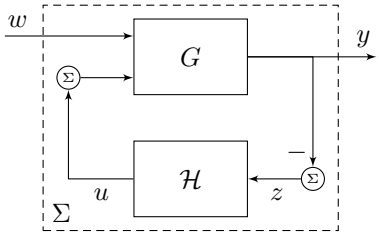

Figure 4.1. Feedback interconnection of an LTI system G and HIGS $\mathcal{H}$.

In this figure, the LTI system G is given by

$$G : \begin{cases} \dot{x}_g(t) &= A_g x_g(t) + B_g u(t) + B_w w(t), \\ y(t) &= C_g x_g(t), \end{cases} \tag{4.1}$$

with states $x_g(t) \in \mathbb{R}^m$, exogenous input $w(t) \in PB$ belonging to the class of piecewise Bohl functions (conform Chapter 2), controlled output $y(t) \in \mathbb{R}$, and

control input $u(t) \in \mathbb{R}$ at time $t \in \mathbb{R}_{\geq 0}$. It is assumed that (A_g, B_g, C_g) is minimal and the transfer functions from u to y and w to y are denoted by

$$G_{yu}(s) = C_g(sI - A_g)^{-1}B_g, \tag{4.2a}$$
$$G_{yw}(s) = C_g(sI - A_g)^{-1}B_w. \tag{4.2b}$$

Conform Assumption 2.3.1 the transfer functions in (4.2) have a relative degree of at least two, which implies that $C_gB_g = C_gB_w = 0$.

A hybrid integrator-gain system $\mathcal{H}$ in Figure 4.1 is described by a piecewise linear (PWL) system with discontinuous right-hand side

$$\mathcal{H} : \begin{cases} \dot{x}_h(t) &= \omega_h z(t), \quad \text{if } (z(t), u(t), \dot{z}(t)) \in \mathcal{F}_1, \\ x_h(t) &= k_h z(t), \quad \text{if } (z(t), u(t), \dot{z}(t)) \in \mathcal{F}_2, \\ u(t) &= x_h(t), \end{cases} \tag{4.3}$$

where $x_h(t) \in \mathbb{R}$ denotes the state of the integrator, $z(t) = -y(t) \in \mathbb{R}$ is the input to HIGS, which in the context of Figure 4.1 (recall Chapter 2) is differentiable, $\dot{z}(t) = -\dot{y}(t)$ denotes the corresponding time-derivative, and $u(t) \in \mathbb{R}$ is the generated output at time $t \in \mathbb{R}_{\geq 0}$. The sets $\mathcal{F}_1$ and $\mathcal{F}_2$ dictating, respectively, the integrator-mode and gain-mode in (4.3) are given by

$$\mathcal{F}_1 = \left\{(z, u, \dot{z}) \in \mathbb{R}^3 \mid k_h z u \geq u^2 \wedge (z, u, \dot{z}) \notin \mathcal{F}_2\right\}, \tag{4.4a}$$
$$\mathcal{F}_2 = \left\{(z, u, \dot{z}) \in \mathbb{R}^3 \mid u = k_h z \wedge \omega_h z^2 > k_h \dot{z} z\right\}, \tag{4.4b}$$

for which the union is given by the "$[0, k_h]$-sector", defined as

$$\mathcal{F} = \mathcal{F}_1 \cup \mathcal{F}_2 = \left\{(z, u, \dot{z}) \in \mathbb{R}^3 \mid k_h z u \geq u^2\right\}. \tag{4.5}$$

The closed-loop system in Figure 4.1 with G as in (4.1), and $\mathcal{H}$ as in (4.3), (4.4) can be written as the PWL system

$$\Sigma : \begin{cases} \dot{x}(t) &= A_i x(t) + Bw(t), \quad \text{if } x(t) \in \mathcal{X}_i,\ i \in \{1, 2\}, \\ y(t) &= Cx(t), \end{cases} \tag{4.6}$$

with augmented state vector $x(t) = [x_g(t)^\top, x_h(t)]^\top \in \mathbb{R}^n$, where $n = m + 1$. The sets $\mathcal{X}_i$, $i \in \{1, 2\}$, in (4.6) are given by

$$\mathcal{X}_i = \{x \in \mathbb{R}^n \mid Ex \in \mathcal{F}_i\}, \tag{4.7}$$

in which the matrix E is such that $Ex = [z\ u\ \dot{z}]^\top$, and is, therefore, given by

$$E^\top = \begin{bmatrix} -C_g^\top & 0 & -(C_gA_g)^\top \\ 0 & 1 & 0 \end{bmatrix}. \tag{4.8}$$

The mode-dependent system matrices are given by

$$A_1 = \begin{bmatrix} A_g & B_g \\ -\omega_h C_g & 0 \end{bmatrix}, \quad \text{and} \quad A_2 = \begin{bmatrix} A_g & B_g \\ -k_h C_g A_g & 0 \end{bmatrix}, \tag{4.9}$$

and furthermore $B = [B_w^\top \; 0]^\top$, and $C = [C_g \; 0]$. Recall from Chapter 2 that for all inputs $w \in PB$, global existence and forward completeness of solutions to the discontinuous differential equation in (4.6) is guaranteed.

Remark 4.2.1. *The system matrix A_2 in* (4.9) *results from explicit differentiation of the algebraic constraint $x_h - k_h z = 0$ in gain-mode. Consequently, A_2 is rank deficient and has at least one zero eigenvalue. In the upcoming parts it will be useful to remove this rank deficiency. This can be accomplished by adding the algebraic constraint in gain-mode to A_2, giving $\mathcal{A}_2 := A_2 + \mu b H$ with $\mu \in \mathbb{R}$, $b = [0 \; 1]^\top$ and $H = [-k_h C_g \; -1]$. Since $A_2 x = \mathcal{A}_2 x$ for all $x \in \mathcal{X}_2$, this extension is not changing the dynamics in* (4.6). *Using the matrix $\mathcal{A}_2$ rather than A_2 is particularly useful in further analysis where the dynamics in gain-mode are required to be stable, and thus the matrix $\mathcal{A}_2$ must be Hurwitz.*

4.2.2 Problem formulation

Stability properties of the closed-loop system in (4.6) are studied through the notion of input-to-state stability (ISS), for which the definition has been given earlier in Definition 2.3.6. According to Theorem 2.3.11 in Chapter 2, the closed-loop system in (4.6) is ISS, if it admits an ISS-Lyapunov function in the sense of Definition 2.3.10. Linearity of the individual sub-dynamics in (4.6) motivates the choice for considering a candidate ISS-Lyapunov function V to be of a quadratic form, *i.e.*, $V(x) = x^\top P x$ with $P = P^\top \in \mathbb{S}^{n \times n}$. The next theorem presents sufficient conditions in the form of linear matrix inequalities (LMIs) for guaranteeing the existence of a quadratic ISS-Lyapunov function for the HIGS-controlled system in (4.6), thereby proving ISS.

Theorem 4.2.2. *Consider the closed-loop system in* (4.6) *and depicted in Figure 4.1. Suppose there exist a symmetric matrix $P = P^\top \in \mathbb{S}^{n \times n}$ and constants $\tau_i \geq 0$, $i \in \{1, 2, 3\}$, that satisfy the LMIs*

$$P - \tau_1 S^\top J S \succ 0, \tag{4.10a}$$

$$A_1^\top P + P A_1 + \tau_2 S^\top J S \prec 0, \tag{4.10b}$$

$$\Theta^\top (A_2^\top P + P A_2 + \tau_3 T^\top J T) \Theta \prec 0, \tag{4.10c}$$

where

$$S = \begin{bmatrix} C_u \\ k_h C_z - C_u \end{bmatrix}, \quad T = \begin{bmatrix} C_u \\ C_z \left(\omega_h I - k_h A_2\right) \end{bmatrix}, \quad J = \begin{bmatrix} 0 & 1 \\ 1 & 0 \end{bmatrix}, \tag{4.11}$$

with $C_z = [-C_g \;\; 0]$, $C_u = [0 \;\; 1]$, *and* $\Theta^\top = [I \;\; -k_h C_g^\top]$. *Then, the closed-loop system* (4.6) *is ISS in the sense of Definition 2.3.6 with an ISS-Lyapunov function given by* $V(x) = x^\top P x$.

Proof. The proof is based on showing that, under the hypothesis of the theorem, $V(x) = x^\top P x$ satisfies the conditions in Definition 2.3.10 thereby qualifying as a suitable ISS-Lyapunov function for the closed-loop system in (4.6).

Feasibility of the LMI in (4.10a) implies $V(x) = x^\top P x > \tau_1 x^\top S^\top J S x$ for any $x \in \mathbb{R}^n \setminus \{0\}$. Since $x^\top S^\top J S x = 2(k_h z - u)u \geq 0$ for all $x \in \mathcal{X}_1 \cup \mathcal{X}_2$, and $\tau_1 \geq 0$, it follows by virtue of the S-procedure that V is positive definite, such that the first condition (see (2.34)) is satisfied.

In a similar manner, feasibility of the LMI in (4.10b) implies

$$\begin{aligned} \nabla V(x)(A_1 x + Bw) &= x^\top (A_1^\top P + P A_1) x + 2 x^\top P B w \\ &\leq -\epsilon \|x\|^2 - \tau_2 x^\top S^\top J S x + 2 x^\top P B w \\ &\leq -\alpha_1 \|x\|^2 + \beta_1 \|w\|^2, \end{aligned} \tag{4.12}$$

for sufficiently small $\epsilon > 0$ and positive values for α_1 and β_1. For obtaining the last inequality in (4.12), use is made of the S-procedure and Young's inequality.

In gain-mode one finds $x_h = k_h z = -k_h C_g x_g$ with $x_g \in \mathbb{R}^m$ the states of the LTI part of the system, such that $x = \Theta x_g$. Then, by virtue of Finsler's lemma (Boyd et al., 1994), satisfaction of the inequality in (4.10c) implies the existence of some $\mu \in \mathbb{R}$ such that for all $x \in \mathcal{X}_2$

$$\begin{aligned} \nabla V(x)(A_2 x + Bw) &= x^\top (A_2^\top P + P A_2) x + 2 x^\top P B w \\ &\leq -\epsilon_2 \|x\|^2 - x^\top \left(\tau_3 T^\top J T + \mu H^\top H \right) x + 2 x^\top P B w \\ &\leq -\alpha_2 \|x\|^2 + \beta_2 \|w\|^2, \end{aligned} \tag{4.13}$$

with $H = [-k_h C_g \; -1]$, and for some sufficiently small $\epsilon_2 > 0$ and positive values for α_2 and β_2. The last inequality in (4.13) follows from use of the S-procedure relaxation terms $x^\top T^\top J T x = 2(\omega_h z - k_h \dot{z})u > 0$ and $Hx = k_h z - u = 0$, which hold for all $x \in \mathcal{X}_2$. Taking $\alpha = \min\{\alpha_1, \alpha_2\}$ and $\beta = \max\{\beta_1, \beta_2\}$, it immediately follows that the second condition in Definition 2.3.10 is satisfied (see (2.35)), and thus $V(x) = x^\top P x$ is an ISS-Lyapunov function for the closed-loop system in (4.6). Invoking the result in Theorem 2.3.11 completes the proof. □

The next result demonstrates that the conditions in Theorem 4.2.2 provide somewhat stronger robust (with respect to arbitrary small state perturbations) stability guarantees for the closed-loop system in (4.6). It is an immediate consequence from the use of a quadratic Lyapunov function, and the fact that the S-procedure relaxation inequalities hold true for all $x \in \overline{\mathcal{X}}_i$, $i = \{1, 2\}$.

Corollary 4.2.3. *If the conditions in Theorem 4.2.2 are satisfied, then the Krasovskii regularization of* (4.6) *(see* (2.41) *in Section 2.3.4) is ISS.*

Although numerically tractable, solving the LMIs in (4.10) requires a parametric model, which, in practice, may be hard to obtain if one desires an accurate model description. Moreover, the conditions provide limited insight in the (re)design of HIGS-based controllers for guaranteed (robust) stability when the set of LMIs (4.10) turns out to be infeasible. Motivated by these concerns, the main objective in this chapter is to establish frequency-domain conditions that exploit non-parametric models for guaranteeing the existence of a solution to the inequalities in (4.10). This allows for making the transition from time-domain conditions to frequency-domain conditions for guaranteeing ISS.

4.3 Frequency-domain conditions for ISS

4.3.1 Existing results

Before presenting the main results, existing frequency-domain conditions for switched systems as presented in Kamenetskiy, 2017; King et al., 2011; Van Loon et al., 2017 are tailored to the specific class of HIGS-controlled systems (see also Deenen et al., 2021 in this regard). The equivalence between these conditions and the existence of a *particular* solution to the LMI problem in (4.10) is provided explicitly in the next two theorems, the first which relates to the results in Deenen et al., 2021; Van Loon et al., 2017, and the second which relates to Kamenetskiy, 2017; King et al., 2011.

Theorem 4.3.1. *Suppose the matrix A_g in* (4.1) *is Hurwitz, thereby having that the linear part of the closed-loop system in* (4.6) *is ISS. The following conditions are equivalent:*

(i) The frequency-domain inequality

$$1 + \mathrm{Re}\left\{k_h C_g (j\omega I - A_g)^{-1} B_g\right\} > 0 \tag{4.14}$$

is satisfied for all $\omega \in \mathbb{R} \cup \{\infty\}$.

(ii) The LMIs in (4.10) *admit a solution of the form $P = \mathrm{diag}(M, m) \succ 0$, with $M \in \mathbb{S}^{(n-1)\times(n-1)}$, $m > 0$, $\tau_1 = 0$, $\tau_2, \tau_3 \geq 0$.*

Proof. A proof is given in Appendix 4.A.3. □

Theorem 4.3.2. *Suppose the matrix A_1 in* (4.9) *is Hurwitz, thereby having that the integrator-mode subsystem in* (4.6) *is ISS. The following conditions are equivalent:*

(i) There exist constants $\alpha_1 \geq 0$ and $\alpha_2 \in \mathbb{R}$ such that the frequency-domain inequality

$$1 + \mathrm{Re}\left\{c(j\omega I - A_1)^{-1} b\right\} > 0 \tag{4.15}$$

with $c = C_z(\omega_h I - k_h A_2) + \alpha_1 C_z + \alpha_2 H$, $H = k_h C_z - C_u$, and $b = [0\ 1]^\top$, is satisfied for all $\omega \in \mathbb{R} \cup \{\infty\}$.

(ii) The LMIs in (4.10) *admit a solution of the form* $P \succ 0$, $\tau_1 = \tau_2 = 0$, $\tau_3 \geq 0$.

Proof. A proof is given in Appendix 4.A.4. □

The frequency-domain conditions in (4.14) and (4.15) arise from applying specific loop transformations to the original feedback configuration as depicted in Figure 4.2. In particular, specific properties of HIGS are exploited for rearranging the original feedback interconnection into an equivalent interconnection of two passive subsystems (Khalil, 2002; van der Schaft, 2017). The loop transformation underlying (4.14) is shown in Figure 4.2b, and transforms HIGS into a dynamical system $\bar{\mathcal{H}}$ with input $\bar{z} = z - u/k_h$ and output $\bar{u} = u/k_h$. Sector-boundedness yields $\bar{z}\bar{u} \geq 0$ such that $\bar{\mathcal{H}}$ preserves input-output passivity properties. The linear system is transformed to

$$\bar{G}_{yu}(s) = 1 + k_h G_{yu}(s) = 1 + k_h C_g (sI - A_g)^{-1} B_g,$$

which, under condition (4.14), is a strictly passive system. Using standard passivity arguments (see, *e.g.*, Khalil, 2002, Theorem 6.3) one finds the original feedback interconnection to be (strictly) passive, which, possibly under some additional observability conditions may imply asymptotic stability. In a comparable manner, the loop transformation underlying the frequency-domain condition in (4.15) is depicted in Figure 4.2c. In this figure, HIGS is transformed into a dynamical system $\bar{\mathcal{H}}$ with input $\bar{z} = k_h \dot{z} + (k + \omega_h) z + \alpha_2 u - \dot{u}$, where $k = -\omega_h - \alpha_1 - k_h \alpha_2$, and output $\bar{u} = \dot{u} - \omega_h z$. Note that $x_h = u$ is differentiable for almost all times $t \in \mathbb{R}_{\geq 0}$. In integrator-mode, one finds $\bar{u} = 0$ such that $\bar{z}\bar{u} = 0$, and in gain-mode one has $\bar{z}\bar{u} = \alpha_1 z(\omega_h z - k_h \dot{z}) \geq 0$, such that overall $\bar{z}\bar{u} \geq 0$, and the transformed system $\bar{\mathcal{H}}$ preserves input-output passivity properties. The linear part in Figure 4.2c is transformed according to

$$\bar{G}_{yu}(s) = 1 + \frac{G_{yu}(s)(k_h s + k) + \alpha_2}{s + \omega_h G_{yu}(s)} = 1 + c(sI - A_1)^{-1} b,$$

which, when satisfying the frequency-domain inequality (4.15), is guaranteed to be a (strictly) passive system. By virtue of, *e.g.*, Khalil, 2002, Theorem 6.3, one can eventually conclude on passivity of the original system. Under some additional observability conditions this, in turn, can imply asymptotic stability of the closed-loop system. Interestingly, the loop transformation underlying condition (4.14) only exploits *static* input-output properties of HIGS, whereas the transformation underlying condition (4.15) also exploits knowledge of the internal (integrator) dynamics of HIGS.

Regarding Theorem 4.3.1 and Theorem 4.3.2, more observations can be made:

1. As a consequence of the fact that both theorems guarantee the existence of a solution to the LMI problem (4.10) with $\tau_1 = 0$, an ISS-Lyapunov

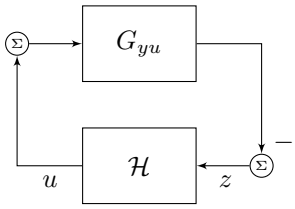

(a) Original system.

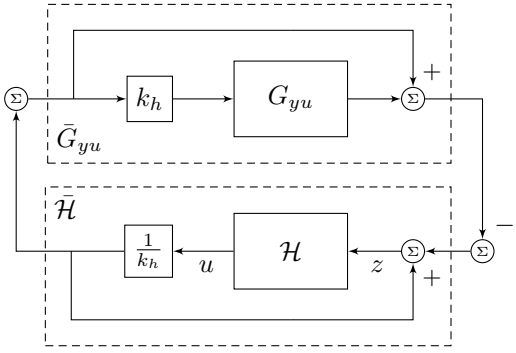

(b) Loop transformation applied in Theorem 4.3.1.

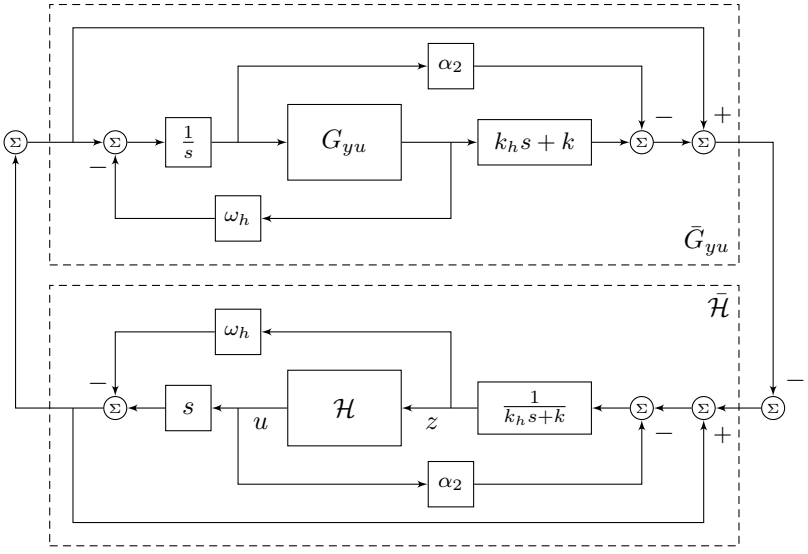

(c) Loop transformation applied in Theorem 4.3.2 with $k = -\omega_h - \alpha_1 - k_h\alpha_2$.

Figure 4.2. Loop transformations underlying the frequency-domain inequalities (4.14) and (4.15) in Theorem 4.3.1 and Theorem 4.3.2, respectively.

function $V(x) = x^\top Px$ is found that is guaranteed to be positive in the full state space $\mathbb{R}^n$, while the states of the closed-loop system only evolve in part of the state space. This observation reveals possible restrictions on the considered class of Lyapunov function candidates that are used in Theorem 4.3.1–4.3.2. In that sense, the conditions potentially become conservative.

2. Theorem 4.3.1 is applicable to HIGS-based control systems for which the LTI part G_{yu} is stable. However, in many applications that may benefit from HIGS-based control, such as motion systems, the linear part of the dynamics contains simple integrators, which renders Theorem 4.3.1 not straightforwardly applicable as G_{yu} is not stable. As indicated before, the interplay between the LTI dynamics and the integrator-dynamics of HIGS is not exploited in the conditions of Theorem 4.3.1, and HIGS is regarded as a static sector-bounded nonlinearity. This is also visible from the fact that the frequency-domain inequality in (4.14) does not depend on ω_h.

3. Theorem 4.3.2 is only applicable to HIGS-based control systems having stable linear dynamics in integrator mode. This narrows down the scope of applications for which Theorem 4.3.2 may be a useful tool for stability analysis. In fact, one may argue that unstable integrator-mode dynamics largely contribute to potential performance improvements with HIGS, and therefore is a desirable property of a HIGS-based controller design.

4. Closer inspection of the proofs of Theorem 4.3.1 and Theorem 4.3.2 reveals that the conditions (4.14) and (4.15) imply the existence of a common quadratic Lyapunov function (CQLF) for the pairs $(A_g, A_g - k_h B_g C_g)$ and $(A_1, A_1 - bc)$, respectively. Existence of a CQLF for $(A_g, A_g - k_h B_g C_g)$ is only possible when the gain-mode dynamics are asymptotically stable, *i.e.*, the matrix $A_g - k_h B_g C_g$ is Hurwitz. On the other hand, when considering a CQLF for $(A_1, A_1 - bc)$, one finds that since $A_1 - bc = A_2 - b(\alpha_1 C_z + \alpha_2 H)$, restricting $\alpha_1 = 0$ leads to a CQLF for the integrator-mode and gain-mode dynamics (recall from Remark 4.2.1 that α_2 does not alter the gain-mode dynamics). This is equivalent to saying that the piecewise linear system (4.6) is asymptotically stable under arbitrary switching. As switching of HIGS is dictated by state-dependent conditions only, this possibly leads to conservative results.

In conclusion, although the results in Theorem 4.3.1 and Theorem 4.3.2 are of interest, they suffer from specific restrictions that are not always beneficial for HIGS-based design as indicated in the above observations. Therefore, lifting these restrictions in the sense of obtaining less conservative conditions is considered important for useful practical applications.

4.3.2 Main results

To address the previously discussed issues and provide less restrictive conditions, consider the next theorem, which forms the main result of this chapter.

Theorem 4.3.3. *Suppose the matrix $A_g - k_h B_g C_g$ is Hurwitz, thereby having that the gain-mode subsystem in (4.6) is ISS. If there exist numbers $\lambda \geq 0$, $k \geq 1$ such that for all $\omega \in \mathbb{R} \cup \{\infty\}$ the frequency-domain inequality*

$$1 + \mathrm{Re}\left\{ \left(\lambda k C_u + F + \left(\lambda + k\frac{\omega_h}{k_h} \right) H \right) (j\omega I - \mathcal{A}_2)^{-1} b \right\} > 0 \tag{4.16}$$

is satisfied, with $\mathcal{A}_2 = A_2 + k\frac{\omega_h}{k_h} bH$, $H = k_h C_z - C_u$, and $F = C_z (k_h A_1 - \omega_h I)$, then the LMI problem (4.10) admits a feasible solution of the form $P = (M + \lambda H^\top H) + \tau_1 S^\top J S$ with $M = M^\top \succ 0$, $\tau_1 = \lambda k$, $\tau_2 = \lambda k(k-1)\omega_h/k_h$ and $\tau_3 = 0$.

Proof. The proof can be found in Appendix 4.A.5. □

To obtain insights in the frequency-domain condition (4.16), it is instructive to study aspects of the underlying loop transformation depicted in Figure 4.3, in particular, passivity of the transformed system $\bar{\mathcal{H}}$. Passivity properties of the LTI loop-transformed system $\bar{G}_{yu}$ are discussed thereafter, and finally the connection with the existence of an ISS-Lyapunov function is highlighted.

Observe that in Figure 4.3 the loop-transformed nonlinear system $\bar{\mathcal{H}}$ admits an input $\bar{z} = (W + k_h L^{-1})z - (K + L^{-1})u = (\omega_h z - \dot{u}) - \lambda(k_h z - (1-k)u)$, and output $\bar{u} = L^{-1}(u - k_h z) = \dot{u} - k_h \dot{z} + k\frac{\omega_h}{k_h}(u - k_h z)$. Passivity of $\bar{\mathcal{H}}$ does not directly follow from a similar reasoning as for the transformations studied in the previous section, since non-negativity of the input-output product $\bar{z}\bar{u}$ does not necessarily hold point-wise in time. However, observe that for almost all times $t \in \mathbb{R}_{\geq 0}$ one may write

$$\bar{z}(t)\bar{u}(t) = \tau R\left(z(t), u(t)\right) + \dot{U}\left(z(t), u(t)\right) + O\left(z(t), u(t), \dot{z}(t), \dot{u}(t)\right) \tag{4.17}$$

in which $\tau = \lambda k(k-1)\omega_h/k_h \geq 0$, and

$$R(z,u) = u(k_h z - u), \tag{4.18a}$$

$$U(z,u) = \lambda \left(ku(k_h z - u) + \frac{1}{2}(k_h z - u)^2 \right), \tag{4.18b}$$

and where

$$O(z,u,\dot{z},\dot{u}) = (\omega_h z - \dot{u})(\dot{u} - k_h \dot{z} + (K+\lambda)(k_h z - u)). \tag{4.19}$$

From sector-boundedness of HIGS in (4.3), one finds point-wise in time that $R(z(t),u(t)) \geq 0$, $U(z(t),u(t)) \geq 0$, and since $\dot{u} = \omega_h z$ in integrator-mode and

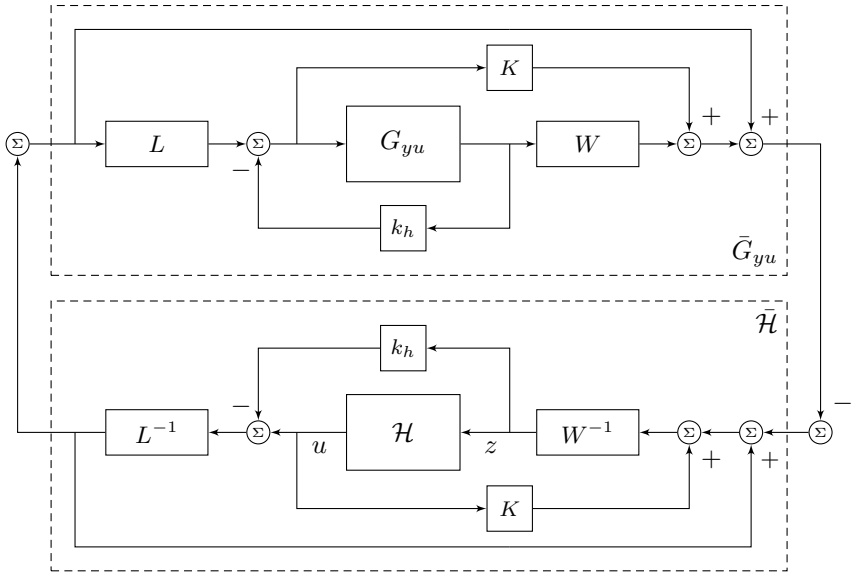

Figure 4.3. Loop transformation underlying the frequency-domain inequality in (4.16) in Theorem 4.3.3, where $K = \lambda(k-1) - k\omega_h/k_h$, $L(s) = (s + k\omega_h/k_h)^{-1}$, and $W(s) = \omega_h(1-k) - \lambda k_h - k_h s$.

both $u = k_h z$ and $\dot{u} = k_h \dot{z}$ in gain-mode, one has $O(z(t), u(t), \dot{z}(t), \dot{u}(t)) = 0$ for almost all times t. Since $\tau \geq 0$, one then finds (with some abuse of notation for $R(t)$ and $O(t)$)

$$U(0) + \int_0^T \bar{z}(t)\bar{u}(t)dt = U(T) + \int_0^T (\tau R(t) + O(t))\, dt \geq 0, \tag{4.20}$$

which implies that the transformed system $\bar{\mathcal{H}}$ in Figure 4.3 preserves input-output passivity properties. Note that the key difference with the transformations employed in Theorem 4.3.1 and Theorem 4.3.2 is that, besides static input-output properties and knowledge regarding the underlying dynamics, also integral properties are exploited here.

Next, passivity properties of the transformed LTI system $\bar{G}_{yu}(s)$ in Figure 4.3 are studied. Observe from Figure 4.3 that this transfer function is given by

$$\bar{G}_{yu}(s) = 1 + \left(\frac{K + W(s)G_{yu}(s)}{1 + k_h G_{yu}(s)} \right) L(s). \tag{4.21}$$

To see the relation with the frequency-domain condition in (4.16), first observe

that (4.21) admits the state-space formulation

$$\bar{\Sigma} : \begin{cases} \dot{\bar{x}} &= \bar{\mathcal{A}}\bar{x} + \bar{\mathcal{B}}\bar{u}, \\ \bar{y} &= \bar{\mathcal{C}}\bar{x} + \bar{\mathcal{D}}\bar{u} \end{cases} \tag{4.22}$$

with state $\bar{x} \in \mathbb{R}^n$, input and output $\bar{u}, \bar{y} \in \mathbb{R}$, and matrices

$$\left[\begin{array}{c|c} \bar{\mathcal{A}} & \bar{\mathcal{B}} \\ \hline \bar{\mathcal{C}} & \bar{\mathcal{D}} \end{array}\right] = \left[\begin{array}{cc|c} A_g - k_h B_g C_g & B_g & 0 \\ 0 & -k\frac{\omega_h}{k_h} & 1 \\ \hline F_g - \lambda k_h k C_g & K & 1 \end{array}\right], \tag{4.23}$$

in which $F_g = C_g(\omega_h I - k_h A_g)$ and $K = \lambda(k-1) - k\omega_h/k_h$. Consider the state transformation $x = T\bar{x}$ with

$$T = \begin{bmatrix} I & 0 \\ -k_h C_g & 1 \end{bmatrix}, \quad \text{and} \quad T^{-1} = \begin{bmatrix} I & 0 \\ k_h C_g & 1 \end{bmatrix}. \tag{4.24}$$

Using this transformation, one finds an equivalent state-space description as

$$\left[\begin{array}{c|c} T\bar{\mathcal{A}}T^{-1} & T\bar{\mathcal{B}} \\ \hline \bar{\mathcal{C}}T^{-1} & \bar{\mathcal{D}} \end{array}\right] = \left[\begin{array}{c|c} \mathcal{A}_2 & \mathcal{B} \\ \hline \mathcal{C} & \mathcal{D} \end{array}\right] = \left[\begin{array}{cc|c} A_g & B_g & 0 \\ -k_h C_g A_g - k\omega_h C_g & -k\frac{\omega_h}{k_h} & 1 \\ \hline F_g - (\lambda k_h + k\omega_h) C_g & K & 1 \end{array}\right], \tag{4.25}$$

such that, in turn, (4.21) is equivalent to

$$\begin{aligned} \bar{G}_{yu}(s) &= \mathcal{C}\left(sI - \mathcal{A}_2\right)^{-1}\mathcal{B} + \mathcal{D} \\ &= \left(\lambda k C_u + F + \left(\lambda + k\frac{\omega_h}{k_h}\right) H\right)\left(sI - \mathcal{A}_2\right)^{-1} b + 1. \end{aligned} \tag{4.26}$$

As such, the frequency-domain condition in (4.16) implies the LTI part $\bar{G}_{yu}$ in Figure 4.3 to be (strictly) passive, such that, in turn, the interconnection in Figure 4.3 is (strictly) passive.

To see the connection with an ISS-Lyapunov function and feasibility of the LMIs in (4.10), first note that strict passivity of $\bar{G}_{yu}$ is equivalent (Khalil, 2002; van der Schaft, 2017) to the existence of a quadratic storage function $W(x) = x^\top M x > 0$ satisfying

$$\begin{aligned} \dot{W}(x) &= x^\top \left(\mathcal{A}_2^\top M + M\mathcal{A}_2\right) x + x^\top M b\bar{u} + \bar{u}^\top b^\top M x + 2x^\top M B w \\ &= -\epsilon x^\top M x - 2\bar{z}\bar{u} + 2x^\top M B w. \end{aligned} \tag{4.27}$$

This, however, is not an appropriate ISS-Lyapunov function in the sense of Definition 2.3.10. On the other hand, consider the function

$$V(x) = W(x) + 2\lambda U(z, x_h) > 0, \quad \text{for all} \quad x \in \mathcal{X} = \mathcal{X}_1 \cup \mathcal{X}_2, \tag{4.28}$$

where $U(z, x_h) = kx_h(k_h z - x_h) + \frac{1}{2}(k_h z - x_h)^2$, and $\lambda \geq 0$. The inequality in (4.28) follows from the fact that $W(x) > 0$ for all non-zero $x \in \mathbb{R}^n$ and $U(z, x_h) \geq 0$ for all $x \in \mathcal{X}$. The time-derivative of V satisfies for all $x \in \mathcal{X}$ and almost all time $t \in \mathbb{R}_{\geq 0}$

$$\dot{V}(x) \leq -\epsilon x^\top M x - 2\bar{z}\bar{u} + 2\dot{U}(z, x_h) + 2x^\top MBw < -\alpha\|x\|^2 + \beta\|w\|^2, \quad (4.29)$$

where for obtaining the second inequality it is used that $\bar{z}(t)\bar{u}(t) = \tau R(t) + \dot{U}(t) + O(t)$, with $\tau R(t) + O(t) \geq 0$. Hence, V is an ISS-Lyapunov function that is guaranteed to be positive definite for all $x \in \mathcal{X}$, and for which the existence is guaranteed by the frequency-domain inequality in (4.16). In fact, one can write $V(x) = x^\top P x$ with $P = M + \lambda H^\top H + \tau_1 S^\top J S$ and $\tau_1 = \lambda k$, which coincides with the specific ISS-Lyapunov function that results from Theorem 4.3.3. The connection between the frequency-domain inequality and the existence of the quadratic ISS-Lyapunov function (and, therefore, feasibility of the LMIs in (4.10)) is formally shown in the proof of Theorem 4.3.3 as provided in Appendix 4.A.5

Remark 4.3.4. *Satisfying the inequality in* (4.16) *with* $\lambda = 0$ *results in a common quadratic Lyapunov function for the piecewise linear system* (4.6)*, which follows from the fact that this choice yields* $\bar{z}\bar{u} = 0$ *for all times. Hence, in this case no further information about HIGS is exploited, and the condition is found to be equivalent to* (4.15) *with* $\alpha_1 = 0$ *and* $\alpha_2 = k\omega_h/k_h$*.*

4.3.3 Verifying the frequency-domain conditions

While the above discussion helps in establishing links with results from the literature and insights in the existence of a particular ISS-Lyapunov function, at this point in the analysis it is not immediately clear how to verify the frequency-domain condition (4.16) in an effective manner. In order to derive a practical method for verifying the conditions, recall that the relevant transfer function is given by

$$\begin{aligned}\bar{G}_{yu}(s) &= 1 + \left(\lambda(kC_u + H) + F + k\frac{\omega_h}{k_h}H\right)(sI - \mathcal{A}_2)^{-1}b \\ &= 1 + \left(KS(s) + \frac{1}{k_h}W(s)T(s)\right)L(s) \\ &= 1 + \left(\frac{\omega_h}{k_h}(T(s) - k) - sT(s)\right)L(s) - \lambda(1 - kS(s))L(s),\end{aligned} \quad (4.30)$$

where $S(s) = 1/(1 + k_h G_{yu}(s))$ and $T(s) = k_h G_{yu}(s) S(s)$ with $G_{yu}(s)$ given in (4.2) equal the sensitivity and complementary sensitivity functions in gain-mode.

For verifying the conditions of Theorem 4.3.3, one should first verify if the gain-mode dynamics are input-to-state stable. This can be done by applying the

Nyquist stability criterion (Franklin et al., 2005, Section 6.3) to the open-loop characteristics $1+k_hG_{yu}(j\omega)$. Note that (part of) the characteristics of $G_{yu}(j\omega)$ may be obtained from frequency-response function (FRF) measurements. Next, condition (4.16) can be verified by searching for parameters $\lambda \geq 0$, $k \geq 1$ such that the frequency-domain inequality $\mathrm{Re}(\bar{G}_{yu}(j\omega)) > 0$ with $\bar{G}_{yu}(j\omega)$ given in (4.30) holds for all $\omega \in \mathbb{R}$. This amounts to verifying the inequality

$$1 + X(j\omega, k) - \lambda Y(j\omega, k) > 0, \tag{4.31}$$

where

$$\begin{aligned} X(j\omega,k) &= \mathrm{Re}\left\{\left(\left(\frac{\omega_h}{k_h} - j\omega\right)T(j\omega) - k\frac{\omega_h}{k_h}\right)L(j\omega,k)\right\} \\ &= \frac{\omega_h}{k_h}\mathrm{Re}\left\{(T(j\omega)-k)L(j\omega,k)\right\} + \omega\mathrm{Im}\left\{T(j\omega)L(j\omega,k)\right\}, \end{aligned} \tag{4.32a}$$

and

$$\begin{aligned} Y(j\omega,k) &= \mathrm{Re}\left\{(kT(j\omega) - k + 1)\,L(j\omega,k)\right\} \\ &= k\mathrm{Re}\left\{T(j\omega)L(j\omega,k)\right\} + (1-k)\mathrm{Re}\left\{L(j\omega,k)\right\}. \end{aligned} \tag{4.32b}$$

For any fixed k, condition (4.31) can be verified graphically by inspecting if the (X,Y)-curve lies to the right of the line $1+X-\lambda Y = 0$, *i.e.*, a line in the (X,Y)-plane that passes through the point $(X,Y) = (-1,0)$ with a slope of $1/\lambda$. The parameter $k \geq 1$ can be used for shaping the (X,Y)-curve. This graphical test shows resemblance with the classical Popov plot (Khalil, 2002).

A few useful insights that follow from the representation in (4.31) are established in the following corollaries.

Corollary 4.3.5. *If the conditions in Theorem 4.3.1 are satisfied, then the conditions in Theorem 4.3.3 are satisfied as well.*

Proof. Choose $\lambda = \omega_h/k_h$ and observe that with this choice one finds $\lim_{k\to\infty}(1+X(j\omega,k)) = 0$ and

$$\lim_{k\to\infty} \lambda Y(j\omega,k) = \mathrm{Re}\left\{T(j\omega) - 1\right\} = -\mathrm{Re}\left\{\frac{1}{1+k_hG_{yu}(j\omega)}\right\}. \tag{4.33}$$

Hence, for $k \to \infty$ condition (4.31) reduces to

$$\mathrm{Re}\left\{\frac{1}{1+k_hG_{yu}(j\omega)}\right\} = \frac{1 + k_h\mathrm{Re}\left\{G_{yu}(j\omega)\right\}}{\|1+k_hG_{yu}(j\omega)\|^2} > 0. \tag{4.34}$$

Obviously, if (4.14) is satisfied, then the matrix $A_g - k_hB_gC_g$ is Hurwitz, and the inequality in (4.34) is also satisfied. □

Corollary 4.3.5 implies that the conditions in Theorem 4.3.3 are equally or less restrictive than the conditions in Theorem 4.3.1.

Corollary 4.3.6. *Consider the closed-loop system in* (4.6) *and suppose that the gain-mode subsystem is input-to-state stable for all* $\omega_h \geq \omega_h^*$ *with* $\omega_h^* \geq 0$. *Then for any* $\omega_h > \max\{\omega_h^*, 2\mu k_h\}$, *with* $\mu = \sup_{\omega_h \geq \omega_h^*} \|\omega T(j\omega, \omega_h)\|_\infty$, *the closed-loop system* (4.6) *is ISS.*

Proof. Choose $\lambda = \frac{\omega_h}{k k_h}$ such that (4.31) evaluates to

$$1+X(j\omega,k)-\lambda Y(j\omega,k) = 1+\omega \mathrm{Im}\left\{T(j\omega)L(j\omega)\right\}-\frac{\omega_h}{k_h}\left(\frac{k^2-k+1}{k}\right)\mathrm{Re}\left\{L(j\omega)\right\}. \tag{4.35}$$

Since

$$\mathrm{Re}\left\{L(j\omega)\right\} = \frac{k k_h \omega_h}{k_h^2\omega^2 + (k\omega_h)^2} \leq \frac{k_h}{k\omega_h}, \quad \text{for all } \omega \in \mathbb{R}, \tag{4.36}$$

and $k(k-1) \geq 0$, one finds that (4.35) is bounded from below by

$$1 + X(j\omega,k) - \lambda Y(j\omega,k) \geq \left(\frac{k-1}{k^2}\right) + \omega \mathrm{Im}\left\{T(j\omega)L(j\omega)\right\}. \tag{4.37}$$

From the assumption that the gain-mode is stable for any $\omega_h \geq \omega_h^*$, it holds that $\|\omega T(j\omega,\omega_h)\|_\infty \leq \tilde{\mu}(\omega_h) \leq \mu$ with $\mu = \sup_{\omega_h \geq \omega_h^*} \|\omega T(j\omega,\omega_h)\|_\infty$, and, therefore, $\|\omega T(j\omega)L(j\omega)\|_\infty \leq \|\omega T(j\omega)\|_\infty \|L(j\omega)\|_\infty \leq \mu k_h/(k\omega_h)$. This, in turn, implies

$$|\omega \mathrm{Im}\left\{T(j\omega)L(j\omega)\right\}| \leq \mu \frac{k_h}{k\omega_h}. \tag{4.38}$$

Choose $k = 2$ such that (4.37) yields

$$\left(\frac{k-1}{k^2}\right) + \omega \mathrm{Im}\left\{T(j\omega)L(j\omega)\right\} \geq \frac{1}{4} - \frac{\mu k_h}{2\omega_h}. \tag{4.39}$$

Hence, for $\omega_h > \max\{\omega_h^*, 2\mu k_h\}$ one finds that (4.31) holds. The conditions of Theorem 4.3.3 are satisfied, thereby guaranteeing ISS of (4.6). □

Remark 4.3.7. *In case* $T(j\omega)$ *is independent of* ω_h, *one has* $\omega_h^* = 0$, *and* $\mu = \|\omega T(j\omega)\|_\infty$.

The result in Corollary 4.3.6 is not surprising. As the time-domain behaviour of HIGS tends to a gain for $\omega_h \to \infty$, the characteristics of the piecewise linear closed-loop system (4.6) tend to that of the gain-mode dynamics. Stability properties of the closed-loop system are then determined by stability properties of the gain-mode dynamics. Hence, in this manner the nonlinear contribution of HIGS can be mitigated. This, in turn, shows that it is always possible for a HIGS-based control system to fall back onto a linear design when choosing ω_h sufficiently large, thereby demonstrating a simple mechanism to balance between dominant "linear" and "nonlinear" behaviour of the closed-loop system.

These observations also allow for an intuitive tuning approach for HIGS-based control systems with guaranteed stability. One can start with choosing ω_h sufficiently large and a stable gain-mode design, the latter obtained via, *e.g.*, loop-shaping techniques (Steinbuch and Norg, 1998). By gradually decreasing ω_h, the minimum value ω_h^* can be found for which the frequency-domain condition (4.31) is satisfied. By decreasing ω_h, the effect of the nonlinearity is made more pronounced. Using a (time-domain) performance objective, one can iteratively search for an appropriate value for $\omega_h \geq \omega_h^*$. Small values for ω_h have been observed to benefit transient performance properties, see for instance the example discussed in Chapter 3. Interestingly, for the example considered in Chapter 3, ISS can be verified on the basis of Theorem 4.3.3.

4.3.4 Example: Mass-spring-damper system

To demonstrate the potential improvements resulting from the frequency-domain condition (4.16) in Theorem 4.3.3, a comparative study is made for the control configuration given in Figure 4.4.

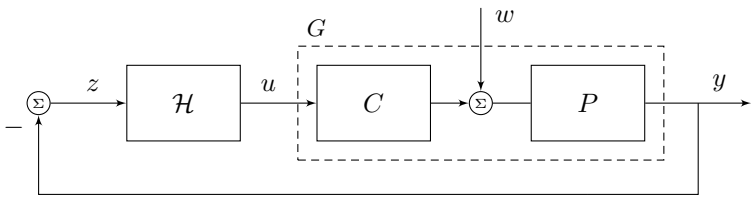

Figure 4.4. Mass-spring-damper example with HIGS.

In this example, the plant is a mass-spring-damper system represented by the transfer function

$$P(s) = \frac{1}{ms^2 + bs + k}, \tag{4.40}$$

with $m = 1$ kg, $b = 0.0564$ Ns/m, and $k = 1$ N/m, and the linear part of the HIGS-based feedback controller is given by a first-order lead filter

$$C(s) = k_p \left(\frac{s + \omega_z}{s + \omega_p} \right), \tag{4.41}$$

with $k_p = 1.4$ Nm, $\omega_z = 5$ rad/s, and $\omega_p = 6.95$ rad/s. The transfer function from u to y is given by $G_{yu}(s) = C(s)P(s)$, and the transfer function from w to y is given by $G_{yw}(s) = P(s)$. In this control configuration, HIGS is deployed as a first-order low-pass filter with less phase-lag than its linear counterpart. For this system, the LMIs in (4.10), as well as the frequency-domain conditions in Theorem 4.3.1–4.3.3 are verified for several values of the parameters ω_h and k_h. The corresponding results are shown in Figure 4.5.

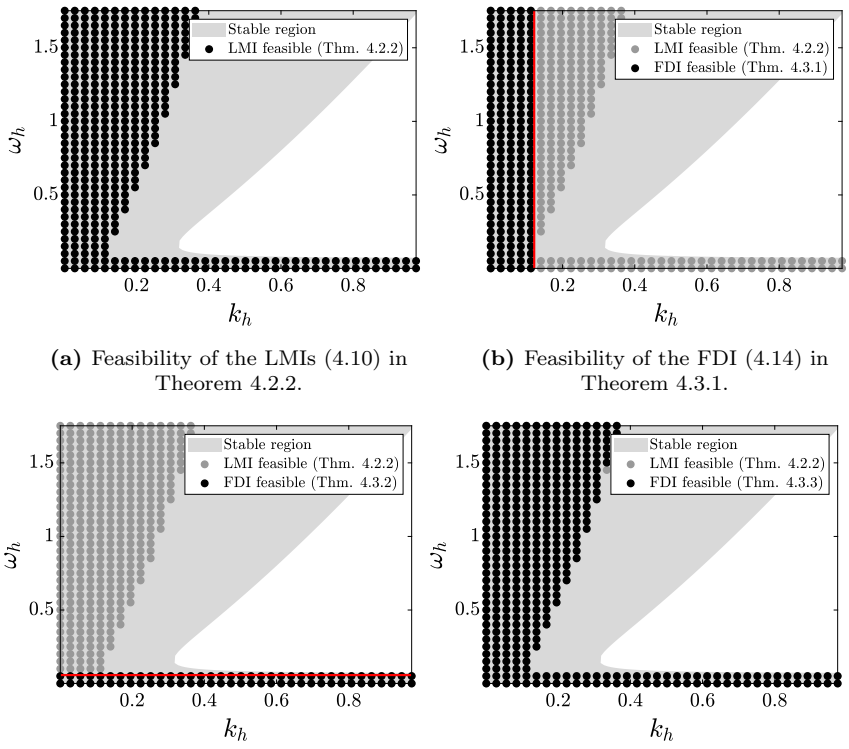

(a) Feasibility of the LMIs (4.10) in Theorem 4.2.2.

(b) Feasibility of the FDI (4.14) in Theorem 4.3.1.

(c) Feasibility of the FDI (4.15) in Theorem 4.3.2.

(d) Feasibility of the FDI (4.16) in Theorem 4.3.3.

Figure 4.5. A comparison between the time-domain conditions (LMIs) in Theorem 4.2.2 and the frequency-domain conditions (FDIs) in Theorem 4.3.1–4.3.3 for different values of the HIGS parameters ω_h and k_h.

As can be seen from Figure 4.5b, the conditions in Theorem 4.3.1 guarantee a solution to the LMI problem in (4.10) for $k_h \leq 0.12$. This value results from the fact that condition (4.14) treats HIGS as a generic sector-bounded nonlinearity, and, therefore, does not take into account its integrator dynamics. This is manifested by the fact that (4.14) is independent of ω_h. Since (for values $k_h > 0.12$) a solution to the LMIs in (4.10) clearly depends on ω_h as well, (4.14) can never be satisfied beyond this point.

Similarly, the conditions in Theorem 4.3.2 are found to guarantee a solution for all $\omega_h \leq 0.056$ rad/s as is shown in Figure 4.5c. This bound is the result from the fact that for $\omega_h > 0.056$ rad/s, the integrator dynamics are unstable and, therefore, Theorem 4.3.2 cannot be applied to these cases. Compared to the actual region in Figure 4.5a where the LMIs in (4.10) admit a solution, the results

obtained with Theorem 4.3.1 and Theorem 4.3.2 appear quite conservative.

On the other hand, as can be seen from Figure 4.5d, the conditions in Theorem 4.3.3 lead to a close match with the region where the LMIs in (4.10) have a solution. In fact, the frequency-domain inequality (FDI) in (4.16) and the LMIs in (4.10) almost appear to be identical for the given example (Figure 4.5a versus Figure 4.5d). A graphical check of the conditions in (4.31) through a Popov-like plot as discussed previously is shown in Figure 4.6 for the pair $k_h = 0.23$ and $\omega_h = 1.05$, with $k = 4$ and $\lambda = 1.35$.

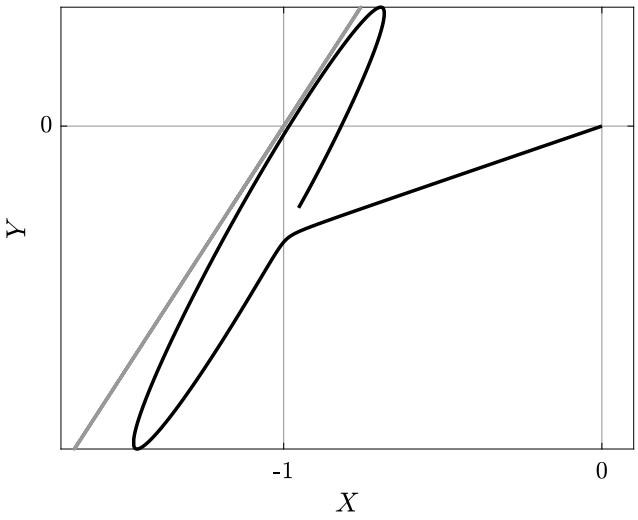

Figure 4.6. Popov-like plot of the (X, Y)-curve for the system in Figure 4.4 with $k_h = 0.23$ and $\omega_h = 1.05$. The stability parameters k, λ for satisfying (4.31) are found to be $k = 4$ and $\lambda = 1.35$.

It is stressed that, when compared to the actual stable region obtained by time-domain simulations (grey area), the LMIs in (4.10) resulting from a quadratic Lyapunov function still introduce conservatism in the analysis. Other techniques such as the construction of piecewise quadratic Lyapunov functions (Rantzer and Johansson, 2000) should be used for further reducing this conservatism. The construction of piecewise quadratic Lyapunov functions for HIGS-based control systems is discussed in Chapter 5. For the example discussed it will be shown later in Section 5.5 that a stability analysis based on such an approach can approximate the grey area in Figure 4.5 very closely.

4.4 Robustifying the conditions

The transition from time-domain tools toward frequency-domain tools for stability analysis of nonlinear systems allows for an intuitive extension toward dealing with plant uncertainties. This is particularly useful for industrial applications where one often designs a single controller for a population of systems that includes many system realizations. For the classical circle- and Popov critera, extensions toward robust stability have been made in, *e.g.*, Impram and Munro, 2001; Tsypkin and Polyak, 1992. Inspired by these works, the frequency-domain criteria presented in Theorem 4.3.3 are extended toward systems with multiplicative uncertainties.

4.4.1 Stability criteria for plants with multiplicative uncertainty

Suppose that the SISO LTI plant $G_{yu}(s)$ in (4.2) is not exactly known, but instead is known to belong to the multiplicative uncertainty set

$$\Pi = \{G_{yu}(s) \mid G_{yu}(s) = G_0(s)(1 + W(s)\Delta(s)), \Delta(s) \in \mathcal{RH}_\infty \text{ and } \|\Delta\|_\infty \leq 1\}, \tag{4.42}$$

where $G_0(s)$ is a nominal model of the plant, $W(s)$ is a proper and stable weighting function that captures magnitude information on uncertainties in the system, and $\Delta(s)$ is the (normalized) uncertainty which can be represented by an arbitrary proper and stable transfer function that satisfies $\|\Delta\|_\infty \leq 1$. For more details on uncertainty modelling and appropriate weighting filter selection for SISO LTI systems, see, *e.g.*, Skogestad and Postlethwaite, 2010, Chapter 7.

To verify stability of the HIGS-based control system (4.6) for all possible plants $G_{yu}(s) \in \Pi$, one essentially has to check two conditions: 1) stability of the nominal gain-mode dynamics with respect to all allowable perturbations, and 2) satisfaction of the frequency-domain inequality (4.31) for all $G_{yu}(s) \in \Pi$. In the next proposition, these conditions are formalized and expressed in terms of requirements on the nominal system, *i.e.*, with $\Delta(s) = 0$.

Proposition 4.4.1. *Suppose that the LTI part of the closed-loop system* (4.6) *dictating the transfer from u to y satisfies $G_{yu}(s) \in \Pi$ with Π the uncertainty set given in* (4.42)*, and assume that the nominal gain-mode dynamics with $\Delta(s) = 0$ are input-to-state stable. If for all $\omega \in \mathbb{R}$ the closed-loop system* (4.6) *satisfies*

$$\|W(j\omega)L_0(j\omega)\| < \|1 + L_0(j\omega)\|, \tag{4.43}$$

with $L_0(s) = k_h G_0(s)$, and there exist numbers $\lambda \geq 0, k \geq 1$ such that for all $\omega \in \mathbb{R}$ the frequency-domain inequality

$$1 + X_0(\omega, k) - \lambda Y_0(\omega, k) - \rho(\omega)\sqrt{\left(\frac{\omega_h}{k_h} - \lambda k\right)^2 + \omega^2} > 0, \tag{4.44}$$

is satisfied, where

$$X_0(\omega,k) = \frac{\omega_h}{k_h}\mathrm{Re}\left\{(T_0(j\omega)-k)C_l(j\omega)\right\} + \omega\mathrm{Im}\left\{T_0(j\omega)C_l(j\omega)\right\}, \tag{4.45a}$$

$$Y_0(\omega,k) = k\mathrm{Re}\left\{T_0(j\omega)C_l(j\omega)\right\} + (1-k)\mathrm{Re}\left\{C_l(j\omega)\right\}, \tag{4.45b}$$

with

$$T_0(s) = \frac{L_0(s)}{1+L_0(s)}, \quad \text{and} \quad C_l(s) = \frac{1}{s+k\frac{\omega_h}{k_h}}, \tag{4.46}$$

and where

$$\rho(\omega) = \frac{\|T_0(j\omega)W(j\omega)C_l(j\omega)\|}{\|1+L_0(j\omega)\| - \|W(j\omega)L_0(j\omega)\|}, \tag{4.47}$$

then, the overall closed-loop system (4.6) *is ISS for all plants* $G_{yu}(s) \in \Pi$.

Proof. The proof can be found in Appendix 4.A.6. □

Condition (4.43) is standard practice in robust control theory for LTI systems, and can be verified by plotting the Nyquist diagram of the nominal open-loop characteristics $L_0(j\omega)$. At each frequency ω superimpose a circle with center $L_0(j\omega)$ and radius $r(\omega) := \|W(j\omega)L_0(j\omega)\|$. If none of these circles in the complex plane cover the critical point $(-1,0)$, then (4.43) is satisfied which means that the gain-mode dynamics are robustly stable with respect to all allowable plant perturbations contained in Π.

Due to the nonlinear appearance of λ in (4.44), however, it is not immediately clear how to check this condition graphically. One possible approach is to plot the nominal (X_0, Y_0) locus and for each frequency ω draw an ellipse centered at (X_0, Y_0) and described by the quadratic equation

$$x^2 - 2\frac{\omega_h}{kk_h}xy + \left(\frac{\omega_h^2}{k^2k_h^2} + \frac{\omega^2}{k^2}\right)y^2 - (\omega\rho(\omega))^2 = 0. \tag{4.48}$$

The resulting hull of the ellipses should lie to the right of the line $1+x-\lambda y = 0$.

A less involved, but possibly more conservative method, follows from the inequality (Tsypkin and Polyak, 1992)

$$\sqrt{\left(\frac{\omega_h}{k_h} - \lambda k\right)^2 + \omega^2} \leq \sqrt{\left(\frac{\omega_h}{k_h}\right)^2 + \omega^2} + \lambda k.$$

One can construct a lower-bound for the left-hand side in (4.44) as

$$\begin{aligned} 1 + \left(X_0(\omega,k) - \rho(\omega)\sqrt{\left(\frac{\omega_h}{k_h}\right)^2 + \omega^2}\right) - \lambda\left(Y_0(\omega,k) + k\rho(\omega)\right) \\ = 1 + X_0'(\omega,k) - \lambda Y_0'(\omega,k). \end{aligned} \tag{4.49}$$

Hence, if (4.49) is positive, then the inequality in (4.44) is satisfied. Positiveness of (4.49) can be verified by inspecting if the shifted locus (X_0', Y_0') lies to the right of the straight line defined by $1 + x - \lambda y = 0$ for some $\lambda \geq 0$, $k \geq 1$.

4.4.2 Example: Rotating beam

To illustrate the applicability of the conditions for robust stability in Proposition 4.4.1, consider a rotating beam with a mass located at the tip, representing, for example, a robotic arm with end effector (Sciavicco and Siciliano, 2000). The plant dynamics from input torque τ to the tip deflection θ are not exactly known, but instead are known to belong to the set

$$\Pi = \{P(s) = P_0(s)\,(1 + W(s)\Delta(s)) \mid \Delta(s) \in \mathcal{RH}_\infty \text{ and } \|\Delta\|_\infty \leq 1\}\,, \quad (4.50)$$

where $P_0(s) = 1/s^2$ is a rigid body model of the beam, and

$$W(s) = \frac{3.5s^2 + 4.9s + 3.5}{s^2 + 27.2s + 289} \quad (4.51)$$

is a second-order weighting filter that accounts for unmodelled high-frequency dynamics such as, *e.g.*, the flexible modes of the beam or actuator/sensor dynamics (Sciavicco and Siciliano, 2000). For robustly stabilizing the beam around the horizontal position defined by $\theta^* = 0$, a HIGS-based feedback controller, being the series interconnection of HIGS and an LTI filter, is considered. The closed-loop configuration is depicted in Figure 4.7.

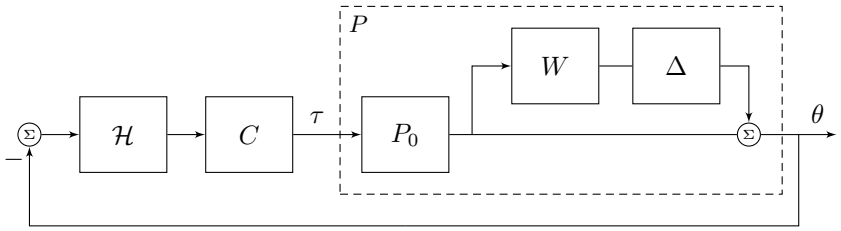

Figure 4.7. Feedback control configuration for the rotating flexible beam.

The linear part of the controller is constructed as the series interconnection of a lead filter, a second-order low-pass filter, and an additional zero, that is,

$$C(s) = k_p \left(\frac{s + \omega_z}{s + \omega_p}\right) \frac{\omega_{lp}^2 (s + \omega_c)}{s^2 + 2\beta\omega_{lp}s + \omega_{lp}^2}. \quad (4.52)$$

The lead filter in (4.52) is used for stabilizing the gain-mode dynamics, whereas the second-order low-pass filter is used for providing sufficient roll-off at high frequencies. The zero in (4.52) at ω_c in series with HIGS provides a (local) phase lag reduction in the control loop, intended to improve the transient properties of the closed-loop system, see also the design rationale as discussed earlier in Chapter 3. The controller (4.52) is initially designed on the basis of the nominal rigid-body model $P_0(s)$ in such a manner that the nominal closed-loop in

gain-mode is stable and satisfies a peaking constraint of 4 dB on the sensitivity function. Note that enforcing such a robustness bound helps in keeping the perturbation term (4.47) small, as this directly relates to the worst-case sensitivity in gain-mode. The resulting parameters are given by $k_p = 10$ N/m, $\omega_z = 0.8$ rad/s, $\omega_p = 9$ rad/s, $\omega_{lp} = 11$ rad/s, $\beta = 1.2$ and $\omega_c = \omega_h|1+4j\pi|$ rad/s, $k_h = 1$ and $\omega_h = 3.5$ rad/s.

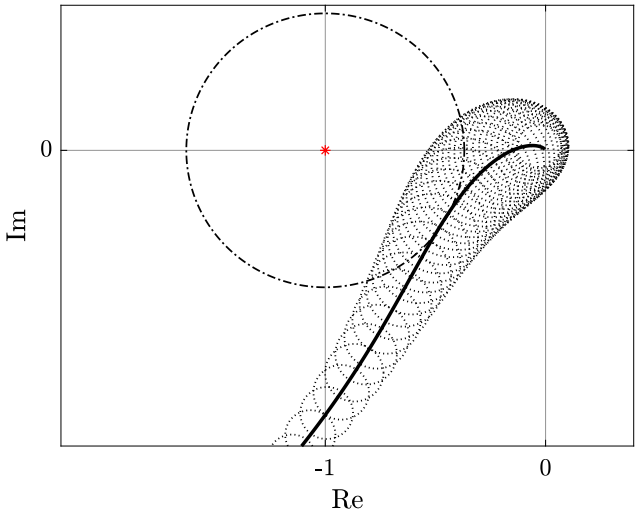

Figure 4.8. Uncertainty region around the nominal open-loop $L_0(j\omega) = k_h C(j\omega)P_0(j\omega)$ (black) generated by the multiplicative uncertainty. The critical point $(-1, 0)$ is not covered by this region, so the nominal gain-mode dynamics are robustly stable against the given uncertainty. The dashed-dotted circle indicates a 4 dB robustness bound (modulus margin) on the nominal system.

The nominal open-loop characteristics $L_0(j\omega) = k_h C(j\omega)P_0(j\omega)$ together with the uncertainty region generated by the multiplicative uncertainty are shown in Figure 4.8. From this figure it is concluded that condition (4.43) is satisfied, and the gain-mode dynamics are stable for all possible plants $P(s) \in \Pi$.

Verification of the frequency-domain condition in (4.44) is done by means of inspecting the shifted (X_0, Y_0)-locus in (4.49), as well as the uncertainty region around the nominal (X_0, Y_0)-locus generated by ellipsoids of the form described in (4.48). The corresponding plots (with $k = 10$) are given in Figure 4.9. First note on the basis of the nominal locus (black curve) in the figure that the nominal HIGS-based control system is ISS. Remark that for this case the conditions in Theorem 4.3.1 and Theorem 4.3.2 are not applicable due to the presence of a double integrator in the plant, and the unstable integrator-mode dynamics.

Regarding stability of the perturbed system, no conclusions can be drawn on

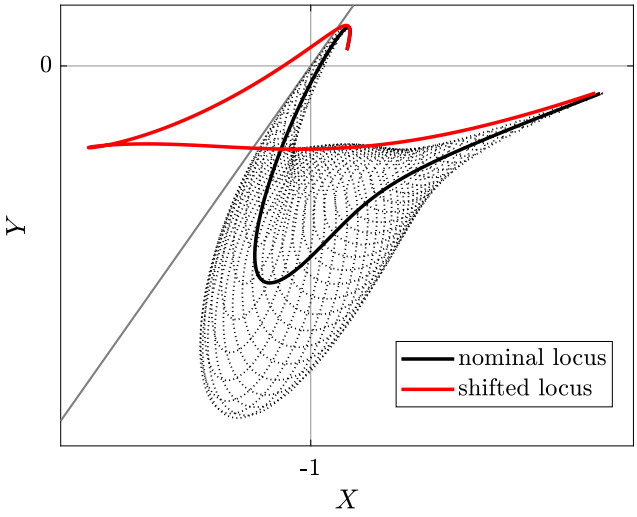

Figure 4.9. Verifying inequality (4.44) by means of *i*) the shifted (X_0, Y_0)-locus (red), and *ii*) the uncertainty region around the nominal (X_0, Y_0)-locus (black) generated by the ellipses described in (4.48). Stability for all $P(s) \in \Pi$ is verified by means of the latter approach with $k = 10$ and $\lambda = 1.05$.

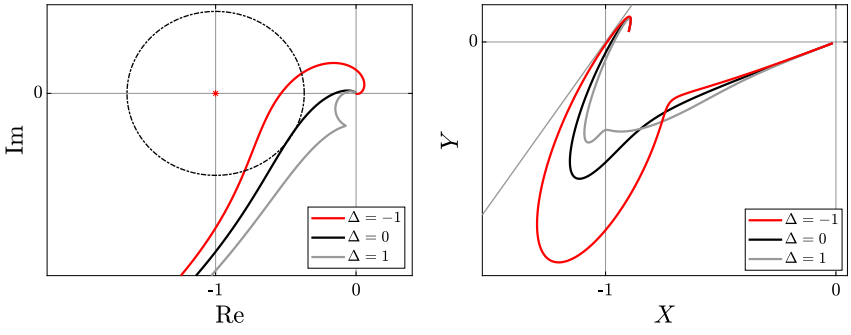

(a) Nyquist plot of the gain-mode. **(b)** Popov-like plot.

Figure 4.10. Graphical illustration of the conditions in Theorem 4.3.3 for the nominal plant $P(s) = P_0(s)$, and two perturbed plants $P(s) = P_0(s)(1 - W(s))$ and $P(s) = P_0(s)(1 + W(s))$.

the basis of the shifted (X_0, Y_0)-locus (red curve), as there is no $\lambda \geq 0$ such that this curve lies to the right of the line $1 + x - \lambda y = 0$. On the other hand, the ellipse-based uncertainty region (dotted) around the nominal locus is found to

remain to the right of such line with $\lambda = 1.05$ and thus (4.44) holds with $k = 10$ and $\lambda = 1.05$. This clearly illustrates that, despite its computational advantage, using the shifted locus for verifying inequality (4.44) can be more conservative than the approach using ellipses. Since all conditions in Proposition 4.4.1 are satisfied, one can conclude that the HIGS-based control system is ISS for all $P(s) \in \Pi$. For a final demonstration, two perturbed plants are considered with $\Delta(s) = -1$ and $\Delta(s) = 1$ for which the relevant plots are given in Figure 4.10. Conform the previous results, the conditions in Theorem 4.3.3 are satisfied and the corresponding closed-loop systems are ISS. A numerically obtained solution to the LMI problem in (4.10) for these cases that follows from satisfying the frequency-domain conditions in Theorem 4.3.3 is provided in Appendix 4.B.

4.5 Application to a motor-load motion system

In this section, applicability of the presented tools is demonstrated on an experimental motion control application. The set-up is shown in Figure 4.11 and consists of two rotating masses connected by a thin, flexible shaft. Non-collocated actuation is considered, *i.e.*, measurements by the encoder at the load side (right-side) are separated from actuation at the motor side (left side), see, *e.g.*, Preumont, 1997 for further details on these type of systems. The measured frequency-response function (FRF) of the plant $P(j\omega)$ from actuator input to encoder position of the load is shown in Figure 4.12, and is obtained from closed-loop measurements with a sampling frequency of 2 kHz.

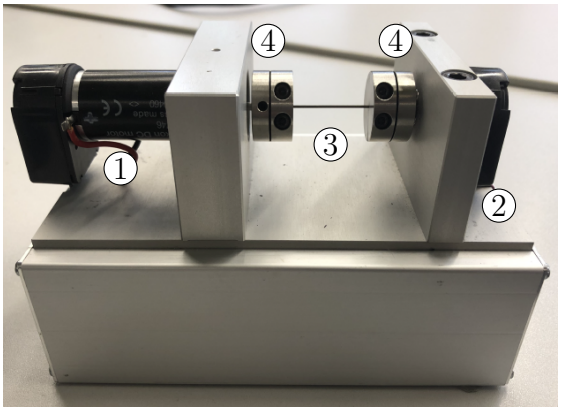

Figure 4.11. Experimental motor-load motion system set-up with ①: actuator (motor side), ②: encoder (load side), ③: flexible shaft, and ④: rotating masses.

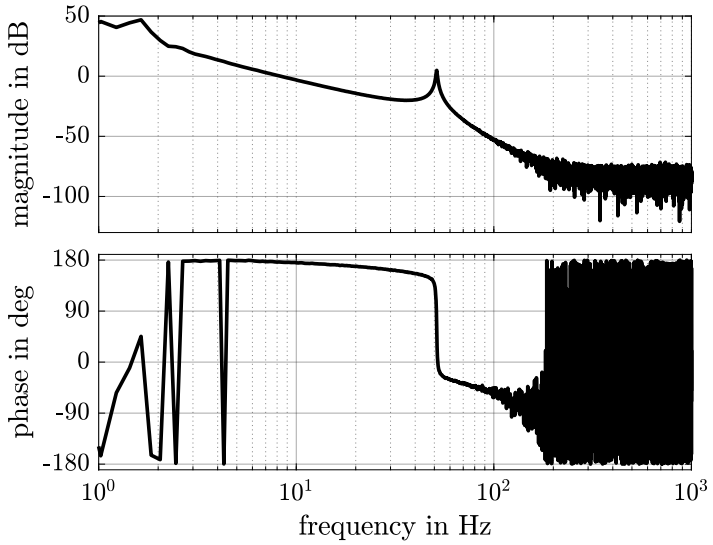

Figure 4.12. Measured frequency response function (FRF) of the experimental motor-load motion system.

4.5.1 Controller design

Consider the feedback control scheme as depicted in Figure 4.13. Given a reference command $r(t) \in \mathbb{R}$, a servo error signal $e(t)$ is constructed using the relation $e(t) = r(t) - q(t)$, where $q(t) \in \mathbb{R}$ represents the measured output of the motor-load motion system P at time $t \in \mathbb{R}_{\geq 0}$. This system is subject to an input disturbance $d(t) \in \mathbb{R}$ for $t \in \mathbb{R}_{\geq 0}$. For dealing with external (set-point

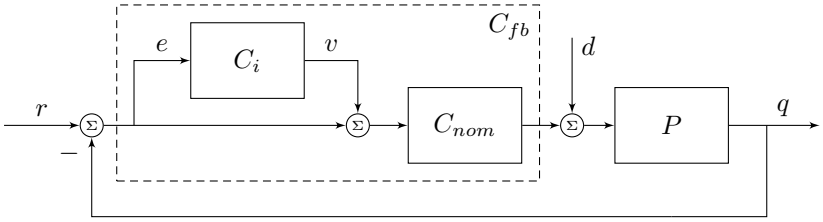

Figure 4.13. Feedback control scheme for the motor-load motion system.

induced) disturbances, a feedback controller $C_{fb} = (1 + C_i)C_{nom}$ with integral action is designed. The nominal LTI filter $C_{nom}(s)$ is given by

$$C_{nom}(s) = k_p \left(\frac{s + \omega_z}{s + \omega_p} \right) \left(\frac{\omega_{lp}^2}{s^2 + 2\beta_{lp}\omega_{lp}s + \omega_{lp}^2} \right), \tag{4.53}$$

whereas C_i is a HIGS-based integrator as depicted in Figure 4.14 with $\omega_c = \omega_h|1 + 4j/\pi|/k_h$. This specific HIGS-based integrator design stems from the ideas in Chapter 3 and is intended for balancing transient and steady-state performance properties in a more desirable manner.

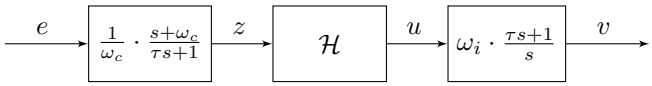

Figure 4.14. HIGS-based integrator C_i.

Tuning of the controller is done on the basis of the approach discussed previously in Section 4.3.3 by initially setting $\omega_h = \infty$ such that C_i effectively reduces to an LTI integrator and the linear scheme $C_{fb}(s) = (1 + \frac{\omega_i}{s})C_{nom}(s)$ is effectively recovered. Using classical loop-shaping techniques, a stable LTI design is obtained with $k_p = 3.3$ Nm, $\omega_i = 8 \cdot 2\pi$ rad/s, $\omega_z = 2 \cdot 2\pi$ rad/s, $\omega_p = 50 \cdot 2\pi$ rad/s, $\omega_{lp} = 50 \cdot 2\pi$ rad/s, and $\beta_{lp} = 0.5$. After fixing $k_h = 1$, and $\tau = 2 \cdot 10^{-3}$, the HIGS integrator frequency ω_h is reduced to $\omega_h = 5 \cdot 2\pi$ rad/s.

To verify ISS of the closed-loop system design, first observe that due to the simple integrators in C_i and P, one cannot apply Theorem 4.3.1 and thus one should resort to Theorem 4.3.2 or Theorem 4.3.3. The open-loop characteristics of the individual integrator- and gain-modes, given by

$$L_{int}(j\omega) = \left(1 + \frac{\omega_h}{j\omega}\left(\frac{\omega_i}{\omega_c} + \frac{\omega_i}{j\omega}\right)\right) C_{nom}(j\omega)P(j\omega),$$

$$L_{gain}(j\omega) = \left(1 + k_h\left(\frac{\omega_i}{\omega_c} + \frac{\omega_i}{j\omega}\right)\right) C_{nom}(j\omega)P(j\omega),$$

are inspected through the Nyquist plot depicted in Figure 4.15. On the basis of the Nyquist stability criterion, it immediately follows from this figure that the integrator-mode is unstable, whereas the gain-mode is stable. Hence, one cannot apply Theorem 4.3.2 either, and, hence, one should resort to the new result in Theorem 4.3.3 for a frequency-domain stability analysis. Note that in the configuration of Figure 4.13, the relevant transfer function from $y = -z$ to u needed for verifying the frequency-domain inequality in (4.31) is identified as

$$G_{yu}(j\omega) = \left(\frac{\omega_i}{\omega_c} + \frac{\omega_i}{j\omega}\right) \cdot \frac{C_{nom}(j\omega)P(j\omega)}{1 + C_{nom}(j\omega)P(j\omega)}. \tag{4.54}$$

The corresponding Popov-like plot with $k = 15$, and $\lambda = 10$ is shown in Figure 4.16. Clearly, for these values the frequency-domain inequality in (4.31) is satisfied, such that, together with stability of the gain-mode subsystem, all conditions of Theorem 4.3.3 are satisfied. Hence, the closed-loop system is ISS. Interestingly, the smallest value for which ISS could be shown on the basis of Theorem 4.3.3 was found to be $\omega_h = 1.5 \cdot 2\pi$ rad/s. For smaller values of ω_h,

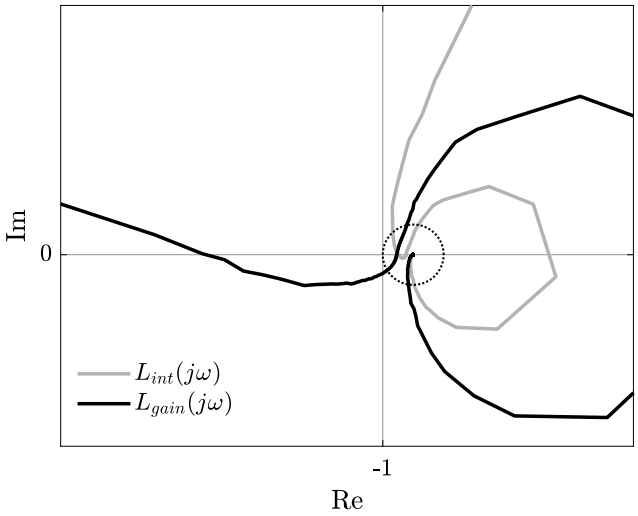

Figure 4.15. Nyquist plot of the open-loop characteristics of the integrator- and gain-mode using the measured FRF of the motor-load motion system.

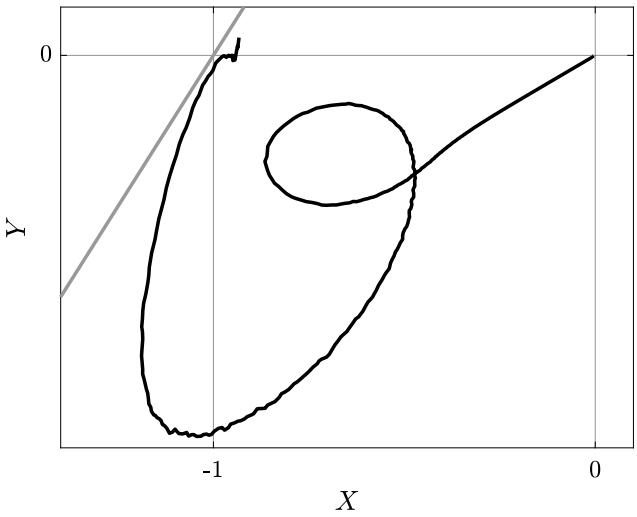

Figure 4.16. Popov-like plot constructed on the basis of the measured FRF of the motor-load motion system and parameter values $k = 15$, $\lambda = 10$.

satisfaction of the conditions in Theorem 4.3.3 is limited by the fact that the gain-mode dynamics become unstable. Nevertheless, for smaller values stable closed-loop behaviour was observed during experiments. For improving upon this aspect, it may be useful to refine the conditions in Theorem 4.3.3 to allow for unstable gain-mode dynamics as well.

Typical step-responses of the closed-loop system for $\omega_h \in \{5, 10, 100\} \cdot 2\pi$ rad/s are shown in Figure 4.17, and clearly demonstrate the beneficial effect of reducing ω_h on transient properties such as overshoot and settling times.

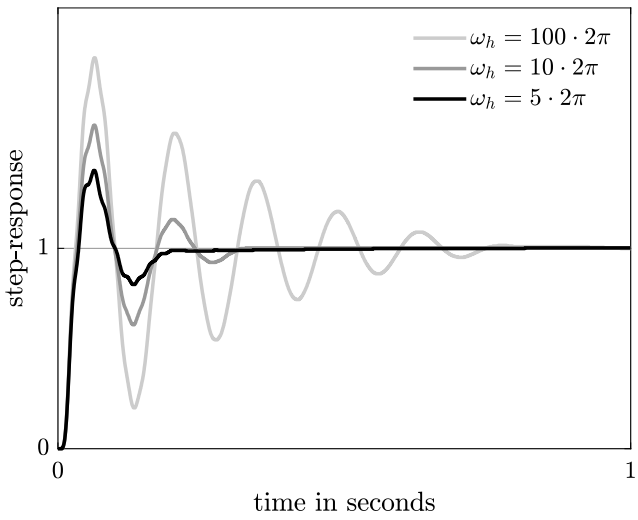

Figure 4.17. Measured time-responses of the closed-loop system with $\omega_h \in \{5, 10, 100\} \cdot 2\pi$ rad/s when subject to a step input $r(t) = 1$, $t \in \mathbb{R}_{\geq 0}$.

4.6 Summary

In this chapter, novel frequency-domain conditions for input-to-state stability (ISS) of HIGS-based control systems have been presented. The conditions result from exploiting integral properties of HIGS, and guarantee the existence of a quadratic Lyapunov function that is strictly positive only within the relevant subregion of the state-space where the dynamics of HIGS are active. As such, these conditions may provide a substantial advantage over existing results such as the circle-criterion in the sense of reducing conservatism in the analysis. The derived frequency-domain conditions can be verified graphically in a manner that is comparable to the classical Popov plot. An extension is made for verifying ISS of systems that are subject to multiplicative uncertainty, and several design

insights for (robust) HIGS-based controller design are addressed. Effectiveness of the presented tools is demonstrated by means of an experimental case-study on a benchmark motion control application.

Although the presented frequency-domain conditions for (robust) stability are particularly valuable for practical design and analysis purposes, at the same time these can still be conservative. This conservatism is a result from the fact that underlying the conditions is the use of a common quadratic Lyapunov function for an essentially piecewise linear system. In the next chapter, a stability and performance analysis based on *piecewise* quadratic Lyapunov functions is pursued. Such functions are known to introduce a significant amount of flexibility in the analysis, which can lead to reduced conservatism, though potentially at the expense of losing the more practically verifiable frequency-domain interpretation.

4.A Proofs and technical results

4.A.1 Preliminaries

Before stating the proofs of several theorems presented in this chapter, some useful preliminary results are given first. The following general version of the Kalman-Yakubovich-Popov (KYP)-lemma, which is free of any hypothesis on minimality of the system, is provided. This result will play a central role in the upcoming proofs (see also Leonov et al., 1996; Narendra and Taylor, 1973 for other versions of the KYP-lemma).

Theorem 4.A.1 (Rantzer, 1996, Theorem 1)**.** *Given $A \in \mathbb{R}^{n\times n}$, $B \in \mathbb{R}^{n\times m}$, $Q = Q^\top \in \mathbb{R}^{(n+m)\times(n+m)}$ with $\det(j\omega I - A) \neq 0$ for all $\omega \in \mathbb{R}$. The following two statements are equivalent:*

1. *For all $\omega \in \mathbb{R} \cup \{\infty\}$ the following inequality is satisfied*

$$\begin{bmatrix}(j\omega I - A)^{-1}B\\ I\end{bmatrix}^* Q \begin{bmatrix}(j\omega I - A)^{-1}B\\ I\end{bmatrix} \prec 0; \tag{4.55}$$

2. *There exists a symmetric matrix $P = P^\top \in \mathbb{R}^{n\times n}$ such that*

$$\begin{bmatrix}A^\top P + PA & PB\\ B^\top P & 0\end{bmatrix} + Q \prec 0. \tag{4.56}$$

The corresponding equivalence holds for non-strict inequalities in both (4.55) *and* (4.56)*, if the pair (A, B) is controllable.*

The following useful result for the scalar case ($m = 1$) is a special case of Theorem 4.A.1.

Lemma 4.A.2. *Given a Hurwitz matrix A, a vector $B \in \mathbb{R}^n$ and a matrix*

$$Q = \begin{bmatrix} 0 & -Q_{12} \\ -Q_{12}^\top & q_{22} \end{bmatrix} \tag{4.57}$$

with $q_{22} < 0$ and arbitrary $Q_{12} \in \mathbb{R}^n$ for which the conditions in Theorem 4.A.1 are satisfied. Then there exist a positive definite matrix $P \in \mathbb{R}^{n\times n}$, a positive semi-definite matrix $N = N^\top \in \mathbb{R}^{n\times n}$, a vector $L \in \mathbb{R}^n$ and a number $\varepsilon > 0$ that satisfy

$$A^\top P + PA = -L^\top L - N - \varepsilon P \tag{4.58}$$

$$PB = Q_{12} - \sqrt{|q_{22}|}L^\top. \tag{4.59}$$

Proof. Note that since A is Hurwitz, $\det(j\omega I - A) \neq 0$ for all $\omega \in \mathbb{R}$, such that Theorem 4.A.1 can be applied for A, B, and Q as in (4.57). Since $q_{22} < 0$ it follows by virtue of the Schur complement that (4.56) is equivalent to

$$A^\top P + PA + \frac{1}{|q_{22}|}\left(PB - Q_{12}\right)\left(PB - Q_{12}\right)^\top \prec 0, \tag{4.60}$$

which implies the existence of a matrix $\hat{N} = \hat{N}^\top \succ 0$ and a number $\varepsilon > 0$ such that

$$A^\top P + PA + \frac{1}{|q_{22}|}\left(PB - Q_{12}\right)\left(PB - Q_{12}\right)^\top = -(\hat{N} - \varepsilon P) - \varepsilon P. \tag{4.61}$$

By choosing ε sufficiently small, one can always ensure the matrix $N := \hat{N} - \varepsilon P$ to be positive (semi-)definite. Define

$$L^\top = \frac{1}{\sqrt{|q_{22}|}}\left(PB - Q_{12}\right) \tag{4.62}$$

and substitute this identity in (4.61) to obtain (4.58) and (4.59). It remains to show that P is positive definite. Since (4.58) implies $A^\top P + PA \prec 0$ and A is Hurwitz, the result is immediate (see, *e.g.*, Leonov et al., 1996, Lemma 1.10.1). This completes the proof. □

4.A.2 Summary of relevant matrices

The upcoming proofs heavily exploit structure in the system matrices defined in the main text of this chapter. For readability of the proofs, relevant matrices are briefly summarized here. Matrices related to the closed-loop system in (4.6) are given by

$$A_1 = \begin{bmatrix} A_g & B_g \\ -\omega_h C_g & 0 \end{bmatrix}, \quad A_2 = \begin{bmatrix} A_g & B_g \\ -k_h C_g A_g & 0 \end{bmatrix}, \quad B = \begin{bmatrix} B_w \\ 0 \end{bmatrix}, \tag{4.63}$$

and $C = \begin{bmatrix} C_g & 0 \end{bmatrix}$, with matrices (A_g, B_g, B_w, C_g) given in (4.1). Furthermore, the extended system matrix in gain-mode is given by $\mathcal{A}_2 = A_2 + k\frac{\omega_h}{k_h} bH$ with

$$b = \begin{bmatrix} 0 & 1 \end{bmatrix}^\top, \quad \text{and} \quad H = \begin{bmatrix} -k_h C_g & -1 \end{bmatrix} = k_h C_z - C_u, \tag{4.64}$$

and in which

$$C_z = -C = \begin{bmatrix} -C_g & 0 \end{bmatrix}, \quad \text{and} \quad C_u = b^\top = \begin{bmatrix} 0 & 1 \end{bmatrix}. \tag{4.65}$$

Additional S-procedure matrices related to the set of LMIs in Theorem 4.2.2 are given by $\Theta^\top = [I \;\; -k_h C_g^\top]$, and

$$S = \begin{bmatrix} C_u \\ k_h C_z - C_u \end{bmatrix}, \quad T = \begin{bmatrix} C_u \\ C_z\left(\omega_h I - k_h A_2\right) \end{bmatrix}, \quad J = \begin{bmatrix} 0 & 1 \\ 1 & 0 \end{bmatrix}. \tag{4.66}$$

Other matrices relevant in the proofs will be specified in detail when needed.

4.A.3 Proof of Theorem 4.3.1

$(i) \implies (ii)$. First observe that by Assumption 2.3.1 one has $\lim_{\omega\to\infty}\left(1 + \mathrm{Re}\left\{k_h C_g (j\omega I - A_g)^{-1} B_g\right\}\right) > 0$. Indeed, due to the assumption on the relative degree of $G_{yu}(s) = C_g(sI - A_g)^{-1}B_g$ one has $\lim_{|\omega|\to\infty} G_{yu}(j\omega) = 0$. Remark that satisfaction of the frequency-domain inequality (4.14) implies that $1 - \epsilon + \mathrm{Re}\left\{k_h G_{yu}(j\omega)\right\} > 0$ for all $\omega \in \mathbb{R} \cup \{\infty\}$ must be satisfied for some sufficiently small $0 < \epsilon < 1$. Since A_g is Hurwitz, one finds $\det(j\omega I - A_g) \neq 0$, such that (4.55) in item 1 of Theorem 4.A.1 is satisfied for

$$Q = \begin{bmatrix} 0 & k_h C_g^\top \\ k_h C_g & -2(1-\epsilon) \end{bmatrix}.$$

Furthermore, by Lemma 4.A.2 there exist matrices $M = M^\top \succ 0$, $N = N^\top \succeq 0$ and L, and a constant $\varepsilon > 0$ such that

$$A_g^\top M + M A_g = -L^\top L - \varepsilon M - N, \tag{4.67a}$$

$$M B_g = k_h C_g^\top - \sqrt{2(1-\epsilon)} L^\top. \tag{4.67b}$$

Take $P = \mathrm{diag}(M, m)$ with $m = \mu/\omega_h$ and $\mu > 0$ such that $P \succ 0$. As such, (4.10a) is satisfied with $\tau_1 = 0$. Next, observe that with this choice for P together with the equalities in (4.67), one finds

$$\begin{aligned} A_1^\top P + P A_1 &= \begin{bmatrix} A_g^\top M + M A_g & M B_g - \mu C_g^\top \\ B_g^\top M - \mu C_g & 0 \end{bmatrix} \\ &= -U^\top U + \begin{bmatrix} -\varepsilon M - N & (k_h - \mu) C_g^\top \\ (k_h - \mu) C_g & 2(1-\epsilon) \end{bmatrix}, \end{aligned} \tag{4.68}$$

with $U = [L, \sqrt{2(1-\epsilon)}]$. Next, note that

$$S^\top JS = \begin{bmatrix} 0 & -k_h C_g^\top \\ -k_h C_g & -2 \end{bmatrix}, \tag{4.69}$$

such that one finds

$$A_1^\top P + PA_1 + S^\top JS = -U^\top U + \begin{bmatrix} -\varepsilon M - N & -\mu C_g^\top \\ -\mu C_g & -2\epsilon \end{bmatrix}. \tag{4.70}$$

Via the Schur complement, it follows that the right-hand side of (4.70) is negative definite if $-\varepsilon M + \frac{\mu^2}{2\epsilon} C_g^\top C_g \prec 0$. Since M is positive definite, one finds

$$-\varepsilon M + \frac{\mu^2}{2\epsilon} C_g^\top C_g \preceq \left(-\varepsilon \lambda_{\min}(M) + \frac{\mu^2}{2\epsilon} \lambda_{\max}(C_g^\top C_g) \right) I, \tag{4.71}$$

which, by choosing $0 < \mu < \sqrt{\varepsilon \lambda_{\min}(M) / (2\epsilon \lambda_{\max}(C_g^\top C_g))}$ ensures (4.70) to be negative definite. Hence, (4.10b) is satisfied with $\tau_2 = 1$.

In a similar manner, observe that the above choice for P together with the equalities in (4.67) leads to

$$\begin{aligned} A_2^\top P + PA_2 &= \begin{bmatrix} A_g^\top M + MA_g & MB_g - \mu \frac{k_h}{\omega_h} (C_g A_g)^\top \\ B_g^\top M - \mu \frac{k_h}{\omega_h} C_g A_g & 0 \end{bmatrix} \\ &= -U^\top U + \begin{bmatrix} -\varepsilon M - N & k_h C_g^\top - \mu \frac{k_h}{\omega_h} (C_g A_g)^\top \\ k_h C_g - \mu \frac{k_h}{\omega_h} C_g A_g & 2(1-\epsilon) \end{bmatrix}, \end{aligned} \tag{4.72}$$

and note that

$$T^\top JT = \begin{bmatrix} 0 & (k_h A_g - \omega_h I)^\top C_g^\top \\ C_g (k_h A_g - \omega_h I) & 0 \end{bmatrix}. \tag{4.73}$$

Now consider $\Gamma = [0, 1]$ and $m = \mu/\omega_h$, and observe that one then finds

$$A_2^\top P + PA_2 + mT^\top JT + \Gamma^\top H + H^\top \Gamma = -U^\top U + \begin{bmatrix} -\varepsilon M - N & -\mu C_g^\top \\ -\mu C_g & -2\epsilon \end{bmatrix}. \tag{4.74}$$

A similar choice for μ as above makes the right-hand side of (4.74) negative definite. Since $H\Theta = 0$ one finds

$$\Theta^\top \left(A_2^\top P + PA_2 + mT^\top JT \right) \Theta \prec 0, \tag{4.75}$$

such that (4.10c) is satisfied with $\tau_3 = m = \mu/\omega_h$.

$(ii) \implies (i)$. Suppose the LMIs (4.10) are feasible with $P = \operatorname{diag}(M, m) \succ 0$, $\tau_1 = 0$, $\tau_2, \tau_3 \geq 0$. Then, one finds from (4.10b)

$$A_1^\top P + PA_1 + \tau_2 S^\top JS = \begin{bmatrix} A_g^\top M + MA_g & MB_g - \gamma k_h C_g^\top \\ B_g^\top M - \gamma k_h C_g & -2\tau_2 \end{bmatrix} \prec 0, \tag{4.76}$$

with $\gamma = \tau_2 + m\omega_h/k_h > 0$. From this inequality it immediately follows that

$$\begin{bmatrix} A_g^\top L + L A_g & L B_g - k_h C_g^\top \\ B_g^\top L - k_h C_g & -2 \end{bmatrix} \prec 0, \tag{4.77}$$

with $L = M/\gamma$. By the KYP-lemma (Theorem 4.A.1) this implies

$$1 + \mathrm{Re}\left\{k_h C_g (j\omega I - A_g)^{-1} B_g\right\} > 0 \tag{4.78}$$

for all $\omega \in \mathbb{R} \cup \{\infty\}$, which completes the proof.

4.A.4 Proof of Theorem 4.3.2

$(i) \implies (ii)$. First of all, observe that the transfer function defined by $W(j\omega) = c(j\omega I - A_1)^{-1} b$ has a relative degree of one such that $\lim_{|\omega|\to\infty} \mathrm{Re}\{W(j\omega)\} = 0$. Since by assumption A_1 is Hurwitz, one finds $\det(j\omega I - A_1) \neq 0$ for all $\omega \in \mathbb{R}$. Together with satisfaction of the frequency-domain inequality (4.15) this implies the transfer function $1 + W(j\omega)$ to satisfy the frequency-domain inequality in Theorem 4.A.1 with

$$Q = \begin{bmatrix} 0 & c^\top \\ c & -2 \end{bmatrix}, \tag{4.79}$$

in which $c = C_z(\omega_h I - k_h A_2) + \alpha_1 C_z + \alpha_2 H$. By Lemma 4.A.2 it follows that this is equivalent to the existence of matrices $P = P^\top \succ 0$, $N = N^\top \succeq 0$ and L, and a constant $\varepsilon > 0$ such that

$$A_1^\top P + P A_1 = -L^\top L - \varepsilon P - N \tag{4.80a}$$

$$P b = c^\top - \sqrt{2} L^\top. \tag{4.80b}$$

It immediately follows that (4.10a) and (4.10b) are satisfied with $\tau_1 = \tau_2 = 0$. Next, observe that $A_2 = A_1 - bK$ with $b = [0, 1]$ and $K = C_z(\omega_h I - k_h A_2)$, and consider

$$\begin{aligned} A_2^\top P + P A_2 &= A_1^\top P + P A_1 - P b K - (bK)^\top P \\ &= -L^\top L - \varepsilon P - N - \mathrm{He}\left(c^\top K - \sqrt{2} L^\top K\right) \\ &\preceq -(L - \sqrt{2}K)^\top (L - \sqrt{2}K) - \mathrm{He}\left((\alpha_1 C_z + \alpha_2 H)^\top K\right) \end{aligned} \tag{4.81}$$

where $H = k_h C_z - C_u$ and $\mathrm{He}(X) = X^\top + X$. From this, one can find

$$\begin{aligned} &A_2^\top P + P A_2 + (\alpha_1 + \alpha_2)(H^\top K + K^\top H) + \tau_3 T^\top J T \\ &\quad \preceq -\varepsilon P - (L - \sqrt{2}K)^\top (L - \sqrt{2}K) + \left(\tau_3 - \frac{\alpha_1}{k_h}\right)(C_u^\top K + K^\top C_u), \end{aligned} \tag{4.82}$$

such that the choice $\tau_3 = \alpha_1/k_h$ makes (4.82) negative definite. Since $H\Theta = 0$, one finds that negative definiteness of the matrix in the left-hand side of (4.82) implies

$$\Theta^\top \left(A_2^\top P + P A_2 + \tau_3 T^\top J T\right) \Theta \prec 0. \tag{4.83}$$

Hence, (4.10c) is satisfied with $\tau_3 = \alpha_1/k_h$.
$(ii) \implies (i)$. Suppose that the LMIs (4.10) are feasible for some $P \succ 0$, $\tau_1 = \tau_2 = 0$ and $\tau_3 \geq 0$. From Finsler's lemma it follows that there exists a constant $\gamma \in \mathbb{R}$ such that the following set of LMIs is satisfied:

$$A_1^\top P + PA_1 \prec 0, \tag{4.84a}$$
$$A_2^\top P + PA_2 + \tau_3 T^\top JT + \gamma H^\top H \prec 0. \tag{4.84b}$$

Two possible cases arise: $\gamma \geq 0$ and $\gamma < 0$. In both cases it still holds that $A_1^\top P + PA_1 - |\gamma| H^\top H \prec 0$ and $A_2^\top P + PA_2 + \tau_3 T^\top JT - |\gamma| H^\top H \prec 0$. Using the identities $A_2 = A_1 - bK$, $T^\top JT = C_u^\top K + K^\top C_u$, and $b = C_u^\top$, the second inequality can equivalently be written as

$$A_1^\top P + PA_1 - (P - \tau_3 I)bK - (bK)^\top (P - \tau_3 I) - |\gamma| H^\top H \prec 0. \tag{4.85}$$

As the difference between (4.85) and the inequality $A_1^\top P + PA_1 - |\gamma| H^\top H \prec 0$ is given by $(Pb - \tau_3 b)K - K^\top (b^\top P + \tau_3 b^\top)$, it immediately follows from Kamenetskiy, 2017, Theorem 1 that there exists a number $\varepsilon_1 > 0$ such that

$$\begin{aligned} &A_1^\top P + PA_1 - |\gamma| H^\top H \\ &+ \left(\frac{\varepsilon_1}{\sqrt{2}} Pb - \frac{1}{\varepsilon_1 \sqrt{2}} (\tau C_u + K)^\top \right) \left(\frac{\varepsilon_1}{\sqrt{2}} Pb - \frac{1}{\varepsilon_1 \sqrt{2}} (\tau C_u + K)^\top \right)^\top \prec 0, \end{aligned} \tag{4.86}$$

where $\tau = \tau_3 \varepsilon_1^2$. By using the vector property $aa^\top - bb^\top = \frac{1}{2}(a+b)(a-b)^\top + \frac{1}{2}(a-b)(a+b)^\top$ together with (4.86) and the fact that $A_1^\top P + PA_1 \prec 0$, it again follows from Kamenetskiy, 2017, Theorem 1 that there exists a number $\varepsilon_2 > 0$ such that

$$A_1^\top P + PA_1 + \left(\frac{\varepsilon_2}{\sqrt{2}} p + \frac{1}{\varepsilon_2 \sqrt{2}} q \right) \left(\frac{\varepsilon_2}{\sqrt{2}} p + \frac{1}{\varepsilon_2 \sqrt{2}} q \right)^\top \prec 0, \tag{4.87}$$

with

$$p = \left(\frac{\varepsilon_1}{2} Pb - \frac{1}{2\varepsilon_1} (\tau C_u + K)^\top \right) + \sqrt{\frac{|\gamma|}{2}} H^\top, \tag{4.88a}$$
$$q = \left(\frac{\varepsilon_1}{2} Pb - \frac{1}{2\varepsilon_1} (\tau C_u + K)^\top \right) - \sqrt{\frac{|\gamma|}{2}} H^\top. \tag{4.88b}$$

Denote $\bar{b} = \frac{\varepsilon_1}{2} b$, $\bar{c} = \frac{1}{2\varepsilon_1} (\tau C_u + K)^\top$, and $\bar{h} = \sqrt{\frac{|\gamma|}{2}} H^\top$ such that $p = P\bar{b} - \bar{c} + \bar{h}$ and $q = P\bar{b} - \bar{c} - \bar{h}$, and (4.87) can be written as

$$A_1^\top P + PA_1 + \rho^2 \left(P\bar{b} - \bar{c} + \kappa \bar{h} \right) \left(P\bar{b} - \bar{c} + \kappa \bar{h} \right)^\top \prec 0, \tag{4.89}$$

where $\rho = \frac{\varepsilon_2}{\sqrt{2}} + \frac{1}{\varepsilon_2\sqrt{2}}$ and $\kappa = 1 - 2/(\rho\varepsilon_2\sqrt{2}) = 1 - 2/(\varepsilon_2^2+1)$. Note that $-1 < \kappa < 1$ and $\rho \geq \sqrt{2}$ for all $\varepsilon_2 > 0$, and thus (4.89) implies that

$$A_1^\top P + PA_1 + 2\left(P\bar{b} - \bar{c} + \kappa\bar{h}\right)\left(P\bar{b} - \bar{c} + \kappa\bar{h}\right)^\top \prec 0 \tag{4.90}$$

also holds. By applying the Schur complement to (4.90) one finds

$$\begin{bmatrix} A_1^\top P + PA_1 & \sqrt{2}(P\bar{b} - \bar{c} + \kappa\bar{h}) \\ \sqrt{2}(P\bar{b} - \bar{c} + \kappa\bar{h})^\top & -1 \end{bmatrix} \prec 0, \tag{4.91}$$

which, by the KYP-lemma (Theorem 4.A.1) is equivalent to the frequency-domain inequality for all $\omega \in \mathbb{R} \cup \{\infty\}$

$$\begin{aligned} &1+4\mathrm{Re}\left\{(\bar{c} - \kappa\bar{h})(j\omega I - A_1)^{-1}\bar{b}\right\} \\ &\quad = 1 + \mathrm{Re}\left\{(F + \beta_1 C_u + \beta_2 H(j\omega I - A_1)^{-1}b\right\} > 0, \end{aligned} \tag{4.92}$$

with $\beta_1 = \tau$ and $\beta_2 = -\kappa\varepsilon_1\sqrt{2|\gamma|}$. This corresponds to the frequency-domain inequality (4.15) with $\alpha_1 = k_h\beta_1$ and $\alpha_2 = \beta_2 - \beta_1$. This completes the proof.

4.A.5 Proof of Theorem 4.3.3

First note that from the assumption that $A_g - k_h B_g C_g$ is Hurwitz and $k \geq 1$, it follows that the matrix $\mathcal{A}_2 = A_2 + k\frac{\omega_h}{k_h}bH$ is Hurwitz. To see this, consider the similarity transformation $T\mathcal{A}_2T^{-1}$ with

$$T = \begin{bmatrix} I & 0 \\ k_h C_g & 1 \end{bmatrix}, \quad \text{and} \quad T^{-1} = \begin{bmatrix} I & 0 \\ -k_h C_g & 1 \end{bmatrix}, \tag{4.93}$$

which leads to

$$\bar{\mathcal{A}}_2 := T\mathcal{A}_2T^{-1} = \begin{bmatrix} A_g - k_h B_g C_g & B_g \\ 0 & -k\frac{\omega_h}{k_h} \end{bmatrix}. \tag{4.94}$$

Due to its upper triangular structure, the eigenvalues of the matrix $\bar{\mathcal{A}}_2$ in (4.94) are given by the eigenvalues of $A_g - k_h B_g C_g$ and $-k\omega_h/k_h$. Therefore, $\bar{\mathcal{A}}_2$ is Hurwitz, and thus also $\mathcal{A}_2$ is Hurwitz.

Next, observe that the transfer function

$$W(j\omega) = \left(\lambda k C_u + F + \left(\lambda + k\frac{\omega_h}{k_h}\right)H\right)(j\omega I - \mathcal{A}_2)^{-1}b$$

with $F = C_z(k_h A_1 - \omega_h I)$ has a relative degree of at least one. Hence, one finds $\lim_{|\omega|\to\infty} \mathrm{Re}\{W(j\omega)\} = 0$. Since $\mathcal{A}_2$ is Hurwitz, it follows that $\det(j\omega I - \mathcal{A}_2) \neq 0$ for all $\omega \in \mathbb{R}$. Together with satisfaction of the frequency-domain inequality

in (4.16), this implies the transfer function $1 + W(j\omega)$ to satisfy the frequency-domain inequality in Theorem 4.A.1 with

$$Q = \begin{bmatrix} 0 & \left(\lambda k C_u + F + \left(\lambda + k\frac{\omega_h}{k_h}\right) H\right)^\top \\ \lambda k C_u + F + \left(\lambda + k\frac{\omega_h}{k_h}\right) H & -2 \end{bmatrix}. \quad (4.95)$$

By virtue of Lemma 4.A.2 this implies the existence of matrices $M = M^\top \succ 0$, $N = N^\top \succeq 0$ and L, and a constant $\varepsilon > 0$ such that

$$\mathcal{A}_2^\top M + M\mathcal{A}_2 = -L^\top L - \varepsilon M - N \quad (4.96a)$$

$$Mb = \lambda(kC_u + H)^\top + F^\top + k\frac{\omega_h}{k_h} H^\top - \sqrt{2} L^\top. \quad (4.96b)$$

Since $\mathcal{A}_2 = A_1 + bG$ with $G = F + k\frac{\omega_h}{k_h} H$ the equalities in (4.96) yield

$$\begin{aligned} &A_1^\top M + M A_1 = -G^\top b^\top M - MbG - L^\top L - \varepsilon M - N \\ &= -\mathrm{He}\left(\left(\lambda(kC_u + H)^\top + G^\top - \sqrt{2} L^\top\right) G\right) - L^\top L - \varepsilon M - N \\ &= -\left(L - \sqrt{2} G\right)^\top \left(L - \sqrt{2} G\right) - \mathrm{He}\left(\lambda(kC_u + H)^\top G\right) - \varepsilon M - N \\ &\prec -\lambda \left((kC_u + H)^\top \left(F + k\frac{\omega_h}{k_h} H\right) + \left(F + k\frac{\omega_h}{k_h} H\right)^\top (kC_u + H) \right), \end{aligned} \quad (4.97)$$

where $\mathrm{He}(X) = X^\top + X$. Observe that one can write $F = HA_1$ such that

$$(kC_u + H)^\top F = (kC_u + H)^\top H A_1 = (kS^\top JS + H^\top H) A_1 - k\omega_h H^\top C_z, \quad (4.98)$$

where use is made of the identities $S^\top JS = C_u^\top H + H^\top C_u$, and $C_u A_1 = \omega_h C_z$. Substituting (4.98) in (4.97) yields

$$\begin{aligned} A_1^\top M + M A_1 + \lambda \mathrm{He} \Bigg(&(kS^\top JS + H^\top H) A_1 \\ &\left(k\frac{\omega_h}{k_h}(kC_u + H) - k\omega_h C_z\right)^\top H \Bigg) \prec 0. \end{aligned} \quad (4.99)$$

Choose $P = (M + \lambda H^\top H) + \lambda k S^\top JS$ and observe that since $M \succ 0$, this choice yields $P - \lambda k S^\top JS \succ 0$. Hence, (4.10a) is satisfied with $\tau_1 = \lambda k \geq 0$. Furthermore, with this choice for P, (4.99) evaluates to

$$A_1^\top P + P A_1 + \lambda \frac{\omega_h}{k_h} \mathrm{He}\left((k(kC_u + H) - kk_h C_z)^\top H\right) \prec 0. \quad (4.100)$$

Since $C_z = \frac{1}{k_h}(H + C_u)$ the last term in the left-hand side of (4.100) yields

$$\lambda k(kC_u + H)^\top H - \lambda k k_h C_z^\top H = \lambda k(k-1) C_u^\top H. \quad (4.101)$$

Under the assumption that $\lambda \geq 0, k \geq 1$, and with the identity $S^\top JS = C_u^\top H + H^\top C_u$ this yields

$$A_1^\top P + PA_1 + \tau_2 S^\top JS \prec 0, \tag{4.102}$$

with $\tau_2 = \lambda k \omega_h (k-1)/k_h \geq 0$. As such, (4.10b) is satisfied. Additionally, with the choice for P, one finds from the equality in (4.96a) that

$$\mathcal{A}_2^\top M + M\mathcal{A}_2 = \mathcal{A}_2^\top P + P\mathcal{A}_2 - \lambda \mathrm{He}\left(H^\top \left((H + kC_u)\mathcal{A}_2 - k^2 C_u^\top H\right)\right) \prec 0. \tag{4.103}$$

Since $H\Theta = 0$, (4.10c) is satisfied with $\tau_3 = 0$. This completes the proof.

4.A.6 Proof of Proposition 4.4.1

The proof is based on showing that, when (4.43) and (4.44) are satisfied, the conditions of Theorem 4.3.3 hold for all $G_{yu}(s) \in \Pi$. Namely, for all possible plants 1) the gain-mode dynamics are stable, and 2) the frequency-domain inequality (4.16) is satisfied.

1) **Stability of the gain-mode dynamics for all $G_{yu}(s) \in \Pi$.**
Consider the open-loop characteristics of the gain-mode dynamics, which, under the assumption of multiplicative uncertainties, can be represented as

$$L(s) = k_h G_{yu}(s) = L_0(s)(1 + W(s)\Delta(s)), \tag{4.104}$$

where $L_0(s) = k_h G_0(s)$ denotes the nominal open-loop. From the assumption that the nominal closed-loop gain-mode dynamics are stable, it immediately follows from Skogestad and Postlethwaite, 2010, Section 7.5 that when (4.43) holds for all $\omega \in \mathbb{R}$, the nominal gain-mode dynamics are robustly stable with respect to all allowable perturbations. Therefore, under the hypothesis of the proposition, the gain-mode dynamics are stable for all $G_{yu}(s) \in \Pi$.

2) **Satisfying the frequency-domain inequality in** (4.16) **for all $G_{yu}(s) \in \Pi$.**
Observe that the complementary sensitivity function $T(s)$ can be written as

$$T(s) = \frac{k_h G_{yu}(s)}{1 + k_h G_{yu}(s)} = \frac{L(s)}{1 + L(s)} = T_0(s)(1 + W(s)\Delta_T(s)), \tag{4.105}$$

with

$$T_0(s) = \frac{L_0(s)}{1 + L_0(s)}, \quad \text{and} \quad \Delta_T(s) = \frac{\Delta(s)}{1 + L(s)}. \tag{4.106}$$

Since $\Delta(s) \in \mathcal{RH}_\infty$, it follows that whenever the gain-mode is robustly stable, one has $\Delta_T(s) \in \mathcal{RH}_\infty$. The magnitude of the relative uncertainty

in $T(s)$ then admits an upper-bound of

$$\|\Delta_T(j\omega)\| \leq \frac{1}{\|1 + L_0(j\omega)\| - \|W(j\omega)L_0(j\omega)\|}, \tag{4.107}$$

which follows from selecting the worst-case perturbation $\|\Delta(j\omega)\| = 1$ for all $\omega \in \mathbb{R}$ such that the complex numbers $1 + L_0(j\omega)$ and $W(j\omega)\Delta(j\omega)L_0(j\omega)$ point in opposite directions. Observe that this corresponds to an upper-bound on the magnitude of all possible sensitivity functions $S(s) = 1 - T(s)$.

From substituting the perturbed system (4.105) in the frequency-domain inequality (4.31), it follows that this inequality is satisfied for all possible plants $G_{yu}(s) \in \Pi$ if

$$1 + (X_0(\omega, k) + \delta_x(\omega, k)) - \lambda(Y_0(\omega, k) + \delta_y(\omega, k)) > 0. \tag{4.108}$$

Here, the nominal terms are given by

$$\begin{aligned} X_0(\omega, k) &= \frac{\omega_h}{k_h}\mathrm{Re}\left\{(T_0(j\omega) - k)C_l(j\omega)\right\} + \omega\mathrm{Im}\left\{T_0(j\omega)C_l(j\omega)\right\}, \\ Y_0(\omega, k) &= k\mathrm{Re}\left\{T_0(j\omega)C_l(j\omega)\right\} + (1 - k)\mathrm{Re}\left\{C_l(j\omega)\right\}, \end{aligned}$$

and the perturbations are expressed as

$$\begin{aligned} \delta_x(\omega, k) &= \frac{\omega_h}{k_h}\delta_u(\omega) + \omega\delta_v(\omega), \\ \delta_y(\omega, k) &= k\delta_u(\omega), \end{aligned}$$

in which δ_u and δ_v are given by

$$\begin{aligned} \delta_u(\omega) &= \mathrm{Re}\left\{T_0(j\omega)W(j\omega)\Delta_T(j\omega)C_l(j\omega)\right\}, \\ \delta_v(\omega) &= \mathrm{Im}\left\{T_0(j\omega)W(j\omega)\Delta_T(j\omega)C_l(j\omega)\right\}, \end{aligned}$$

and satisfy the constraint

$$\sqrt{\delta_u^2(\omega) + \delta_v^2(\omega)} \leq \frac{\|T_0(j\omega)W(j\omega)C_l(j\omega)\|}{\|1 + L_0(j\omega)\| - \|W(j\omega)L_0(j\omega)\|} := \rho(\omega). \tag{4.111}$$

The minimum of (4.108) subject to the constraint in (4.111) can be estimated as follows. Observe that one may write

$$\delta_u(\omega) = \nu(\omega)\cos(\theta), \quad \text{and} \quad \delta_v(\omega) = \nu(\omega)\sin(\theta), \tag{4.112}$$

where $\nu(\omega) \leq \rho(\omega)$, and $\theta \in [0, 2\pi]$. Then, using the standard trigonometric identity $a\cos(\phi) + b\sin(\phi) = \sqrt{a^2 + b^2}\cos(\phi - \psi)$ with $\psi = \arctan(b/a)$ it follows that (4.108) reads

$$1 + X_0(\omega, k) - \lambda Y_0(\omega, k) + \gamma(\omega)\cos(\theta - \varphi) > 0 \tag{4.113}$$

where

$$\gamma(\omega) = \nu(\omega)\sqrt{\left(\frac{\omega_h}{k_h} - \lambda k\right)^2 + \omega^2}, \quad \text{and} \quad \varphi = \arctan\left(\frac{(k_h\omega)^2}{(\omega_h - \lambda k k_h)^2}\right).$$

The minimum of the left-hand side in (4.113) over all possible perturbations is given by

$$1 + X_0(\omega, k) - \lambda Y_0(\omega, k) - \rho(\omega)\sqrt{\left(\frac{\omega_h}{k_h} - \lambda k\right)^2 + \omega^2} > 0. \tag{4.114}$$

Hence, satisfying (4.114) for some $\lambda \geq 0$ and $k \geq 1$ implies that the inequality in (4.31), and, therefore the one in (4.16) is satisfied for all $G_{yu}(s) \in \Pi$.

It follows that the conditions of Theorem 4.3.3 are satisfied for all possible plants $G_{yu}(s)$, and therefore the HIGS-based control system (4.6) is robustly ISS with respect to all perturbed plants $G_{yu}(s) \in \Pi$. This completes the proof.

4.B Numerical results for the rotating beam example

By virtue of the KYP-lemma, see Theorem 4.A.1, satisfaction of the frequency-domain inequality (4.16) (or equivalently (4.31)) is equivalent to feasibility of the matrix inequality

$$\begin{bmatrix} \mathcal{A}_2^\top M + M\mathcal{A}_2 & Mb - (\lambda(kC_u + H)^\top + F^\top + k\frac{\omega_h}{k_h}H^\top) \\ \star & -2 \end{bmatrix} \prec 0, \tag{4.115}$$

with some matrix $M = M^\top \succ 0$. Positive definiteness of M follows from the fact that $\mathcal{A}_2$ is Hurwitz. For the considered plants $P(s) = P_0(s)(1 + W(s)\Delta(s))$ with $\Delta(s) = \{-1, 0, 1\}$, the frequency-domain inequality (4.16) is satisfied with $k = 10$ and $\lambda = 1.05$. The numerical values for M obtained by solving the LMI in (4.115) with $k = 10, \lambda = 1.05$ for each plant are provided next. For the sake of presentation, the matrix M is partitioned as

$$M = \begin{bmatrix} M_{11} & M_{12} \\ M_{12}^\top & M_{22} \end{bmatrix}.$$

Nominal case $P(s) = P_0(s)$:

$$M_{11} = \begin{bmatrix} 3271.2854 & 82193.7721 & 534807.0409 \\ 82193.7721 & 3004106.9455 & 19530867.0090 \\ 534807.0409 & 19530867.0090 & 178395426.3242 \end{bmatrix},$$

$$M_{12} = \begin{bmatrix} 1574208.5725 & 1204195.6982 & 193.6223 \\ 55267119.4324 & 42759474.2704 & 5322.5116 \\ 532538659.7802 & 395523311.3937 & 42307.3639 \end{bmatrix},$$

$$M_{22} = \begin{bmatrix} 2026477013.5053 & 1493823228.4453 & 160464.7104 \\ 1493823228.4453 & 2160096399.0418 & 111424.8123 \\ 160464.7104 & 111424.8123 & 22.7148 \end{bmatrix}.$$

Perturbed case $P(s) = P_0(s)(1 - W(s))$:

$$M_{11} = \begin{bmatrix} 4880.7755 & 251826.0241 & 4191785.8755 & 39016697.2764 \\ 251826.0241 & 16510934.0492 & 302309543.5827 & 2743984637.6464 \\ 4191785.8755 & 302309543.5827 & 7587169458.3818 & 72761822581.433 \\ 39016697.2764 & 2743984637.6464 & 72761822581.433 & 881540530984.12 \end{bmatrix},$$

$$M_{12} = \begin{bmatrix} 199224663.4201 & 472787522.7299 & 328062752.3567 & 194.3089 \\ 13092392632.769 & 29888238457.862 & 20575239560.836 & 9294.7132 \\ 338418179289.5 & 767746791900.84 & 517746603541.71 & 186354.9208 \\ 4599831505793.6 & 9963315985129.3 & 7358773017871 & 2476973.7529 \end{bmatrix},$$

$$M_{22} = \begin{bmatrix} 27545089834524 & 65932522976148 & 46503156198819 & 16452428.8539 \\ 65932522976148 & 191562522048800 & 135108155437422 & 46019570.0211 \\ 46503156198819 & 135108155437422 & 183015500663288 & 31124546.6947 \\ 16452428.8539 & 46019570.0211 & 31124546.6947 & 23.2877 \end{bmatrix}.$$

Perturbed case $P(s) = P_0(s)(1 + W(s))$:

$$M_{11} = \begin{bmatrix} 5236.2926 & 279488.5565 & 4949323.5059 & 40714645.3085 \\ 279488.5565 & 17085147.7713 & 324839323.4501 & 2753567067.9138 \\ 4949323.5059 & 324839323.4501 & 7594793298.9262 & 70205901470.309 \\ 40714645.3085 & 2753567067.9138 & 70205901470.309 & 760739074665.45 \end{bmatrix},$$

$$M_{12} = \begin{bmatrix} 94681293.0386 & 511850879.0378 & 346410474.6424 & 222.5935 \\ 12829886381.139 & 31995174956.989 & 21948710840.095 & 10894.7828 \\ 331294005217.72 & 823668242739.55 & 564716797770.18 & 216726.8692 \\ 4049693004175.1 & 10108792675510 & 7305193912176.1 & 2238633.8050 \end{bmatrix},$$

$$M_{22} = \begin{bmatrix} 24473169128149 & 65339497795751 & 47724442948185 & 15035711.6402 \\ 65339497795751 & 194151848611488 & 149313749273044 & 49491927.7282 \\ 47724442948185 & 149313749273044 & 182828306824733 & 30773635.4780 \\ 15035711.6402 & 49491927.7282 & 30773635.4780 & 26.9618 \end{bmatrix}.$$

A numerical solution to the LMIs in (4.10) for each plant is then given by

$$P = M + \lambda H^\top H + \lambda k (C_u^\top H + H^\top C_u),$$

with $\tau_1 = \lambda k = 10.5$, $\tau_2 = \lambda k \omega_h (k-1)/k_h = 330.75$, $\tau_3 = 0$, and the resulting quadratic (ISS-)Lyapunov function is given by $V(x) = x^\top P x$.

Chapter 5

Time-Domain Tools for Stability and Performance Analysis: An LMI Approach

5.1 Introduction

In the previous chapter, frequency-domain conditions for (robust) stability and performance of hybrid integrator-gain systems (HIGS) have been derived. The power of these conditions is represented by the fact that these do not require the use of parametric models, but rather can be verified (often graphically) on the basis of easy-to-measure frequency response function (FRF) data. Moreover, these conditions allow for intuitive controller tuning procedures. Such aspects make the frequency-domain conditions valuable tools in an industrial environment. The advantages, however, can possibly come at the expense of increased conservatism in the analysis, which is mainly attributed to the underlying use of a *quadratic* Lyapunov function for an essentially piecewise linear (PWL) system. It is known, see, *e.g.*, Johansson and Rantzer, 1998; Johansson, 2002; Rantzer and Johansson, 2000 that some stable PWL systems do not admit a quadratic Lyapunov function, thereby narrowing down applicability of these tools for systems containing HIGS. To deal with this issue and improve upon the previous results, in this chapter use of more flexible *piecewise quadratic* (PWQ) Lyapunov functions is considered (Ambrosino and Garone, 2015; Branicky, 1998; Deenen et al., 2021; Hassibi and Boyd, 1998; Iervolino et al., 2015; Johansson and Rantzer, 1998; Johansson, 2002; Pettersson and Lennartson, 1996; Rantzer and Johansson, 2000; Xie et al., 1997).

The use of PWQ Lyapunov functions for stability and performance analysis

of switched/hybrid systems has been successfully applied to numerous fields of control applications, including reset control systems, see, *e.g.*, Aangenent et al., 2010; Loquen et al., 2010; Nešić et al., 2008; Zaccarian et al., 2011. Key in the works on constructing PWQ Lyapunov functions for reset systems is a partitioning of subsets of the state-space that dictate flow of the reset control system into smaller regions, each to which a different quadratic function is assigned. Since each function has to satisfy certain demands in the associated subregions only, the set of admissible Lyapunov functions may be significantly increased, thereby reducing conservatism.

Inspired by the approaches mentioned above, and the work in Deenen et al., 2021, in this chapter an extension toward HIGS-based control systems is made. In particular, the three-dimensional subspace determining the active dynamics of HIGS is partitioned into convex polyhedral cones. There are many possible choices for the sizes and shapes of the polyhedral cones. For example, in Deenen et al., 2021 a polyhedral partitioning based on a spherical division of the three-dimensional region of HIGS is proposed. In this chapter, however, an alternative approach is pursued in which the relevant subspace is divided into three-dimensional *simplicial* cones, *i.e.*, polyhedral convex cones that are generated by the intersection of three half-spaces (Concini and Procesi, 2010; Iervolino et al., 2015). This choice is mainly motivated by numerical considerations. Namely, when considering polyhedral cones that result from a larger number of intersecting half-spaces such as in Deenen et al., 2021, ensuring continuity of the PWQ function in a numerical search procedure should typically be done by posing explicit equality constraints. From a computational point-of-view, such constraints are particularly hard to satisfy as numerical solvers work with finite precision and can therefore only approximate a solution (Oehlerking, 2011, Chapter 4, Section 4.5). On the other hand, when using simplicial cones, one can exploit a compact matrix parametrization of piecewise quadratic functions on polyhedral partitions in a manner as introduced in Johansson, 2002. This parametrization allows for the continuity requirement to be directly incorporated in the description of each local quadratic function, thereby guaranteeing continuity a priori, and making the need for equality constraints in the eventual set of constraints redundant. Moreover, for the partitioning considered, this way of ensuring continuity is shown to be done in a non-conservative manner.

On the basis of this partitioning strategy, rigorous conditions for stability and performance of HIGS-based control systems are formulated in this chapter. Two performance measures are considered, namely the $\mathcal{L}_2$-gain, which characterizes the worst-case energy gain of the system with respect to a specific class of inputs, and the $\mathcal{H}_2$-norm, which reflects the transient behaviour through the energy in the system's impulse response. These measures are well-established for linear time-invariant (LTI) systems (Boyd et al., 1994; Scherer et al., 1997; Willems, 2007) and have also been extensively studied for reset control systems (Aangenent et al., 2010; Carrasco et al., 2010; Mercader et al., 2013; Nešić et al.,

2011; Zhao and Wang, 2016). The relevance of these particular measures for systems with HIGS comes from the possibility to improve disturbance suppression properties and transient properties as illustrated in Chapter 3.

By exploiting a tailored partitioning with PWQ functions, the conditions for stability and performance of HIGS-based control systems are formulated in terms of linear matrix inequalities (LMIs) in a manner that is robust from a numerical perspective. In addition, novel algebraic conditions are presented that provide relevant insights regarding (in)feasibility of the LMIs. These results rigorously demonstrate the benefits obtained from exploiting partition refinements, and help in guiding such refinements as to increase the possibility of finding a solution to the presented LMI conditions. To the best of the authors knowledge, algebraic results formally demonstrating the benefits of a partition refinement have not appeared in the literature before.

The remainder of this chapter is organized as follows. In Section 5.2 the closed-loop system setting with HIGS is presented. In Section 5.3, the partitioning strategy for the construction of PWQ functions is discussed. This approach is subsequently used in Section 5.4 in deriving rigorous time-domain conditions for stability and performance. Applicability of the presented analysis tools is demonstrated through numerical examples in Section 5.5. Section 5.6 provides a summary of the main conclusions.

5.1.1 Notation

The following notations are adopted throughout this chapter. The set of real symmetric matrices in $\mathbb{R}^{n\times n}$ is denoted by $\mathbb{S}^{n\times n}$, and the set of real symmetric matrices having non-negative elements is denoted by $\mathbb{S}^{n\times n}_{\geq 0}$. A symmetric matrix $M \in \mathbb{S}^{n\times n}$ is positive (negative) definite, denoted by $M \succ 0$ ($M \prec 0$), if $x^\top Mx > 0$ ($x^\top Mx < 0$) for all $x \in \mathbb{R}^n \setminus \{0\}$. The symbols $>, \geq, <, \leq$ for vectors are understood componentwise. The interior and closure of a set $\mathcal{X} \subseteq \mathbb{R}^n$ are denoted by $\text{int}(\mathcal{X})$ and $\overline{\mathcal{X}}$, respectively. For a signal, $t \mapsto v(t)$ the notation dom v denotes its projection on the time (t) axis, and $T_v = \sup \text{dom } x$ indicates the maximal time of the domain. The set of square-integrable functions is denoted by $\mathcal{L}_2$ and endowed with the $\mathcal{L}_2$-norm defined as $\|v\|_2 = (\int_0^{T_v} \|v(t)\|^2 dt)^{\frac{1}{2}}$.

5.2 System setting and problem formulation

5.2.1 Closed-loop system description

For the sake of readability, the generic closed-loop system setting with HIGS that is considered throughout this thesis and is discussed in detail in Chapter 2 is repeated in this section. The setting is depicted in Figure 5.1 in which G is a generalized plant that contains the interconnection to be controlled, and filters

related to the LTI part of the controller, possibly augmented with LTI input-output weighting filters. The latter weighting filters are added for the purpose of including problem-specific input knowledge into the system description, *e.g.*, through known spectra of exogenous signals, and penalizing regulated output variables (see also van de Wal et al., 2002).

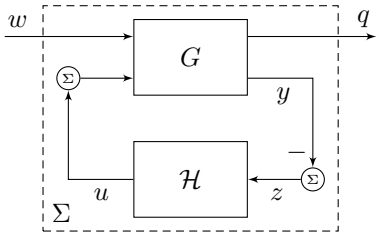

Figure 5.1. Feedback interconnection of a MIMO LTI system G and a SISO HIGS $\mathcal{H}$ with inputs w and performance channel q.

In state-space representation, G is represented as the LTI multi-input multi-output (MIMO) system

$$G : \begin{cases} \dot{x}_g(t) &= A_g x_g(t) + B_g u(t) + B_w w(t), \\ q(t) &= C_q x_g(t) + D_u u(t) + D_q w(t), \\ y(t) &= C_g x_g(t), \end{cases} \tag{5.1}$$

with states $x_g(t) \in \mathbb{R}^m$, performance channel $q(t) \in \mathbb{R}^r$ which contains performance variables such as servo errors and control actions, and $w(t) \in \mathbb{R}^p$ denotes the inputs, such as disturbances, noise, and reference profiles at time $t \in \mathbb{R}_{\geq 0}$. In the setting considered, w is assumed to belong to the class of piecewise Bohl functions (PB). The input to and output of HIGS $\mathcal{H}$ are denoted by $z(t) = -y(t) \in \mathbb{R}$, and $u(t) \in \mathbb{R}$, respectively. Recall that the matrices (A_g, B_g, C_g) are minimal and by virtue of the standing assumption on the relative degree (Assumption 2.3.1) one has $C_g B_g = C_g B_w = 0$.

In Figure 5.1 the hybrid integrator-gain system $\mathcal{H}$ is given by

$$\mathcal{H} : \begin{cases} \dot{x}_h(t) = \omega_h z(t) & \text{if } (z(t), u(t), \dot{z}(t)) \in \mathcal{F}_1, \\ x_h(t) = k_h z(t) & \text{if } (z(t), u(t), \dot{z}(t)) \in \mathcal{F}_2, \\ u(t) = x_h(t), \end{cases} \tag{5.2}$$

where $x_h(t) \in \mathbb{R}$ denotes the state of the integrator, $z(t) \in \mathbb{R}$ is the input, which in the closed-loop setting of Figure 5.1 is at least one time differentiable, $\dot{z}(t) \in \mathbb{R}$ is the corresponding time-derivative, and $u(t) \in \mathbb{R}$ is the generated output. The sets $\mathcal{F}_1$ and $\mathcal{F}_2$ are given by

$$\mathcal{F}_1 = \left\{ (z, u, \dot{z}) \in \mathbb{R}^3 \mid k_h z u \geq u^2 \wedge (z, u, \dot{z}) \notin \mathcal{F}_2 \right\}, \tag{5.3a}$$

$$\mathcal{F}_2 = \left\{ (z, u, \dot{z}) \in \mathcal{F} \mid u = k_h z \wedge \omega_h z^2 > k_h \dot{z} z \right\}, \tag{5.3b}$$

and

$$\mathcal{F} = \mathcal{F}_1 \cup \mathcal{F}_2 = \left\{(z, u, \dot{z}) \in \mathbb{R}^3 \mid k_h z u \geq u^2\right\}, \tag{5.4}$$

which is often referred to as the "$[0, k_h]$-sector". For a detailed discussion and motivation for HIGS, and visualization of the sets $\mathcal{F}_1$, $\mathcal{F}_2$, and $\mathcal{F}$, see Chapter 2.

The interconnection of the LTI system G as in (5.1) and HIGS $\mathcal{H}$ in (5.2) is written as the PWL system

$$\Sigma : \begin{cases} \dot{x}(t) &= A_i x(t) + B w(t), \quad \text{if } x(t) \in \mathcal{X}_i,\ i \in \{1, 2\}, \\ q(t) &= C x(t) + D w(t), \end{cases} \tag{5.5}$$

with augmented state vector $x(t) = [x_g(t)^\top, x_h(t)]^\top \in \mathbb{R}^n$, where $n = m + 1$. The sets $\mathcal{X}_i$, $i \in \{1, 2\}$ in (5.5) are given by

$$\mathcal{X}_i = \{x \in \mathbb{R}^n \mid Ex \in \mathcal{F}_i\}, \tag{5.6}$$

where the matrix E is such that $Ex = (z\ u\ \dot{z})^\top$, and, therefore, is given by

$$E^\top = \begin{bmatrix} -C_g^\top & 0 & -(C_g A_g)^\top \\ 0 & 1 & 0 \end{bmatrix}. \tag{5.7}$$

The mode-dependent system matrices are given by

$$A_1 = \begin{bmatrix} A_g & B_g \\ -\omega_h C_g & 0 \end{bmatrix}, \quad \text{and} \quad A_2 = \begin{bmatrix} A_g & B_g \\ -k_h C_g A_g & 0 \end{bmatrix}, \tag{5.8}$$

and furthermore $B = [B_w^\top, 0]^\top$, $C = [C_g, 0]$, and $D = D_q$. Recall from Chapter 2 that under the assumption that $w \in PB$, global existence and forward completeness of solutions to the discontinuous differential equation in (5.5) with $x(0) \in \mathcal{X}_1 \cup \mathcal{X}_2 = \mathcal{X} = \{x \in \mathbb{R}^n \mid Ex \in \mathcal{F}\}$ is guaranteed, see also the details in Deenen et al., 2021; Sharif et al., 2019.

5.2.2 Problem formulation

This chapter is mainly concerned with formulating potentially less conservative conditions for stability and performance of a HIGS-controlled system as in (5.5). Stability is meant here in the sense of input-to-state stability (ISS), for which the definition has been given earlier in Chapter 2, Definition 2.3.6. Performance is quantified in terms of two measures, being the $\mathcal{L}_2$-gain and the $\mathcal{H}_2$-norm.

The $\mathcal{L}_2$-gain is often considered as a steady-state performance measure, characterizing the system's energy transmission from an input w to the output q. Formally, the $\mathcal{L}_2$-gain is defined as follows.

Definition 5.2.1. *The closed-loop system in* (5.5) *is said to have an $\mathcal{L}_2$-gain from w to q smaller than or equal to γ, if there exists a $\mathcal{K}_\infty$-function ν such*

that for any $w \in \mathcal{L}_2$*, and any initial condition* $x(0) = x_0 \in \mathcal{X}$*, all corresponding solutions to* (5.5) *with* dom $q \neq \{0\}$ *satisfy*

$$\|q\|_2 \leq \nu(\|x_0\|) + \gamma\|w\|_2. \tag{5.9}$$

One of the possible interpretations of the $\mathcal{H}_2$-norm is the total energy content of the output q due to an impulsive input w. For LTI systems, the response to such impulsive input is equivalent to the response when the system is subject to an initial condition $x_0 = B$, where B denotes the input column. This interpretation of the $\mathcal{H}_2$-norm is adopted in this chapter, and motivates the following definition for the $\mathcal{H}_2$-norm (see also Aangenent et al., 2010 in the context of reset control).

Definition 5.2.2. *The closed-loop system in* (5.5) *with* $w = 0$ *is said to have an* $\mathcal{H}_2$*-norm smaller than or equal to* γ *if for a specific initial value* $x(0) = x_0 \in \mathcal{X}$ *the corresponding solutions to* (5.5) *with* dom $q \neq \{0\}$ *satisfy*

$$\|q\|_{2,x_0} \leq \gamma. \tag{5.10}$$

Note that the above definitions allow for (maximal) solutions not being forward complete, as was also done in the definition for ISS (Definition 2.3.6). As in the previous chapter, ISS can be verified by finding a suitable ISS-Lyapunov function, see Definition 2.3.10. For assessing performance in terms of the $\mathcal{L}_2$-gain and $\mathcal{H}_2$-norm, the concept of dissipativity as introduced in Chapter 2, Definition 2.3.12 is useful. Recall that the closed-loop system in (5.5) admits a finite $\mathcal{L}_2$-gain from w to q smaller than or equal to γ, if it is dissipative with respect to the supply function $s(w, q, x) = \gamma^2\|w\|^2 - \|q\|^2$. By a comparable reasoning, it has an $\mathcal{H}_2$-norm smaller than or equal to γ for some initial condition x_0, if it is dissipative with respect to the supply function $s(w, q, x) = -\|q\|^2$. Hence, determining upper-bounds on the $\mathcal{L}_2$-gain and $\mathcal{H}_2$-norm amounts to finding appropriate storage functions that satisfy the conditions in Definition 2.3.12 with the corresponding supply functions. Given this rationale, the main objective in this chapter is to provide computationally tractable conditions for the existence of ISS-Lyapunov/storage functions to characterize stability and performance of the closed-loop system in (5.5) under an as small as possible level of conservatism. For that purpose, an approach, which is inspired by the works in Aangenent et al., 2010; Deenen et al., 2021; Johansson, 2002; Loquen et al., 2010; Nešić et al., 2011; Rantzer and Johansson, 2000; Zaccarian et al., 2005, and exploits piecewise quadratic functions is pursued.

5.3 Partition strategy, PWQ functions, and constraint matrices

Key in the construction of PWQ functions is the division of (a subset of) the state-space of the considered system into smaller sub-regions. This section dis-

cusses the specific partitioning strategy for HIGS, and provides a procedure for efficiently constructing the matrices associated with the computation of PWQ functions. Before going into detail, some definitions regarding cones and conical partitions are introduced.

Definition 5.3.1 (Positive hull, Concini and Procesi, 2010)**.** *The positive hull of a set $\mathcal{R} \subset \mathbb{R}^n$ is the set of all positive combinations of elements from $\mathcal{R}$, i.e.,*

$$\operatorname{pos}(\mathcal{R}) = \left\{ \sum_{m=1}^{M} \lambda_m r_m \mid r_m \in \mathcal{R}, \lambda_m \geq 0, m = 1, \ldots, M, \text{ for some } M \in \mathbb{N}_{>0} \right\}.$$

Definition 5.3.2 (Polyhedral cone, Concini and Procesi, 2010)**.** *A polyhedral cone is the positive hull of a minimal (non-redundant) set $\mathcal{R} := \{r_1, \ldots, r_M\}$ with a finite number of elements. In this case $\mathcal{R}$ is called the generating set of the polyhedral cone, and $r_1, \ldots, r_M$ are generators.*

Definition 5.3.3 (Simplicial cone, Concini and Procesi, 2010)**.** *A simplicial cone in $\mathbb{R}^n$ is the positive hull of a set $\mathcal{R}$ with n linearly independent generators.*

Polyhedral and simplical cones can be written as

$$\mathcal{S} = \{x \in \mathbb{R}^n \mid Sx \geq 0\},$$

for some suitable matrix $S \in \mathbb{R}^{q \times n}$ of full rank (Concini and Procesi, 2010). For simplicial cones it follows that the matrix S is a square invertible matrix. The notation $-\mathcal{S}$ indicates the set $\{x \in \mathbb{R}^n \mid -x \in \mathcal{S}\}$, also denoted by its negative complement. In the remainder, a set $\mathcal{F}$ is called *symmetric* if it is formed as the union between a set and its negative complement, that is, $\mathcal{F} = \mathcal{S} \cup -\mathcal{S}$. For an in-depth discussion on the topic of polyhedral and simplicial cones, see, *e.g.,* Concini and Procesi, 2010.

Definition 5.3.4 (Simplicial partition, Iervolino et al., 2015)**.** *Let a set $\mathcal{F} \subseteq \mathbb{R}^n$ and an integer $N > 0$ be given. A simplicial partition of $\mathcal{F}$ is a family $\mathcal{P}_\mathcal{F} = \{\mathcal{S}_1, \ldots, \mathcal{S}_N\}$ consisting of a finite number of simplicial cones $\mathcal{S}_n$, $n \in \mathcal{N} := \{1, \ldots, N\}$, that satisfy $\mathcal{F} = \bigcup_{n \in \mathcal{N}} \mathcal{S}_n$, and $\operatorname{int}(\mathcal{S}_n) \cap \operatorname{int}(\mathcal{S}_m) = \emptyset$ for $n \neq m$.*

5.3.1 Simplicial partitioning of $\mathcal{F}$

As discussed in the introduction, for the approach in this chapter, the three-dimensional region $\mathcal{F}$ as defined in (5.4) and shown in Figure 5.2 is partitioned into simplicial cones, see Definition 5.3.4. A simplicial partition of the region $\mathcal{F}$ is constructed in the following manner. From (5.4) and Figure 5.2, it can be seen that $\mathcal{F}$ is formed as the union of two polyhedral cones $\hat{\mathcal{S}}$ and $-\hat{\mathcal{S}}$, that is, $\mathcal{F} = \hat{\mathcal{S}} \cup -\hat{\mathcal{S}}$, with

$$\hat{\mathcal{S}} := \left\{ \xi \in \mathbb{R}^3 \mid \hat{S}\xi \geq 0 \right\}, \tag{5.11}$$

where $\xi = [z, u, \dot{z}]^\top$, and

$$\hat{S} = \begin{bmatrix} 0 & 1 & 0 \\ k_h & -1 & 0 \end{bmatrix}. \tag{5.12}$$

The intersection of $\hat{\mathcal{S}}$ and $-\hat{\mathcal{S}}$ is defined by $\hat{S}\xi = 0$, and coincides with the line

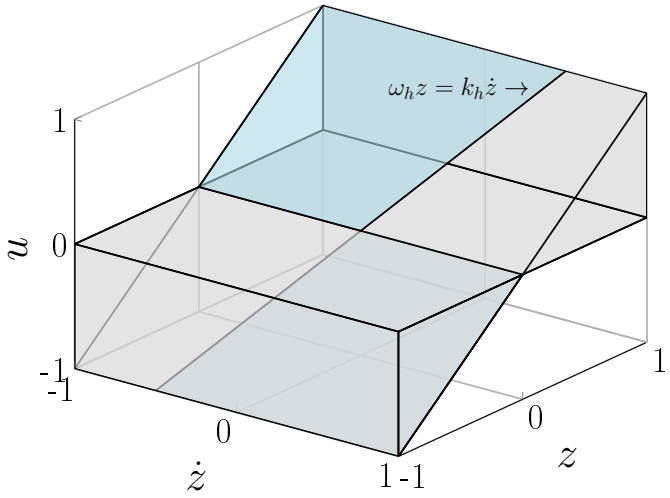

Figure 5.2. Three-dimensional region $\mathcal{F}$ as defined in (5.4). In this figure, the integrator mode region $\mathcal{F}_1$ in (5.3a) is depicted in gray, and the gain mode region $\mathcal{F}_2$ in (5.3b) is depicted in blue.

$\xi = \left\{[0, 0, \dot{z}]^\top \mid \dot{z} \in \mathbb{R}\right\}$, see Figure 5.2. According to Concini and Procesi, 2010, Lemma 1.40, polyhedral cones with non-empty interior can always be partitioned into a finite number of simplicial cones. This result allows the polyhedral cone $\hat{\mathcal{S}}$ in (5.11) to be partitioned into N simplicial cones $\hat{\mathcal{S}}_n$ given by

$$\hat{\mathcal{S}}_n = \left\{\xi \in \mathbb{R}^3 \mid \hat{S}_n \xi \geq 0\right\}, \quad n \in \mathcal{N} := \{1, \ldots, N\}, \tag{5.13}$$

with $\hat{S}_n \in \mathbb{R}^{3\times 3}$ an invertible matrix. An illustration of a simplicial cone $\hat{\mathcal{S}}_n$ is provided in Figure 5.3. The cone is spanned by three unit vectors r_n^1, r_n^2, r_n^3, denoted as the generators such that $\hat{\mathcal{S}}_n = \operatorname{pos}\left\{r_n^1, r_n^2, r_n^3\right\}$, and the generating set (see Definition 5.3.2) is given by $\mathcal{R}_n = \left\{r_n^1, r_n^2, r_n^3\right\}$.

Denote the simplicial partition of $\hat{\mathcal{S}}$ into N simplicial cones by

$$\mathcal{P}_{\hat{\mathcal{S}}} := \left\{\hat{\mathcal{S}}_1, \ldots, \hat{\mathcal{S}}_N\right\}. \tag{5.14}$$

A generating set $\mathcal{R}$ of the partition $\mathcal{P}_{\hat{\mathcal{S}}}$ is constructed as the union of the generating sets $\mathcal{R}_n$ of each simplicial cone $\hat{\mathcal{S}}_n \in \mathcal{P}_{\hat{\mathcal{S}}}$, *i.e.*, $\mathcal{R} = \bigcup_{n\in\mathcal{N}} \mathcal{R}_n$. In what

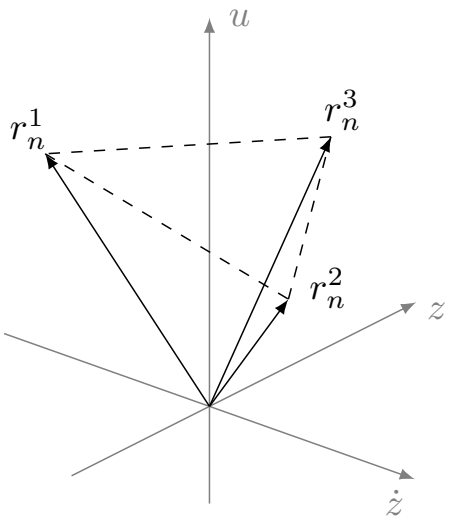

Figure 5.3. Illustration of a simplicial cone $\hat{\mathcal{S}}_n$, which is spanned by three vectors r_n^1, r_n^2, r_n^3, referred to as generators such that $\hat{\mathcal{S}}_n = \operatorname{pos}\{r_n^1, r_n^2, r_n^3\}$. The generating set of the cone is given by $\mathcal{R}_n = \{r_n^1, r_n^2, r_n^3\}$.

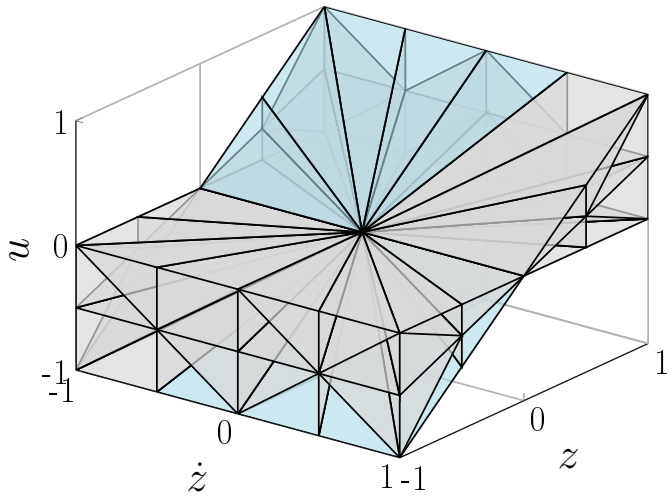

Figure 5.4. Impression of a simplicial partition of $\mathcal{F}$ into N simplicial cones $\hat{\mathcal{S}}_n$. The blue shaded regions correspond to "boundary planes" $\hat{\mathcal{T}}_m$, $m \in \mathcal{M}$ that partition the gain-mode region $\mathcal{F}_2$.

follows, it is assumed that the simplicial partition $\mathcal{P}_{\hat{\mathcal{S}}}$ is constructed in such a manner that the unit vectors $[0,0,1]^\top$ and $[0,0,-1]^\top$ are generators, and thus $\{[0,0,1],[0,0,-1]\} \in \mathcal{R}$. Moreover, it is assumed that the (normalized) vector defining the line $u = k_h z$, $\omega_h = k_h \dot{z}$ describing a common boundary of the set $\mathcal{F}_1$ and $\mathcal{F}_2$ is a generator of the partition as well. Clearly, a partition of $-\hat{\mathcal{S}}$ directly results from a partitioning of $\hat{\mathcal{S}}$, and is denoted by $-\mathcal{P}_{\hat{\mathcal{S}}} := \{-\hat{\mathcal{S}}_1, \ldots, -\hat{\mathcal{S}}_N\}$. Due to symmetry of the region $\mathcal{F}$, a simplicial partition of $\mathcal{F}$ is then given by $\mathcal{P}_{\mathcal{F}} := \mathcal{P}_{\hat{\mathcal{S}}} \cup -\mathcal{P}_{\hat{\mathcal{S}}}$. An impression of a possible partition of $\mathcal{F}$ into simplicial cones is illustrated in Figure 5.4. Several efficient numerical procedures can be employed for constructing an appropriate simplicial division of an n-dimensional space, such as bisection along the longest edge techniques (Iervolino et al., 2015), and ray-gridding algorithms (Yfoulis and Shorten, 2004).

Since $\overline{\mathcal{F}}_1 = \mathcal{F}$, a partition of the integrator-mode region $\mathcal{F}_1$ in (5.3a), denoted by $\mathcal{P}_{\mathcal{F}_1}$ is equivalent to a partition of the full region $\mathcal{F}$, *i.e.*, $\mathcal{P}_{\mathcal{F}_1} = \mathcal{P}_{\mathcal{F}}$. As $\mathcal{F}_2$ forms a "boundary set" of $\mathcal{F}$, it follows that a partitioning of $\mathcal{F}$ induces a simplicial partitioning of $\mathcal{F}_2$, denoted by $\mathcal{P}_{\mathcal{F}_2}$. The cones belonging to the partitioning $\mathcal{P}_{\mathcal{F}_2}$ are described by $\hat{\mathcal{T}}_m = \operatorname{pos}\{r_m^i, r_m^j\}$, $m \in \mathcal{M}$, $(i,j) \in \{1,2,3\}$, where the set $\mathcal{M} \subset \mathcal{N}$ contains the indices of the cones $\hat{\mathcal{S}}_m$, $m \in \mathcal{N}$ for which $\mathcal{F}_2 \cap \mathcal{S}_m \neq \emptyset$, and r_m^i, r_m^j are those generators of $\hat{\mathcal{S}}_m$ that satisfy $r_m^i, r_m^j \in \overline{\mathcal{F}}_2$. As such, the generating set of $\hat{\mathcal{T}}_m$ is given by $\mathcal{R}'_m = \{r_m^i, r_m^j\}$. Clearly, $\hat{\mathcal{T}}_m$ are polyhedral cones in $\mathbb{R}^3$, and can alternatively be described by

$$\hat{\mathcal{T}}_m = \left\{ \xi \in \mathbb{R}^3 \mid \hat{T}_m \geq 0 \wedge h\xi = 0 \right\}, \quad m \in \mathcal{M} \subset \mathcal{N}, \tag{5.15}$$

where $\hat{T}_m \in \mathbb{R}^{2\times 3}$ is a full row rank matrix, and $h = [k_h, -1, 0]$. The partition $\mathcal{P}_{\mathcal{F}_2}$ of the gain-mode region is then given by

$$\mathcal{P}_{\mathcal{F}_2} = \left\{ \hat{\mathcal{T}}_{m_1}, \ldots, \hat{\mathcal{T}}_{m_M} \right\} \cup \left\{ -\hat{\mathcal{T}}_{m_1}, \ldots, -\hat{\mathcal{T}}_{m_M} \right\} = \mathcal{P}_{\hat{\mathcal{T}}} \cup -\mathcal{P}_{\hat{\mathcal{T}}}, \tag{5.16}$$

where $\{m_1, \ldots, m_M\} = \mathcal{M}$ and $M \leq N$ denotes the number of elements in $\mathcal{M}$. The generating set $\mathcal{R}'$ of the partition $\mathcal{P}_{\mathcal{F}_2}$ is formed as $\mathcal{R}' := \bigcup_{m\in\mathcal{M}} \mathcal{R}'_m$, and contains all generators r_n, $n \in \mathcal{N}$ of the partition $\mathcal{P}_{\mathcal{F}}$ that satisfy $r_n \in \overline{\mathcal{F}}_2$.

5.3.2 PWQ function parametrization and constraint matrices

The main advantages of using a simplicial partitioning as discussed above, are 1) the possibility to directly incorporate continuity properties in the definition of the PWQ function, and 2) doing so without introducing additional conservatism. Particularly, by exploiting a compact matrix parametrization of piecewise quadratic functions on polyhedral partitions, adopted from Johansson and Rantzer, 1998; Rantzer and Johansson, 2000 (see also Ambrosino and Garone,

2015; Iervolino et al., 2015), and defined as

$$V_i(x) = x^\top P_i x = x^\top F_i^\top \Phi F_i x, \tag{5.17}$$

where $F_i \in \mathbb{R}^{r\times n}$, $i \in \mathcal{N}$ form the so-called *continuity matrices* satisfying $F_i x = F_j x$ for all x on a boundary shared by two polyhedral regions, and $\Phi \in \mathbb{S}^{r\times r}$ is a symmetric matrix that contains the decision variables, continuity of the PWQ functions over cell boundaries is guaranteed (see Lemma 4.2 in Johansson, 2002). This formulation makes explicit equality constraints obsolete, which has computational advantages.

Based on the partitioning strategy as illustrated in Figure 5.4, the following two propositions present useful results for the construction of the matrices $\hat{S}_i$ in (5.13) and $\hat{T}_i$ in (5.15) describing the simplicial cones, and the continuity matrices used in (5.17). These results are based on the ideas outlined in the seminal works Johansson and Rantzer, 1998, and Johansson, 2002. In formulating the propositions, it will be useful to collect the generators of a simplicial cone $\hat{\mathcal{S}}_i \in \mathcal{P}_{\hat{\mathcal{S}}}$ in a matrix $R_i := [r_i^1, r_i^2, r_i^3] \in \mathbb{R}^{3\times 3}$, $i \in \mathcal{N}$, and the generators of a cone $\hat{\mathcal{T}}_j \in \mathcal{P}_{\hat{\mathcal{T}}}$ in a matrix $R'_j := [r_j^1, r_j^2] \in \mathbb{R}^{3\times 2}$, $j \in \mathcal{M}$.

Proposition 5.3.5. *Consider a simplicial partition $\mathcal{P}_{\hat{\mathcal{S}}}$. The matrices*

$$\hat{S}_i = R_i^{-1}, \qquad i \in \mathcal{N} \tag{5.18}$$

$$\hat{T}_j = \left((R'_j)^\top R'_j\right)^{-1} (R'_j)^\top, \qquad j \in \mathcal{M} \tag{5.19}$$

and $h = [k_h, -1, 0]$ satisfy the inequalities in (5.13) *and* (5.15)*, respectively.*

Proof. The proof can be found in Appendix 5.A.1. □

Proposition 5.3.6. *Consider a simplicial partition $\mathcal{P}_{\hat{\mathcal{S}}}$. Define the set $\bar{\mathcal{R}} := \mathcal{R} \setminus \left\{[0,0,-1]^\top\right\}$, and collect its elements in the matrix $\bar{R} := [r_1, \dots r_p] \in \mathbb{R}^{3\times p}$. Let the matrices $E_i \in \mathbb{R}^{p\times 3}$, $i \in \mathcal{N}$ have its q-th row equal to zero for all $q \in \{1, \dots, p\}$ such that $r_q \notin \mathcal{S}_i$, and the remaining rows equal to the rows of a three-dimensional identity matrix such that $\bar{R}E_i = R_i$, in which no distinction is made between the generators $[0,0,1]^\top$ and $[0,0,-1]^\top$. Then, the matrices*

$$\hat{F}_i = E_i \left(\bar{R}E_i\right)^{-1}, \quad i \in \mathcal{N}, \tag{5.20}$$

satisfy the property $\hat{F}_i\xi = \hat{F}_j\xi$ for all $\xi \in \hat{\mathcal{S}}_i \cap \hat{\mathcal{S}}_j$ and $\xi \in -\hat{\mathcal{S}}_i \cap -\hat{\mathcal{S}}_j$, $i, j \in \mathcal{N}\times\mathcal{N}$, $i \neq j$, and all $\xi \in \hat{\mathcal{S}}_i \cap -\hat{\mathcal{S}}_j$, $i, j \in \mathcal{N} \times \mathcal{N}$.

Proof. A proof is given in Appendix 5.A.2. □

Example 5.3.7. *In order to emphasize the subtlety in Proposition 5.3.6 of making no distinction between the generators $[0,0,1]^\top$ and $[0,0,-1]^\top$ for constructing the continuity matrices, consider Figure 5.5 which shows an example of a*

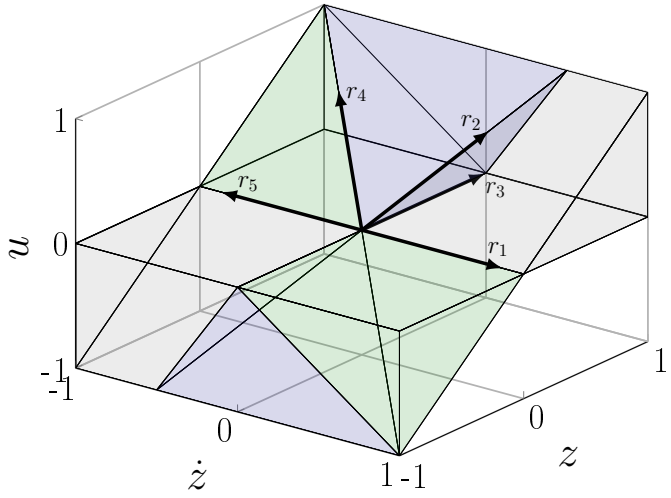

Figure 5.5. Example of a simplicial partitioning of the symmetric set $\mathcal{F}$. The regions $\hat{\mathcal{S}}$ and $-\hat{\mathcal{S}}$ are partitioned into three simplicial cones $\hat{\mathcal{S}}_n$, $n = \{1, 2, 3\}$. The unit vectors r_i, $i = \{1, \ldots, 5\}$ are the generators of the partitioning, and the simplicial cones are given by $\hat{\mathcal{S}}_1 = \text{pos}\{r_1, r_2, r_3\}$ (grey), $\hat{\mathcal{S}}_2 = \text{pos}\{r_2, r_3, r_4\}$ (blue), and $\hat{\mathcal{S}}_3 = \text{pos}\{r_3, r_4, r_5\}$ (green).

simplicial partitioning of the three-dimensional region $\hat{\mathcal{S}}$ (respectively $-\hat{\mathcal{S}}$) into three simplicial cones. The generating set $\mathcal{R}$ of the partitioning is given by $\mathcal{R} = \{r_1, r_2, r_3, r_4, r_5\}$, with generators

$$r_1 = \begin{bmatrix} 0 \\ 0 \\ 1 \end{bmatrix},\ r_2 = \frac{1}{\sqrt{3}} \begin{bmatrix} 1 \\ 1 \\ 1 \end{bmatrix},\ r_3 = \begin{bmatrix} 1 \\ 0 \\ 0 \end{bmatrix},\ r_4 = \frac{1}{\sqrt{3}} \begin{bmatrix} 1 \\ 1 \\ -1 \end{bmatrix},\ r_5 = \begin{bmatrix} 0 \\ 0 \\ -1 \end{bmatrix}.$$

The reduced set $\bar{\mathcal{R}}$ is given by $\bar{\mathcal{R}} = \mathcal{R} \setminus \{[0, 0, -1]^\top\} = \{r_1, r_2, r_3, r_4\}$. The simplicial cones $\hat{\mathcal{S}}_n$, $n = \{1, 2, 3\}$ are formed by $\hat{\mathcal{S}}_1 = \text{pos}\{r_1, r_2, r_3\}$, $\hat{\mathcal{S}}_2 = \text{pos}\{r_2, r_3, r_4\}$, and $\hat{\mathcal{S}}_3 = \text{pos}\{r_3, r_4, r_5\}$, see also Figure 5.5. The selection matrices E_n are then constructed as

$$E_1 = \begin{bmatrix} 1 & 0 & 0 \\ 0 & 1 & 0 \\ 0 & 0 & 1 \\ 0 & 0 & 0 \end{bmatrix}, \quad E_2 = \begin{bmatrix} 0 & 0 & 0 \\ 1 & 0 & 0 \\ 0 & 1 & 0 \\ 0 & 0 & 1 \end{bmatrix}, \quad \text{and} \quad E_3 = \begin{bmatrix} 0 & 0 & 1 \\ 0 & 0 & 0 \\ 1 & 0 & 0 \\ 0 & 1 & 0 \end{bmatrix},$$

and the continuity matrices as in (5.20) *follow as*

$$\hat{F}_1 = \begin{bmatrix} 0 & -1 & 1 \\ 0 & \sqrt{3} & 0 \\ 1 & -1 & 0 \\ 0 & 0 & 0 \end{bmatrix}, \quad \hat{F}_2 = \begin{bmatrix} 0 & 0 & 0 \\ 0 & \frac{\sqrt{3}}{2} & \frac{\sqrt{3}}{2} \\ 1 & -1 & 0 \\ 0 & \frac{\sqrt{3}}{2} & -\frac{\sqrt{3}}{2} \end{bmatrix}, \quad \text{and} \quad \hat{F}_3 = \begin{bmatrix} 0 & 1 & 1 \\ 0 & 0 & 0 \\ 1 & -1 & 0 \\ 0 & \sqrt{3} & 0 \end{bmatrix}.$$

Consider the point $\xi = [z, u, \dot{z}]^\top = [2, 1, 1]^\top$*, which is located on the boundary between* $\hat{\mathcal{S}}_1$ *and* $\hat{\mathcal{S}}_2$*. For this point one finds* $\hat{F}_1\xi = \hat{F}_2\xi = [0, \sqrt{3}, 1, 0]^\top$*. For the point* $\xi = [2, 1, -1]^\top$ *located on the boundary between* $\hat{\mathcal{S}}_2$ *and* $\hat{\mathcal{S}}_3$ *one finds* $\hat{F}_2\xi = \hat{F}_3\xi = [0, 0, 1, \sqrt{3}]^\top$*. For* $\xi = [0, 0, -1]^\top$*, which is on the boundary between* $\hat{\mathcal{S}}_3$ *and* $-\hat{\mathcal{S}}_1$*, one finds* $\hat{F}_1\xi = \hat{F}_3\xi = [-1, 0, 0]^\top$*. If the vector* r_5 *would have been taken into account for constructing the continuity matrices* $\hat{F}_i$*,* $i = 1, 2, 3$*, then for* $\xi = [0, 0, -1]^\top$ *one finds* $\hat{F}_1\xi = [1, 0, 0, 0, 0]^\top$ *and* $\hat{F}_3\xi = [0, 0, 0, 0, -1]^\top$*. Hence,* $\hat{F}_1\xi \neq \hat{F}_3\xi$ *for all* $\xi \in \{\hat{\mathcal{S}}_1 \cap -\hat{\mathcal{S}}_3\} \cup \{-\hat{\mathcal{S}}_1 \cap \hat{\mathcal{S}}_3\}$*. The reason for this is that the common boundary is described by both* r_1 *and* $r_5 = -r_1$*. Eliminating* r_5 *(or* r_1*) ensures that this boundary is represented by only one vector in* $\overline{\mathcal{R}}$*.*

Using $\xi = Ex$, with E given in (5.7), the sets $\hat{\mathcal{S}}_i$, $i \in \mathcal{N}$ in (5.18) and $\hat{\mathcal{T}}_j$, $j \in \mathcal{M}$ in (5.19) are transformed to

$$\mathcal{S}_i = \{x \in \mathbb{R}^n \mid S_i x \geq 0\}, \tag{5.21a}$$
$$\mathcal{T}_j = \{x \in \mathbb{R}^n \mid T_j x \geq 0 \wedge Hx = 0\}, \tag{5.21b}$$

where

$$S_i = \hat{S}_i E, \quad T_j = \hat{T}_j E, \quad \text{and} \quad H = hE, \tag{5.22}$$

for describing the polyhedral partitions in the state space of the closed-loop system (5.5). The continuity matrices are extended to

$$F_i = \left[(\hat{F}_i E)^\top, I\right]^\top, \tag{5.23}$$

where $\hat{F}_i$ is defined in (5.20), and I is an $n \times n$ identity matrix that is added for the purpose of ensuring full rank of F_i. Note that $\bigcup_{i\in\mathcal{N}} \{\mathcal{S}_i \cup -\mathcal{S}_i\} = \overline{\mathcal{X}}_1 = \mathcal{X}$, and $\bigcup_{j\in\mathcal{M}} \{\mathcal{T}_j \cup -\mathcal{T}_j\} = \overline{\mathcal{X}}_2$, where $\mathcal{X} = \mathcal{X}_1 \cup \mathcal{X}_2$ is defined in (5.6).

It may appear that the parametrization (5.17) with the continuity matrices as in (5.23) can introduce some conservatism in the analysis due to fixing the structure of the matrices P_i a priori. This is indeed true when the region $\mathcal{Z} := \{(z, \dot{z}) \in \mathbb{R}^2 \mid z \geq 0\}$, (alternatively $-\mathcal{Z}$), *i.e.*, the $(z, \dot{z})$-plane with $z \geq 0$ (or $z \leq 0$) is divided into only two regions. In that case, one finds for $u = 0$ and $v = (z, \dot{z}) \in \mathbb{R}^2$ that $F_i H v = F_j H v = Fv$, where $\mathrm{im} H = \ker U$ with $U = [0, 1, 0]$. Hence, in that case the PWQ function V as in (5.17) degenerates to a quadratic function in that plane, *i.e.*, $V = v^\top H^\top P_i H v = v^\top H^\top P_j H v = v^\top F^\top \Phi F v = v^\top P v$. This follows from the fact that F_i and F_j are based on the same generating

vectors in $\mathcal{Z}$. It is relatively simple to construct examples for which a piecewise quadratic function can still be constructed with this partitioning, and thus using a quadratic one introduces conservatism. A degenerate case can be found in Example 5.3.7. When dividing $\mathcal{Z}$ into more than two regions, however, ensuring the continuity property through the parametrization in (5.17) is done in a non-conservative manner, as follows from the next proposition.

Proposition 5.3.8. *Consider a symmetric simplicial partitioning of $\mathcal{F}$ in which the region $\mathcal{Z} = \left\{(z, \dot{z}) \in \mathbb{R}^2 \mid z \geq 0\right\}$ is divided into more than two regions. Then, the following statements are equivalent:*

i) A PWQ function of the form

$$V(x) = x^\top P_i x, \quad \text{if } x \in \mathcal{S}_i \cup -\mathcal{S}_i, \quad i \in \mathcal{N}, \tag{5.24}$$

with $P_i = P_i^\top$ defined over a polyhedral partition $\mathcal{P}_\mathcal{X} = \{\mathcal{S}_1, \ldots, \mathcal{S}_N\} \cup \{-\mathcal{S}_1, \ldots, -\mathcal{S}_N\}$, with $\mathcal{S}_i$ given in (5.21a), is continuous.

ii) There exists a symmetric matrix $\Phi \in \mathbb{R}^{r \times r}$ such that

$$P_i = F_i^\top \Phi F_i, \quad i \in \mathcal{N}, \tag{5.25}$$

with F_i given in (5.23).

iii) There exist symmetric matrices $P_i = P_i^\top$, $i \in \mathcal{N}$ that satisfy

$$Z_{ij}^\top (P_i - P_j) Z_{ij} = 0, \tag{5.26}$$

where $\operatorname{im} Z_{ij} = \ker H_{ij}$, and H_{ij} describes the boundary between $\mathcal{S}_i$ and $\mathcal{S}_j$.

Proof. See Appendix 5.A.3. □

It is also worth mentioning in this regard that compared to a generic polyhedral partitioning strategy, a simplicial partitioning strategy itself does not introduce more conservatism in the analysis. Namely, since each polyhedral cone with non-empty interior can be partitioned into a finite number of simplical cones (Concini and Procesi, 2010, Lemma 1.40), then when defining a continuous function over a polyhedral partitioning such as discussed in Deenen et al., 2021, this same function can be defined over a simplicial partitioning as well. The converse, however, not necessarily holds true.

5.4 LMI conditions for stability and performance

5.4.1 Main results

This section presents the main results of this chapter in the form of LMI conditions which, if feasible, guarantee the existence of PWQ ISS-Lyapunov and stor-

age functions that can be used for certifying ISS and computing upper-bounds on the $\mathcal{L}_2$-gain and $\mathcal{H}_2$-norm of the closed-loop system in (5.5).

Theorem 5.4.1. *Consider the closed-loop system in* (5.5) *with* $w \in \mathcal{L}_2$*, and let a polyhedral symmetric partition* $\mathcal{P}_\mathcal{X} = \{\mathcal{S}_1, \dots, \mathcal{S}_N\} \cup \{-\mathcal{S}_1, \dots, -\mathcal{S}_N\}$ *with* $\mathcal{S}_i$ *as in* (5.21a) *be given. Suppose there exist matrices* U_i, $W_i \in \mathbb{S}^{3\times 3}_{\geq 0}$ *for all* $i \in \mathcal{N}$*, and* $V_j \in \mathbb{S}^{2\times 2}_{\geq 0}$, $L_j \in \mathbb{R}^q$ *for all* $j \in \mathcal{M}$*, a matrix* $\Phi \in \mathbb{S}^{q\times q}$*, and constant* $\gamma > 0$*, such that* $P_i = F_i^\top \Phi F_i$*,* $i \in \mathcal{N}$ *satisfies the following LMI conditions:*

$$P_i - S_i^\top W_i S_i \succ 0, \quad i \in \mathcal{N}, \tag{5.27}$$

$$\begin{bmatrix} A_1^\top P_i + P_i A_1 + S_i^\top U_i S_i & P_i B & C^\top \\ B^\top P_i & -\gamma I & D^\top \\ C & D & -\gamma I \end{bmatrix} \prec 0, \quad i \in \mathcal{N}, \tag{5.28}$$

$$\begin{bmatrix} \bar{A}_2^\top P_j + P_j \bar{A}_2 + T_j^\top V_j T_j + Q_j & P_j B & C^\top \\ B^\top P_j & -\gamma I & D^\top \\ C & D & -\gamma I \end{bmatrix} \prec 0, \quad j \in \mathcal{M}, \tag{5.29}$$

in which $Q_j = L_j H + (L_j H)^\top$*, and* $\bar{A}_2 = A_2 + \mu b H$*, with* $b = [0, 1]^\top$ *and* $\mu \in \mathbb{R}$ *a fixed number, and where* S_i*,* T_j*,* H*, and* F_i *are given in* (5.22) *and* (5.23)*. Then the closed-loop system in* (5.5) *is input-to-state stable (ISS) and has a finite* $\mathcal{L}_2$*-gain from* w *to* q *smaller than or equal to* γ*.*

Proof. The proof can be found in Appendix 5.A.4. □

Remark 5.4.2. *The motivation for using the extended system matrix* $\bar{A}_2 = A_2 + \mu b H$ *rather than* A_2*, comes from numerical considerations. Since* A_2 *results from explicit differentiation of the algebraic constraint in gain-mode, this matrix is singular. Consequently, the LMI problem in* (5.27)*,* (5.28) *may become ill-conditioned, which potentially leads to numerical issues; note that* $\bar{A}_2$ *being singular corresponds to* $\mu = 0$*. By appending* A_2 *with an additional matrix* $\mu b \Pi$*, the resulting matrix* $\bar{A}_2$ *becomes non-singular, thereby leading to numerically more favourable conditions, see also the related discussion in Chapter 4, Remark 4.2.1. Note that the gain-mode dynamics remain unchanged, that is,* $A_2 x = \bar{A}_2 x$ *for all* $x \in \mathcal{X}_2$*. A suitable choice for* μ *may be one that minimizes the condition number of* $\bar{A}_2$*.*

Inspired by the results for generic PWL systems in Johansson and Rantzer, 1998; Rantzer and Johansson, 2000, and reset control systems in, *e.g.*, Aangenent et al., 2010; Nešić et al., 2011, the following theorem presents conditions for computing an upper-bound on the $\mathcal{H}_2$-norm of the closed-loop system in (5.5).

Theorem 5.4.3. *Consider the closed-loop system in* (5.5) *with* $w = 0$ *and an initial condition* $x(0) = x_0 \in \mathcal{X}$*. Let a polyhedral partition* $\mathcal{P}_\mathcal{X} = \{\mathcal{S}_1, \dots, \mathcal{S}_N\} \cup \{-\mathcal{S}_1, \dots, -\mathcal{S}_N\}$ *with* $\mathcal{S}_i$ *as in* (5.21a) *be given. Suppose there exist matrices* U_i*,*

$W_i \in \mathbb{S}^{3\times 3}_{\geq 0}$ for all $i \in \mathcal{N}$, and $V_j \in \mathbb{S}^{2\times 2}_{\geq 0}$, $L_j \in \mathbb{R}^q$, for all $j \in \mathcal{M}$, a matrix $\Phi \in \mathbb{S}^{q\times q}$, and a constant $\gamma > 0$, such that $P_i = F_i^\top \Phi F_i$, $i \in \mathcal{N}$ satisfies the following LMI conditions

$$P_i - S_i^\top W_i S_i \succ 0, \quad i \in \mathcal{N}, \tag{5.30}$$

$$A_1^\top P_i + P_i A_1 + S_i^\top U_i S_i + C^\top C \prec 0, \quad i \in \mathcal{N}, \tag{5.31}$$

$$\bar{A}_2^\top P_j + P_j \bar{A}_2 + T_j^\top K_j T_j + Q_j + C^\top C \prec 0, \quad j \in \mathcal{M}, \tag{5.32}$$

$$\gamma^2 - x_0^\top P_q x_0 \geq 0, \quad q \in \mathcal{J}(x_0) \tag{5.33}$$

in which $Q_j = L_j H + (L_j H)^\top$, $\bar{A}_2 = A_2 + \mu b H$, with $b = [0, 1]^\top$ and $\mu \in \mathbb{R}$ a fixed number, S_i, T_i, H, and F_i are defined in (5.22) *and* (5.23)*, and where $\mathcal{J}(x_0) := \{i \in \mathcal{N} \mid x_0 \in \mathcal{S}_i \cup -\mathcal{S}_i\}$. Then, for initial condition $x_0 \in \mathcal{X}$, the closed-loop system in* (5.5) *has an $\mathcal{H}_2$-norm smaller than or equal to γ.*

Proof. Taking similar steps as in the proof of Theorem 5.4.1, it follows that conditions (5.30)–(5.32) imply $V(x(t)) - V(x(0)) \leq -\|q\|^2$. Using $V(x(t)) \geq 0$, $x(0) = x_0$, and (5.33) yields $\|q\|_{2,x_0} \leq \gamma$, thereby completing the proof. □

The following result shows that, similar to the quadratic case in Chapter 4, the conditions in Theorem 5.4.1 and 5.4.3 resulting from the use of a PWQ function provide stronger robust (with respect to arbitrary small state perturbations) stability and performance guarantees for the closed-loop system in (5.5).

Corollary 5.4.4. *If the conditions in Theorem 5.4.1 and Theorem 5.4.3 are satisfied, then the Krasovskii regularization of* (5.5) *(see* (2.41) *in Section 2.3.4) is ISS and has a finite $\mathcal{L}_2$-gain/$\mathcal{H}_2$-norm smaller than or equal to γ.*

Proof. Note that by construction, in each cell $\mathcal{T}_j \subset \mathcal{S}_j$, $j \in \mathcal{M}$ with $\mathcal{M} \subset \mathcal{N}$ a "common" P_j is employed for both the integrator-mode and gain-mode. As such, it readily follows that for all $x \in \mathcal{T}_j \cup -\mathcal{T}_j$, $j \in \mathcal{M}$

$$x^\top \nabla P_j \, (\overline{\text{co}}(A_1 x, A_2 x) + Bw) \leq s(w, q, x). \tag{5.34}$$

The remaining point to worry about is the point where $Ex = (z, u, \dot{z}) = 0$, since in that point all piecewise functions come together, and (5.34) needs to hold for all $j \in \mathcal{N}$. Note, however, that for $Ex = 0$ one has $A_1 x = A_2 x$. Since $x^\top \nabla P_i (A_1 x + Bw) \leq s(w, q, x)$, for all $x \in \mathcal{S}_i \cup -\mathcal{S}_i$, $i \in \mathcal{N}$, which contains the point $Ex = 0$, the result immediately follows. □

5.4.2 On (in)feasibility of the LMI conditions

When the LMIs in Theorem 5.4.1 or Theorem 5.4.3 turn out to be infeasible for a certain partitioning, this partitioning can be iteratively refined to increase the possibility of finding a solution, if existing. In this regard, it might be useful to

know in advance under which conditions and for which partitioning the LMIs will not be feasible, such that these cases do not have to be considered. In general, this is difficult to assess since the LMI conditions are only sufficient conditions for stability. However, some insights regarding (in)feasibility of the LMIs can be obtained when one or both submodes of the HIGS-controlled system are unstable. This is formalized in the following proposition.

Proposition 5.4.5. *Let a simplicial partitioning $\mathcal{P}_{\mathcal{F}}$ be given. The LMI conditions in Theorem 5.4.1 and Theorem 5.4.3 do not admit a feasible solution for that specific partitioning $\mathcal{P}_{\mathcal{F}}$ if one (or both) of the following conditions holds:*

C1. *The matrix A_1 given in* (5.8) *has eigenvalues $\lambda \in \mathbb{C}$ with $\mathrm{Re}(\lambda) > 0$ that satisfy for some $i \in \mathcal{N}$*

$$\left\{ \begin{bmatrix} \mathrm{Re}(\lambda) \\ \omega_h \\ \mathrm{Re}(\lambda)^2 - \mathrm{Im}(\lambda)^2 \end{bmatrix}, \begin{bmatrix} \mathrm{Im}(\lambda) \\ 0 \\ 2\mathrm{Re}(\lambda)\mathrm{Im}(\lambda) \end{bmatrix} \right\} \subset \hat{\mathcal{S}}_i \cup -\hat{\mathcal{S}}_i, \tag{5.35}$$

with $\hat{\mathcal{S}}_i$ defined in (5.13).

C2. *The matrix $A_g + k_h B_g C_z$ with A_g, B_g, C_z given in* (5.1) *has eigenvalues $\lambda \in \mathbb{C}$ with $\mathrm{Re}(\lambda) > 0$ that satisfy for some $j \in \mathcal{M}$*

$$\left\{ \begin{bmatrix} 1 \\ \mathrm{Re}(\lambda) \end{bmatrix}, \begin{bmatrix} 0 \\ \mathrm{Im}(\lambda) \end{bmatrix} \right\} \subset \hat{\mathcal{T}}_j \cup -\hat{\mathcal{T}}_j, \tag{5.36}$$

with $\hat{\mathcal{T}}_j$ defined in (5.15).

Proof. The proof is given in Appendix 5.A.5. □

The result of Proposition 5.4.5 shows the benefits of considering a partitioning in the full $(z, u, \dot{z})$-space in contrast to, *e.g.,* a partitioning in the (z, u)-space. Namely, when (5.35) and/or (5.36) are true, one can refine the partitioning to render these conditions false, whereas for a simpler partitioning and refinement strategy this may not be possible due to limited flexibility. For example, in case the gain-mode region is not partitioned (see for instance the partitioning strategy in Van den Eijnden et al., 2019), one has $\hat{\mathcal{T}} \cup -\hat{\mathcal{T}} = \overline{\mathcal{F}}_2$ such that (5.36) is always satisfied for any eigenvalue λ of the matrix $A_g + k_h B_g C_z$ that satisfies $0 \leq \mathrm{Re}(\lambda) \leq \frac{\omega_h}{k_h}$ and $\mathrm{Im}(\lambda) \in \mathbb{R}$. When the gain-mode region is partitioned, this is not necessarily true. With these conditions one may test upfront if a simpler, computationally less demanding partitioning could potentially work, or a more involved three-dimensional partitioning should be considered. Moreover, these conditions give direct insights into some of the necessary properties that a partition refinement should admit. The application and relevance of Proposition 5.4.5 will be illustrated in Section 5.5.

Closer inspection of the results in Proposition 5.4.5 reveals that, under some simple algebraic conditions on the eigenvalues related to the system matrices in integrator-mode and gain-mode, there exists no partitioning for which the LMIs are feasible. These conditions are summarized in the following corollary.

Corollary 5.4.6. *There is no simplicial symmetric partitioning $\mathcal{P}_\mathcal{F}$ of $\mathcal{F}$ such that the LMI conditions in Theorem 5.4.1 and Theorem 5.4.3 admit a feasible solution, if one or both of the following conditions hold:*

(i) there is a real eigenvalue λ of A_1 that satisfies $\lambda > \frac{\omega_h}{k_h}$;

(ii) there is a real eigenvalue λ of $A_g + k_h B_g C_z$ that satisfies $0 \leq \lambda < \frac{\omega_h}{k_h}$.

Proof. Consider the vectors

$$v_1 = \begin{bmatrix} \mathrm{Re}(\lambda) \\ \omega_h \\ \mathrm{Re}(\lambda)^2 - \mathrm{Im}(\lambda)^2 \end{bmatrix}, \quad \text{and} \quad v_2 = \begin{bmatrix} 1 \\ k_h \\ \mathrm{Re}(\lambda) \end{bmatrix}. \tag{5.37}$$

Suppose that (i) holds. Since $\mathrm{Im}(\lambda) = 0$ by assumption, it follows that $v_1 \in \mathcal{F}_1$. As $\hat{\mathcal{S}}_i \cup -\hat{\mathcal{S}}_i \subset \mathcal{F}_1$ for all $i \in \mathcal{N}$, there always exists a region $\hat{\mathcal{S}}_i \cup -\hat{\mathcal{S}}_i$ such that $v_1 \in \hat{\mathcal{S}}_i \cup -\hat{\mathcal{S}}_i$. Similarly, assume that (ii) holds such that $v_2 \in \mathcal{F}_2$. Since $\mathrm{Im}(\lambda) = 0$ and $\hat{\mathcal{T}}_j \cup -\hat{\mathcal{T}}_j \subset \mathcal{F}_2$ for all $j \in \mathcal{M}$, there always exists a region $\hat{\mathcal{T}}_j \cup -\hat{\mathcal{T}}_j$ such that $v_2 \in \hat{\mathcal{T}}_j \cup -\hat{\mathcal{T}}_j$. Consequently, condition (5.35) and/or (5.36) are satisfied for all partitions, and thus the LMIs are not feasible. □

Interestingly, this geometric result can directly be interpreted in terms of unstable closed-loop system behaviour. Indeed, the vectors v_1 and v_2 in (5.37) define a possible direction along which the $(z, u, \dot{z})$-trajectory can evolve in the regions $\mathcal{F}_1$ or $\mathcal{F}_2$. When condition (i) in Corollary 5.4.6 is satisfied, the z-trajectory evolves at a rate of at least $1/k_h$ times faster than the u-trajectory, *i.e.,* $0 \leq du/dz < k_h$. Consequently, the sector boundary $u = k_h z$ cannot be reached such that switching, as a potentially stabilizing mechanism, is not initiated. A similar interpretation is given for the gain-mode. When condition (ii) is satisfied, the $\dot{z}$-trajectory evolves at least ω_h/k_h times slower than the z-trajectory. As such, $0 \leq d\dot{z}/dz < \omega_h/k_h$ and the switching boundaries $\omega_h z = k_h \dot{z}$ or $z = 0$ cannot be reached. Note that a condition on the magnitude of the eigenvalues is thus a consequence of the fact that trajectories of HIGS evolve in a sector. The above observations can be translated into *necessary* conditions for input-to-state stability as formalized in the following theorem.

Theorem 5.4.7. *A necessary condition for the closed-loop system in* (5.5) *to be input-to-state stable is that none of the conditions in Corollary 5.4.6 hold true.*

Proof. If the conditions in Corollary 5.4.6 are satisfied, then one (or both) of the sub-modes is unstable, and according to Corollary 5.4.6 (see also the proof of

Proposition 5.4.5) it follows that the eigenvector $v \in \mathbb{R}^m$ corresponding to the unstable real eigenvalue satisfies $Ev = \alpha_1 v_1 \in \mathcal{F}_1$ or $E\Theta v = \alpha_2 v_2 \in \mathcal{F}_2$, with v_1, v_2 given in (5.37) and $\alpha_1, \alpha_2 \in \mathbb{R}$. When starting in the integrator-mode with initial condition $x(0) = v$ and $w = 0$, the corresponding trajectory evolves according to $x(t) = e^{\lambda t} v$. For the integrator-mode one finds for all $t \geq 0$

$$(z(t), u(t), \dot{z}(t)) = e^{\lambda t} Ev \in \mathcal{F}_1. \tag{5.38}$$

Similarly, starting with initial condition $x(0) = \Theta v$ in gain-mode yields $x(t) = e^{\lambda t}\Theta v$ such that for $t \geq 0$

$$(z(t), u(t), \dot{z}(t)) = e^{\lambda t} E\Theta v \in \mathcal{F}_2. \tag{5.39}$$

The $(z, u, \dot{z})$-trajectory moves along the line spanned by $Ev \in \mathcal{F}_1$ or $E\Theta v \in \mathcal{F}_2$. The system cannot switch: it remains in the unstable linear mode and thus there is a trajectory that diverges exponentially from the origin. This directly violates the property of an ISS system that for zero inputs, the origin is asymptotically stable for any admissible initial condition $x_0 \in \mathbb{R}^n$. □

Remark 5.4.8. *For planar HIGS-controlled systems, being the interconnection of HIGS with a one-dimensional linear plant, the conditions in Theorem 5.4.7 can be shown to be necessary and sufficient, see also a related result for reset systems in Nešić et al., 2011, Theorem 3 and linear complementary systems in Camlibel et al., 2003, Theorem III.3.*

5.5 Numerical examples

In this section, applicability of the time-domain tools for stability and performance analysis is demonstrated by means of two numerical examples. In the first example, the potential for reducing conservatism in the analysis when using PWQ functions is illustrated for the mass-spring-damper system discussed previously in Chapter 4. In the second example, stability and performance of a HIGS-based control design for a fourth-order motion system is studied in detail. For this example, the relevance of Proposition 5.4.5 is highlighted in particular.

5.5.1 Mass-spring-damper system revisited

Recall the example presented earlier in Chapter 4, Section 4.3, in which a mass-spring-damper system, given by

$$P(s) = \frac{1}{ms^2 + bs + k}, \tag{5.40}$$

with $m = 1$ kg, $b = 0.0564$ Ns/m, and $k = 1$ N/m, is placed in feedback with the series interconnection of HIGS and an LTI filter, the latter given by

$$C(s) = k_p \left(\frac{s + \omega_z}{s + \omega_p} \right), \tag{5.41}$$

where $k_p = 1.4$ N/m, $\omega_z = 5$ rad/s, and $\omega_p = 6.95$ rad/s. Note that this example serves the purpose of demonstrating the potential benefits when using a state-space partition in a stability and performance analysis, and is not necessarily designed to achieve the best performance in $\mathcal{L}_2$ or $\mathcal{H}_2$ sense.

Stability analysis

For assessing ISS of the closed-loop system, the LMI-conditions in Theorem 5.4.1 are solved by means of the `MATLAB` toolbox `YALMIP` (Löfberg, 2004) together with the external solver `MOSEK` (Andersen et al., 2003) for different values of ω_h and k_h, and using different partitioning strategies. In particular, a comparison is made between *i*) using no partitioning (leading to a single quadratic Lyapunov function as in Chapter 4), *ii*) a two-dimensional partitioning in which the $[0, k_h]$-sector in the (z, u)-space is iteratively partitioned into a maximum of 1200 smaller sub-sectors, and *iii*) a three-dimensional partitioning in which the $(z, u, \dot{z})$-space is iteratively partitioned into at most 1200 three-dimensional subregions. The results are presented in Figure 5.6.

From Figure 5.6a it can be seen that, compared to the simulation-based stable region (grey) obtained from applying a unit step input to the system, a considerable degree of conservatism remains in concluding on ISS of the closed-loop system when using an LMI-based approach without partitioning (black dots). This is a result from considering a common (smooth) quadratic ISS-Lyapunov function. In Figure 5.6b, it is shown that a two-dimensional partitioning of the $[0, k_h]$-sector (see also the strategy discussed in Van den Eijnden et al., 2019) is able to partly alleviate this problem, resulting in a significantly larger set of parameters for which ISS can be guaranteed. For parameter pairs close to the edge of the stable region, however, also this approach is consistently unable to provide stability guarantees. Finally, Figure 5.6c illustrates the potential of a three-dimensional partitioning in terms of reducing conservatism. The resulting range of (k_h, ω_h)-values for which closed-loop stability can be concluded on the basis of the LMI conditions closely coincides with the stable region found from time-series simulations. In fact, the results seem to closely resemble what would be expected from a necessary condition for closed-loop stability of the nonlinear feedback system.

Performance analysis - $\mathcal{L}_2$-gain

An upper-bound on the $\mathcal{L}_2$-gain of the closed-loop system from w to y with $k_h = 0.23$ and for various values of ω_h is computed by minimizing γ in Theorem 5.4.1 under the LMI constraints (5.27)–(5.29), and with different partition-

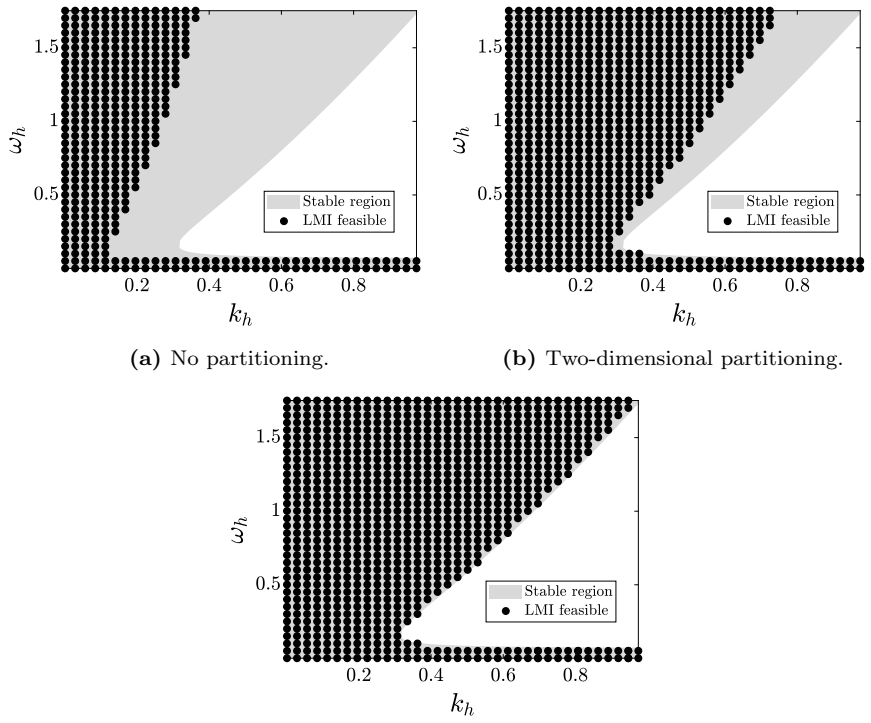

(a) No partitioning.

(b) Two-dimensional partitioning.

(c) Three-dimensional partitioning.

Figure 5.6. A comparison between solving the LMI conditions in Theorem 5.4.1 using different partitioning strategies for different parameter values of ω_h and k_h. See also Figure 4.5 in Chapter 4 for a similar analysis but on the basis of frequency-domain conditions.

ing strategies. The results from solving the LMIs are shown in Figure 5.7.

In addition, an estimate obtained from simulated experiments is provided in this figure. For this purpose, a truncated sinusoid, defined by

$$w(t) = \begin{cases} \sin(\omega t) & \text{for all } t \in [0, T], \\ 0 & \text{otherwise,} \end{cases} \tag{5.42}$$

with $T = 100 \cdot 2\pi/\omega$ and $\omega > 0$ is applied to the closed-loop system at various frequencies. The simulation time is set to $t_s = 10T$ seconds to ensure the response has sufficiently settled. A lower-bound on the $\mathcal{L}_2$-gain is then estimated by taking the maximum ratio of the $\mathcal{L}_2$-norms of the input w and output $q = y$.

The result in Figure 5.7 clearly illustrates the benefits of a state-space par-

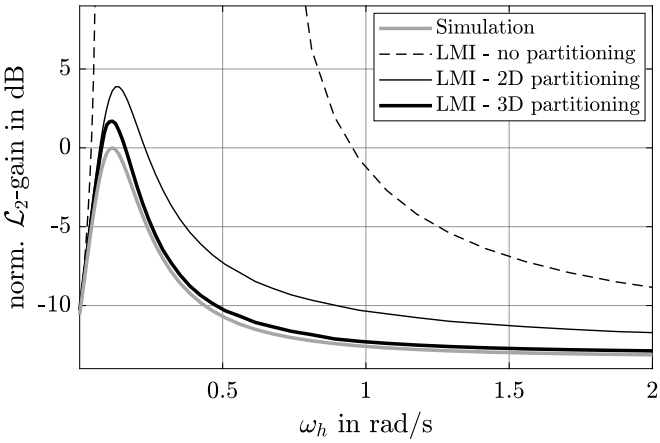

Figure 5.7. Estimated $\mathcal{L}_2$-gain (normalized) obtained by means of *i*) Theorem 5.4.1 with different partitioning strategies, and *ii*) time-domain simulations.

tition as the estimates become significantly tighter. Note that for certain values of ω_h a small discrepancy between the estimates resulting from the LMIs with a three-dimensional partitioning and the time-domain simulations remains. This may be caused by *i*) numerical artefacts, *ii*) remaining conservatism in the analysis due to a finite partitioning, and *iii*) the chosen class of input signals, which may only provide a lower-bound for the true $\mathcal{L}_2$-gain, that is, $\gamma_{\text{sim}} \leq \gamma_{\text{true}} \leq \gamma_{\text{LMI}}$.

Performance analysis - $\mathcal{H}_2$-norm
An upper-bound on the $\mathcal{H}_2$-norm of the closed-loop system with $w = 0$, and when subject to an initial condition $x(0)$ that corresponds to an initial state $y(0) = 1$, $\dot{y}(0) = 0$ of the simply supported mass, is computed for $k_h = 0.23$ and various ω_h. Specifically, γ in Theorem 5.4.3 is minimized under the LMI constraints (5.27)–(5.29), and with different partitionings. The results are shown in Figure 5.8, along with the true $\mathcal{H}_2$-norm obtained from time-series simulations.

Again, a clear benefit can be seen from using a three-dimensional partitioning strategy as the estimate of the $\mathcal{H}_2$-norm closely corresponds to the true value obtained by simulations, underlining the accuracy of the LMIs.

5.5.2 Fourth-order motion system

For the second example, consider a typical motion system represented by the fourth-order transfer function

$$P(s) = \frac{1}{ms^2} - \frac{1}{m(s^2 + 2\beta_0\omega_0 s + \omega_0^2)}, \tag{5.43}$$

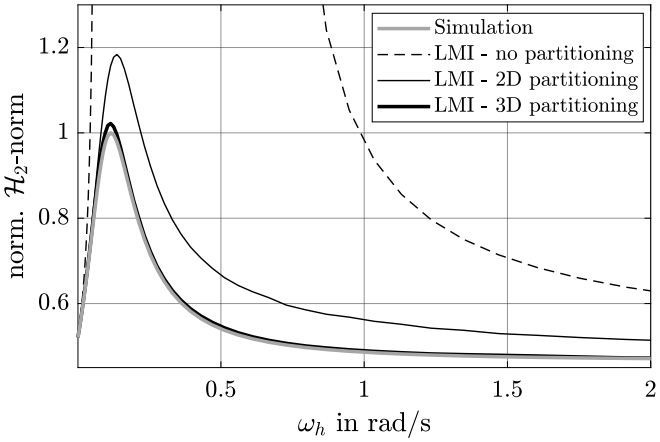

Figure 5.8. Estimated $\mathcal{H}_2$-norm (normalized) obtained by means of Theorem 5.4.3 with different partitioning strategies, and the true $\mathcal{H}_2$-norm obtained through time-domain simulations.

which is a combination of rigid-body and non-rigid-body dynamics, and where $m = 18$ kg, $\omega_0 = 1200 \cdot 2\pi$ rad/s, and $\beta_0 = 0.03$. This system is placed in feedback with a controller C_{fb} being the series interconnection of a linear PID-filter $C_{pid}(s)$, a second-order low-pass filter $C_{lp}(s)$, and a notch filter $C_n(s)$. The individual filters are constructed as

$$C_{pid}(s) = k_p \left(1 + \frac{\omega_i}{s} + \frac{s}{\omega_d}\right), \tag{5.44}$$

$$C_{lp}(s) = \frac{\omega_{lp}^2}{s^2 + 2\beta\omega_{lp}s + \omega_{lp}^2}, \tag{5.45}$$

$$C_n(s) = \frac{\omega_p^2}{\omega_z^2} \cdot \frac{s^2 + 2\beta_z\omega_z s + \omega_z^2}{s^2 + 2\beta_p\omega_p s + \omega_p^2}. \tag{5.46}$$

To potentially improve transient and steady-state performance, HIGS is added in series with an additional output filter $C_z(s) = \frac{s+\omega_c}{\omega_c}$ with $\omega_c = \frac{\omega_h}{k_h}|1 + \frac{4j}{\pi}|$. The linear portion of the controller is then given by

$$C(s) := C_z(s)C_{lp}(s)C_{pid}(s)C_n(s). \tag{5.47}$$

The system is subject to a bounded input disturbance $d \in \mathcal{L}_2$, and a unit step-input $r(t) = 1$ for $t \geq 0$, $r(t) = 0$ otherwise. The specific closed-loop configuration is depicted in Figure 5.9, and satisfies Assumption 2.3.1.

An initial controller is designed by means of a loop-shaping procedure (Franklin et al., 2005; Skogestad and Postlethwaite, 2010; Steinbuch and Norg,

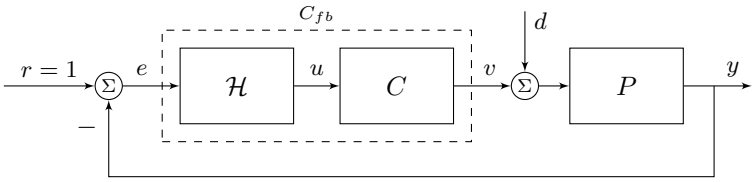

Figure 5.9. Schematic representation of the closed-loop system.

1998) in which HIGS is replaced by its describing function $\mathcal{D}(j\omega)$ (see Chapter 2). The aim is to maximize the bandwidth, *i.e.*, the frequency at which the quasi-linear open-loop frequency response function $L(j\omega) := P(j\omega)C(j\omega)\mathcal{D}(j\omega)$ crosses 0 dB for the first time, while satisfying a peaking constraint of 8 dB on the quasi-linear sensitivity function $S(j\omega) := (1 + L(j\omega))^{-1}$. The phase benefits associated with HIGS may allow for an increase in bandwidth as compared to an LTI design. The loop-shaping design procedure exploited here will be discussed in detail in Chapter 7.

On the basis of this approach, the following parameter values are obtained: $k_p = 4.816 \cdot 10^7$ N/m, $\omega_i = 150 \cdot 2\pi$ rad/s, $\omega_d = 240 \cdot 2\pi$ rad/s, $\omega_{lp} = 1400 \cdot 2\pi$ rad/s, $\beta = 0.7$, $\omega_z = 1160 \cdot 2\pi$ rad/s, $\beta_z = 0.01$, $\omega_p = 850 \cdot 2\pi$, $\beta_p = 0.3$, $\omega_h = 300 \cdot 2\pi$ rad/s, $k_h = 1$, and the bandwidth is 305 Hz. A Nyquist-like plot of the describing function $L(j\omega)$, together with the open-loop characteristics of the linear gain- and integrator-mode is shown in Figure 5.10.

Stability Analysis

For verifying input-to-state stability of the resulting design, the conditions in Theorem 5.4.1 are checked. However, before doing so, note from Figure 5.10 that the individual LTI integrator-mode subsystem and gain-mode subsystem are unstable. In fact, it turns out that one of the complex eigenvalue pairs of the system matrix in gain-mode is given by $\lambda = 52.2 \pm 5102j$, and satisfies

$$0 \leq \mathrm{Re}(\lambda) = 52.2 \leq \omega_h / k_h = 300 \cdot 2\pi.$$

According to Proposition 5.4.5 the closed-loop system does not admit a common quadratic Lyapunov function, but also there does not exist a PWQ Lyapunov function with *any* two-dimensional partitioning, *i.e.*, a partitioning in which the gain-mode region is not partitioned (see also Aangenent et al., 2010; Loquen et al., 2010; Van den Eijnden et al., 2019). Therefore, when existing, a PWQ (ISS)-Lyapunov function can only be found with a three-dimensional partitioning (or more). A feasible solution to the LMIs in Theorem 5.4.1 was found with a division of the region $\hat{\mathcal{S}}$ into a total of 28 simplicial cones.

The closed-loop system is simulated with $r = d = 0$, and random initial conditions for the plant and LTI part of the controller, whereas the initial state of HIGS is set to $x_h(0) = 0$. The corresponding evolution of the Lyapunov function

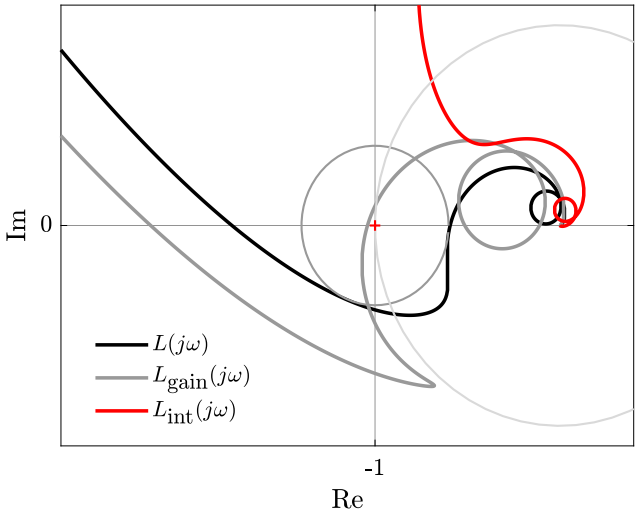

Figure 5.10. Nyquist plot of the quasi-linear open-loop frequency response function $L(j\omega)$ (black) together with the associated linear gain-mode characteristics (grey) and linear integrator-mode characteristics (red).

along trajectories of the system is shown in Figure 5.11. As can be seen for a specific solution, this function is positive, continuous, and monotonically decreasing.

Performance analysis - $\mathcal{L}_2$-gain

Next, performance in terms of the $\mathcal{L}_2$-gain is studied using Theorem 5.4.1. Similar as before, γ is minimized under the LMI constraints (5.27)–(5.29). The result for an increasing number of subdivisions N of the three-dimensional region $\mathcal{F}$ is given in Table 5.1, together with an estimate for the lower-bound obtained from simulations with the truncated sinusoid in (5.42) as an input disturbance d at different frequencies ω. The maximum for this lower-bound was found at an input frequency of $\omega = 229.78 \cdot 2\pi$ rad/s.

Table 5.1. $\mathcal{L}_2$-gain estimation.

	$N = 70$	$N = 100$	$N = 250$	$N = 700$	$N = 1200$
γ_{sim} $(\cdot 10^7)$	1.24	1.24	1.24	1.24	1.24
γ_{LMI} $(\cdot 10^7)$	4.59	3.17	2.25	1.93	1.73
Δ	270%	155%	81%	56%	39%

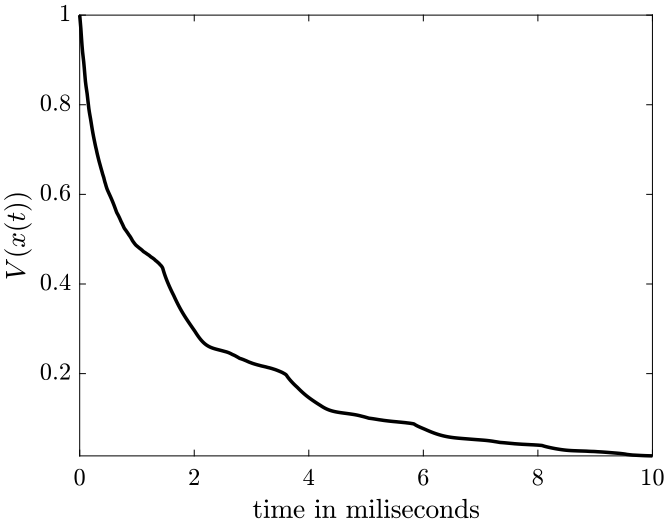

Figure 5.11. Time-evolution of the PWQ Lyapunov function (normalized) along the trajectories of the system.

The results in Table 5.1 show the benefit of a partition refinement for improving the accuracy of the LMI approximation. Remark that a gap between the LMI approximation and the simulation result remains due to the fact that the chosen input signal may not necessarily reflect the worst-case disturbance for the closed-loop system, numerical artefacts, and remaining conservatism.

Performance analysis - $\mathcal{H}_2$-norm

For a final exposition of the tools presented in this chapter, an estimate for the $\mathcal{H}_2$-norm of the error response when the system is subject to a unit-step input is computed. For this purpose, a state-transformation is applied as follows. When being in a state of equilibrium with $(z, u) = (0, 0)$ the system must be in integrator mode. The equilibrium state is determined as $x^* = -A_1^{-1}B$, where invertibility of A_1 follows from the absence of zero eigenvalues. Remark that due to the presence of an integrator in C_{fb}, the only possibility for the tracking error $e = r - y$ is to be zero when the system is in equilibrium. Consider the transformation $\xi := x - x^*$ for which simple calculations show that the dynamics of the transformed system read

$$\dot{\xi} = A_i \xi, \quad \text{when} \quad \xi \in \mathcal{X}_i, \quad i = \{1, 2\},$$

with initial condition $\xi(0) = -A_1^{-1}B$. The LMI conditions in Theorem 5.4.3 are solved for this transformed autonomous system with an increasing number of

subdivisions N of $\mathcal{F}$. The results are provided in Table 5.2, along with the true $\mathcal{H}_2$-norm obtained from time-series simulations. Note that as an alternative for computing the $\mathcal{H}_2$-norm, one could have approximated the unit-step input by an LTI input filter $W_r(s) = \frac{1}{s+\epsilon}$ with small $\epsilon > 0$ and initial state $x_r(0) = 1$, see also Aangenent et al., 2010 for such an approach. A step-response of the closed-loop system is shown in Figure 5.12.

Table 5.2. $\mathcal{H}_2$-norm estimation.

	$N = 70$	$N = 100$	$N = 250$	$N = 700$	$N = 1200$
γ_{sim}	0.041	0.041	0.041	0.041	0.041
γ_{LMI}	0.101	0.075	0.061	0.058	0.056
Δ	146%	83%	49%	42%	36%

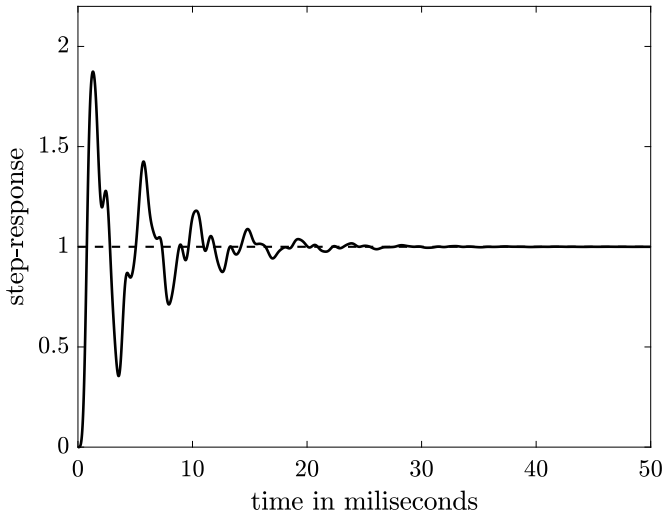

Figure 5.12. Step-response of the closed-loop system.

Although refinement of the partitioning shows a significant benefit for improving an estimation of the $\mathcal{H}_2$-norm, a discrepancy of 36% still remains. This difference may partly be due to remaining conservatism in the analysis. To potentially refine the results, one can use a different partitioning or search for, *e.g.*, alternative (piecewise) polynomial storage functions (Chesi, 2010; Garulli et al., 2013). It is furthermore expected that the increased computational complexity

due to an increased system dimension may lead to numerical problems, and, as such, contributes to this gap. Also note that for the previous (numerically simpler) example, the conditions lead to a very tight estimate of the true $\mathcal{H}_2$-norm. Moreover, one should keep in mind that for the current example a feasible solution to the LMIs does not even exist at all when using either no partitioning or a two-dimensional partitioning, making the conditions still relevant.

Remark 5.5.1. *To improve overall numerical conditioning of the LMIs for this example, a Gramian-based balancing of the closed-loop state-space realization has been performed (Laub et al., 1987; Moore, 1981). Hereto, a similarity transformation $x_b = Tx$ is computed on the basis of the state-space description in integrator-mode, which is subsequently applied to both the integrator-mode and gain-mode state-space models for constructing a balanced closed-loop model. In addition, input/output scaling has been used. Namely, the input matrix B in* (5.5) *has been multiplied with a factor of* 10^4 *for lifting the $\mathcal{L}_2$-gain, thereby leading to more favourable numerical conditions. Output scaling has been applied to $\dot{z}$ such that z, u and $\dot{z}$ are approximately of the same order of magnitude.*

5.6 Summary

This chapter presented rigorous time-domain conditions for stability and performance of HIGS-based control systems. For potentially reducing conservatism in the analysis and obtain tighter performance estimates, the conditions exploit flexible piecewise quadratic functions defined over a tailored and a numerically robust state-space partition. The latter is constructed by dividing the full region that determines mode-switching of HIGS into smaller, conic regions, each to which a quadratic function is assigned. On the basis of this partition with piecewise quadratic functions, conditions for stability and performance are formulated as a convex optimization problem in terms of numerically verifiable LMIs. For achieving more insights regarding (in)feasibility of the LMIs, sufficient conditions are given under which the LMIs cannot be solved, guiding partition refinements which are important for obtaining accurate stability and performance estimates. The effectiveness of the presented tools (along with some shortcomings) has been demonstrated on numerical control examples.

Despite the $\mathcal{L}_2$-gain considered in this chapter being a valuable measure for (steady-state) time-domain performance of HIGS-based control systems, it may be conservative as it applies to a broad class of input signals and may not always reflect the actual performance objective. However, one often has more knowledge about external signals acting on the system. Therefore, it is of interest to seek for alternative ways in quantifying (steady-state) time-domain performance of systems containing HIGS. In the next chapter, the notion of *convergent systems* is adopted, which opens up the possibility for accurately characterizing steady-state performance in both time- and frequency-domain.

5.A Proofs and technical results

5.A.1 Proof of Proposition 5.3.5

First, it is shown that $\xi \in \hat{\mathcal{S}}_i \iff \hat{S}_i\xi \geq 0$ for all $i \in \mathcal{N}$.

- $\xi \in \hat{\mathcal{S}}_i \Rightarrow \hat{S}_i\xi \geq 0$. Since $\hat{\mathcal{S}}_i = \text{pos}\left\{r_i^1, r_i^2, r_i^3\right\}$ is a simplicial cone, each $\xi \in \hat{\mathcal{S}}_i$ can uniquely be written as a positive combination of columns from $R_i = [r_i^1, r_i^2, r_i^3]$, that is,

$$\xi = R_i\lambda, \text{ with } 0 \leq \lambda \in \mathbb{R}^3. \tag{5.48}$$

  Invertibility of R_i results in $\lambda = R_i^{-1}\xi \geq 0$, which by the choice $\hat{S}_i = R_i^{-1}$ yields the inequality.

- $\hat{S}_i\xi \geq 0 \Rightarrow \xi \in \hat{\mathcal{S}}_i$. Suppose $\hat{S}_i\xi = \lambda \geq 0$. Invertibility of $\hat{S}_i$ yields $\xi = R_i\lambda$ and thus $\xi \in \text{pos}\left\{r_i^1, r_i^2, r_i^3\right\} = \hat{\mathcal{S}}_i$. The result follows.

Next it is shown that $\xi \in \hat{\mathcal{T}}_j \iff \hat{T}_j\xi \geq 0, h\xi = 0$ for all $j \in \mathcal{M}$.

- $\xi \in \hat{\mathcal{T}}_j \Rightarrow \hat{T}_j\xi \geq 0, h\xi = 0$. The equality $h\xi = 0$ follows immediately from the observation that $\hat{\mathcal{T}}_j \subset \mathcal{F}_2$, and thus each $\xi \in \hat{\mathcal{T}}_j$ is perpendicular to the vector defined by h. Since $\hat{\mathcal{T}}_j = \text{pos}\left\{r_j^1, r_j^2\right\}$ is a polyhedral cone, each $\xi \in \hat{\mathcal{T}}_j$ can be written as the positive combination of columns in $R'_j = [r_j^1, r_j^2]$, that is

$$\xi = R'_j\lambda, \text{ with } 0 \leq \lambda \in \mathbb{R}^2. \tag{5.49}$$

  Since R'_j has linearly independent columns, it follows that the matrix product $(R'_j)^\top R'_j$ also has linearly independent columns and, therefore, is invertible. Multiplying (5.49) from the left by $((R'_j)^\top R'_j)^{-1}(R'_j)^\top$ yields

$$\left((R'_j)^\top R'_j\right)^{-1}(R'_j)^\top\xi = \lambda \geq 0.$$

  From the choice for $\hat{T}_j$ in (5.15) the result follows.

- $\hat{T}_j\xi \geq 0, h\xi = 0 \Rightarrow \xi \in \hat{\mathcal{T}}_j$. Suppose $\hat{T}_j\xi = \lambda$ with $\lambda \geq 0$. Premultiplication of this equality with $(R'_j)^\top R'_j$ yields $(R'_j)^\top\xi = (R'_j)^\top R'_j\lambda$, which, in turn, yields

$$(R'_j)^\top\left(\xi - R'_j\lambda\right) = 0. \tag{5.50}$$

  Clearly, since $R'_j \in \mathbb{R}^{3\times 2}$ there is no unique solution to this equation. Consider a solution that satisfies $\xi - R'_j\lambda \neq 0$. Since the columns of R'_j both belong to the plane defined by $\ker(h)$, it must hold that the vector $\xi - R'_j\lambda$ is perpendicular to this plane. However, since $R'_j\lambda \in \ker(h)$, this contradicts the assumption that $\xi \in \ker(h)$. As such, the only solution that can satisfy (5.50) when $h\xi = 0$ holds, is $\xi = R'_j\lambda$. For $\lambda \geq 0$ this implies $\xi \in \text{pos}\left\{r_j^1, r_j^2\right\} = \hat{\mathcal{T}}_j$.

5.A.2 Proof of Proposition 5.3.6

The first part of the proof follows similar arguments as in Johansson, 2002, Section A.4. First, the continuity property is shown for all $\xi \in \hat{\mathcal{S}}_i \cap \hat{\mathcal{S}}_j$, $i, j \in \mathcal{N} \times \mathcal{N}$, $i \neq j$. Observe that each $\xi \in \hat{\mathcal{S}}_i$ can be written as a linear combination of elements from $\bar{\mathcal{R}}$, such that

$$\xi = \sum_{q=1}^{p} r_q w_{q,i} = \bar{R}\bar{w}_i, \tag{5.51}$$

where $\bar{w}_i = [w_{1,i}, \ldots, w_{p,i}]^\top \in \mathbb{R}^p$ collects the weights $w_{q,i}$. One can set $w_{q,i} = 0$ for all q such that $r_q \notin \hat{\mathcal{S}}_i$ (where no distinction is made between $[0, 0, 1]^\top$ and $[0, 0, -1]^\top$). By doing so, it follows that $\bar{w}_i = E_i E_i^\top \bar{w}_i$, such that (5.51) can equivalently be written as $\xi = \bar{R}E_i E_i^\top \bar{w}_i$. Since E_i extracts those columns from $\bar{R}$ that coincide with the generators of $\hat{\mathcal{S}}_i$, it follows that the columns of the matrix $\bar{R}E_i$ are linearly independent and thus $\bar{R}E_i$ is invertible. From this, one finds the mapping $\bar{w}_i = E_i \left(\bar{R}E_i\right)^{-1} \xi$. On the boundary shared by two simplicial cones $\hat{\mathcal{S}}_i$ and $\hat{\mathcal{S}}_j$, the only non-zero elements of $w_{q,i}, w_{q,j}$ are those that describe this common boundary. Therefore, $w_{q,i}(\xi) = w_{q,j}(\xi)$ for all $\xi \in \hat{\mathcal{S}}_i \cap \hat{\mathcal{S}}_j$. The result trivially follows for $\xi \in -\hat{\mathcal{S}}_i \cap -\hat{\mathcal{S}}_j$, $i, j \in \mathcal{N} \times \mathcal{N}$, $i \neq j$.

It remains to show that (5.20) also yields the continuity property for $\xi \in \hat{\mathcal{S}}_i \cap -\hat{\mathcal{S}}_j$, $i, j \in \mathcal{N} \times \mathcal{N}$ which corresponds to the line $\xi = [0, 0, \dot{z}]^\top$. Since the vector $[0, 0, -1]^\top$ is excluded from $\bar{\mathcal{R}}$, this common boundary is represented by only one column in $\bar{R}$, being the vector $[0, 0, 1]^\top$. Therefore, for each $\xi \in \hat{\mathcal{S}}_i \cap -\hat{\mathcal{S}}_j$, $i, j \in \mathcal{N} \times \mathcal{N}$, the only non-zero element in $w_{q,i}$ and $w_{q,j}$ describes this common boundary. This concludes the proof.

5.A.3 Proof of Proposition 5.3.8

Parts of the proof are inspired by the proofs of Ambrosino and Garone, 2015, Lemma 1, and Ambrosino and Garone, 2015, Theorem 2.

i) $\implies$ *ii)*: Suppose V in (5.24) is continuous. Consider the state transformation $\bar{x} = Tx$, with $T = \begin{bmatrix} E^\top & U^\top \end{bmatrix}^\top$, and where $\mathrm{Im}(U) = \ker(E)$, such that one finds $\bar{x} = [\xi^\top, \hat{x}^\top]^\top$ with $\xi = [z, u, \dot{z}]^\top \in \mathbb{R}^3$ and $\hat{x} \in \mathbb{R}^{n-3}$. Note that T has full rank and thus is invertible. In terms of the transformed coordinates, the function V reads as $V(\bar{x}) = \bar{x}^\top \bar{P}_i \bar{x}^\top$ with $\bar{P}_i = T^{-\top} P_i T^{-1}$. Partition the matrix $\bar{P}_i$, $i \in \mathcal{N}$ as

$$\bar{P}_i = \begin{bmatrix} \bar{P}_i^{11} & \bar{P}_i^{12} \\ \bar{P}_1^{21} & \bar{P}_i^{22} \end{bmatrix}, \tag{5.52}$$

with $\bar{P}_i^{12} = (\bar{P}_i^{21})^\top$, such that

$$V(\bar{x}) = \xi^\top \bar{P}_i^{11} \xi + 2\hat{x}^\top \bar{P}_i^{12} \xi + \hat{x}^\top P_i^{22} \hat{x}. \tag{5.53}$$

Continuity of V then implies for all $\xi \in \hat{\mathcal{S}}_i \cap \hat{\mathcal{S}}_j$, $(i,j) \in \mathcal{N} \times \mathcal{N}$ and all $\hat{x} \in \mathbb{R}^{n-3}$

$$\xi^\top (P_i^{11} - P_j^{11})\xi + 2\hat{x}^\top (P_i^{12} - P_j^{12})\xi + \hat{x}^\top (P_i^{22} - P_j^{22})\hat{x} = 0. \tag{5.54}$$

First consider all $p \in \mathcal{N}$ and all $\xi \in \hat{\mathcal{S}}_p$. Since $\xi = 0 \in \left\{\hat{\mathcal{S}}_i \cap \hat{\mathcal{S}}_j\right\}$ for all $(i,j) \in \mathcal{N} \times \mathcal{N}$, it should hold that $\hat{x}^\top (P_i^{22} - P_j^{22})\hat{x} = 0$ for all $\hat{x} \in \mathbb{R}^{n-3}$. This is only possible if there exists a symmetric matrix $\Phi^{22} \in \mathbb{S}^{(n-3)\times(n-3)}$ such that for all $i \in \mathcal{N}$ one has $P_i^{22} = \Phi^{22}$.

In a similar manner, when $\hat{x} = 0$, it should hold for all $\xi \in \left\{\hat{\mathcal{S}}_i \cap \hat{\mathcal{S}}_j\right\}$, $(i,j) \in \mathcal{N} \times \mathcal{N}$ that $\xi^\top (P_i^{11} - P_j^{11})\xi = 0$. On the basis of Ambrosino and Garone, 2015, Theorem 2, one can conclude that the equalities

$$r_m^\top \bar{P}_i^{11} r_m = r_m^\top \bar{P}_j^{11} r_m = \phi_{mm} \tag{5.55a}$$
$$r_m^\top \bar{P}_i^{11} r_n = r_m^\top \bar{P}_j^{11} r_n = \phi_{mn}, \tag{5.55b}$$

hold true for all $r_m, r_n \in \mathcal{R}_i \cap \mathcal{R}_j$, where $\mathcal{R}_i$ denotes the set of generators of $\hat{\mathcal{S}}_i$. Note that for all $r_m, r_n \in \mathcal{R}_i \cap \mathcal{R}_j$, with $r_n = [0,0,-1]$ one has

$$r_n^\top \bar{P}_i^{11} r_n = r_n^\top \bar{P}_j^{11} r_n = r_k^\top \bar{P}_i^{11} r_k = r_k^\top \bar{P}_j^{11} r_k = \phi_{nn} = \phi_{kk} \tag{5.56a}$$
$$r_m^\top \bar{P}_i^{11} r_n = r_m^\top \bar{P}_j^{11} r_n = -r_m^\top \bar{P}_i^{11} r_k = -r_m^\top \bar{P}_j^{11} r_k = \phi_{mn} = -\phi_{mk}, \tag{5.56b}$$

with $r_k = -r_n = [0,0,1]^\top$. Note that in case r_m and r_k already are generators of a region $\hat{\mathcal{S}}_l$, $l \neq j$, $l \neq i$, then ϕ_{mk} is already defined, and one should consider both r_k, and r_n as separate generators, otherwise there will be overlap in the ϕ-elements. This degenerate situation, however, only arises when the $(z, \dot{z})$ region is divided into two regions. For divisions into more than two regions, there is no need to make a distinction between the vectors $[0,0,1]^\top$ and $[0,0,-1]^\top$ since it is always possible to express the constraints in terms of either one of these vectors without creating overlap.

Considering the non-degenerate cases, by the result in Ambrosino and Garone, 2015, Lemma 1 there exists a symmetric matrix $\Phi^{11} = \{\phi_{pq}\} \in \mathbb{S}^{r\times r}$ for all $p = 1, \ldots, r$ and all $q = 1, \ldots, r$. Note that Φ^{11} can always be constructed by simply collecting the elements in (5.56). Moreover, if for a couple (m,n) and an integer i such that $r_m, r_n \in \mathcal{R}_i$ does not exist, then ϕ_{mn} remains unconstrained.

On a per region basis, one can write

$$R_i^\top \bar{P}_i^{11} R_i = \Phi_i^{11} = E_i^\top \Phi^{11} E_i, \tag{5.57}$$

with R_i the matrix collecting the generators of $\hat{\mathcal{S}}_i$, and Φ_i^{11} the matrix containing the parameters associated with the region $\hat{\mathcal{S}}_i$. The second inequality in

(5.57) explicitly follows from the construction of the extraction matrices E_i as in Proposition 5.3.6. Since R_i is invertible, one finds

$$\bar{P}_i^{11} = R_i^{-\top}\Phi_i R_i^{-1} = (\bar{R}E_i)^{-\top}\Phi_i(\bar{R}E_i)^{-1} = (\bar{R}E_i)^{-\top}E_i^{\top}\Phi^{11}E_i(\bar{R}E_i)^{-1}, \tag{5.58}$$

with $\bar{R}$ the matrix collecting the distinct generators of the partitioning $\mathcal{P}_{\hat{\mathcal{S}}}$. Due to symmetry, the identity (5.58) also applies to all $\xi \in -\hat{\mathcal{S}}_p$, $p \in \mathcal{N}$. Note that continuity over the boundary defined by the vector $[0,0,-1]^{\top}$ is implied by (5.56). From the definition of the continuity matrices as $\hat{F}_i = E_i(\bar{R}E_i)^{-1}$, it follows that

$$\bar{P}_i = \hat{F}_i^{\top}\Phi^{11}\hat{F}_i. \tag{5.59}$$

Since $\hat{x}^{\top}(P_i^{22} - P_j^{22})\hat{x} = 0$ for all $\hat{x} \in \mathbb{R}^{n-3}$, and $\xi^{\top}(P_i^{11} - P_j^{11})\xi = 0$ for all $\xi \in \pm\hat{\mathcal{S}}_i \cap \pm\hat{\mathcal{S}}_j$, $i,j \in \mathcal{N}\times\mathcal{N}$, it must also be true that $\hat{x}^{\top}(P_i^{12} - P_j^{12})\xi = 0$ for all $(\hat{x},\xi) \in \left\{\mathbb{R}^{n-3}\right\} \times \left\{\pm\hat{\mathcal{S}}_i \cap \pm\hat{\mathcal{S}}_j\right\}$. In a similar manner as before, one finds the equality

$$P_i^{12}r_m = P_j^{12}r_m = \phi_m \tag{5.60}$$

to hold for all $r_m \in \mathcal{R}_i \cap \mathcal{R}_j$. Moreover, for all $r_m \in \mathcal{R}_i \cap \mathcal{R}_j$ with $r_m = [0,0,-1]^{\top}$ one finds

$$P_i^{12}r_m = P_j^{12}r_m = \phi_m = -P_i^{12}r_n = -P_j^{12}r_n = -\phi_n, \tag{5.61}$$

where $r_n = -r_m = [0,0,-1]^{\top}$. Similar as before, there is no need to make a distinction between $[0,0,1]^{\top}$ and $[0,0,-1]^{\top}$. Collect all elements in a matrix $\Phi^{12} = \{\phi_p\} \in \mathbb{R}^{3\times r}$ for all $p = 1,\ldots,r$, and observe that

$$\bar{P}_i^{12}R_i = \Phi_i^{12} = \Phi^{12}E_i. \tag{5.62}$$

Since R_i is invertible, it follows that

$$\bar{P}_i^{12} = \Phi^{12}E_iR_i^{-1} = \Phi^{12}E_i(\bar{R}E_i)^{-1} = \Phi^{12}\hat{F}_i. \tag{5.63}$$

As such, the partitioned matrix in (5.52) is equivalently written as

$$\bar{P}_i = \begin{bmatrix} \hat{F}_i^{\top}\Phi^{11}\hat{F}_i & \Phi^{12}\hat{F}_i \\ \hat{F}_i^{\top}\Phi^{21} & \Phi^{22} \end{bmatrix} = \begin{bmatrix} \hat{F}_i & 0 \\ 0 & I \end{bmatrix}^{\top} \begin{bmatrix} \Phi^{11} & \Phi^{12} \\ \Phi^{21} & \Phi^{22} \end{bmatrix} \begin{bmatrix} \hat{F}_i & 0 \\ 0 & I \end{bmatrix}. \tag{5.64}$$

Pre- and post-multiplying this with $\bar{x} = [\xi^{\top}, \hat{x}^{\top}]^{\top}$ yields

$$\begin{aligned} \bar{x}^{\top}\bar{P}_i\bar{x} &= \xi^{\top}\hat{F}_i^{\top}\Phi^{11}\hat{F}_i\xi + 2\hat{x}^{\top}\Phi^{12}\hat{F}_i\xi + \hat{x}^{\top}\Phi^{22}\hat{x} \\ &= \xi^{\top}\hat{F}_i^{\top}\Phi^{11}\hat{F}_i\xi + \bar{x}^{\top}\Gamma\Phi^{12}\hat{F}_i\xi + \xi^{\top}\hat{F}_i^{\top}\Phi^{21}\Gamma\bar{x} + \bar{x}^{\top}\Gamma^{\top}\Phi^{22}\Gamma\bar{x}, \end{aligned} \tag{5.65}$$

with $\Gamma = [0, I]$. As such, one finds

$$\begin{aligned}\bar{x}\bar{P}_i\bar{x} &= \begin{bmatrix}\xi\\ \bar{x}\end{bmatrix}^\top \begin{bmatrix}\hat{F}_i^\top \Phi^{11}\hat{F}_i & \hat{F}_i^\top \Phi^{12}\Gamma\\ \Gamma^\top\Phi^{21}\hat{F}_i & \Gamma^\top\Phi^{22}\Gamma\end{bmatrix}\begin{bmatrix}\xi\\ \bar{x}\end{bmatrix}\\ &= \begin{bmatrix}\xi\\ \bar{x}\end{bmatrix}^\top \begin{bmatrix}\hat{F}_i & 0\\ 0 & I\end{bmatrix}^\top \begin{bmatrix}\Phi^{11} & \Phi^{12}\Gamma\\ \Gamma^\top\Phi^{21} & \Gamma^\top\Phi^{22}\Gamma\end{bmatrix}\begin{bmatrix}\hat{F}_i & 0\\ 0 & I\end{bmatrix}\begin{bmatrix}\xi\\ \bar{x}\end{bmatrix}.\end{aligned} \tag{5.66}$$

Then, using $P_i = T^\top \bar{P}_i T$, and $[\xi^\top, \bar{x}^\top]^\top = [E^\top, T]^\top x$ with $T = [E^\top, U^\top]^\top$, one finds

$$\begin{aligned}P_i &= \begin{bmatrix}\hat{F}_i E\\ T\end{bmatrix}^\top \begin{bmatrix}\Phi^{11} & \Phi^{12}\Gamma\\ \Gamma^\top\Phi^{21} & \Gamma^\top\Phi^{22}\Gamma\end{bmatrix}\begin{bmatrix}\hat{F}_i E\\ T\end{bmatrix}\\ &= \begin{bmatrix}\hat{F}_i E\\ I\end{bmatrix}^\top \begin{bmatrix}\Phi^{11} & \Phi^{12}U\\ U^\top\Phi^{21} & U^\top\Phi^{22}U\end{bmatrix}\begin{bmatrix}\hat{F}_i E\\ I\end{bmatrix} = F_i^\top \Phi F_i.\end{aligned} \tag{5.67}$$

Hence, continuity of V implies the existence of a symmetric matrix Φ such that $P_i = F_i^\top \Phi F_i$.

ii) $\implies$ *iii)*. Suppose that there exists a symmetric matrix Φ such that $P_i = F_i^\top \Phi F_i$ for all $i \in \mathcal{N}$, and where $F_i = [(E_i R_i^{-1} E)^\top, I]$. By partitioning Φ as

$$\Phi = \begin{bmatrix}\Phi^{11} & \Phi^{12}\\ \Phi^{21} & \Phi^{22}\end{bmatrix}, \tag{5.68}$$

one can write

$$P_i = \Phi^{22} + (\hat{F}_i E)^\top \Phi^{11}\hat{F}_i E + \Phi^{12}\hat{F}_i E + (\hat{F}_i E)^\top \Phi^{21}, \tag{5.69}$$

with $\hat{F}_i = E_i R_i^{-1}$. Now observe that for all $(i, j) \in \mathcal{N} \times \mathcal{N}$ such that $\mathcal{S}_i \cap \mathcal{S}_j \neq \emptyset$, the boundary between two adjacent regions can be written as

$$H_{ij} = (E_i R_i^{-1} - E_j R_j^{-1})E = (\hat{F}_i - \hat{F}_j)E, \tag{5.70}$$

which clearly by construction of the continuity matrices implies $H_{ij}x = 0$ for all $x \in \mathcal{S}_i \cap \mathcal{S}_j$. In turn, one finds $\hat{F}_i E = H_{ij} + \hat{F}_j E$. Then for all $(i, j) \in \mathcal{N} \times \mathcal{N}$ such that $\mathcal{S}_i \cap \mathcal{S}_j \neq \emptyset$ the difference $P_i - P_j$ after simplification reads

$$P_i - P_j = \left(\Phi^{12} + \Phi^{11}\hat{F}_j E\right)^\top H_{ij} + H_{ij}^\top \left(\Phi^{21} + \Phi^{11}\hat{F}_j E\right). \tag{5.71}$$

Since $\mathrm{im} Z_{ij} = \ker H_{ij}$ it holds true that $H_{ij} Z_{ij} = 0$, from which it immediately follows that $Z_{ij}^\top (P_i - P_j) Z_{ij} = 0$.

iii) $\implies$ *i)*. Assume there exist matrices P_i such that $Z_{ij}^\top(P_i - P_j)Z_{ij} = 0$. On the boundary between two regions $\mathcal{S}_i$ and $\mathcal{S}_j$, one can write $x = Z_{ij}v$ with $v \in \mathbb{R}^{n-2}$. Assuming the equality holds, then for any $v \in \mathbb{R}^{n-2}$ one finds

$$v^\top Z_{ij}^\top(P_i - P_j)Z_{ij}v = x^\top(P_i - P_j)x = x^\top P_i x - x^\top P_j x = 0, \tag{5.72}$$

which clearly implies a function of the form $V_i(x) = x^\top P_i x$ if $x \in \mathcal{S}_i \cup -\mathcal{S}_i$ to be continuous. This completes the proof.

5.A.4 Proof of Theorem 5.4.1

Consider the piecewise quadratic function

$$V(x) = V_i(x) := x^\top P_i x, \text{ when } x \in \mathcal{S}_i \cup -\mathcal{S}_i, i \in \mathcal{N}, \tag{5.73}$$

where $P_i = F_i^\top \Phi F_i$. The proof is based on showing that, under the conditions of the theorem, V classifies both as a storage function, as well as a suitable ISS-Lyapunov function for the closed-loop system in (5.5) (see Definition 2.3.10).

First, observe that solutions to (5.5) are locally absolutely continuous, and V is composed by locally Lipschitz continuous functions. By virtue of Proposition 5.3.6, V is continuous over the boundaries of the partitioning, making V a (non-smooth) locally Lipschitz continuous function on the set $\mathcal{X} = \{x \in \mathbb{R}^n \mid Ex \in \mathcal{F}\}$.

Positive definiteness of V (and thus satisfaction of condition (2.34) in Definition 2.3.10) is implied by (5.27). Indeed, from the results in Proposition 5.3.5 and non-negativity of the elements in W_i, it follows that

$$x^\top S_i^\top W_i S_i x \geq 0, \text{ when } x \in \mathcal{S}_i \cup -\mathcal{S}_i, \, i \in \mathcal{N}. \tag{5.74}$$

Application of the S-procedure then shows that

$$V(x) > x^\top S_i^\top W_i S_i x \geq 0 \text{ if } 0 \neq x \in \mathcal{S}_i \cup -\mathcal{S}_i, \, i \in \mathcal{N}. \tag{5.75}$$

The strict inequality implies the existence of some sufficiently small $\alpha_1 > 0$ such that $V(x) \geq \alpha_1 \|x\|^2$. Furthermore, due to the piecewise quadratic construction of V there exists $\alpha_2 > 0$ such that $V(x) \leq \alpha_2 \|x\|^2$. Hence, one finds

$$\alpha_1 \|x\|^2 \leq V(x) \leq \alpha_2 \|x\|^2, \tag{5.76}$$

which yields the corresponding result.

Next, it is shown that the LMIs in (5.28) and (5.29) imply satisfaction of the condition (2.35) in Definition 2.3.10. Hereto, consider first the LMI condition in (5.28). Using the results from Proposition 5.3.5, and non-negativity of the elements in U_i, one finds that $x^\top S_i^\top U_i S_i x \geq 0$ when $x \in \mathcal{S}_i \cup -\mathcal{S}_i$. Application of the S-procedure in combination with the Schur complement of (5.28) shows that

the inequality in (5.28) implies for $i \in \mathcal{N}$ that at all points where the gradient of V is defined, it satisfies

$$\begin{aligned}\nabla V_i(x)(A_1x + Bw) &= x^\top \left(A_1^\top P_i + P_i A_1\right) x + 2x^\top P_i B w \\ &\leq -\epsilon\|x\|^2 - (Cx + Dw)^\top (Cx + Dw) + \gamma^2\|w\|^2 \\ &= -\epsilon\|x\|^2 - \|q\|^2 + \gamma^2\|w\|^2.\end{aligned}$$

In a similar manner, consider the LMI condition in (5.29). Combining the results of Proposition 5.3.5 with non-negativity of the elements in V_j shows that $x^\top T_j^\top V_j T_j x \geq 0$ for all $x \in \mathcal{T}_j \cup -\mathcal{T}_j$, $j \in \mathcal{M}$. Application of the S-procedure, Finsler's lemma, and the Schur complement then shows that the inequality in (5.29) at all points where the gradient of V is defined it satisfies

$$\begin{aligned}\nabla V_j(x)(A_2x + Bw) &= x^\top \left(A_2^\top P_j + P_j A_2\right) x + 2x^\top P_j B w + 2\mu x^\top P_j (b\Pi) x \\ &\leq -\epsilon\|x\|^2 - (Cx + Dw)^\top (Cx + Dw) + \gamma^2\|w\|^2 \\ &= -\epsilon\|x\|^2 - \|q\|^2 + \gamma^2\|w\|^2,\end{aligned}$$

where the algebraic relation $Hx = 0$ is used, which holds true for all $x \in \mathcal{T}_j \cup -\mathcal{T}_j$, $j \in \mathcal{M}$. From the above inequalities, one can conclude that

$$\max_{(p,q)\in\mathcal{PQ}} \nabla V_p(x)(A_q x + Bw) \leq -\epsilon\|x\|^2 + \gamma^2\|w\|^2, \tag{5.77}$$

where $\mathcal{PQ} := \{\{1\} \times \mathcal{N}\} \cup \{\{2\} \times \mathcal{M}\}$. This implies condition (2.35) to hold, thereby demonstrating that under the hypothesis of the theorem, V classifies as an ISS-Lyapunov function. By virtue of Theorem 2.3.11 this implies ISS of the closed-loop system in (5.5).

In a similar manner, from the above inequalities one can conclude

$$\max_{(p,q)\in\mathcal{PQ}} \nabla V_p(x)(A_q x + Bw) \leq -\|q\|^2 + \gamma^2\|w\|^2 \tag{5.78}$$

to hold, such that V classifies as a storage function with supply rate $s(w, q, x) = -\|q\|^2 + \gamma^2\|w\|$. The proof can be finished using standard arguments such as in, *e.g.*, Khalil, 2002 and van der Schaft, 2017 for showing that the closed-loop system in (5.5) admits an $\mathcal{L}_2$-gain smaller than or equal to γ.

5.A.5 Proof of Proposition 5.4.5

For proving infeasibility of the LMIs (5.27), (5.28) and (5.30)–(5.33), it is sufficient to prove that the LMIs

$$P_i - S_i^\top W_i S_i \succ 0, \tag{5.79a}$$

$$A_1^\top P_i + P_i A_1 + S_i^\top U_i S_i \prec 0, \tag{5.79b}$$

$$\bar{A}_2^\top P_j + P_j \bar{A}_2 + T_j^\top K_j T_j + L_j H + (L_j H)^\top \prec 0, \tag{5.79c}$$

with S_i, T_j, and H defined in (5.22), cannot be feasible for some $i \in \mathcal{N}$ and $j \in \mathcal{M}$ under conditions (5.35) and/or (5.36).

C1. Consider the integrator-mode subsystem. When feasible, the conditions in (5.79) imply that for any complex nonzero vector $v \in \mathbb{C}^m$ and its complex conjugate $\bar{v}$ it holds that $\bar{v}^\top \left(P_i - S_i^\top W_i S_i\right) v > 0$ and $\bar{v}^\top \left(A_1^\top P_i + P_i A_1 + S_i^\top U_i S_i\right) v < 0$. Choose v to be an eigenvector of A_1 such that $A_1 v = \lambda v$ with $\lambda \in \mathbb{C}$ the corresponding eigenvalue. Observe the identity

$$Ev \overset{(5.7)}{=} \begin{bmatrix} C_z & 0 \\ 0 & 1 \\ C_z A_g & 0 \end{bmatrix} v = \begin{bmatrix} \frac{1}{\omega_h} C_u A_1 \\ C_u \\ \frac{1}{\omega_h} C_u A_1^2 \end{bmatrix} v = \rho C_u v \tag{5.80}$$

with $C_u := [0_{1\times p}, 1]$, $\rho := \begin{bmatrix} \frac{\lambda}{\omega_h} & 1 & \frac{\lambda^2}{\omega_h} \end{bmatrix}^\top$ and the matrices A_g, $C_z = -C$ are given in (5.1) and (5.8), respectively. Note that here use is made of the fact that $C_z B_g = 0$ by virtue of Assumption 2.3.1. Assume $\lambda \in \mathbb{C}$ such that

$$\rho = \frac{1}{\omega_h} \left(\begin{bmatrix} \mathrm{Re}(\lambda) \\ \omega_h \\ \mathrm{Re}(\lambda)^2 - \mathrm{Im}(\lambda)^2 \end{bmatrix} + j \begin{bmatrix} \mathrm{Im}(\lambda) \\ 0 \\ 2\mathrm{Re}(\lambda)\mathrm{Im}(\lambda) \end{bmatrix} \right). \tag{5.81}$$

By construction of S_i as in (5.22), it follows that

$$\begin{aligned} S_i v &= R_i^{-1} E v = R_i^{-1} \rho C_u v \\ &= R_i^{-1} \left(\mathrm{Re}(\rho) + j\mathrm{Im}(\rho)\right) C_u v. \end{aligned} \tag{5.82}$$

Note that, additionally,

$$S_i \bar{v} = R_i^{-1} \left(\mathrm{Re}(\rho) - j\mathrm{Im}(\rho)\right) C_u \bar{v}.$$

If $\mathrm{Re}(\rho), \mathrm{Im}(\rho) \in \hat{\mathcal{S}}_i$ then $R_i^{-1}\mathrm{Re}(\rho) \geq 0$ and $R_i^{-1}\mathrm{Im}(\rho) \geq 0$ hold entry-wise. Similarly, for $\mathrm{Re}(\rho), \mathrm{Im}(\rho) \in -\hat{\mathcal{S}}_i$ one has $R_i^{-1}\mathrm{Re}(\rho) \leq 0$ and $R_i^{-1}\mathrm{Im}(\rho) \leq 0$. Moreover, if $\mathrm{Re}(\rho) \in \pm\hat{\mathcal{S}}_i$ and $\mathrm{Im}(\rho) \in \mp\hat{\mathcal{S}}_i$, then $R_i^{-1}\mathrm{Re}(\rho)$ and $R_i^{-1}\mathrm{Im}(\rho)$ have opposite signs. For any symmetric matrix X_i with non-negative elements one finds

$$\bar{v}^\top S_i^\top X_i S_i v = \bar{v}^\top C_u^\top \begin{bmatrix} \mathrm{Re}(\rho) \\ \mathrm{Im}(\rho) \end{bmatrix}^\top Q_i \begin{bmatrix} \mathrm{Re}(\rho) \\ \mathrm{Im}(\rho) \end{bmatrix} C_u v \geq 0, \tag{5.83}$$

with $Q_i = \mathrm{diag}\left(R_i^{-\top} X_i R_i^{-1}, R_i^{-\top} X_i R_i^{-1}\right)$ a block diagonal matrix. Note that the cross product of real and imaginary parts cancels.

Suppose (5.79a) holds. Through (5.83) with $X_i = W_i$, this implies $\bar{v}^\top P_i v > 0$, which, in turn, for $\mathrm{Re}(\lambda) > 0$ implies

$$\begin{aligned} &\bar{v}^\top \left(A_1^\top P_i + P_i A_1\right) v + \bar{v}^\top S_i^\top U_i S_i v \\ &= 2\mathrm{Re}(\lambda) \bar{v}^\top P_i v + \bar{v}^\top S_i^\top U_i S_i v > 0. \end{aligned} \tag{5.84}$$

Hence, under condition (5.35) the inequalities in (5.79) cannot be satisfied, which shows that the LMIs in Theorem 5.4.1 and Theorem 5.4.3 are infeasible in this case.

C2. Consider the gain-mode subsystem. As these dynamics are defined in a lower-dimensional region of $\mathcal{F}$, namely $\mathcal{F}_2$ in (5.3b), it follows from Finsler's lemma that for any $j \in \mathcal{M}$, the first and third LMI in (5.79) can equivalently be written as

$$\Theta^\top \left(P_j - S_j^\top W_j S_j\right) \Theta \succ 0, \tag{5.85a}$$

$$\Theta^\top \left(A_2^\top P_j + P_j A_2\right) \Theta + \Theta^\top T_j^\top V_j T_j \Theta \prec 0, \tag{5.85b}$$

with $\Theta = [I, k_h C_z^\top]^\top$ and A_2 is given in (5.8). Also note that $H\Theta = 0$. Next, observe that

$$A_2\Theta = \begin{bmatrix} A_g & B_g \\ k_h C_z A_g & 0 \end{bmatrix} \begin{bmatrix} I \\ k_h C_z \end{bmatrix} = \begin{bmatrix} A_g + k_h B_g C_z \\ k_h C_z A_g \end{bmatrix} = \Theta \hat{A}_2,$$

where $\hat{A}_2 := A_g + k_h B_g C_z$ with A_g, B_g, $C_z = -C$ given in (5.1) and (5.8), and use is made of the fact that $C_z B_g = 0$. Consider $v \in \mathbb{C}^{m-1}$ to be an eigenvector of $\hat{A}_2$ such that $\hat{A}_2 v = \lambda v$ with $\lambda \in \mathbb{C}$ the corresponding eigenvalue. Then the following identity holds

$$E\Theta v = \begin{bmatrix} C_z & 0 \\ 0 & 1 \\ C_z A_g & 0 \end{bmatrix} \begin{bmatrix} I \\ k_h C_z \end{bmatrix} v = \begin{bmatrix} C_z \\ k_h C_z \\ C_z \bar{A}_2 \end{bmatrix} v = \rho C_z v, \tag{5.86}$$

with $\rho := \begin{bmatrix} 1 & k_h & \lambda \end{bmatrix}^\top$. Assume $\lambda \in \mathbb{C}$ such that

$$\rho = \begin{bmatrix} 1 \\ k_h \\ \mathrm{Re}(\lambda) \end{bmatrix} + j \begin{bmatrix} 0 \\ 0 \\ \mathrm{Im}(\lambda) \end{bmatrix}. \tag{5.87}$$

The vectors $\mathrm{Re}(\rho)$ and $\mathrm{Im}(\rho)$ both belong to the plane in $\mathcal{F}$ defined by $h\xi = [k_h, -1, 0]\xi = 0$, $\xi \in \mathbb{R}^3$, *i.e.,* the two-dimensional plane in $\mathcal{F}$ on which the gain-mode is defined. Consequently, since $\hat{\mathcal{T}}_j$, $j \in \mathcal{M}$ is a subset of this plane, and $\hat{\mathcal{T}}_j \subset \hat{\mathcal{S}}_j$ for all $j \in \mathcal{M}$, it follows that

$$\left\{ \begin{bmatrix} 1 \\ \mathrm{Re}(\lambda) \end{bmatrix}, \begin{bmatrix} 0 \\ \mathrm{Im}(\lambda) \end{bmatrix} \right\} \subset \hat{\mathcal{T}}_j \Leftrightarrow \{\mathrm{Re}(\rho), \mathrm{Im}(\rho)\} \subset \hat{\mathcal{S}}_j.$$

Using a similar reasoning as before, it follows that if (5.36) is true, then $\bar{v}^\top \Theta S_j^\top W_j S_j \Theta v \geq 0$ and $\bar{v}^\top \Theta T_j^\top V_j T_j \Theta v \geq 0$. Suppose (5.85a) is feasible. Together with the above this implies $\bar{v}^\top \bar{P}_j v > 0$ with $\bar{P}_j := \Theta^\top P_j \Theta$. Consequently

it must be true that

$$\begin{aligned} &\bar{v}^\top \left(\hat{A}_2^\top \bar{P}_j + \bar{P}_j \hat{A}_2 \right) v + \bar{v} \Theta T_j^\top V_j T_j \Theta v \\ &= 2\mathrm{Re}(\lambda) \bar{v}^\top \bar{P}_j v + \bar{v}^\top \Theta T_j^\top V_j T_j \Theta v > 0. \end{aligned} \tag{5.88}$$

This contradicts (5.85), which implies that (5.79) cannot be feasible when (5.36) is true. In turn, this shows that for this case the LMIs in Theorem 5.4.1 and Theorem 5.4.3 cannot be feasible. This completes the proof.

Chapter 6

Steady-State Performance Analysis: A Convergent Dynamics Approach

6.1 Introduction

Steady-state performance of a feedback control system indicates, in a certain sense, the sensitivity of its steady-state response to external inputs. In the previous chapter, (steady-state) performance of hybrid integrator-gain systems (HIGS) has been characterized through the notion of the $\mathcal{L}_2$-gain, which is often interpreted as a measure for the worst-case system's energy transmission from an input to an output. Although such an approach is valid for a broad class of input signals and provides a worst-case performance metric, it does not take into account additional knowledge regarding the nature of the inputs, and in that sense can be conservative when dealing with specific inputs, such as periodic inputs. To characterize the steady-state performance of control systems containing HIGS in a more accurate manner, this chapter pursues an alternative approach that exploits the notion of *convergent systems*.

The term convergent system was first coined in the Russian literature (Demidovich, 1967; Pliss, 1964) and refers to nonlinear systems having the property that, when excited by an arbitrary bounded input, there exists a *unique* time-varying solution (related to the input) that is bounded on the whole time axis and is globally asymptotically stable. Regardless of the initial conditions of the system, all other solutions converge to this steady-state solution. Contrary to asymptotically stable linear systems, this property does not hold for nonlinear systems in general. Moreover, it is not trivially established. However, proving

the convergence property leads to the guarantee of having a unique and bounded steady-state response, which opens up the possibility for characterizing steady-state performance in an exact manner using a variety of numerical tools such as forward integration, periodic solvers (Ascher et al., 1988) or the more efficient mixed time-frequency (MTF) algorithm (Pavlov et al., 2013) to name but a few. Besides, it facilitates a means to construct nonlinear Bode plots (Alcorta Garcia et al., 2010; Pavlov et al., 2007; Thenozhi and Tang, 2016) and quantify the accuracy of approximate methods such as the describing function (Pavlov et al., 2008; Pogromsky and van den Berg, 2014). Notions closely related to convergence, *i.e.*, describing the property of solutions converging to each other, are known in the literature as incremental stability and contraction, see, *e.g.*, Angeli, 2002; Forni and Sepulchre, 2012; Fromion et al., 1996; Li et al., 2014; Lohmiller and Slotine, 1998; Russo et al., 2010; Waitman et al., 2016 and the references therein.

Motivated by the aforementioned desirable properties and tools related to convergence, the main objective in this chapter is to investigate the relevant convergence property for HIGS-controlled systems. For systems containing a scalar, memoryless nonlinearity, conditions for convergence typically hinge upon the nonlinearity satisfying an incremental sector condition (Ghodrat and Marquez, 2021; Pavlov et al., 2006a; Romanchuk and Smith, 1999). HIGS, however, inherently violates such incremental sector condition due to its underlying dynamics in combination with the discontinuous vector field. Moreover, discontinuous vector fields can significantly complicate a convergence analysis as is also highlighted in Pavlov et al., 2006b, where conditions for convergence of piecewise affine (PWA) systems with discontinuous right-hand sides are formulated in terms of linear matrix inequalities (LMIs). In said work, discontinuities may only occur due to affine terms in the dynamics. For HIGS, however, discontinuities in the dynamics also result from other terms, such that the results in Pavlov et al., 2006b do not translate to the setting considered here. In Morinaga et al., 2004; Waitman et al., 2016; Waitman et al., 2019 piecewise quadratic/polynomial Lyapunov functions are used for deriving incremental stability properties of classes of PWA systems. These results, however, do not exploit knowledge regarding (incremental) properties of the closed-loop system dynamics, possibly making them conservative in the current context.

In this chapter, a piecewise quadratic approach is pursued as well, but different from the results in Morinaga et al., 2004; Waitman et al., 2016, here specific incremental properties of the vector field of HIGS are taken into account. In particular, by partitioning HIGS' incremental input-output space, regional properties are identified that can be conveniently exploited for constructing appropriate piecewise incremental Lyapunov functions. Essentially, these functions result from "connecting" separate incremental storage functions (each linked to different incremental properties) in a suitable manner. In order to make the results applicable to a larger class of systems, the integrator-mode in HIGS is

replaced by a generic nonlinear vector field. Under certain assumptions on this vector field, conditions for convergence are established which, in turn, can be formulated in terms of numerically tractable LMIs. A frequency-domain interpretation of the LMIs, which allows for a graphical verification of the conditions and may yield valuable tuning insights, is presented as well. The conditions are further extended to provide rigorous error bounds on steady-state performance predictions based on the describing function approximation.

The organization of this chapter is as follows. In Section 6.2 the system set-up and a modification to the original HIGS description are discussed. In Section 6.3, the incremental form of the closed-loop dynamics is formulated, and local properties are identified that play an essential role in the analysis. The main results of this chapter are presented in Section 6.4 and Section 6.5 in the form of time- and frequency-domain conditions for convergence. An extension toward steady-state performance estimation is made in Section 6.6. Application of the presented tools is demonstrated on a numerical example in Section 6.7. The main findings in this chapter are summarized in Section 6.8.

6.1.1 Notations

Along with the notations from previous chapters, in this chapter use is made of some additional notations. The Euclidian inner product between two vectors $a \in \mathbb{R}^n$ and $b \in \mathbb{R}^n$, denoted by $\langle a, b\rangle$, is defined as $\langle a, b\rangle = a^\top b$. A "weighted" inner product based on a symmetric matrix P, denoted by $\langle \cdot, \cdot \rangle_P$, is defined as $\langle a, b\rangle_P = a^\top P b$. The root-mean-square (RMS) value of a periodic signal y with period $T > 0$, *i.e.*, $y(t) = y(t+T)$ is defined by $\|y\|_{2,T} = (\frac{1}{T}\int_0^T |y(t)|^2 dt)^{\frac{1}{2}}$.

6.2 System setting and problem formulation

This chapter is concerned with Lur'e-type systems as shown in Figure 6.1, which represent the feedback interconnection of a single-input single-output (SISO) linear time-invariant (LTI) system G, and a sector-bounded integrator $\mathcal{H}$.

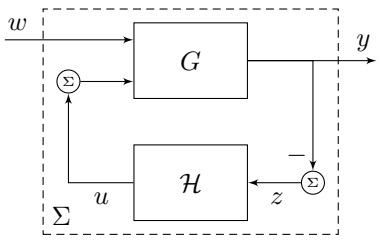

Figure 6.1. Lur'e-type system interconnection of an LTI system G and a sector-bounded, dynamic nonlinearity $\mathcal{H}$.

Similar as in previous chapters, the linear portion of the closed-loop system is described by the state-space formulation

$$G : \begin{cases} \dot{x}_g(t) &= A_g x_g(t) + B_g u(t) + B_w w(t), \\ y(t) &= C_g x_g(t) \end{cases} \tag{6.1}$$

with state $x_g(t) \in \mathbb{R}^m$, external input $w(t) \in \mathbb{R}$, control input $u(t) \in \mathbb{R}$, and output $y(t) \in \mathbb{R}$ at time $t \in \mathbb{R}_{\geq 0}$. The system description in (6.1) is assumed to be a minimal representation, and

$$G_{yu}(s) = C_g \left(sI - A_g\right)^{-1} B_g, \tag{6.2a}$$

$$G_{yw}(s) = C_g \left(sI - A_g\right)^{-1} B_w, \tag{6.2b}$$

denote the transfer functions from u to y, and w to y, respectively. Recall from Assumption 2.3.1 that the transfer functions $G_{yu}(s)$ and $G_{yw}(s)$ in (6.2) have a relative degree of at least two, such that $C_g B_g = C_g B_w = 0$.

6.2.1 An extended hybrid integrator design

In the original description of HIGS as provided in Chapter 2, the dynamics in integrator-mode are linear. To introduce more flexibility from a design point-of-view, as well as more generality from a system-theoretic perspective, below extended versions of HIGS are presented in which the underlying integrator dynamics are allowed to be nonlinear. In particular, consider the nonlinear discontinuous dynamical system described by

$$\mathcal{H} : \begin{cases} \dot{x}_h(t) &= f(x_h(t), z(t)), & \text{if } (z(t), u(t), \dot{z}(t)) \in \hat{\mathcal{F}}_1, \\ x_h(t) &= k_h z(t), & \text{if } (z(t), u(t), \dot{z}(t)) \in \hat{\mathcal{F}}_2, \\ u(t) &= x_h(t), \end{cases} \tag{6.3}$$

where $x_h(t) \in \mathbb{R}$ denotes the state, $z(t) \in \mathbb{R}$ is the input, $\dot{z}(t)$ denotes the time-derivative of z at time t, and $u(t) \in \mathbb{R}$ is the output. The signal z is assumed to be continuously differentiable and $f : \mathbb{R} \times \mathbb{R} \to \mathbb{R}$ is a (non)linear function. On the basis of a similar reasoning as discussed in Chapter 2, Section 2.2, the sets $\hat{\mathcal{F}}_1$ and $\hat{\mathcal{F}}_2$ dictating the active dynamics of (6.3) are defined as

$$\hat{\mathcal{F}}_1 := \left\{ (z, u, \dot{z}) \in \mathbb{R}^3 \mid k_h z u \geq u^2 \wedge (z, u, \dot{z}) \notin \hat{\mathcal{F}}_2 \right\}, \tag{6.4a}$$

$$\hat{\mathcal{F}}_2 := \left\{ (z, u, \dot{z}) \in \mathbb{R}^3 \mid u = k_h z \wedge f(x_h, z) z > k_h \dot{z} z \right\}, \tag{6.4b}$$

where the union $\hat{\mathcal{F}} := \hat{\mathcal{F}}_1 \cup \hat{\mathcal{F}}_2$ defines the $[0, k_h]$-sector. The terms "integrator-mode" and "integrator-dynamics" are sometimes used throughout the rest of this chapter to indicate the mode of (6.3), where the nonlinear dynamics $\dot{x}_h = f(x_h, z)$ are active.

Concerning the function f in (6.3), the following assumptions are made.

Assumption 6.2.1. *The nonlinear function f in (6.3) satisfies $f(0,0) = 0$ and $f(0,z)z \geq 0$.*

Assumption 6.2.2. *There exist constants $c_1, c_2 \in \mathbb{R}$ such that the nonlinear function f in (6.3) satisfies for all $x_h, z, x_h', z' \in \mathbb{R}$*

$$((f(x_h,z) - f(x_h',z'))\,\delta x_h \leq c_1 \delta x_h^2 + c_2 \delta x_h \delta z, \tag{6.5}$$

where $\delta x_h := x_h - x_h'$, and $\delta z := z - z'$.

Assumption 6.2.1 ensures $(x_h, z) = (0,0)$ to be an equilibrium point of (6.3) for zero input, and ensures for $x_h = 0$, $z \neq 0$ that the vector field in integrator-mode points toward the interior of $\hat{\mathcal{F}}_1$. The latter is important for guaranteeing that trajectories of (6.3) cannot escape the $[0, k_h]$-sector through the line $(z,u) = (z,0)$. Assumption 6.2.2 can be seen as a monotonicity type of condition. For functions of the form $f(x_h,z) = g(x_h) + \omega_h z$, with $\omega_h \in \mathbb{R}_{\geq 0}$, $g(\cdot)$ a globally Lipschitz continuous function, and $g(0) = 0$, Assumption 6.2.1 and Assumption 6.2.2 are always satisfied. A simple choice for $g(\cdot)$ includes (but is not limited to) $g(x_h) = \alpha x_h$, $\alpha \in \mathbb{R}$, leading to first-order linear dynamics in integrator-mode. This choice strongly links to a first-order reset element (FORE) as discussed in, *e.g.*, Chait and Hollot, 2002; Horowitz and Rosenbaum, 1975. For $\alpha = 0$, one recovers $f(x_h,z) = \omega_h z$, *i.e.*, the description of HIGS as considered in the previous chapters.

6.2.2 Closed-loop system formulation

Due to the piecewise nonlinear nature of $\mathcal{H}$ in (6.3), the closed-loop system resulting from the feedback interconnection of G in (6.1) (with $z = -y = -C_g x_g$) and $\mathcal{H}$ in (6.3) admits the state-space description

$$\Sigma : \begin{cases} \dot{x}(t) = A_1 x(t) + bF(x(t)) + Bw(t) & \text{if } Ex(t) \in \hat{\mathcal{F}}_1, \\ \dot{x}(t) = A_2 x(t) + Bw(t) & \text{if } Ex(t) \in \hat{\mathcal{F}}_2, \\ y(t) = Cx(t) \end{cases} \tag{6.6}$$

with states $x(t) = [x_g(t)^\top, x_h(t)]^\top \in \mathbb{R}^n$, $n = m + 1$, exogenous input $w(t) \in \mathbb{R}$, output $y(t) \in \mathbb{R}$ at time $t \in \mathbb{R}_{\geq 0}$, and where (with some abuse of notation) $F(x) = f(x_h, -C_g x_g)$. The mode-dependent system matrices are given by

$$A_1 = \begin{bmatrix} A_g & B_g \\ 0 & 0 \end{bmatrix}, \quad \text{and} \quad A_2 = \begin{bmatrix} A_g & B_g \\ -k_h C_g A_g & 0 \end{bmatrix}, \tag{6.7}$$

and furthermore $b = [0\ 1]^\top$, $B = [B_w^\top\ 0]^\top$, and $C = [C_g\ 0]$. The signals that determine mode switching are extracted by the matrix E, which is given by

$$E^\top = \begin{bmatrix} -C_g^\top & 0 & -k_h(C_g A_g)^\top \\ 0 & 1 & 0 \end{bmatrix} = \begin{bmatrix} -C^\top & b^\top & -k_h(CA_1)^\top \end{bmatrix}, \tag{6.8}$$

i.e., $Ex = (z, u, \dot{z})$. Note that the matrix A_2 results from explicit differentiation of the algebraic constraint in gain-mode, see also Chapter 4, Remark 4.2.1.

A few words on well-posedness properties of the nonlinear closed-loop system in (6.6) are in order. For the system with $f(x_h, z) = \omega_h z$, *i.e.*, the original description of HIGS, global existence of absolutely continuous (AC) solutions to (6.6) is formally guaranteed for all inputs w that belong to the class of piecewsie Bohl functions (Deenen et al., 2021; Sharif et al., 2019). The results in Sharif et al., 2019 can be extended to guarantee global existence of solutions to (6.6) for all "Bohl inputs" w if f is linear and satisfies Assumption 6.2.1. More general guarantees on global existence of solutions is considered as interesting and important future work. In the remainder of this chapter, it is assumed that for inputs w to the system (6.6) belonging to the class of piecewise Bohl (PB) functions, AC solutions to (6.6) exist globally (for all $t \in [0, \infty)$).

Remark 6.2.3. *For assessing input-to-state stability and/or $\mathcal{L}_2/\mathcal{H}_2$ performance properties of the closed-loop system in* (6.6)*, one may extend the tools developed in Chapters 4 and 5 accordingly. In case $f(x_h, z) = -\alpha x_h + \omega_h z$, i.e., the underlying dynamics are linear, such an extension is straightforward. On the other hand, when f is nonlinear and Assumption 6.2.2 holds, using state strict passivity of $\mathcal{H}$ (which results from the fact that $k_h z u - x_h^2 \geq 0$), one is still able to apply Theorem 4.3.1 (circle-criterion) directly, but application of the other results may be more involved. One possible approach to extend the existing tools in this case is by viewing* (6.6) *as a "perturbed" version of a nominal piecewise linear (PWL) system. In particular, consider the system*

$$\Sigma : \begin{cases} \dot{x}(t) = A_1 x(t) + b(F(x(t)) + (\alpha C_u - \omega_h C_z)x(t)) + Bw(t) & \text{if } Ex(t) \in \hat{\mathcal{F}}_1, \\ \dot{x}(t) = A_2 x(t) + Bw(t) & \text{if } Ex(t) \in \hat{\mathcal{F}}_2, \\ y(t) = Cx(t) \end{cases} \tag{6.9}$$

where $C_u, C_z \in \mathbb{R}^n$ are defined such that $C_u x = x_h$ and $C_z x = z$, and

$$A_1 = \begin{bmatrix} A_g & B_g \\ \omega_h C_z & -\alpha \end{bmatrix}, \quad \text{and} \quad A_2 = \begin{bmatrix} A_g & B_g \\ k_h C_z A_g & 0 \end{bmatrix}. \tag{6.10}$$

By assuming that $|F(x) + (\alpha C_u - \omega_h C_z)x| \leq \epsilon |x|$ for some $\epsilon \geq 0$, one can derive stability and performance conditions for the true piecewise nonlinear system by combining tools from Chapters 4 and 5 for the nominal PWL system with, e.g., small-gain type of arguments, see also Khalil, 2002, Chapter 9 and related ideas presented in Rantzer and Johansson, 2000, Section VII. In dealing with the (possibly non-convex) set $\hat{\mathcal{F}}_2$, conditions related to the gain-mode dynamics in (6.9) *should be posed for the inflated set $\tilde{\mathcal{F}}_2$, defined by*

$$\tilde{\mathcal{F}}_2 := \left\{ (z, u, \dot{z}) \in \mathbb{R}^3 \mid u = k_h z \wedge (k_h c_1 + c_2) z^2 > k_h \dot{z} z \right\}, \tag{6.11}$$

allowing for formulating LMI conditions. This inflated set along with $c_1, c_2 \in \mathbb{R}$ *is a consequence of applying Assumption 6.2.2 to the inequality* $f(x_h, z)z > k_h \dot{z} z$ *in gain-mode. Clearly one finds that* $\hat{\mathcal{F}}_2 \subseteq \tilde{\mathcal{F}}_2$*, so that when conditions hold for all* $Ex \in \tilde{\mathcal{F}}_2$*, these also hold for all* $Ex \in \hat{\mathcal{F}}_2$*. For the nonlinear case, the tooling presented in earlier chapters is thus still highly relevant.*

6.2.3 Incremental stability, convergence, and problem formulation

This chapter is concerned with studying the behaviour of (steady-state) solutions to the closed-loop system in (6.6). Of particular interest is the stability of solutions with respect to each other. This property can be characterized through the notions of incremental (input-to-state) stability (δISS), and (input-to-state) convergence (ISC).

Definition 6.2.4 (Angeli, 2002)**.** *The closed-loop system* (6.6) *is said to be uniformly incrementally asymptotically stable (*δ*UAS), if there exists a* $\mathcal{KL}$*-function* β *such that for any input* $w \in PB \cap \mathcal{L}_\infty$*, and initial conditions* $x_0, x_0' \in \mathcal{X}$ *at time* $t = 0$*, with*

$$\mathcal{X} := \left\{ x \in \mathbb{R}^n \mid Ex \in \hat{\mathcal{F}} \right\}, \tag{6.12}$$

all solutions to (6.6) *satisfy*

$$\|x(t, x_0, w) - x(t, x_0', w)\| \leq \beta \left(\|x_0 - x_0'\|, t \right), \tag{6.13}$$

for all $t \in \mathbb{R}_{\geq 0}$*.*

Definition 6.2.5 (Angeli, 2002)**.** *The closed-loop system* (6.6) *is said to be incrementally input-to-state stable (*δ*ISS), if there exist a* $\mathcal{KL}$*-function* β *and a* $\mathcal{K}$*-function* γ *such that for inputs* $w, w' \in PB \cap \mathcal{L}_\infty$*, and all initial conditions* $x_0, x_0' \in \mathcal{X}$ *at time* $t = 0$*, all solutions to* (6.6) *satisfy*

$$\|x(t, x_0, w) - x(t, x_0', w')\| \leq \beta \left(\|x_0 - x_0'\|, t \right) + \gamma \left(\sup_{0 \leq \tau \leq t} \|w(\tau) - w'(\tau)\| \right), \tag{6.14}$$

for all $t \in \mathbb{R}_{\geq 0}$*.*

Definition 6.2.6 (Demidovich, 1967; Pavlov et al., 2006a)**.** *The closed-loop system* (6.6) *is said to be uniformly convergent (UC), if*

1. *all solutions* x *corresponding to an initial condition* $x_0 \in \mathcal{X}$ *at time* $t = 0$ *and some input* $w \in PB \cap \mathcal{L}_\infty$ *exist for all* $t \in [0, \infty)$*;*
2. *there exists a solution* $\bar{x}_w$ *of* (6.9)*, depending on the input* w*, defined and bounded for all* $t \in \mathbb{R}$*;*

3. *the solution $\bar{x}_w$ is uniformly asymptotically stable, i.e., there exists a $\mathcal{KL}$-function β such that for any $x_0 \in \mathcal{X}$ at time $t = 0$ and any input $w \in PB \cap \mathcal{L}_\infty$, all solutions x to* (6.6) *satisfy for the same input w*

$$\|x(t, x_0, w) - \bar{x}_w(t, \bar{x}_{w,0}, w)\| \leq \beta(\|x_0 - \bar{x}_{w,0}\|, t), \tag{6.15}$$

for all $t \in \mathbb{R}_{\geq 0}$.

Definition 6.2.7 (Demidovich, 1967; Pavlov et al., 2006a)**.** *The closed-loop system* (6.6) *is said to be input-to-state convergent (ISC), if it is UC, and additionally there exist a $\mathcal{KL}$-function β, and a $\mathcal{K}_\infty$-function γ such that solutions x of the system* (6.6) *corresponding to inputs $w, w' \in PB$ satisfy*

$$\|x(t, x_0, w') - \bar{x}_w(t, \bar{x}_{w,0}, w)\| \leq \beta(\|x_0 - \bar{x}_{w,0}\|, t) + \gamma\left(\sup_{0 \leq \tau \leq t} |w'(\tau) - w(\tau)|\right), \tag{6.16}$$

for all times $t \in \mathbb{R}_{\geq 0}$.

In general, the properties of incremental (input-to-state) stability and uniform (input-to-state) convergence are not equivalent. However, as shown in Ruffer et al., 2013, uniform convergence and incremental stability are equivalent on compact positively invariant sets. By virtue of this fact, for proving convergence of the closed-loop system in (6.6) it is then sufficient to 1) verify incremental stability to guarantee any two solutions to converge to each other, and 2) verify for bounded inputs w the existence of a compact positively invariant set to guarantee the existence of at least one solution $\bar{x}_w(t)$ that is bounded on $\mathbb{R}$ (Demidovich, 1967; Yakubovich, 1964). The next result presents a Lyapunov characterization of these sufficient conditions for convergence.

Theorem 6.2.8 (Pavlov et al., 2006a)**.** *Consider the closed-loop system in* (6.6)*. If there exist a locally Lipschitz continuous function $V : \mathbb{R}^n \times \mathbb{R}^n \to \mathbb{R}_{\geq 0}$, class $\mathcal{K}_\infty$-function α_1, and class $\mathcal{K}$-functions α_2, α, β satisfying for all $x, x' \in \mathcal{X}$, and all inputs $w, w' \in PB \cap \mathcal{L}_\infty$*

$$\alpha_1(|x - x'|) \leq V(x, x') \leq \alpha_2(|x - x'|), \tag{6.17a}$$

$$\max_{p \in \partial V(x,x')} \max_{f \in F(x,w,x',w')} \langle p, f \rangle \leq -\alpha(|x - x'|) + \beta(|w - w'|), \tag{6.17b}$$

then the closed-loop system in (6.6) *is input-to-state convergent (ISC).*

In proving this theorem, the following auxiliary result will be useful.

Lemma 6.2.9 (Pavlov et al., 2006a; Yakubovich, 1964)**.** *Consider system* (6.6) *with input $w \in PB \cap \mathcal{L}_\infty$. Suppose that*

(i) the system (6.6) *admits a unique solution on $\mathbb{R}_{\geq 0}$ for every initial state $x_0 \in \mathcal{X}$ at time $t = 0$ and for the input w;*

(ii) these solutions depend on the initial state x_0 in a continuous manner;

(iii) there exists a compact set $D \subseteq \mathcal{X}$, which is positively invariant with respect to system (6.6) *for the input $w \in PB \cap \mathcal{L}_\infty$.*

Then there exists at least one solution $\bar{x}_w$ depending on the input w that is defined and bounded for all $t \in \mathbb{R}_{\geq 0}$.

Proof of Theorem 6.2.8. By Theorem 2.3.9 and Theorem 2.3.11, it can be shown that conditions (6.17a) and (6.17b) imply the closed-loop system in (6.6) to be incrementally input-to-state stable (δISS), and, in turn, uniformly incrementally asymptotically stable (δUAS). From the definition of δUAS (Definition 6.2.4) it then immediately follows that solutions corresponding to an initial state $x_0 \in \mathcal{X}$ at time $t = 0$ and input $w \in PB$ are unique, and depend continuously on these initial states.

Next, take $(x(t), w(t))$ with $w \in PB$ to be an arbitrary trajectory of the system and let $w'(t) \equiv 0$, $x'(t) \equiv 0$ for all $t \in \mathbb{R}$. Due to Assumption 6.2.1, it follows that $f(0,0) = 0$, and the point $(x, w) = (0, 0)$ is an equilibrium of the system (6.6). Then, using standard arguments it follows that (6.17a) and (6.17b) imply the set $D(c) := \left\{x \in \mathbb{R}^n \mid V(x) \leq \alpha_2 \circ \alpha^{-1} \circ \beta(c)\right\}$ to be a compact positively invariant set for every input $w \in PB \cap \mathcal{L}_\infty$ satisfying $|w(t)| \leq c$ for all $t \in \mathbb{R}$. Here, $\circ$ denotes the composition of functions. By Lemma 6.2.9 there exists a solution $\bar{x}_w$ that is defined and bounded for all $t \in \mathbb{R}_{\geq 0}$. From the fact that the system is δUAS, it follows that this solution is uniformly asymptotically stable, and, as a consequence, the system is uniformly convergent.

Furthermore, since the system is δISS, one finds by setting $x'(t) = \bar{x}_w(t)$ that (6.14) implies (6.16) to hold for some appropriate functions β and γ. Hence, the system is input-to-state convergent (ISC). This completes the proof. □

Remark 6.2.10. *It is worthwhile noting that an immediate consequence of satisfying the conditions in Theorem 6.2.8 is the guarantee for uniqueness of solutions corresponding to an initial state $x_0 \in \mathcal{X}$. Hence, establishing δUAS properties provides sufficient conditions for uniqueness of solutions, which for HIGS-based control systems has been an open issue.*

The main challenge in satisfying the conditions of Theorem 6.2.8 lies in finding an appropriate *incremental* Lyapunov function V. In line with the previous chapters, the main objective in this chapter is to formulate constructive time- and frequency-domain conditions for guaranteeing the existence of such function. In doing so, properties of the *incremental form* of the LTI system (6.1) and the modified HIGS in (6.3) are studied first.

6.3 Incremental form and system properties

For assessing convergence properties of the closed-loop system in (6.6) it is instructive to study the incremental form of the LTI system G in (6.1) and the nonlinearity $\mathcal{H}$ in (6.3). This section presents the incremental dynamics along with some properties that serve a key purpose in deriving useful conditions for guaranteeing convergence.

6.3.1 Incremental dynamics

Define $\delta x_g(t) := x_g(t) - x'_g(t) \in \mathbb{R}^m$ as the difference between two trajectories $x_g(t) = x_g(t, x_{g,0}, w(t), u(t))$ and $x'_g(t) = x_g(t, x'_{g,0}, w'(t), u'(t))$ generated by the linear system (6.1) subject to inputs $w, u, w', u' \in \mathbb{R}$, and initial conditions $x_{g,0}, x'_{g,0} \in \mathbb{R}^m$, respectively, at time $t \in \mathbb{R}_{\geq 0}$. The incremental form of the linear system G in (6.1) then reads

$$\delta G : \begin{cases} \delta \dot{x}_g(t) = A_g \delta x_g(t) + B_g \delta u(t) + B_w \delta w(t), \\ \delta y(t) \ \ = C_g \delta x_g(t), \end{cases} \tag{6.18}$$

with $\delta u(t) := u(t) - u'(t) \in \mathbb{R}$ the incremental control input, $\delta w(t) := w(t) - w'(t) \in \mathbb{R}$ the incremental external input, and $\delta y(t) := y(t) - y'(t) \in \mathbb{R}$ the incremental output, at time $t \in \mathbb{R}_{\geq 0}$. Clearly, when the system matrix A_g is Hurwitz, this linear sub-system is convergent.

Consider $\delta x_h(t) := x_h(t) - x'_h(t) \in \mathbb{R}$ as an increment of the state of the nonlinearity $\mathcal{H}$ in (6.3). The incremental dynamics of $\mathcal{H}$ are then given by

$$\delta \dot{x}_h(t) = \begin{cases} f(x_h(t), z(t)) - f(x'_h(t), z'(t)), & \text{if } (q(t), q'(t)) \in \hat{\mathcal{F}}_1 \times \hat{\mathcal{F}}_1, \\ k_h \delta \dot{z}(t), & \text{if } (q(t), q'(t)) \in \hat{\mathcal{F}}_2 \times \hat{\mathcal{F}}_2, \\ f(x_h(t), z(t)) - k_h \dot{z}'(t), & \text{if } (q(t), q'(t)) \in \hat{\mathcal{F}}_1 \times \hat{\mathcal{F}}_2, \\ k_h \dot{z}(t) - f(x'_h(t), z'(t)), & \text{if } (q(t), q'(t)) \in \hat{\mathcal{F}}_2 \times \hat{\mathcal{F}}_1, \end{cases} \tag{6.19}$$

where $\delta z(t) := z(t) - z'(t) = -\delta y(t) \in \mathbb{R}$ is the incremental input, and in which $(q, q') = \left(q^\top, q'^\top\right)^\top$ with $q = (z, u, \dot{z}) \in \mathbb{R}^3$, and $q' = (z', u', \dot{z}') \in \mathbb{R}^3$. The output generated by the incremental dynamics in (6.19) is given by $\delta u(t) = \delta x_h(t)$. Note that the last three lines in (6.19) result from explicit differentiation of the algebraic constraint in gain-mode.

6.3.2 Properties

The following properties of the incremental system in (6.19) appear particularly useful for deriving convergence properties. These essentially shows that, under Assumption 6.2.2 on the vector field f, in subregions of the incremental input-output space the system in (6.19) satisfies certain monotonicity-like properties.

Property 6.3.1. *Suppose that Assumption 6.2.2 is satisfied. Then, the incremental system in* (6.19) *satisfies*

$$(\delta x_h)^2 \leq k_h \delta z \delta x_h, \quad \text{for all } (\delta z, \delta x_h) \in \Omega_1, \tag{6.20a}$$

$$(\delta \dot{x}_h)\delta x_h \leq c_1 \delta x_h^2 + c_2 \delta x_h \delta z, \quad \text{for all } (\delta z, \delta x_h) \in \Omega_2, \tag{6.20b}$$

where

$$\Omega_1 := \left\{ (\delta z, \delta x_h) \in \mathbb{R}^2 \mid \delta z \delta x_h \geq \frac{1}{k_h} \delta x_h^2 \right\}, \tag{6.21a}$$

$$\Omega_2 := \mathbb{R}^2 \setminus \Omega_1. \tag{6.21b}$$

Proof. A proof can be found in Appendix 6.A.1. □

Property 6.3.2. *Suppose that Assumption 6.2.2 is satisfied. Then, the incremental system in* (6.19) *satisfies for all* $(\delta z, \delta x_h) \in \Omega_2$ *with* Ω_2 *defined in* (6.21) *the inequality*

$$\delta \dot{x}_h (\delta x_h - k_h \delta z) \leq (c_1 \delta x_h + c_2 \delta z)(\delta x_h - k_h \delta z), \quad \text{for } (\delta z, \delta x_h) \in \Omega_2. \tag{6.22}$$

Proof. For all $(\delta z, \delta x_h) \in \Omega_2$ it holds that $\delta x_h (\delta x_h - k_h \delta z) > 0$, and thus δx_h and $\delta x_h - k_h \delta z$ have similar signs and are both non-zero. Then, from (6.20b) as an immediate consequence one finds for all $(\delta z, \delta x_h) \in \Omega_2$

$$\delta \dot{x}_h (\delta x_h - k_h \delta z) \leq (c_1 \delta x_h + c_2 \delta z)(\delta x_h - k_h \delta z). \tag{6.23}$$

This yields the result. □

It is interesting to observe that both Property 6.3.1 and Property 6.3.2 resemble regional monotonicity-like characteristics of the vector field of (6.19). The concept of monotonicity (which can also be related to a one-sided Lipschitz condition (Hu, 2006)) often plays an important role in characterizing asymptotic stability, incremental stability and convergence of non-smooth systems through quadratic Lyapunov functions, see, *e.g.*, Brogliato and Tanwani, 2019; Heemels et al., 2020. Property 6.3.1 and Property 6.3.2 will turn out to be instrumental in formulating conditions for input-to-state convergence (ISC), as will be seen in the next sections.

6.4 Time-domain conditions for ISC

6.4.1 A small-gain condition

Before discussing the use of monotonicity properties in deriving conditions for convergence, consider the following observation. Regarding $\delta z(t)$ as an input

to the incremental system in (6.19), one may recognize from (6.20b) in Property 6.3.1 that δx_h^2 could resemble a regional δISS-Lyapunov function for this system in case $c_1 < 0$. Combining this with the incremental gain property in (6.20a), in fact, suggests (6.19) to be ISS. This important insight is formalized in the next result.

Lemma 6.4.1. *Consider the incremental nonlinear system in* (6.19)*. Suppose that Assumptions 6.2.2–6.2.1 are satisfied with $c_1 < 0$ and furthermore suppose that δz is bounded in the sense that $|\delta z(\tau)|$ is finite for all $t \in \mathbb{R}_{\geq 0}$. Then,* (6.19) *satisfies*

$$\|\delta x_h(t)\| \leq e^{-\epsilon t}\|\delta x_h(0)\| + \gamma_z \left(\sup_{0\leq\tau\leq t} |\delta z(\tau)| \right) \tag{6.24}$$

with $\gamma_z = \max\left\{k_h, \frac{c_2}{|c_1|-\epsilon}\right\}$ *and* $0 < \epsilon < |c_1|$.

Proof. Consider the set

$$M := \left\{(\delta z, \delta x_h) \in \mathbb{R}^2 \mid \|\delta z\| \leq \rho, \|\delta x_h\| \leq \gamma_z \rho\right\}, \quad \rho := \sup_{0\leq\tau\leq t} \|\delta z(\tau)\|, \tag{6.25}$$

which is visualized in Figure 6.2 by the black rectangle.

Suppose that $(\delta z(0), \delta x_h(0)) \notin M$. Note from the fact that $-\rho \leq \delta z(0) \leq \rho$, this implies that $\|\delta x_h(t)\| > \gamma_z \rho \geq \gamma_z \|\delta z(t)\|$ for all $t \geq 0$ for which $(\delta z(t), \delta x_h(t)) \notin M$, such that $(\delta z(t), \delta x_h(t)) \in \Omega_2$, see also Figure 6.2. Then, it immediately follows from Property 6.3.1 with $c_1 < 0$ that (6.20b) satisfies

$$(\delta \dot{x}_h)\delta x_h \leq c_1 \delta x_h^2 + c_2 \delta x_h \delta z \leq -\epsilon \delta x_h^2, \tag{6.26}$$

due to $\|\delta z(t)\| \leq \frac{1}{\gamma_z}\|\delta x_h(t)\| \leq \frac{|c_1|-\epsilon}{c_2}\|\delta x_h(t)\|$. By the Bellmann-Gronwall lemma this leads to

$$\|\delta x_h(t)\| \leq e^{-\frac{\epsilon}{2}t}\|\delta x_h(0)\| \tag{6.27}$$

for all time $t \geq 0$ as long as $(\delta z(t), \delta x_h(t)) \notin M$. Then, there must exist a finite time $t' \geq 0$ for which $(\delta z(t'), \delta x_h(t')) \in M$. Once $(\delta z(t'), \delta x_h(t')) \in M$, it remains there for all times $t \geq t'$, as it follows from (6.27) that M is a positively invariant set, and

$$\|\delta x_h(t)\| \leq \gamma_z \rho \quad \text{for all } t \geq t'. \tag{6.28}$$

In case $(\delta z(0), \delta x_h(0)) \in M$ the above applies with $t' = 0$. Combining the inequalities in (6.27) and (6.28) leads to (6.24). A sketch of the mechanism underlying the ISS property is illustrated in Figure 6.2. □

The next result is a direct consequence of Lemma 6.4.1.

Theorem 6.4.2. *Consider the closed-loop system* (6.6)*, and the incremental systems in* (6.18) *and in* (6.19)*. Suppose the matrix A_g in* (6.18) *is Hurwitz and the small-gain relation*

$$\gamma_z \gamma_u < 1 \tag{6.29}$$

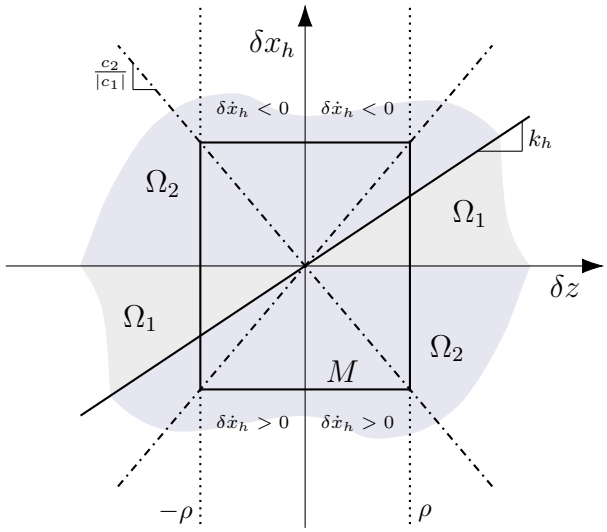

Figure 6.2. Visualization of the mechanism underlying the ISS property of the incremental system in (6.19) with $\gamma_z = \frac{c_2}{|c_1|-\epsilon}$.

is satisfied, where $\gamma_z = \max\left\{k_h, \frac{c_2}{|c_1|}\right\}$ *and* $\gamma_u = \int_0^\infty |C_g e^{A_g \tau} B_p| d\tau$. *Then the closed-loop system* (6.6) *is input-to-state convergent (ISC).*

Proof. For a proof, see Appendix 6.A.2. □

Note that $\gamma_u = \int_0^\infty |C_g e^{A_g \tau} B_g| dt = \int_0^\infty |\mathcal{L}^{-1}\{G_{yu}(s)\}| dt$ corresponds to the induced $\mathcal{L}_\infty$-norm of the SISO LTI system described by $G_{yu}(s) = C_g(A_g - sI)^{-1}B_g$, which is equivalent to the $\mathcal{L}_1$-norm of its impulse response, see also Skogestad and Postlethwaite, 2010, p. 540, and γ_z is an upper-bound on the induced $\mathcal{L}_\infty$-norm of (6.19).

6.4.2 Lyapunov-based conditions

In deriving Lyapunov-based conditions for convergence, the following definition and auxiliary result that follows directly from the previously discussed properties will be particularly helpful in understanding the rationale behind the upcoming results.

Definition 6.4.3 (Heemels et al., 2020)**.** *A function* $g : \mathbb{R}^m \to \mathbb{R}^n$ *is called* α*-strongly* P*-monotone if there exists* $\alpha > 0$ *such that*

$$\langle (g(x) - g(y)), x - y \rangle_P \geq \alpha \|x - y\|_P^2 \tag{6.30}$$

for all $x, y \in \mathbb{R}^m$.

Lemma 6.4.4. *Suppose Assumption 6.2.2 is satisfied, and there exist a positive definite symmetric matrix P and a number $0 \leq \tau \leq 1$ that satisfy*

$$A^\top P + PA \prec 0 \quad \text{and} \quad Pb = C_u^\top - \tau k_h C_z^\top \tag{6.31}$$

with matrices

$$A = \begin{bmatrix} A_g & B_g \\ -c_2 C_g & c_1 \end{bmatrix}, \quad \text{and} \quad b = \begin{bmatrix} 0 \\ 1 \end{bmatrix}, \tag{6.32}$$

then for all $(\delta z, \delta x_h) \in \Omega_2$ the incremental system (6.18)–(6.19) satisfies the α-strongly P-monotone condition

$$\langle -\delta \dot{x}, \delta x \rangle_P \geq \alpha \|\delta x\|_P^2 \tag{6.33}$$

with $\delta x = \left[\delta x_g^\top, \delta x_h\right]^\top$ and some $\alpha > 0$.

Proof. One can write the incremental dynamics as

$$\delta \dot{x} = A\delta x + b\phi, \tag{6.34}$$

where $\phi = \delta \dot{x}_h - c_1 \delta x_h - c_2 \delta z$. From this, it follows that for all $(\delta z, \delta x_h) \in \Omega_2$

$$\langle \delta \dot{x}, \delta x \rangle_P = \langle P\delta \dot{x}, \delta x \rangle = \langle PA\delta x, \delta x \rangle + \langle Pb\phi, \delta x \rangle \leq -\nu \|\delta x\|^2, \tag{6.35}$$

for some positive ν, where it is used that $\delta x^\top (A^\top P + PA)\delta x \leq -\nu \|\delta x\|^2$ and by virtue of Property 6.3.1 and Property 6.3.2 for all $(\delta z, \delta x_h) \in \Omega_2$ one finds

$$\begin{aligned} \langle Pb\phi, \delta x \rangle &= \phi(C_u - \tau k_h C_z)\delta x = \phi(\delta x_h - \tau k_h \delta z) \\ &= (\delta \dot{x}_h - c_1 \delta x_h - c_2 \delta z)\left((1-\tau)\delta x_h + \tau(\delta x_h - k_h \delta z)\right) \leq 0. \end{aligned} \tag{6.36}$$

This shows the α-strongly P-monotone condition. □

The result in Lemma 6.4.4 forms the inspiration for constructing a specific incremental Lyapunov function for the closed-loop system in (6.6) as follows. A function of the form $W(\delta x) = \delta x^\top P \delta x$ with $P \in \mathbb{R}^{m \times m}$ satisfying (6.31) in Lemma 6.4.4 qualifies as a "regional" incremental Lyapunov function for the system in (6.6) when $(\delta z, \delta x_h) \in \Omega_2$, with Ω_2 defined in (6.21). Note that due to the second condition in (6.31), the function W can equivalently be written as $W(\delta x_g) = \delta x_g^\top P_{11} \delta x_g + v(\delta x_h, \delta z)$ with $P_{11} = P_{11}^\top$ and $v(\delta x_h, \delta z) := \delta x_h(\delta x_h - 2\tau k_h \delta z)$. For all $(\delta z, \delta x_h)$ in the region Ω_1, however, this specific function W may not qualify as an incremental Lyapunov function as the monotonicity property in (6.33) is not guaranteed to hold.

On the other hand, for all $(\delta z, \delta x_h) \in \Omega_1$ the incremental sector condition in (6.20a) holds true. Then, a natural incremental Lyapunov function candidate for this region is one that stems from the circle-criterion and is given by $U(\delta x_g) = \delta x_g^\top M x_g$ with $M \in \mathbb{R}^{m \times m}$ a symmetric positive definite matrix that satisfies

the corresponding circle criterion conditions (see, *e.g.*, the conditions posed in Theorem 4.3.1 in Chapter 4).

The question that arises at this point is how to "patch" these functions together over the boundaries shared by Ω_1 and Ω_2 to obtain a continuous function. A particular idea is to fix $\tau = 1/2$ and set $M = P_{11}$ a priori. Then, for all $(\delta x_h, \delta z) \in \Omega_1 \cap \Omega_2$ one finds $v(\delta x_h, \delta z) = 0$ and $W(\delta x) = U(\delta x_g)$. Fixing τ, however, may possibly be restrictive and not necessary. Now observe that when keeping τ variable, $v(\delta x_h, \delta z)$ can be rewritten as $v(\delta x_h, \delta z) = (1-2\tau)\delta x_h^2 + 2\tau\delta x_h(\delta x_h - k_h \delta x_h)$. While the second term vanishes at the boundaries of Ω_1 and Ω_2 where $\delta x_h = 0$ or $\delta x_h = k_h \delta z$, the first term only vanishes at $\delta x_h = 0$. To account for this term, a further partitioning of the incremental input-output space of (6.19) as depicted in Figure 6.3 is proposed. Based on this partitioning, a candidate piecewise quadratic function of the form

$$V(\delta x) = \delta x_g^\top M \delta x_g + k \max\left\{\delta x_h^2, k_h^2 \delta z^2\right\} + \max\left\{0, v(\delta x_h, \delta z)\right\}, \qquad (6.37)$$

with $k > -\frac{1}{2}$ is considered. Essentially, the max functions correspond to "transitions" from one region to another. Note that by construction, V in (6.37) is a locally Lipschitz continuous piecewise quadratic function.

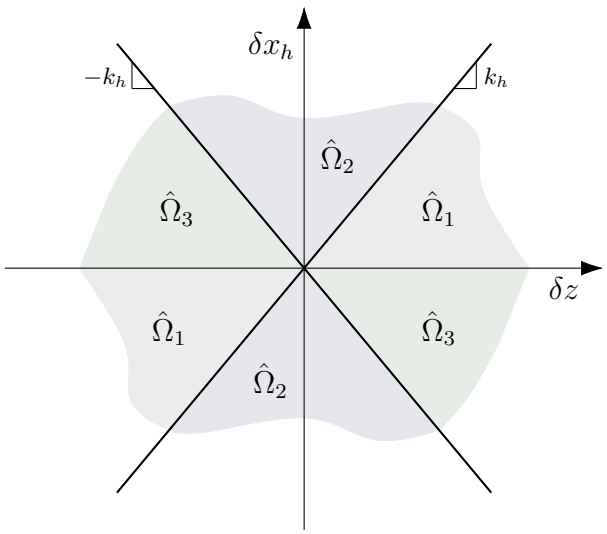

Figure 6.3. Partitioning of the incremental input-output space of (6.19) induced by the piecewise quadratic function V in (6.37) where $\hat{\Omega}_1 = \Omega_1$ and $\hat{\Omega}_2 \cup \hat{\Omega}_3 = \Omega_2$.

Based on the ideas outlined above, the next theorem presents sufficient conditions for V in (6.37) to classify as an incremental Lyapunov function through which input-to-state convergence of the closed-loop system in (6.6) is guaranteed.

Theorem 6.4.5. *Consider the closed-loop system in* (6.6)*, and suppose Assumption 6.2.2 is satisfied. If there exist constants* $k > -\frac{1}{2}$, $\tau_1, \tau_2 \geq 0$ *and a symmetric matrix* $M = M^\top$ *that satisfy the LMI conditions*

$$M + k k_h^2 C_g^\top C_g \succ 0, \tag{6.38a}$$

and

$$\begin{bmatrix} A_g^\top M + M A_g & M B_g \\ B_g^\top M & 0 \end{bmatrix} + k \begin{bmatrix} Q_g & 0 \\ 0 & 0 \end{bmatrix} + \tau_1 S_1 \prec 0, \tag{6.38b}$$

$$\begin{bmatrix} A_g^\top M + M A_g & M B_g \\ B_g^\top M & 0 \end{bmatrix} + k \begin{bmatrix} 0 & -\frac{c_2}{2} C_g^\top \\ -\frac{c_2}{2} C_g & 2c_1 \end{bmatrix} + T \prec 0, \tag{6.38c}$$

$$\begin{bmatrix} A_g^\top M + M A_g & M B_g \\ B_g^\top M & 0 \end{bmatrix} + k \begin{bmatrix} Q_g & 0 \\ 0 & 0 \end{bmatrix} + T + \tau_2 S_2 \prec 0, \tag{6.38d}$$

where $Q_g = A_g^\top C_g^\top C_g + C_g^\top C_g A_g$,

$$T = \begin{bmatrix} -k_h c_2 C_g^\top C_g & \left(\frac{k_h c_1}{2} - c_2\right) C_g^\top + \frac{k_h}{2} A_g^\top C_g^\top \\ C_g \left(\frac{k_h c_1}{2} - c_2\right) + \frac{k_h}{2} C_g A_g & 2c_1 \end{bmatrix}, \tag{6.39a}$$

and

$$S_1 = \begin{bmatrix} 0 & -k_h C_g^\top \\ -k_h C_g & -2 \end{bmatrix}, \qquad S_2 = \begin{bmatrix} 0 & k_h C_g^\top \\ k_h C_g & -2 \end{bmatrix}, \tag{6.39b}$$

then the closed-loop system in (6.6) *is input-to-state convergent (ISC).*

Proof. The proof is provided in Appendix 6.A.3. □

Remark 6.4.6. *Necessary conditions for the LMIs in* (6.38) *to be feasible are* $\tau_1 > 0$*, and* $c_1 < 0$*. Furthermore, the choice* $k = 0$ *makes the LMI in* (6.38d) *redundant since satisfying* (6.38c) *ensures the existence of a sufficiently small* $\tau_2 \geq 0$ *such that* (6.38d) *can always be satisfied as well.*

Remark 6.4.7. *The above results show a strong relation with recently presented results for so-called oblique projected dynamical systems (oPDS) with state constraints. In particular, the conditions presented in Lemma 6.4.4 correspond to typical conditions for δISS of an oPDS with states that are confined to a closed, convex constraint set (see Heemels et al., 2020, Theorem 2). In the context of HIGS, it was shown in Sharif et al., 2021a that, under some additional conditions, a HIGS-controlled system as in* (6.6) *can be reformulated as a switched oPDS. In that case, the positive definite matrix associated with state projections onto a constraint set is given by*

$$P = \begin{bmatrix} P_{11} & -k_h C_z^\top \\ -k_h C_z & 1 \end{bmatrix}, \tag{6.40}$$

which coincides with the matrix that results from the conditions in Lemma 6.4.4 for $\tau = 1$. However, as the constraint set for a HIGS-controlled system is a non-convex set that is given by the union of two convex polyhedral cones, the results in Heemels et al., 2020 for showing δISS of HIGS-controlled systems can not be applied directly. In this regard, Theorem 6.4.5 provides a possible approach for overcoming this hurdle, and may further help in studying δISS properties of more generic oPDS with non-convex constraint sets.

6.5 Frequency-domain conditions for ISC

When studying the set of LMIs in (6.38) in more detail, one may recognize the individual LMI conditions (6.38b)–(6.38d) to resemble certain passivity conditions. Due to the strong link between the concept of passivity and frequency-domain properties via the KYP-lemma (Yakubovich, 1962), it is interesting to verify if the set of LMIs in Theorem 6.2.8 admit a frequency-domain interpretation. As also motivated in Chapter 4, frequency-domain conditions are highly valuable from a practical perspective as these often lead to insights regarding design and robustness aspects.

In order to make the transition from time-domain conditions toward frequency-domain conditions, the LMIs in (6.38) are simplified by a priori assuming $k = 0$ and $c_2 \geq 0$. This assumption is useful for reducing the three LMIs in (6.53b)–(6.53d) to two LMIs. Although such a simplification may restrict the solution space of the LMIs, and in that sense comes at the cost of introducing conservatism, it is believed that the associated frequency-domain conditions can still yield valuable tuning insights and may further aid the development of more advanced (frequency-domain) conditions for convergence.

For $k = 0, c_2 \geq 0$, it is possible to verify that the LMIs in (6.38) admit a solution if there exist a matrix $M \succ 0$ and a constant $\tau > 0$ that satisfy the following LMI conditions

$$\begin{bmatrix} A_g^\top M + M A_g & M B_g \\ B_g^\top M & 0 \end{bmatrix} + \tau \begin{bmatrix} 0 & -k_h C_g^\top \\ -k_h C_g & -2 \end{bmatrix} \prec 0, \tag{6.41a}$$

$$\begin{bmatrix} A_g^\top M + M A_g & M B_g \\ B_g^\top M & 0 \end{bmatrix} + \begin{bmatrix} 0 & \left(\lambda I + \frac{k_h}{2} A_g^\top\right) C_g^\top \\ C_g \left(\lambda I + \frac{k_h}{2} A_g\right) & 2c_1 \end{bmatrix} \prec 0, \tag{6.41b}$$

with $\lambda = \frac{k_h c_1}{2} - c_2$. Note that the term $-k_h c_2 C_g^\top C_g$ in the matrix T in (6.39a) is left out to further simplify the conditions. The next theorem presents a necessary and sufficient condition in the frequency-domain for feasibility of the LMIs in (6.41) with $M \succ 0$.

Theorem 6.5.1. *The linear matrix inequalities in* (6.41) *admit a feasible solution if and only if the transfer function $G(s) = G_{yu}(s) = C_g(sI - A_g)^{-1}B_g$ is*

stable, and there exist constants $\tau, \varepsilon > 0$ *that satisfy for all* $\omega \in \mathbb{R}$

$$\begin{bmatrix} k_h \mathrm{Re}\left\{G(j\omega)\right\} + 1 & \frac{1}{2\sqrt{2}} W(j\omega) \\ \frac{1}{2\sqrt{2}} W^*(j\omega) & 1 - \frac{k_1}{2} \mathrm{Re}\left\{U(j\omega)\right\} \end{bmatrix} \succ 0, \tag{6.42}$$

with $U(j\omega) = (k_2 + k_3 j\omega) G(j\omega)$, $W(j\omega) = \frac{1}{\sqrt{\tau}} U^*(j\omega) - k_1 \sqrt{\tau} k_h G(j\omega)$ *and*

$$k_1 = \left(\varepsilon + \frac{1}{\varepsilon}\right) \sqrt{\frac{1}{2|c_1|}} + \left(\varepsilon - \frac{1}{\varepsilon}\right) \sqrt{\frac{\tau}{2}} k_h, \tag{6.43a}$$

$$k_2 = \left(\varepsilon + \frac{1}{\varepsilon}\right) \sqrt{\frac{1}{2|c_1|}} \left(\frac{k_h c_1}{2} - c_2\right) + \left(\frac{1}{\varepsilon} - \varepsilon\right) \sqrt{\frac{\tau}{2}} k_h, \tag{6.43b}$$

$$k_3 = \left(\varepsilon + \frac{1}{\varepsilon}\right) \sqrt{\frac{1}{2|c_1|}} \frac{k_h}{2}. \tag{6.43c}$$

Proof. The proof is provided in Appendix 6.A.4. □

It is interesting to mention that the diagonal elements of the matrix in (6.42) pose necessary conditions for feasibility of (6.41a) and (6.41b), respectively, which correspond to circle criterion-like conditions (see also the frequency-domain conditions for stability in Chapter 4, Theorem 4.3.1). The off-diagonal elements account for the coupling in the LMIs in (6.41) through the matrix M.

Clearly, the variable ε appears in an awkward manner in (6.42). For the choice $\varepsilon = 1$, however, the frequency-domain inequality in (6.42) simplifies significantly, but at the cost of loosing necessity of the conditions. Still, one obtains sufficient conditions for convergence that can be assessed graphically and may provide some direction toward parameter tuning.

Corollary 6.5.2. *Suppose the transfer function* $G(s) = G_{yu}(s)$ *as in* (6.2a) *is stable. Then the closed-loop system in* (6.6) *is ISC if the following frequency-domain conditions are satisfied:*

1. *The transfer function* $G(s)$ *satisfies for all* $\omega \in \mathbb{R} \cup \{\infty\}$

$$1 + k_h \mathrm{Re}\left\{G(j\omega)\right\} > 0; \tag{6.44}$$

2. *The transfer function* $G(s)$ *satisfies for all* $\omega \in \mathbb{R} \cup \{\infty\}$

$$1 + X(j\omega) - \alpha Y(j\omega) > 0, \tag{6.45}$$

in which $\alpha = 1/c_1$ *and*

$$X(j\omega) = \frac{3k_h}{2} \mathrm{Re}\left\{G(j\omega)\right\} + \frac{k_h^2}{4} G(j\omega)^2, \tag{6.46a}$$

$$Y(j\omega) = c_2 \mathrm{Re}\left\{G(j\omega)\right\} + \frac{k_h}{2} \omega \mathrm{Im}\left\{G(j\omega)\right\} + \frac{k_h c_2}{2} G(j\omega)^2; \tag{6.46b}$$

3. There exists a $\tau > 0$ such that for all $\omega \in \mathbb{R} \cup \{\infty\}$, it follows that

$$\left\| \frac{\sqrt{\tau}}{j\omega + 2\omega_c(\tau)} \right\| > \frac{k_h}{4} \frac{\sqrt{|\alpha|}\|G(j\omega)\|}{\sqrt{1 + X(j\omega) - \alpha Y(j\omega)}}, \tag{6.47}$$

with $\omega_c(\tau) = \sqrt{\left(\frac{1}{2\alpha} - \frac{c_2}{k_h}\right)^2 + \tau^2}$.

Proof. The proof can be found in Appendix 6.A.5. □

The first condition in Corollary 6.5.2 corresponds to a classical circle-criterion condition and can be checked graphically by inspecting the Nyquist plot of $G(j\omega)$. The second condition corresponds to a Popov-like condition that can be verified graphically by inspecting if the (X, Y)-locus remains to the right of a line that passes through the point $(-1, 0)$ and has a slope of $\alpha = 1/c_1$ (see also Chapter 4). The third condition essentially implies that the weighted magnitude characteristics of $G(j\omega)$ should be upper-bounded by the magnitude characteristics of a specific first-order low-pass filter, for which both the gain at $\omega = 0$ and cut-off frequency are determined by the choice of τ. This can be verified in a Bode magnitude plot. Note the resemblance with assessing robust performance for SISO LTI systems (see *e.g.*, Skogestad and Postlethwaite, 2010, Chapter 7) where the low-pass filter represents a specific weighting filter.

6.6 Steady-state performance estimation

The property of convergence paves the way for quantifying the accuracy of approximate, but easy-to-use tools such as the describing function method for steady-state performance analysis of the closed-loop system in (6.6). This section presents a computationally efficient method for quantifying the accuracy of a steady-state performance estimation using a describing function approximation. The presented ideas are inspired by the results in Pavlov et al., 2008; Pogromsky and van den Berg, 2014; van den Berg et al., 2008. A different approach that exploits the notion of contractive systems can be found in Coogan and Margaliot, 2019.

6.6.1 Linear approximation of steady-state solutions

Consider an LTI system of the form

$$\hat{\Sigma} : \begin{cases} \dot{\hat{x}}_g(t) & = A_g \hat{x}_g(t) + B_g \hat{u}(t) + B_w w(t) \\ \hat{y}(t) & = C_g \hat{x}_g(t) \end{cases} \tag{6.48}$$

with states $\hat{x}_g(t) \in \mathbb{R}^m$, external input $w(t) \in \mathbb{R}$, and output $\hat{y}(t) \in \mathbb{R}$ at time $t \in \mathbb{R}_{\geq 0}$. The external input $w : \mathbb{R}_{\geq 0} \to \mathbb{R}$ is assumed to be periodic with period

time $T > 0$. Define the signal $\hat{u} : \mathbb{R}_{\geq 0} \to \mathbb{R}$ as

$$\hat{u}(t) = \frac{1}{2\pi} \int_{-\infty}^{\infty} \hat{U}(j\omega) e^{j\omega t} d\omega \quad \text{with} \quad \hat{U}(j\omega) = -\hat{T}(j\omega) W(j\omega), \tag{6.49}$$

in which $W(j\omega)$ denotes the Fourier series of the periodic input w, and where the complex mapping $\hat{T} : \mathbb{C} \to \mathbb{C}$ is defined as

$$\hat{T}(j\omega) = \frac{\Psi(j\omega) G_{yw}(j\omega)}{1 + \Psi(j\omega) G_{yu}(j\omega)},$$

with transfer functions $G_{yw}(s) = C_g(sI - A_g)^{-1} B_w$ and $G_{yu}(s) = C_g(sI - A_g)^{-1} B_g$, and where $\Psi : \mathbb{C} \to \mathbb{C}$ denotes a harmonic linearization of the nonlinear element $\mathcal{H}$ with respect to a harmonic input. In this regard, Ψ may for example represent the sinusoidal input describing function as derived in Chapter 2, or a two-sinusoidal/incremental input describing function, see, *e.g.*, Gelb and Vander Velde, 1968. It is assumed that $1 + \Psi(j\omega) G_{yu}(j\omega) \neq 0$ for all $\omega \in \mathbb{R} \cup \{\infty\}$. It is important to realize that by definition $\hat{u}(t) = \hat{u}(t + T)$ is periodic with the same fundamental period time T as that of the input $w(t) = w(t + T)$.

Under the assumption that A_g is Hurwitz, and since both $\hat{u}$ and w are harmonic inputs, it follows that the limit (steady-state) solution of the LTI system in (6.48), denoted by $\hat{\bar{y}}$, is unique, periodic with period time T, and is expressed in the frequency-domain as

$$\begin{aligned} \hat{\bar{Y}}(j\omega) &= G_{yu}(j\omega) \hat{U}(j\omega) + G_{yw}(j\omega) W(j\omega) \\ &= \frac{G_{yw}(j\omega)}{1 + \Psi(j\omega) G_{yu}(j\omega)} W(j\omega). \end{aligned} \tag{6.50}$$

Observe that (6.50) is, in fact, the response obtained through a harmonic linearization of the closed-loop system in (6.6) (Khalil, 2002). Note that $\hat{\bar{y}}$ and $\hat{\bar{Y}}$ are fully known, and that $\hat{U}(j\omega) = -\Psi(j\omega) \hat{\bar{Y}}(j\omega) = -\hat{T}(j\omega) W(j\omega)$.

6.6.2 Accuracy of the harmonic linearization

It is of interest to quantify in some way the accuracy of the linear approximation in (6.50). To this end, suppose that the closed-loop system in (6.6) is a uniformly convergent system. As such, when forced by a periodic input $w(t) = w(t+T)$, it admits a unique and periodic steady-state solution $\bar{x}$ satisfying $\bar{x}(t) = \bar{x}(t + T)$ for all $t \in \mathbb{R}_{\geq 0}$ with $\bar{x}(t) = [\bar{x}_g(t)^\top, \bar{x}_h(t)]^\top$, see also Angeli, 2002.

Let ξ be the difference $\xi(t) := \bar{x}_g(t) - \hat{\bar{x}}_g(t)$, where $\hat{\bar{x}}_g(t)$ denotes the unique steady-state solution of (6.48) subject to the same input w, and $\zeta(t) := \bar{x}_h(t) - \hat{\bar{x}}_h(t)$, in which $\hat{\bar{x}}_h(t)$ is the unique response of (6.3) subject to the input $\hat{\bar{z}}(t) = -\hat{\bar{y}}(t)$, *i.e.*, the open-loop response of HIGS. Then, the dynamics of the

differences ξ, ζ can be written as

$$\begin{aligned}\dot{\xi}(t) &= A_g\xi(t) + B_g\zeta(t) + B_g\Delta(t),\\ \dot{\zeta}(t) &\overset{\text{a.e.}}{=} \frac{d}{dt}\left(\bar{x}_h(t) - \hat{\bar{x}}_h(t)\right),\\ q(t) &= C_g\xi(t),\end{aligned} \tag{6.51}$$

where q is the difference between the performance output $\bar{y} = C_g\bar{x}_g$ of the true (convergent and nonlinear) system and the estimate $\hat{\bar{y}} = C_g\hat{\bar{x}}_g$, and where

$$\Delta(t) = \hat{\bar{x}}_h(t) - \hat{u}(t) \tag{6.52}$$

with $\hat{u}$ defined in (6.49). It is important to realize that since $\hat{\bar{y}}$ is known, $\hat{\bar{x}}_h$ is completely known, and the expression in (6.52) can always be computed, either numerically or analytically. Moreover, since $\hat{\bar{y}}(t) = \hat{\bar{y}}(t+T)$, it follows that $\hat{\bar{x}}_h(t) = \hat{\bar{x}}_h(t+T)$, and since $\hat{u}(t) = \hat{u}(t+T)$ it holds that $\Delta(t) = \Delta(t+T)$ for all $t \in \mathbb{R}_{\geq 0}$. As such, one can consider (6.51) as the incremental system (6.18), (6.19) subject to a periodic input $\Delta(t)$. The following theorem presents a method for quantifying the mismatch between the linear approximation in (6.50) and the true nonlinear response of (6.6) in terms of an upper-bound on the root-mean-square (RMS) value of $q = \bar{y} - \hat{\bar{y}}$.

Theorem 6.6.1. *Consider the closed-loop system in* (6.6) *subject to a bounded, T-periodic input w, and assume that this system satisfies Assumption 6.2.2 and is input-to-state convergent (ISC). Suppose there exist constants $k > -1/2$, $\tau_1, \tau_2 \geq 0$, $\mu > 0$ and a symmetric matrix $P = P^\top$ that satisfy the conditions*

$$P + kk_h^2 C_g^\top C_g \succ 0, \tag{6.53a}$$

and

$$\begin{bmatrix} A_g^\top P + PA_g + C_g^\top C_g & PB_g & PB_g \\ B_g^\top P & 0 & 0 \\ B_g^\top P & 0 & -\mu^2 \end{bmatrix} + k \begin{bmatrix} Q_g & 0 & 0 \\ 0 & 0 & 0 \\ 0 & 0 & 0 \end{bmatrix} + \tau_1 S_1 \prec 0, \tag{6.53b}$$

$$\begin{bmatrix} A_g^\top P + PA_g + C_g^\top C_g & PB_g & PB_g \\ B_g^\top P & 0 & 0 \\ B_g^\top P & 0 & -\mu^2 \end{bmatrix} + k \begin{bmatrix} 0 & -\frac{c_2}{2}C_g^\top & 0 \\ -\frac{c_2}{2}C_g & 2c_1 & 0 \\ 0 & 0 & 0 \end{bmatrix} + T \prec 0, \tag{6.53c}$$

$$\begin{bmatrix} A_g^\top P + PA_g + C_g^\top C_g & PB_g & PB_g \\ B_g^\top P & 0 & 0 \\ B_g^\top P & 0 & -\mu^2 \end{bmatrix} + k \begin{bmatrix} Q_g & 0 & 0 \\ 0 & 0 & 0 \\ 0 & 0 & 0 \end{bmatrix} + T + \tau_2 S_2 \prec 0, \tag{6.53d}$$

where $Q_g = A_g^\top C_g^\top C_g + C_g^\top C_g A_g$,

$$T = \begin{bmatrix} -k_h c_2 C_g^\top C_g & \left(\frac{k_h c_1}{2} - c_2\right) C_g^\top + \frac{k_h}{2} A_g^\top C_g^\top & 0 \\ C_g\left(\frac{k_h c_1}{2} - c_2\right) + \frac{k_h}{2} C_g A_g & 2c_1 & 0 \\ 0 & 0 & 0 \end{bmatrix}, \quad (6.54a)$$

and

$$S_1 = \begin{bmatrix} 0 & -k_h C_g^\top & 0 \\ -k_h C_g & -2 & 0 \\ 0 & 0 & 0 \end{bmatrix}, \qquad S_2 = \begin{bmatrix} 0 & k_h C_g^\top & 0 \\ k_h C_g & -2 & 0 \\ 0 & 0 & 0 \end{bmatrix}. \quad (6.54b)$$

Then, the approximation error $q = \bar{y} - \hat{\bar{y}}$ *satisfies*

$$\sqrt{\frac{1}{T}\int_0^T |q(t)|^2 dt} \leq \mu\nu(T), \quad \text{with} \quad \nu(T) = \sqrt{\frac{1}{T}\int_0^T \Delta^2(t) dt}. \quad (6.55)$$

Proof. Consider the piecewise quadratic function

$$V(\xi, \zeta) = \xi^\top P \xi + k \max\left\{\zeta^2, k_h e^2\right\} + \max\left\{0, v(\zeta, e)\right\}, \quad (6.56)$$

with $e = -\bar{y} + \hat{\bar{y}}$, and $v(\zeta, e) = \zeta(\zeta - k_h e)$. Similar to the proof of Theorem 6.4.5 it can be shown that, under the hypothesis of the theorem, V is continuous, positive definite, and its time-derivative satisfies for almost all time

$$\frac{d}{dt} V(\xi(t), \zeta(t)) \leq -q^2(t) + \mu^2 \Delta^2(t). \quad (6.57)$$

Since by assumption the closed-loop system (6.6) is ICS, the steady-state solution $\bar{x}$ is T-periodic, *i.e.*, $\bar{x}(t) = \bar{x}(t+T)$. Moreover, as the steady-state solutions of the LTI system in (6.48) are T-periodic, the differences ξ and ζ are also T-periodic. As such, V is periodic and satisfies $V(t) = V(t+T)$. Integrating (6.57) from t to $t+T$, and using periodicity of V yields the inequality in (6.55). □

By computing the approximation error, one can find an upper- and lower-bound for the RMS value of the performance variable $\bar{y}$ as

$$\|\hat{\bar{y}}\|_{2,T} - \|\bar{y} - \hat{\bar{y}}\|_{2,T} \leq \|\bar{y}\|_{2,T} \leq \|\hat{\bar{y}}\|_{2,T} + \|\bar{y} - \hat{\bar{y}}\|_{2,T}, \quad (6.58)$$

where use is made of the (reverse) triangle inequality. From $\|\bar{y} - \hat{\bar{y}}\|_{2,T} = \|q\|_{2,T}$, the result in (6.58) allows, for instance, for computing upper- and lower-bounds on the RMS ratio of an input $w(t) = \sin(\omega t)$ with $\omega \in \mathbb{R}_{>0}$ and the corresponding steady-state response $\bar{y}$ as

$$\hat{\mathcal{M}}(\omega) - d(\omega) \leq \mathcal{M}(\omega) \leq \hat{\mathcal{M}}(\omega) + d(\omega), \quad (6.59)$$

in which

$$\mathcal{M}(\omega) := \frac{\|\bar{y}\|_{2,T}}{\|w\|_{2,T}}, \quad \text{and} \quad \hat{\mathcal{M}}(\omega) := \frac{\|\hat{y}\|_{2,T}}{\|w\|_{2,T}} = \left\| \frac{G_{qw}(j\omega)}{1 + \Psi(j\omega) G_{qu}(j\omega)} \right\|, \quad (6.60)$$

and where $d(\omega) := \mu\nu(\omega)/\|w\|_{2,T}$. Note that, in this context, $\mathcal{M}(\omega)$ can be seen as a generalization of a traditional transfer function for LTI systems (Pavlov et al., 2008), and $\hat{\mathcal{M}}(\omega)$ is a harmonic approximation with $\Psi(j\omega)$ being the sinusoidal input describing function. The term $d(\omega)$ estimates the mismatch between $\mathcal{M}(j\omega)$ and $\hat{\mathcal{M}}(j\omega)$ due to, for instance, the presence of higher-order harmonics in the true nonlinear response.

6.7 A numerical case-study

To demonstrate the applicability of the tools that are presented in this chapter, consider the feedback interconnection as depicted in Figure 6.4.

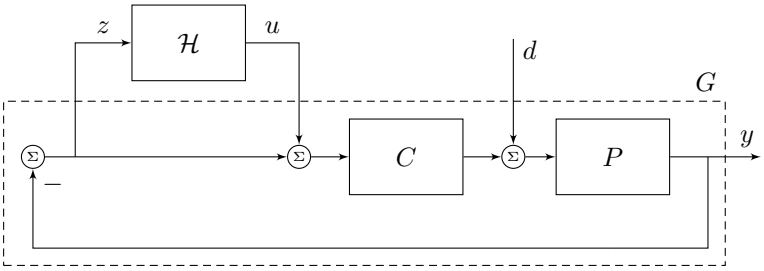

Figure 6.4. Feedback control scheme with nonlinearity $\mathcal{H}$.

Here, the plant P is a second-order LTI system that is described by the transfer function

$$P(s) = \frac{1}{s^2 + 2\beta_0\omega_0 s + \omega_0^2}, \quad (6.61)$$

with natural frequency $\omega_0 = 54 \cdot 2\pi$ rad/s and dimensionless damping coefficient $\beta_0 = 0.009$. The nominal LTI feedback controller C is given by

$$C(s) = k_p \left(\frac{s + \omega_i}{s} \right) \left(\frac{\omega_{lp}^2}{s^2 + 2\beta\omega_{lp} s + \omega_{lp}^2} \right) \quad (6.62)$$

with $k_p = 7 \cdot 10^4$ N/m, $\omega_i = 4.75 \cdot 2\pi$ rad/s, $\omega_{lp} = 6.5 \cdot 2\pi$ rad/s, and $\beta_{lp} = 0.8$.

The nonlinearity $\mathcal{H}$ is given in (6.3) with $f(x_h, z) = -\alpha x_h + \omega_h z$, and $\alpha, \omega_h \in \mathbb{R}_{>0}$, and furthermore $k_h = 0.6$. Note that f satisfies Assumption 6.2.2 with $c_1 = -\alpha$ and $c_2 = \omega_h$. The purpose of adding this element to the existing LTI controller C is to balance between additional suppression of low-frequency

disturbances and transient time-domain response in a more desirable manner (see also Deenen et al., 2017; Gruntjens et al., 2019; Van Loon et al., 2017 for comparable strategies). A derivation of the sinusoidal input describing function for the nonlinearity $\mathcal{H}$, denoted by $\mathcal{D}(j\omega)$ is provided in Appendix 6.B and will be used later for estimating steady-state performance properties of the closed-loop system in Figure 6.4.

The feedback configuration in Figure 6.4 can be rearranged into an equivalent Lur'e form as depicted earlier in Figure 6.1. In the context of this figure one finds $w = d$ and $G(s) = [G_{yu}(s), G_{yw}(s)]$, with

$$G_{yu}(s) = \frac{P(s)C(s)}{1 + P(s)C(s)}, \quad \text{and} \quad G_{yw}(s) = \frac{P(s)}{1 + P(s)C(s)}. \tag{6.63}$$

By design, these transfer functions are Hurwitz and satisfy the standing assumption on the relative degree (Assumption 2.3.1).

6.7.1 Convergence

Convergence of the closed-loop system is studied for different values of $\omega_h \in (0, 10 \cdot 2\pi]$ and different ratios for $\alpha/\omega_h \in [0, 1.8]$. This ratio determines the effect of an additional pole in the integrator dynamics. In principle, the smaller the ratio α/ω_h, the more the characteristics of $\mathcal{H}$ tend to that of HIGS as considered in Chapters 2–5. The corresponding results from evaluating the LMI conditions in Theorem 6.4.5 as well as the frequency-domain conditions in Corollary 6.5.2 are shown in Figure 6.5.

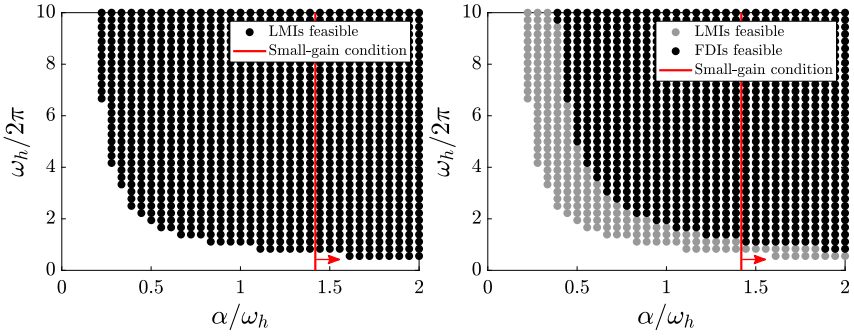

(a) Feasibility of the LMIs in Theorem 6.4.5.

(b) Feasibility of the FDIs in Theorem 6.5.1.

Figure 6.5. A comparison between feasibility of the LMI conditions in Theorem 6.4.5 (left figure), the frequency-domain conditions in Corollary 6.5.2 (right figure), and the small-gain condition in Theorem 6.4.2 (indicated by the region to the right of the red line) for different values of ω_h and ratios α/ω_h.

As expected, the range for which convergence can be shown by means of Theorem 6.4.5 is larger than the one resulting from Corollary 6.5.2 as the latter assumes a specific solution to the LMIs in (6.38). Furthermore, note that since $\mathrm{Re}\{G_{yu}(j\omega)\} \geq -0.209$, by virtue of the circle criterion the closed-loop system in Figure 6.4 is ISS for all $k_h < \frac{1}{0.209} = 3.37$. For the SISO LTI system described by G_{yu} it is easy to verify that the $\mathcal{L}_1$-norm of $G_{yu}(s)$, denoted by γ_1, satisfies $\gamma_1 = 1.419$. Since $\gamma_1 k_h = 0.85 < 1$, it then follows that the small-gain condition in Theorem 6.4.2 is satisfied for all $\alpha/\omega_h > 1.419$. This region is indicated by the region to the right of the red line in Figure 6.5. It is interesting to remark that for small values of ω_h and large ratios of α/ω_h, convergence is guaranteed by the small-gain condition in Theorem 6.4.2, but not by the LMIs and the frequency-domain conditions in Theorem 6.4.5 and Corollary 6.5.2, respectively. This indicates that for the example discussed, the small-gain condition is not necessarily more restrictive than the Lyapunov-based conditions, and in that sense both conditions can complement each other.

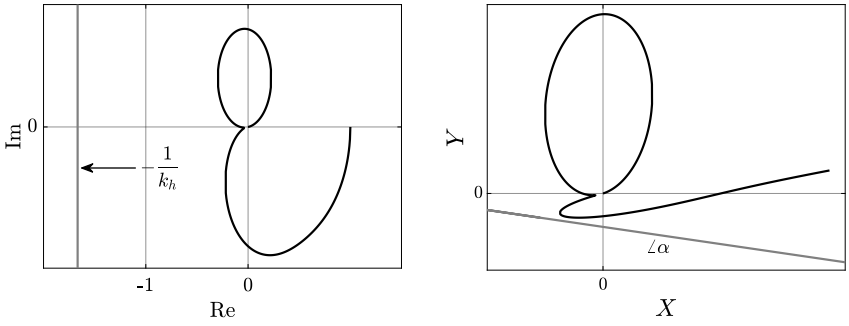

(a) Circle criterion in (6.44). **(b)** Popov-like condition in (6.45).

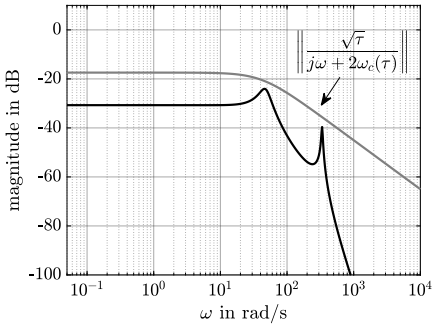

(c) Small-gain-like condition in (6.47).

Figure 6.6. Graphical interpretation of the three frequency-domain conditions in Corollary 6.5.2 for $\omega_h = 4 \cdot 2\pi$ rad/s, $\alpha/\omega_h = 0.6$ and and $\tau = 67.2$.

A graphical illustration of the frequency-domain conditions in Corollary 6.5.2 for $\omega_h = 4{\cdot}2\pi$ rad/s and $\alpha/\omega_h = 0.6$ with $\tau = 67.2$ is provided in Figure 6.6. Note that the circle criterion condition is satisfied with significant margin, whereas the Popov-like condition and small-gain like condition appear more restrictive.

The closed-loop system with $\omega_h = 4 \cdot 2\pi$ rad/s and $\alpha/\omega_h = 0.6$ is simulated for different initial conditions, and with a sinusoidal input disturbance given by $d(t) = \sin(\omega t)$ with input frequency $\omega = 6 \cdot 2\pi$ rad/s. The corresponding steady-state error $e = -y$ and the output u of the nonlinearity are shown in Figure 6.7. Clearly, the solutions converge to a unique steady-state periodic solution (shown in black) that has a fundamental period of 6 Hz, which is the same as that of the input w. Moreover, note that the output u is continuous, but it is not smooth.

6.7.2 Steady-state performance estimation

Next it is shown how the tools from Section 6.6 can be applied for estimating performance of the closed-loop system from Figure 6.4 on the basis of a describing function approximation with guaranteed error margins. For this purpose, suppose that the closed-loop system is subject to a sinusoidal input disturbance $d(t) = \sin(\omega t)$. Steady-state performance is quantified by the RMS ratio between the sinusoidal input d and the corresponding unique steady-state response $\bar{y}$ at various input frequencies ω. For LTI systems, this ratio corresponds to the process sensitivity which indicates how a harmonic input disturbance affects the steady-state output $\bar{y}$, *i.e.*, how well disturbances are rejected by the closed-loop system. For the nonlinear system in Figure 6.4 disturbance rejection properties can be estimated through a describing function-based approximation of the process sensitivity as given by

$$\hat{\mathcal{M}}(j\omega) = \frac{P(j\omega)}{1 + (1 + \Psi(j\omega))P(j\omega)C(j\omega)}, \tag{6.64}$$

in which $\Psi(j\omega) = \mathcal{D}(j\omega)$, with $\mathcal{D}(j\omega) \in \mathbb{C}$ the sinusoidal input describing function of $\mathcal{H}$ in (6.3) with $f(x_h, z) = -\alpha x_h + \omega_h z$ as provided in Appendix 6.B.

Error bounds for the approximation in (6.64) can be established via the inequalities in (6.59). Note that in case of a sinusoidal input and for $\Psi(j\omega) = \mathcal{D}(j\omega)$, the term $\Delta(t)$ that is used for constructing the bounds is specifically computed as

$$\Delta(t) = \|\hat{\mathcal{M}}(j\omega)\| \left(\hat{\bar{u}}(t) - \|\mathcal{D}(j\omega)\| \sin(\omega t + \angle\mathcal{D}(j\omega))\right), \tag{6.65}$$

where $\hat{\bar{u}}$ is the response of $\mathcal{H}$ to a sinusoidal input, and is given by

$$\hat{\bar{u}}(t) = \begin{cases} \frac{\omega_h}{\sqrt{\omega^2+\alpha^2}} \sin(\omega t + \varphi) + \frac{\omega_h}{\omega^2+\alpha^2}\omega e^{-\alpha t}, & \text{if } 0 \le t < \frac{\gamma(\omega)}{\omega}, \\ k_h \sin(\omega t), & \text{if } \frac{\gamma(\omega)}{\omega} \le t < \frac{\pi}{\omega}, \\ \frac{\omega_h}{\sqrt{\omega^2+\alpha^2}} \sin(\omega t + \varphi) - \frac{\omega_h}{\omega^2+\alpha^2}\omega e^{-\alpha\left(t-\frac{\pi}{\omega}\right)}, & \text{if } \frac{\pi}{\omega} \le t < \frac{\pi+\gamma(\omega)}{\omega}, \\ k_h \sin(\omega t), & \text{if } \frac{\pi+\gamma(\omega)}{\omega} \le t < \frac{2\pi}{\omega} \end{cases}$$

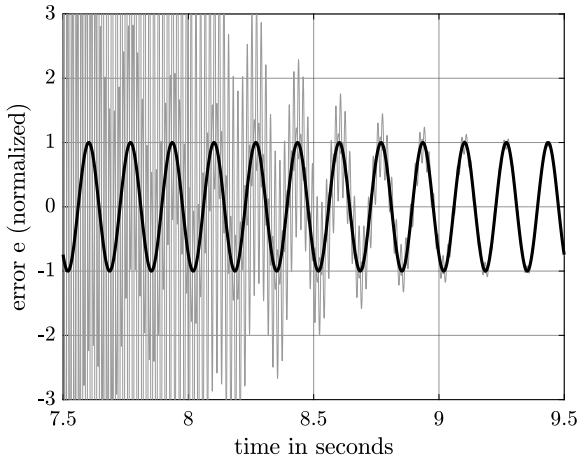

(a) Error response of the closed-loop system.

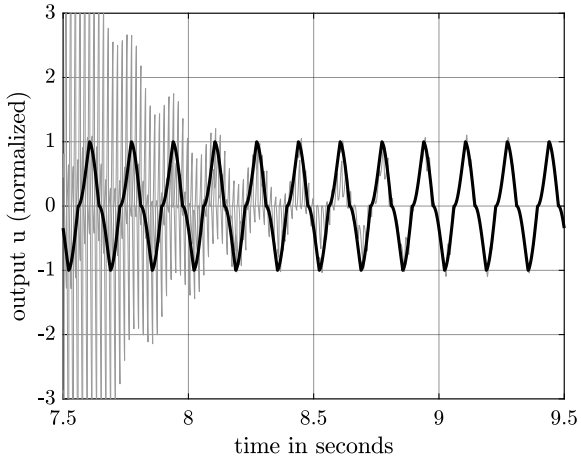

(b) Output of the nonlinearity $\mathcal{H}$.

Figure 6.7. Time-series simulation of the closed-loop system for different initial conditions and input $w(t) = \sin(\omega t)$ with $\omega = 6 \cdot 2\pi$ rad/s. The (transient) responses for different initial conditions are indicated in grey, and the steady-state solution is indicated in black.

with $\gamma(\omega)$ the (numerically obtained) switching instance and $\varphi = \arctan(-\frac{\omega}{\alpha})$. The value for μ as in (6.59) can be found numerically by solving the matrix inequalities in Theorem 6.6.1.

A steady-state performance estimate for the closed-loop system with $\omega_h =$

$4{\cdot}2\pi$ rad/s and $\alpha = 0.6\omega_h$ at various input frequencies is illustrated in Figure 6.8. In this figure, an estimate for the RMS ratio $\|\bar{y}\|_{2,T}/\|d\|_{2,T}$ by means of the approximation in (6.64) is depicted by the red line, and the error bounds with $\mu = 6.101$ are indicated by the dotted black lines. The true RMS ratio obtained by means of time-series simulations is shown by the red dots.

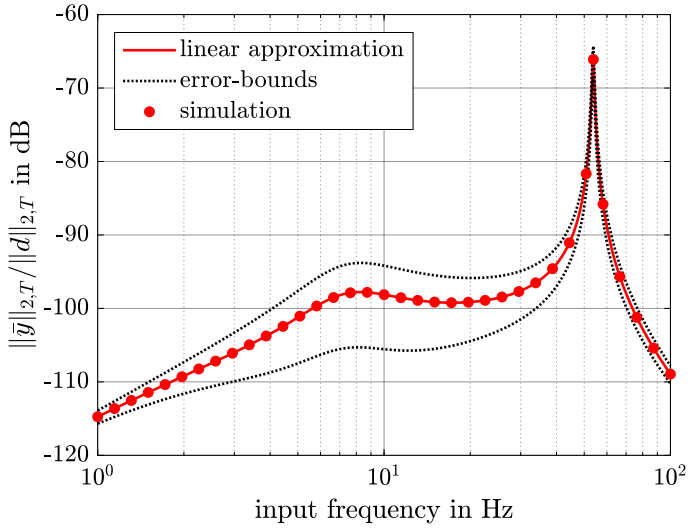

Figure 6.8. Describing function approximation of the RMS ratio between a sinusoidal input $d(t) = \sin(\omega t)$ at various input frequencies and the steady-state response $\bar{y}$ (red line), error-bounds (dotted black), and time-series simulations (red dots).

It can be seen that the error-bounds provide a useful uncertainty interval for steady-state performance and are computationally far less demanding to obtain than the exact RMS ratios via time-series simulations. Furthermore, for this example the describing function approximation seems to provide an accurate prediction of the closed-loop system performance when considering sinusoidal inputs. For each input frequency ω, the error $\|\bar{y} - \hat{\bar{y}}\|_{2,T}$ is shown in Figure 6.9. The largest value for $\|\bar{y} - \hat{\bar{y}}\|_{2,T}$, *i.e.*, the largest discrepancy (in terms of RMS value) between the unique steady-state response and its linear approximation is found to be $2.37 \cdot 10^{-7}$ and occurs at an input frequency of $\omega = 18 \cdot 2\pi$ rad/s. This frequency coincides with 1/3-th of the resonance frequency at 54 Hz in the plant P, such that the third harmonic in the output of $\mathcal{H}$ is amplified in this case. Note that peaks are also visible at 1/5-th and 1/7-th of this resonance frequency. Despite these amplifications, the contribution of higher-harmonics in the output remains small, which may be attributed to the fact that the closed-loop transfer function $G_{yu}(s)$ from u to $z = -y$ has significant low-pass filter characteristics,

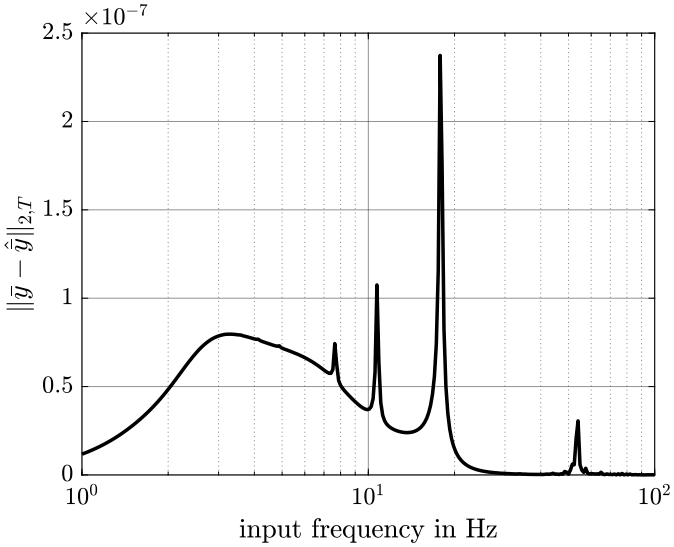

Figure 6.9. RMS value of the steady-state approximation error $\|\bar{y} - \hat{\bar{y}}\|_{2,T}$ at various input frequencies.

thereby largely filtering the higher-order harmonics generated by $\mathcal{H}$.

6.8 Summary

In this chapter, time- and frequency-domain conditions for input-to-state convergence (ISC) of systems consisting of the feedback interconnection of an LTI plant and a hybrid integrator are presented. The latter can be seen as a generalization of HIGS as discussed in earlier chapters. By exploiting incremental properties of the hybrid integrator that hold in a subset of the state-space, a set of numerically tractable LMI conditions is formulated that, when feasible, guarantee the existence of a specific piecewise quadratic incremental Lyapunov function for the system. A frequency-domain interpretation of the LMIs is given which allows for a graphical verification of the conditions. The convergence property is further exploited for estimating steady-state performance on the basis of the describing function with guaranteed error margins.

The tools that have been developed so far are particularly useful for analysis of a given system containing HIGS (or a generalization thereof). Although some of these tools also provide a useful direction for parameter tuning, these do not immediately support intuitive design of a closed-loop controller in its totality for the best interplay between linear and nonlinear parts. To deal with this, in the next chapter two approaches toward the design of HIGS-based controllers

are pursued. The first approach exploits rigorous LMIs for controller synthesis, whereas the second approach is based on heuristics and exploits the describing function within a loop-shaping framework.

6.A Proofs and technical results

6.A.1 Proof of Property 6.3.1

First consider the following observations.

1) Since the region Ω_1 in (6.21) describes the same $[0, k_h]$-sector as defined by $\hat{\mathcal{F}}$, inequality (6.20a) trivially follows.

2) When both trajectories are in 'gain-mode', the sector-condition is inherently satisfied and thus $(\delta z, \delta x_h) \in \Omega_1$. In this case, (6.20a) is satisfied with an equality.

3) When trajectories belong to Ω_2, and are both in 'integrator-mode' it follows that
$$(\delta \dot{x}_h)\delta x_h = (f(x_h, z) - f(x_h', z'))\delta x_h,$$
which, by virtue of Assumption 6.2.2 implies that the inequality in (6.20b) is satisfied.

4) From the definition of the set Ω_2 in (6.21) it follows that all $(\delta z, \delta x_h) \in \Omega_2$ inherently violate the $[0, k_h]$-sector condition as in (6.21a). This implies that the pairs (z, x_h) and (z', x_h') must belong to the same cone $\mathcal{K} \subset \hat{\mathcal{F}}$ or $-\mathcal{K} \subset \hat{\mathcal{F}}$ where the cone $\mathcal{K}$ is described by $\mathcal{K} = \{(z, u) \in \mathbb{R}^2 \mid u \geq 0,\ k_h z \geq u\}$, and, consequently, z, z', x_h, x_h' all have similar signs. Moreover, z, z' are non-zero. The latter follows from the fact that if $z = 0$ (or $z' = 0$), then also $x_h = 0$ (or $x_h' = 0$), and consequently $k_h \delta x_h \delta z = k_h x_h z \geq x_h^2 = \delta x_h^2$ (or $k_h \delta x_h \delta z = k_h x_h' z' \geq x_h'^2 = \delta x_h^2$). Hence, in that case the $[0, k_h]$-sector condition is satisfied and $(\delta x_h, \delta z) \in \Omega_1$. This, however, contradicts the assumption that $(\delta x_h, \delta z) \in \Omega_2$.

It remains to show that (6.20b) holds when $(\delta z, \delta x_h) \in \Omega_2$ and the trajectories are in different modes. To show this, the following claim is proven first.

Claim: for all $(\delta z, \delta x_h) \in \Omega_2$ the following implications hold:

1. if $x_h = k_h z$ then $z \delta x_h > 0$,
2. if $x_h' = k_h z'$ then $z' \delta x_h < 0$.

Proof of the claim. Observe that for all $(\delta z, \delta x_h) \in \Omega_2$, the following inequality is satisfied:
$$\delta x_h^2 > k_h \delta z \delta x_h. \tag{6.66}$$

It will be shown that due to this inequality, the only possible cases when $x_h = k_h z$ or $x'_h = k_h z'$ are given by the implications that are stated in the claim.

- Suppose $x_h = k_h z$, and $\delta x_h < 0$. Dividing both sides in (6.66) by δx_h then yields
$$k_h z - x'_h = x_h - x'_h < k_h(z - z'), \tag{6.67}$$
which, in turn, implies $k_h z' < x'_h$. From the sector condition in (6.4a) it must be true that $z' < 0$, and $x'_h < 0$. As for all $(\delta z, \delta x_h) \in \Omega_2$ the signals z, x_h, z', x'_h have similar signs and z, z' are non-zero, one finds $z < 0$, and thus $z\delta x_h > 0$.

- Suppose $x_h = k_h z$, and $\delta x_h > 0$. Dividing both sides in (6.66) by δx_h yields
$$k_h z - x'_h = x_h - x'_h > k_h(z - z'), \tag{6.68}$$
which implies $k_h z' > x'_h$. Due to the sector condition in (6.4a) it must be true in this case that $z' > 0$, and $x'_h > 0$. As for all $(\delta z, \delta x_h) \in \Omega_2$ the signals z, x_h, z', x'_h have similar signs and are non-zero, one finds $z > 0$, and, consequently, $z\delta x_h > 0$.

- Suppose $x'_h = k_h z'$, and $\delta x_h < 0$. Given these (in)equalities, it follows from (6.66) that
$$x_h - k_h z' = x_h - x'_h < k_h(z - z'), \tag{6.69}$$
which, in turn, implies $x_h < k_h z$. By the sector condition in (6.4a) it must be true that $z > 0$, and $x_h > 0$. Sign-equivalence then yields $z' > 0$, and thus $z'\delta x_h < 0$.

- Suppose $x'_h = k_h z'$, and $\delta x_h > 0$. As before it follows from (6.66) that
$$x_h - k_h z' = x_h - x'_h > k_h(z - z'), \tag{6.70}$$
which implies $x_h > k_h z$. Invoking the sector condition in (6.4a) shows that $z < 0$, and $x_h < 0$. Sign-equivalence then yields $z' < 0$, and thus $z'\delta x_h < 0$.

This proves the claim.

Now suppose the trajectories are in different modes. Then, according to (6.19) two possibilities arise:

$$(\delta \dot{x}_h)\delta x_h = (k_h \dot{z} - f(x'_h, z'))\, \delta x_h, \tag{6.71a}$$
$$(\delta \dot{x}_h)\delta x_h = (f(x_h, z) - k_h \dot{z}')\, \delta x_h. \tag{6.71b}$$

From the previous claim, one finds that whenever the first trajectory is in gain-mode, and thus $x_h = k_h z$, then z and δx_h have similar signs and are non-zero. Exploiting the inequality $k_h \dot{z} z < f(x_h, z)z$ in gain-mode, see (6.4b), yields $k_h \dot{z} \delta x_h < f(x_h, z)\delta x_h$. As such, one finds

$$(k_h \dot{z} - f(x_h', z'))\, \delta x_h \leq (f(x_h, z) - f(x_h', z'))\delta x_h. \tag{6.72}$$

In a similar manner, when the second trajectory is in gain-mode, and thus $x_h' = k_h z'$, then according to the claim z' and δx_h have opposite signs. By the gain mode condition in (6.4b) this leads to $k_h \dot{z}' \delta x_h > f(x_h', z')\delta x_h$. Consequently

$$(f(x_h, z) - k_h \dot{z}')\, \delta x_h \leq (f(x_h, z) - f(x_h', z'))\delta x_h. \tag{6.73}$$

Invoking Assumption 6.2.2 then leads to the inequality in (6.20b). This completes the proof.

6.A.2 Proof of Theorem 6.4.2

Without loss of generality one can assume (possibly after a state transformation) that $\|C_g\| = 1$ such that $\|\delta z(t)\| = \| - C_g \delta x_g(t)\| \leq \|\delta x_g(t)\|$. Since under the small-gain assumption stated in the theorem, the non-incremental system in (6.6), *i.e.*, the interconnection of the LTI system in (6.1) and $\mathcal{H}$ in (6.3) is ISS, it follows that solutions of (6.6) remain bounded and thus $|\delta z|$ is finite for all $t \geq 0$. Hence, the result from Lemma 6.4.1 holds true. The solution of the LTI system in (6.18) is given by

$$\delta x_g(t) = e^{A_g t}\delta x_g(0) + \int_0^t e^{A_g(t-\tau)} B_g \delta u(\tau) d\tau + \int_0^t e^{A_g(t-\tau)} B_w \delta w(\tau) d\tau, \tag{6.74}$$

from which one finds

$$\|\delta z(t)\| \leq \|\delta x_g(t)\| \leq k e^{-\lambda t}\|\delta x_g(0)\| + \gamma_u \left(\sup_{0 \leq t' \leq t} \|\delta u(t')\| \right) + \gamma_w \|\delta w\|_\infty, \tag{6.75}$$

with $\gamma_u = \int_0^\infty |C_g e^{A_g \tau} B_g| d\tau < \infty$, where boundedness of γ_u results from the fact that A_g is Hurwitz. Applying the small-gain theorem for ISS (or in this case input-to-output stable) systems (Jiang et al., 1994, Theorem 2.1) with $\gamma_u \gamma_z < 1$ in (6.29) then shows that there exist $m, \mu, \tilde{\gamma}_w > 0$ such that

$$\|\delta z(t)\| + \|\delta x_h(t)\| \leq m e^{-\mu t}(\|\delta x_g(0)\| + \|\delta x_h(0)\|) + \tilde{\gamma}_w \|\delta w\|_\infty. \tag{6.76}$$

Define $\delta x(t) = [\delta x_g(t)^\top, \delta x_h(t)]^\top$ and observe from the fact that $\|\delta x\| \leq \|\delta x_g\| + \|\delta x_h\|$ that at this point one has the following two inequalities:

$$\|\delta x(t)\| \leq n e^{-\kappa t}\|\delta x(0)\| + \gamma_h \left(\sup_{0 \leq t' \leq t} \|\delta x_h(t')\| \right) + \hat{\gamma}_w \|\delta w\|_\infty \tag{6.77}$$

$$\|\delta x_h(t)\| \leq m e^{-\mu t}\|\delta x(0)\| + \tilde{\gamma}_w \|\delta w\|_\infty. \tag{6.78}$$

Following the same arguments as in the proof of Jiang et al., 1994, Proposition 3.1, then shows that there exist $r, \sigma, \bar{\gamma}_w > 0$ such that

$$\|\delta x(t)\| \leq re^{-\sigma t}\|\delta x(0)\| + \bar{\gamma}_w \|\delta w\|_\infty, \tag{6.79}$$

which shows that the interconnected system (6.18), (6.19) is δISS. The proof can then be completed in a similar manner as the proof of Theorem 6.2.8 to conclude the system to be ISC.

6.A.3 Proof of Theorem 6.4.5

The proof is based on showing that the LMI conditions in (6.38) imply the piecewise quadratic function

$$V(\delta x) = U(\delta x_g) + k \max\left\{\delta x_h^2, k_h \delta z^2\right\} + \max\left\{0, v(\delta x_h, \delta z)\right\}, \tag{6.80}$$

where $U(\delta x_g) := \delta x_g^\top M \delta x_g$ and $v(\delta x_h, \delta z) := \delta x_h(\delta x_h - k_h \delta z)$ to satisfy the hypothesis of Theorem 6.2.8.

Before proceeding, recall that V induces a partitioning of the incremental input-output region of (6.19), which is also depicted in Figure 6.3. It is useful to write out V explicitly in these subregions, leading to

$$V(\delta x) = \begin{cases} V_1(\delta x) = U(\delta x_g) + k k_h^2 \delta z^2 & \text{if } (\delta x_h, \delta z) \in \hat{\Omega}_1, \\ V_2(\delta x) = U(\delta x_g) + k \delta x_h^2 + \delta x_h(\delta x_h - k_h \delta z) & \text{if } (\delta x_h, \delta z) \in \hat{\Omega}_2, \\ V_3(\delta x) = U(\delta x_g) + k k_h^2 \delta z^2 + \delta x_h(\delta x_h - k_h \delta z) & \text{if } (\delta x_h, \delta z) \in \hat{\Omega}_3, \end{cases}$$

where

$$\hat{\Omega}_1 := \left\{(\delta z, \delta x_h) \in \mathbb{R}^2 \mid k_h \delta z \delta x_h \geq (\delta x_h)^2\right\}, \tag{6.81a}$$

$$\hat{\Omega}_2 := \left\{(\delta z, \delta x_h) \in \mathbb{R}^2 \mid (k_h \delta z)^2 \leq (\delta x_h)^2\right\}, \tag{6.81b}$$

$$\hat{\Omega}_3 := \left\{(\delta z, \delta x_h) \in \mathbb{R}^2 \mid -k_h \delta z \delta x_h \geq (\delta x_h)^2\right\}. \tag{6.81c}$$

Remark that $\hat{\Omega}_1 = \Omega_1$ and $\hat{\Omega}_2 \cup \hat{\Omega}_3 = \Omega_2$ with Ω_1, Ω_2 defined in (6.21) (see also Figure 6.3).

Continuity - For showing continuity, it is sufficient to note that U is a Lipschitz continuous function, and the functions $\max\left\{\delta x_h^2, k_h \delta z^2\right\}$ and $\max\left\{0, v(\delta x)h, \delta z)\right\}$ are locally Lipschitz continuous. As such, V is a locally Lipschitz continuous function.

Positive definiteness - Observe that condition (6.38a) implies the existence of $\alpha_1, \alpha_2 > 0$ such that

$$\alpha_1 \|\delta x_g\|^2 \leq V_1(\delta x) \leq \alpha_2 \|\delta x_g\|^2, \tag{6.82}$$

where specifically $\alpha_1 = \lambda_{\min}(M + kk_h^2 C_g^\top C_g)$ and $\alpha_2 = \lambda_{\max}(M + kk_h^2 C_g^\top C_g)$. For all $(\delta x_h, \delta z) \in \hat{\Omega}_1$ the incremental sector condition $\|\delta x_h\| \leq k_h \|\delta z\| \leq k_h \|C_g\| \|\delta x_g\|$ as in (6.20a) holds true such that

$$\alpha_3 \|\delta x\|^2 \leq V(\delta x) = V_1(\delta x) \leq \alpha_4 \|\delta x\|^2, \tag{6.83}$$

with $\alpha_3 = \alpha_1 \cdot \min\left\{\frac{\mu}{(k_h\|C_g\|)^2}, 1-\mu\right\}$, $0 < \mu < 1$, and $\alpha_4 = \alpha_2$. For the left-hand side inequality, specific use is made of the sector condition $\|\delta x_h\|^2 - k_h^2 \|C_g\|^2 \|\delta x_g\|^2 \leq 0$ in an S-procedure manner.

For all $(\delta x_h, \delta z) \in \hat{\Omega}_2$ it holds that $V(\delta x) = V_2(\delta x) = V_1(\delta x) + k(\delta x_h^2 - k_h^2 \delta z^2) + \delta x_h(\delta x_h - k_h \delta z)$. An upper-bound on V for all $(\delta z, \delta x_h) \in \hat{\Omega}_2$ then follows trivially from $\delta x_h(\delta x_h - k_h \delta z) \leq \left(1 + \frac{k_h}{2}\right) \|\delta x_h\|^2 + \frac{k_h}{2} \|C_g\|^2 \|\delta x_g\|^2$ where specific use is made of Young's inequality. For deriving a lower-bound, two cases are considered: i) $k \geq 0$ and ii) $-1/2 < k \leq 0$. Observe that in both cases one has for all $(\delta x_h, \delta z) \in \hat{\Omega}_2$ that $\delta x_h(\delta x_h - k_h \delta z) \geq \nu \delta x_h(\delta x_h - k_h \delta z)$ with $0 < \nu \leq 1$ and $\delta x_h^2 \geq k_h^2 \delta z^2$. Then, for $k \geq 0$ this results in

$$\begin{aligned} V(\delta x) &\geq \alpha_1 \|\delta x_g\|^2 + \nu \delta x_h(\delta x_h - k_h \delta z) \\ &\geq (1-\kappa)\alpha_1 \|\delta x_g\|^2 + \frac{\kappa \alpha_1}{\|C_g\|^2} \delta z^2 + \nu(\delta x_h^2 - k_h \delta x_h \delta z) \\ &= (1-\kappa)\alpha_1 \|\delta x_g\|^2 + \xi^\top Q \xi, \end{aligned} \tag{6.84}$$

where $0 < \kappa < 1$, $\xi := [\delta x_h, \delta z]^\top$, and

$$Q := \begin{bmatrix} \nu & -\frac{\nu k_h}{2} \\ -\frac{\nu k_h}{2} & \frac{\kappa \alpha_1}{\|C_g\|^2} \end{bmatrix}. \tag{6.85}$$

Since $\nu > 0$ it follows that the matrix Q in (6.85) is positive definite if and only if $\frac{\kappa \alpha_1}{\|C_g\|^2} - \frac{\nu k_h^2}{4} > 0$, which is achieved by choosing $0 < \nu < \min\left\{1, \frac{4\kappa\alpha_1}{k_h^2 \|C_g\|^2}\right\}$. Using $\|\xi\|^2 \geq \|\delta x_h\|^2$ one finds for all $(\delta x_h, \delta z) \in \Omega_2$ and $k \geq 0$ that

$$\alpha_5^+ \|\delta x\|^2 \leq V(\delta x) \leq \alpha_6^+ \|\delta x\|^2, \tag{6.86}$$

with

$$\begin{aligned} \alpha_5^+ &= \min\left\{(1-\kappa)\alpha_1, \lambda_{\min}(Q)\right\}, \\ \alpha_6^+ &= \max\left\{\alpha_2 + \frac{k_h}{2}\|C_g\|^2, 1 + k + \frac{k_h}{2}\right\}. \end{aligned}$$

For $-1/2 < k \leq 0$ one finds

$$\begin{aligned} V(\delta x) &\geq \alpha_1 \|\delta x_g\|^2 + |k|(\delta x_h - k_h \delta z)^2 + (1 - 2|k|)\delta x_h(\delta x_h - k_h \delta z) \\ &\geq (1-\kappa)\alpha_1 \|\delta x_g\|^2 + \frac{\kappa \alpha_1}{\|C_g\|^2} \delta z^2 + \varepsilon(\delta x_h^2 - k_h \delta x_h \delta z) \\ &= (1-\kappa)\alpha_1 \|\delta x_g\|^2 + \xi^\top \hat{Q} \xi, \end{aligned} \tag{6.87}$$

where $0 < \kappa < 1$, $0 < \varepsilon < 1 - 2|k|$, $\xi = [\delta x_h, \delta z]^\top$, and

$$\hat{Q} := \begin{bmatrix} \varepsilon & -\frac{\varepsilon k_h}{2} \\ -\frac{\varepsilon k_h}{2} & \frac{\kappa \alpha_1}{\|C_g\|^2} \end{bmatrix}. \tag{6.88}$$

The matrix $\hat{Q}$ is positive definite if $\varepsilon < \frac{4\kappa\alpha_1}{k_h^2 \|C_g\|^2}$. Hence, by choosing $0 < \varepsilon < \min\left\{1 - 2|k|, \frac{4\kappa\alpha_1}{k_h^2\|C_g\|^2}\right\}$ one obtains the bounds

$$\alpha_5^- \|\delta x\|^2 \leq V(\delta x) \leq \alpha_6^- \|\delta x\|^2, \tag{6.89}$$

with

$$\begin{aligned} \alpha_5^- &= \min\left\{(1-\kappa)\alpha_1, \lambda_{\min}(\hat{Q})\right\}, \\ \alpha_6^- &= \max\left\{\alpha_2 + \left(k k_h^2 + \frac{k_h}{2}\right)\|C_g\|^2, 1 + \frac{k_h}{2}\right\}. \end{aligned}$$

As such, it follows that for all $(\delta x_h, \delta z) \in \hat{\Omega}_2$ one finds

$$\alpha_5 \|\delta x\|^2 \leq V(\delta x) \leq \alpha_6 \|\delta x\|^2, \tag{6.90}$$

with $\alpha_5 = \min\left\{\alpha_5^+, \alpha_5^-\right\}$ and $\alpha_6 = \max\left\{\alpha_6^+, \alpha_6^-\right\}$.

Finally, for all $(\delta x_h, \delta z) \in \hat{\Omega}_3$ it holds that $V(\delta x) = V_3(\delta x) = V_1(\delta x) + \delta x_h(\delta x_h - k_h \delta z)$, which admits an equivalent lower-bound as in (6.90). As such, one finds for all $(\delta x_h, \delta z) \in \hat{\Omega}_3$ that

$$\alpha_7 \|\delta x\|^2 \leq V(\delta x) \leq \alpha_8 \|\delta x\|^2, \tag{6.91}$$

where $\alpha_7 = \alpha_5^+$, $\alpha_8 = \max\left\{1 + \frac{k_h}{2}, \alpha_2 + \frac{k_h}{2}\|C_g\|^2\right\}$. Combining (6.83), (6.90) and (6.91) yields a common upper- and lower-bound for all $\delta x \in \mathbb{R}^n$ as

$$\alpha_9 \|\delta x\|^2 \leq V(\delta x) \leq \alpha_{10} \|\delta x\|^2, \tag{6.92}$$

with $\alpha_9 = \min\{\alpha_3, \alpha_5, \alpha_7\}$, and $\alpha_{10} = \max\{\alpha_4, \alpha_6, \alpha_8\}$. Hence, the function V in (6.80) satisfies condition (6.17a) in Theorem 6.2.8.

Generalized derivative - For the time being, consider $w(t) = w'(t)$ for all $t \in \mathbb{R}$. Then, for all $(\delta x_h, \delta z) \in \hat{\Omega}_1$ one finds

$$\partial V(\delta x)\delta \dot{x} = \mathrm{He}\left(\delta x_g^\top (A_g^\top (M + k C_g^\top C_g)\delta x_g + \delta x_g^\top M B_g \delta x_h\right). \tag{6.93}$$

By pre- and post multiplication of the LMI in (6.38b) with δx, and noting that for all $(\delta x_h, \delta z) \in \hat{\Omega}_1$ one has $\tau_1 \delta x^\top S_1 \delta x = 2\tau_1 \delta x_h (k_h \delta z - \delta x_h) \geq 0$, it follows by virtue of the S-procedure that (6.38b) implies $\partial V(\delta x)\delta \dot{x} \leq -\epsilon_1 \|\delta x\|^2$, $\epsilon_1 > 0$, for all $(\delta x_h, \delta z) \in \hat{\Omega}_1$.

For all $(\delta x_h, \delta_z) \in \hat{\Omega}_2$, one finds at almost all t and for all points where $\partial V(\delta x)$ exists that

$$\begin{aligned}\partial V(\delta x)\delta\dot{x} &= \partial U(\delta x_g)\delta\dot{x}_g + 2(k+1)\delta x_h\delta\dot{x}_h - k_h(\delta x_h\delta\dot{z} + \delta z\delta\dot{x}_h)\\ &= \delta x^\top(A^\top P + PA)\delta x + 2\delta x^\top Pb\phi,\end{aligned} \tag{6.94}$$

where A and b are given in (6.32), P is given by

$$P = \begin{bmatrix} M & -\frac{k_h}{2}C_z^\top \\ -\frac{k_h}{2}C_z^\top & 1+k \end{bmatrix}, \tag{6.95}$$

and $\phi = \delta\dot{x}_h - c_1\delta x_h - c_2\delta z$. By observing that $A^\top P + PA$ corresponds to the matrix in the left hand side of the LMI in (6.38c), satisfying the LMI in (6.38c) implies that $A^\top P + PA \prec 0$. Moreover, since $Pb = (1+k)C_u^\top - \frac{k_h}{2}C_z^\top$ it follows that $\delta x^\top Pb\phi = ((1+k)\delta x_h - \frac{k_h}{2}\delta z)\phi$. By virtue of Property 6.3.1 and Property 6.3.2 one finds along all possible vector fields of δx_h that $((1+k)\delta x_h - \frac{k_h}{2}\delta z)\phi \leq 0$ for all $(\delta x_h, \delta z) \in \hat{\Omega}_2$. As such, $\partial V(\delta x)\delta\dot{x} \leq -\epsilon_2\|\delta x\|^2$, $\epsilon_2 > 0$, for all $(\delta x_h, \delta z) \in \hat{\Omega}_2$.

In a similar manner, one finds for all $(\delta x_h, \delta_z) \in \hat{\Omega}_2$ that at those points where $\partial V(\delta x)$ exists, and for almost all t

$$\begin{aligned}\partial V(\delta x)\delta\dot{x} &= \partial U(\delta x_g)\delta\dot{x}_g + 2kk_h^2\delta z\delta\dot{z} + \delta\dot{x}_h(2\delta x_h - k_h\delta z) - k_h\delta x_h\delta\dot{z}\\ &= \delta x^\top(A^\top\bar{P} + \bar{P}A)\delta x + 2\delta x^\top\bar{P}b\phi,\end{aligned} \tag{6.96}$$

where A and b are given in (6.32), $\bar{P}$ is given by

$$\bar{P} = \begin{bmatrix} M + kk_h^2C_z^\top C_z & -\frac{k_h}{2}C_z^\top \\ -\frac{k_h}{2}C_z^\top & 1 \end{bmatrix}, \tag{6.97}$$

and $\phi = \delta\dot{x}_h - c_1\delta x_h - c_2\delta z$. From the fact that for all $(\delta x_h, \delta z) \in \hat{\Omega}_3$ one has $\tau_2\delta x^\top S_2\delta x = -2\tau_1\delta x_h(\delta x_h + k_h\delta z) \geq 0$. It follows by virtue of the S-procedure that the LMI in (6.38d) implies $\delta x^\top(A^\top\bar{P} + \bar{P}A)\delta x < 0$ for all $(\delta x_h, \delta z) \in \hat{\Omega}_3$. Moreover, since $\delta x^\top\bar{P}b\phi = (\delta x_h - \frac{k_h}{2}\delta z)\phi$ it follows by a similar reasoning as before that $\partial V(\delta x)\delta\dot{x} \leq -\epsilon_3\|\delta x\|^2$, $\epsilon_3 > 0$ for all $(\delta x_h, \delta z) \in \hat{\Omega}_3$.

By virtue of Theorem 2.3.9 one finds

$$\frac{d}{dt}V(\delta x(t)) \leq -\epsilon\|\delta x(t)\|^2 \tag{6.98}$$

with $\epsilon = \min\{\epsilon_1, \epsilon_2, \epsilon_3\}$ to hold for almost all times t. For $w \neq w'$, this result is easily extended as $\delta w = w - w'$ enters the incremental LTI system G in (6.18) in an affine manner. By completing squares one finds for almost all times $t \in \mathbb{R}_{\geq 0}$ that

$$\frac{d}{dt}V(\delta x(t)) \leq -(\epsilon - \sigma)\|\delta x(t)\|^2 + \beta\|\delta w(t)\|^2, \tag{6.99}$$

where $0 < \sigma < \epsilon$ and $\beta = 2\|MB_w\|/\sigma$. As such, condition (6.17b) is satisfied, so that all conditions in Theorem 6.2.8 are satisfied and the system is input-to-state convergent (ISC).

6.A.4 Proof of Theorem 6.5.1

The following results is instrumental in formulating the proof.

Lemma 6.A.1 (Kamenetskiy, 2017)**.** *For satisfying a system of two matrix inequalities*

$$I_1 \prec 0, \quad I_2 \prec 0, \tag{6.100}$$

for which the difference can be written as $I_2 - I_1 = Q = pq^\top + qp^\top$*, for some vectors* $p, q \in \mathbb{R}^n$*, it is necessary and sufficient that there exists a number* $\varepsilon > 0$ *such that one inequality*

$$I_1 + Q^+(\varepsilon) = I_2 + Q^-(\varepsilon) \prec 0, \tag{6.101}$$

with

$$Q^\pm(\varepsilon) = \left(\frac{\varepsilon}{\sqrt{2}}p \pm \frac{1}{\varepsilon\sqrt{2}}q\right)\left(\frac{\varepsilon}{\sqrt{2}}p \pm \frac{1}{\varepsilon\sqrt{2}}q\right)^\top \tag{6.102}$$

is satisfied.

Proof. The proof can be found in Kamenetskiy, 2017, Section 3. □

Proof of the theorem - The proof constists of two main steps. In the first step it is shown through application of Lemma 6.A.1 that the feasibility of the two LMIs in (6.41) is equivalent to feasibility of a single matrix inequality. In the second step, it is shown by the Kalman-Yakubovich-Popov (KYP)-lemma that feasibility of this matrix inequality, in turn, is equivalent to satisfying the frequency-domain inequality in (6.42).

First, it is important to note that for feasibility of the LMIs it is necessary that $c_1 < 0$. Via the Schur complement, the LMIs in (6.41a) and (6.41b) can be reformulated as

$$I_1: \quad A_g^\top M + MA_g + \frac{1}{2\tau}\left(MB_g - \tau k_h C_g^\top\right)\left(MB_g - \tau k_h C_g^\top\right)^\top \prec 0, \tag{6.103}$$

$$I_2: \quad A_g^\top M + MA_g + \frac{1}{2|c_1|}\mathrm{Pm}\left(MB_g + \left(\lambda I + \frac{k_h}{2}A_g^\top\right)C_g^\top\right) \prec 0, \tag{6.104}$$

with $\mathrm{Pm}\,(X) = XX^\top$. Consider the difference $I_2 - I_1$ which reads

$$\begin{aligned} I_2 - I_1 = &\frac{1}{2|c_1|}\mathrm{Pm}\left(MB_g + \left(\lambda I + \frac{k_h}{2}A_g^\top\right)C_g^\top\right) \\ &- \frac{1}{2\tau}\left(MB_g - \tau k_h C_g^\top\right)\left(MB_g - \tau k_h C_g^\top\right)^\top. \end{aligned} \tag{6.105}$$

Using the vector relation $aa^\top - bb^\top = \frac{1}{2}(a+b)(a-b)^\top + \frac{1}{2}(a-b)(a+b)^\top$ for all $a, b \in \mathbb{R}^n$ it follows that (6.105) is equivalent to

$$I_2 - I_1 = pq^\top + qp^\top \tag{6.106}$$

in which p and q are given by

$$p = \frac{1}{\sqrt{2}}\left(a_1 M B_g + Q_1 C_g^\top\right), \quad \text{and} \quad q = \frac{1}{\sqrt{2}}\left(a_2 M B_g + Q_2 C_g^\top\right), \tag{6.107}$$

where

$$a_1 = \left(\frac{1}{\sqrt{2|c_1|}} + \frac{1}{\sqrt{2\tau}}\right), \tag{6.108a}$$

$$a_2 = \left(\frac{1}{\sqrt{2|c_1|}} - \frac{1}{\sqrt{2\tau}}\right), \tag{6.108b}$$

$$Q_1 = \frac{1}{\sqrt{2|c_1|}}\left(\lambda I + \frac{k_h}{2} A_g^\top\right) - \sqrt{\frac{\tau}{2}} k_h I, \tag{6.108c}$$

$$Q_2 = \frac{1}{\sqrt{2|c_1|}}\left(\lambda I + \frac{k_h}{2} A_g^\top\right) + \sqrt{\frac{\tau}{2}} k_h I. \tag{6.108d}$$

By Lemma 6.A.1, it follows that solvability of the inequalities I_1, I_2 is equivalent to the existence of $\varepsilon > 0$ such that one inequality is feasible:

$$\begin{aligned} A_g^\top M + M A_g + \frac{1}{2\tau}\left(MB_g - \tau k_h C_g^\top\right)\left(MB_g - \tau k_h C_g^\top\right)^\top \\ + \left(\frac{\varepsilon}{\sqrt{2}} p + \frac{1}{\varepsilon\sqrt{2}} q\right)\left(\frac{\varepsilon}{\sqrt{2}} p + \frac{1}{\varepsilon\sqrt{2}} q\right)^\top \prec 0. \end{aligned} \tag{6.109}$$

Using the expressions for p and q in (6.107), it follows that (6.109) can be written as

$$\begin{aligned} A_g^\top M + M A_g + \frac{1}{2\tau}\left(MB_g - \tau k_h C_g^\top\right)\left(MB_g - \tau k_h C_g^\top\right)^\top \\ + \frac{1}{4}\mathrm{Pm}\left(\left(\varepsilon a_1 + \frac{1}{\varepsilon} a_2\right) M B_g + \left(\varepsilon Q_1 + \frac{1}{\varepsilon} Q_2\right) C_g^\top\right) \prec 0. \end{aligned} \tag{6.110}$$

Define $\bar{B} = [B_1, B_2]$, $\bar{C} = [C_1, C_2]$ with

$$B_1 = B_g, \tag{6.111a}$$

$$B_2 = \frac{\sqrt{2|c_1|}}{2}\left(\varepsilon a_1 + \frac{1}{\varepsilon} a_2\right) B_g, \tag{6.111b}$$

$$C_1 = -\tau k_h C_g^\top, \tag{6.111c}$$

$$C_2 = \frac{\sqrt{2|c_1|}}{2}\left(\varepsilon Q_1 + \frac{1}{\varepsilon} Q_2\right) C_g^\top. \tag{6.111d}$$

With this choice, the inequality in (6.110) can be written more compactly as

$$A_g^\top M + MA_g + \left(M\bar{B} + \bar{C}^\top\right)\Gamma^{-1}\left(M\bar{B} + \bar{C}^\top\right)^\top \prec 0, \tag{6.112}$$

with $\Gamma^{-1} = \mathrm{diag}([1/(2\tau), 1/(2|c_1|)])$. Since Γ is invertible, by virtue of Schur's complement, (6.112) is equivalent to

$$\begin{bmatrix} A_g^\top M + MA_g & M\bar{B} + \bar{C}^\top \\ \bar{B}^\top M + \bar{C}^\top & -\Gamma \end{bmatrix} \prec 0. \tag{6.113}$$

Hence, by Lemma 6.A.1, feasibility of (6.113) is equivalent to feasibility of (6.41).

From the Kalman-Yakubovich-Popov (KYP)-lemma (Rantzer, 1996) it follows that, in turn, feasibility of (6.113) is equivalent to satisfying the frequency-domain inequality (FDI) given by

$$\begin{bmatrix} W_1(j\omega) & W_2(j\omega) \\ 1 & 0 \\ 0 & 1 \end{bmatrix}^* \begin{bmatrix} 0 & C_1^\top & C_2^\top \\ C_1 & -2\tau & 0 \\ C_2 & 0 & -2|c_1| \end{bmatrix} \begin{bmatrix} W_1(j\omega) & W_2(j\omega) \\ 1 & 0 \\ 0 & 1 \end{bmatrix} \prec 0, \tag{6.114}$$

for all $\omega \in \mathbb{R}$, where $W_1(j\omega) = (j\omega I - A_g)^{-1}B_1 \in \mathbb{C}^n$, and $W_2(j\omega) = (j\omega I - A_g)^{-1}B_2 \in \mathbb{C}^n$. Note that under the assumption that $G_{yu}(s)$ is stable, A_g is Hurwitz and M must necessarily be positive definite.

Expanding the left-hand side of (6.114) yields

$$\begin{bmatrix} W_1^*(j\omega)C_1^\top + C_1W_1(j\omega) - 2\tau & W_1^*(j\omega)C_2^\top + C_1W_2(j\omega) \\ C_2W_1(j\omega) + W_2^*(j\omega)C_1^\top & W_2^*(j\omega)C_2^\top + C_2W_2(j\omega) - 2|c_1| \end{bmatrix} = \begin{bmatrix} -2\tau\left(k_h\mathrm{Re}\left\{G(j\omega)\right\} + 1\right) & -\tilde{W}(j\omega) \\ -\tilde{W}^*(j\omega) & -|c_1|\left(2 - k_1\mathrm{Re}\left\{(k_2 + k_3j\omega)G(j\omega)\right\}\right) \end{bmatrix}, \tag{6.115}$$

where

$$\tilde{W}(j\omega) = \frac{\sqrt{2|c_1|}}{2}\left((k_2 - k_3j\omega)G^*(j\omega) - \tau k_h k_1 G(j\omega)\right) \tag{6.116}$$

and

$$k_1 = \left(\varepsilon + \frac{1}{\varepsilon}\right)\sqrt{\frac{1}{2|c_1|}} + \left(\varepsilon - \frac{1}{\varepsilon}\right)\sqrt{\frac{\tau}{2}}k_h, \tag{6.117a}$$

$$k_2 = \left(\varepsilon + \frac{1}{\varepsilon}\right)\sqrt{\frac{1}{2|c_1|}}\left(\frac{k_hc_1}{2} - c_2\right) + \left(\frac{1}{\varepsilon} - \varepsilon\right)\sqrt{\frac{\tau}{2}}k_h, \tag{6.117b}$$

$$k_3 = \left(\varepsilon + \frac{1}{\varepsilon}\right)\sqrt{\frac{1}{2|c_1|}}\frac{k_h}{2}. \tag{6.117c}$$

By performing a congruence transformation to (6.115) with the matrix $T = \text{diag}([1/\sqrt{2\tau}, 1/\sqrt{2|c_1|}])$ and reversing signs one finds the FDI

$$\begin{bmatrix} k_h \text{Re}\{G(j\omega)\} + 1 & W(j\omega) \\ W^*(j\omega) & 1 - \frac{k_1}{2}\text{Re}\{(k_2 + k_3 j\omega)G(j\omega)\} \end{bmatrix} \succ 0 \tag{6.118}$$

with

$$W(j\omega) = \frac{1}{2\sqrt{2\tau}}(k_2 - k_3 j\omega)G^*(j\omega) - \frac{k_h k_1}{2}\sqrt{\frac{\tau}{2}}G(j\omega). \tag{6.119}$$

Hence, satisfying the frequency-domain inequality in (6.118) is equivalent to satisfying (6.114), and, in turn, is equivalent to satisfying the LMIs in (6.41).

Note that the crux in proving necessity and sufficiency of the frequency-domain conditions for feasibility of the LMIs in (6.41) is the possibility to reformulate the two LMIs in (6.41) into a single matrix inequality.

6.A.5 Proof of Corollary 6.5.2

Consider the conditions in Theorem 6.5.1 with the choice $\varepsilon = 1$. In that case, one has

$$k_1 = \sqrt{\frac{2}{|c_1|}}, \quad k_2 = k_1\left(\frac{k_h c_1}{2} - c_2\right), \quad \text{and} \quad k_3 = k_1\frac{k_h}{2},$$

and the frequency-domain inequality in (6.42) reduces to

$$\begin{bmatrix} k_h \text{Re}\{G(j\omega)\} + 1 & \frac{k_1}{2\sqrt{2}}\hat{W}(j\omega) \\ \frac{k_1}{2\sqrt{2}}\hat{W}^*(j\omega) & 1 + \frac{1}{c_1}\text{Re}\left\{\hat{U}(j\omega)\right\} \end{bmatrix} \succ 0, \tag{6.120}$$

with $\hat{U}(j\omega) = \left(\frac{k_h c_1}{2} - c_2 + \frac{k_h}{2}j\omega\right)G(j\omega)$, $\hat{W}(j\omega) = \frac{1}{\sqrt{\tau}}\hat{U}^*(j\omega) - \sqrt{\tau}k_h G(j\omega)$. By invoking a Schur complement, it follows that the necessary and sufficient conditions for the matrix in (6.120) to be positive definite are given by

$$M_{11}(j\omega) > 0, \tag{6.121}$$

$$M_{11}(j\omega)M_{22}(j\omega) - M_{12}(j\omega)M_{12}^*(j\omega) > 0, \tag{6.122}$$

for all $\omega \in \mathbb{R}$, and where

$$\begin{aligned} M_{11}(j\omega) &= k_h \text{Re}\{G(j\omega)\} + 1, \\ M_{22}(j\omega) &= 1 + \frac{\lambda}{c_1}\text{Re}\{G(j\omega)\} - \frac{k_h}{2c_1}\omega\text{Im}\{G(j\omega)\}, \\ M_{12}(j\omega) &= \frac{1}{2\sqrt{|c_1|}}\left(\frac{1}{\sqrt{\tau}}\left(\lambda - \frac{k_h}{2}j\omega\right)G^*(j\omega) - \sqrt{\tau}k_h G(j\omega)\right), \end{aligned}$$

with $\lambda = \left(\frac{k_h c_1}{2} - c_2\right)$. Expansion of the product $M_{12}(j\omega)M_{12}^*(j\omega)$ yields

$$M_{12}(j\omega)M_{12}^*(j\omega) = F_1(j\omega) + F_2(j\omega)$$

with

$$F_1(j\omega) = \frac{k_h}{2c_1}\left(\lambda\left(\mathrm{Re}\left\{G(j\omega)\right\}^2 - \mathrm{Im}\left\{G(j\omega)\right\}^2\right) - k_h\omega \mathrm{Re}\left\{G(j\omega)\right\}\mathrm{Im}\left\{G(j\omega)\right\}\right)$$
$$F_2(j\omega) = \frac{1}{4|c_1|}\left(\frac{1}{\tau}\left(\frac{k_h^2}{4}\omega^2 + \lambda^2\right) + \tau k_h^2\right)G(j\omega)^2.$$

Then, it follows that a necessary condition for satisfying the frequency-domain inequalities in (6.121) and (6.122) is that $M_{11}(j\omega) = 1 + k_h \mathrm{Re}\left\{G(j\omega)\right\} > 0$, hence condition 1 in the corollary.

For satisfying the second condition in (6.122), first observe that since only positive values for τ are considered, one has $F_2(j\omega) \geq 0$ for all $\omega \in \mathbb{R}$. Hence, a necessary condition for the existence of $\tau > 0$ such that th inequality in (6.122) holds is that for all $\omega \in \mathbb{R}$

$$\begin{aligned} &M_{11}(j\omega)M_{22}(j\omega) - F_1(j\omega) = \\ &1 + \left(k_h + \frac{\lambda}{c_1}\right)\mathrm{Re}\left\{G(j\omega)\right\} - \frac{k_h}{2c_1}\omega \mathrm{Im}\left\{G(j\omega)\right\} + \frac{k_h}{2}\frac{\lambda}{c_1}G(j\omega)^2 > 0. \end{aligned} \tag{6.123}$$

Collecting all terms that contain c_1 yields that (6.123) is equivalently written as

$$1 + X(j\omega) - \alpha Y(j\omega) > 0, \tag{6.124}$$

where $\alpha = 1/c_1$ and

$$X(j\omega) = \frac{k_h}{2}\mathrm{Re}\left\{G(j\omega)\left(3 + \frac{k_h}{2}G(j\omega)\right)\right\}, \tag{6.125a}$$
$$Y(j\omega) = \mathrm{Re}\left\{G(j\omega)\left(c_2 - \frac{k_h}{2}j\omega + c_2\frac{k_h}{2}G(j\omega)\right)\right\}. \tag{6.125b}$$

Hence, condition 2 in the corollary.

Finally, observe that (6.122) can be written as $1 + X(j\omega) - \alpha Y(j\omega) > F_2(j\omega)$. Suppose that condition 2 is satisfied, *i.e.*, for all $\omega \in \mathbb{R}$ it holds that $1 + X(j\omega) - \alpha Y(j\omega) > 0$. Then, (6.122) is equivalent to (after division by the left-hand side and taking the square root)

$$\left\|\frac{\sqrt{\tau}}{j\omega + 2\omega_c(\tau)}\right\| > \frac{k_h}{4}\frac{\sqrt{|\alpha|}\|G(j\omega)\|}{\sqrt{1 + X(j\omega) - \alpha Y(j\omega)}}, \tag{6.126}$$

with $\omega_c(\tau) = \sqrt{\left(\frac{1}{2\alpha} - \frac{c_2}{k_h}\right)^2 + \tau^2}$. This results in condition 3.

6.B Describing function for HIGS with an additional pole

Consider the hybrid integrator in (6.3) with $f(x_h, z) = -\alpha x_h + \omega_h z$ representing HIGS with an additional pole $\alpha \in \mathbb{R}$. With this choice, the "extended" hybrid integrator shows a certain resemblance with a first-order reset element (FORE) as considered in, *e.g.*, Horowitz and Rosenbaum, 1975; Zaccarian et al., 2005. When including an additional pole $\alpha > 0$, it can be easily deduced from the proof of Theorem 2.2.4 in Chapter 2 that $\mathcal{H}$ in (6.3) is incrementally uniformly exponentially stable, which is thus a stronger property than what is derived for $\alpha = 0$, for which only incremental asymptotic stability was shown. Also, amplitude invariance can be shown in a similar manner as was done in Theorem 2.2.5. For $\alpha < 0$, however, these properties are harder to verify due to the resulting unstable dynamics in "integrator-mode". Still, for inputs that cross zero in finite time such as sinusoids, it can be shown that there can exist only one steady-state response which is also amplitude invariant. Here, the fact that the input crosses zero in finite time is explicitly used. By the grace of these properties it is possible to conduct a describing function analysis (see also Chapter 2).

Consider $z(t) = \sin(\omega t)$ as an input to (6.3). Then, with $x_h(0) = 0$, the corresponding unique steady-state response is given by

$$u(t) = \begin{cases} \frac{\omega_h}{\omega^2+\alpha^2}\left(\omega e^{-\alpha t} - \omega\cos(\omega t) + \alpha\sin(\omega t)\right), & \text{for } 0 \le t < \frac{\gamma(\omega)}{\omega}, \\ k_h \sin(\omega t), & \text{for } \frac{\gamma(\omega)}{\omega} \le t < \frac{\pi}{\omega}, \\ \frac{\omega_h}{\omega^2+\alpha^2}\left(-\omega e^{-\alpha\left(t-\frac{\pi}{\omega}\right)} - \omega\cos(\omega t) + \alpha\sin(\omega t)\right), & \text{for } \frac{\pi}{\omega} \le t < \frac{\pi+\gamma(\omega)}{\omega}, \\ k_h \sin(\omega t), & \text{for } \frac{\pi+\gamma(\omega)}{\omega} \le t < \frac{2\pi}{\omega}, \end{cases}$$

where $t = \gamma(\omega)/\omega$ is the switching instance, which follows from the intersection

$$\frac{\omega_h}{\omega^2+\alpha^2}\left(\omega e^{-\alpha\frac{\gamma(\omega)}{\omega}} - \omega\cos(\gamma(\omega)) + \alpha\sin(\gamma(\omega))\right) = k_h\sin(\gamma(\omega)). \tag{6.127}$$

While for $\alpha = 0$, the closed-form solution $\gamma(\omega) = 2\arctan\left(k_h\omega/\omega_h\right)$ can be found, for $\alpha \neq 0$ (6.127) does not admit a closed-form solution. Nevertheless, a numerical solution can be found efficiently via, *e.g.*, standard zero-finding algorithms. The steady-state response to a sinusoid for different ratios of α/ω_h is shown in Figure 6.10.

The Fourier coefficients of the first harmonic in u are given by

$$\begin{aligned} a_1(\omega) = &\frac{2\omega}{\pi}\left(\frac{\omega_h}{\omega^2+\alpha^2}\right)\left(\frac{\omega^2}{\omega^2+\alpha^2}\left(\frac{\alpha}{\omega} - e^{-\alpha\frac{\gamma}{\omega}}\left(\frac{\alpha}{\omega}\cos(\gamma) - \sin(\gamma)\right)\right) - \right. \\ &\left.\frac{2\gamma + \sin(2\gamma)}{4}\right) + \left(\frac{\alpha\omega_h}{\omega^2+\alpha^2} - k_h\right)\frac{1-\cos(2\gamma)}{2\pi}, \end{aligned}$$

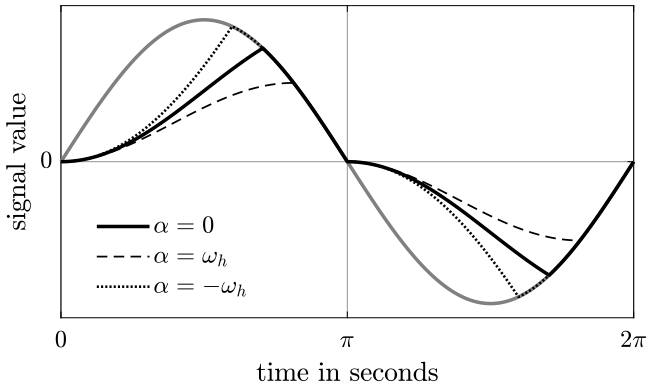

Figure 6.10. Response of $\mathcal{H}$ in (6.3) with $f(x_h, z) = -\alpha x_h + \omega_h z$ to a sinusoidal input for $k_h = 1$, $\omega_h = \pi$ rad/s, and different ratios of α/ω_h.

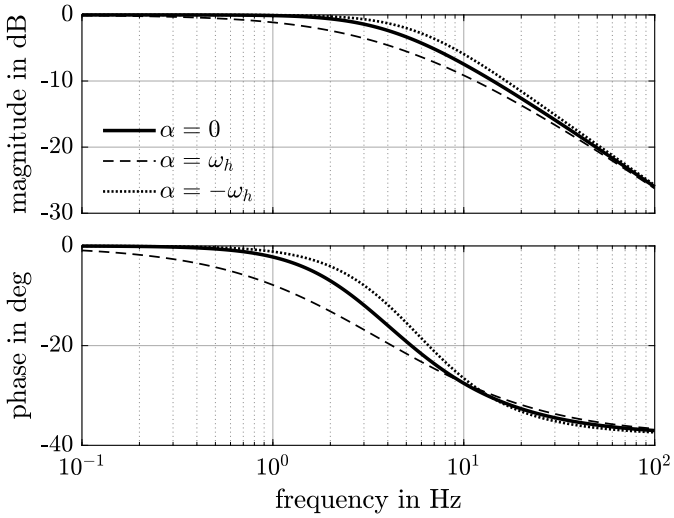

Figure 6.11. Describing function $\mathcal{D}(j\omega)$ of $\mathcal{H}$ in (6.3) with $f(x_h, z) = -\alpha x_h + \omega_h z$ for $k_h = 1$, $\omega_h = \pi$ rad/s, and different ratios of α/ω_h.

and

$$b_1(\omega) = \frac{2\omega}{\pi}\left(\frac{\omega_h}{\omega^2+\alpha^2}\right)\left(\frac{\omega^2}{\omega^2+\alpha^2}\left(1 - e^{-\alpha\frac{\gamma}{\omega}}\left(\cos(\gamma) + \frac{\alpha}{\omega}\sin(\gamma)\right)\right) - \frac{\sin^2(\gamma)}{2}\right) + k_h + \left(\frac{\alpha\omega_h}{\omega^2+\alpha^2} - k_h\right)\frac{2\gamma - \sin(2\gamma)}{2\pi},$$

and the describing function is given by $\mathcal{D}(j\omega) = a_1(\omega) + jb_1(\omega)$. Note that for $\alpha = 0$ one recovers the Fourier coefficients for HIGS as given in (2.16). The corresponding describing function characteristics for different ratios of α/ω_h are shown in Figure 6.11. It can be seen that the choice $\alpha > 0$ (stable pole) results in more damping, whereas the opposite is seen for the choice $\alpha < 0$ (unstable pole). For ratios satisfying $|\alpha/\omega_h| < 1$ the discrepancy with the case $\alpha = 0$ appears to be small. Note that in all cases, $\lim_{\omega\to\infty} \mathcal{D}(j\omega) = \frac{\omega_h}{j\omega}(1+4j/\pi)$, which resembles the describing function of the classical Clegg integrator, see also Chapter 2 and Clegg, 1958; Horowitz and Rosenbaum, 1975.

Part III

Design and Applications

Chapter 7

HIGS-Based Controller Design

7.1 Introduction

The tools that have been developed so far are particularly useful for the purpose of analysis, but provide limited direction toward design of HIGS-based controllers that can achieve improved system performance. As performance improvements do not result from blind application of HIGS, but rather from a careful interplay between its switching mechanism and the remaining linear time-invariant (LTI) parts of the system, there is a need for comprehensive design procedures.

This chapter considers two approaches for HIGS-based controller design. The first approach presents a method for robust controller synthesis by exploiting matrix inequalities that are derived from the frequency-domain conditions presented in Chapter 4, and combines these with the $\mathcal{L}_2$-performance measure as discussed in Chapter 5. The approach links to the work in Arcak et al., 2003 where circle and Popov criteria are used as tools for nonlinear feedback design.

A possible drawback of an approach based on matrix inequalities, however, is the lack of a clear physical interpretation regarding parameter tuning, and limited guidance for re-design when the set of inequalities turns out to be infeasible. In an industrial setting these aspects may be experienced as less desirable. Therefore, as an alternative, a second approach that exploits a describing function characterization of HIGS within a robust loop-shaping framework is presented. Key in this approach is to express the modelling error induced by the describing function approximation as an uncertainty in the controller (Ferreres and Fromion, 1998; Impram and Munro, 2001; Katebi and Zhang, 1995). Controller design with the describing function of HIGS as a frequency-domain approximation of its nonlinear steady-state input-output behaviour then proceeds in a manner similar to that for LTI systems, and entails robustness against both

modelling errors in the plant as well as in the controller. One may argue that design based on describing functions is not relevant (if at all possible) in the given nonlinear control context, for example due to the lack of mathematical rigour in the statements on stability and performance. But, as frequency-domain tools are widely adopted by control engineers in industry, such an approach may be of great practical value and the benefits associated with it cannot be ignored. It is advocated that the approach is not only useful for HIGS-based control design, but applies to the design of other nonlinear strategies, for example reset control (Beker et al., 2001; Clegg, 1958; Nešić et al., 2008) as well. Also notice in this regard that the need for systematic design procedures in general is acknowledged as being one of the open problems in reset and hybrid control (Zhao et al., 2013).

The remainder of this chapter is organized as follows. In Section 7.2 the control design problem formulation is specified. In Section 7.3 robust synthesis of HIGS-based controllers using matrix inequalities is discussed. Section 7.4 presents a design approach that exploits describing functions within a robust loop-shaping framework. The main findings of this chapter are summarized in Section 7.5.

7.2 System description and problem formulation

7.2.1 General system description

Consider the control configuration as depicted in Figure 7.1. Here, G is the generalized plant, which is represented as the linear time-invariant (LTI) multi-input multi-output (MIMO) system

$$G : \begin{cases} \dot{x}_g(t) &= A_g x_g(t) + B_g v(t) + B_w w(t) + B_{w_\Delta} w_\Delta(t), \\ y(t) &= C_g x_g(t) + D_g v(t) + D_w w(t) + D_{w_\Delta} w_\Delta(t), \\ q(t) &= \bar{C}_q x_g(t) + \bar{D}_q v(t) + \bar{D}_w w(t) + \bar{D}_{w_\Delta} w_\Delta(t), \\ q_\Delta(t) &= \hat{C}_q x_g(t) + \hat{D}_q v(t) + \hat{D}_w w(t) + \hat{D}_{w_\Delta} w_\Delta(t), \end{cases} \tag{7.1}$$

where $x_g(t) \in \mathbb{R}^m$ denotes the states of the generalized plant, $q(t) \in \mathbb{R}^r$ contains the performance variables, such as tracking errors and control actions, $w(t) \in \mathbb{R}^l$ are the exogenous input signals, such as disturbances, measurement noise, and reference commands. The matrices (A_g, B_g, C_g, D_g) are assumed to be minimal, and the remaining matrices in (7.1) are of appropriate dimension. The uncertainty channels $w_\Delta(t) \in \mathbb{R}^p$, $q_\Delta(t) \in \mathbb{R}^q$ are related by $w_\Delta = \Delta_G q_\Delta$, where $\Delta_G \in \bar{\Delta}$ is an unstructured plant uncertainty that belongs to the set

$$\bar{\Delta} := \left\{ \Delta_G \in \mathcal{RH}_\infty^{p\times q} \mid \|\Delta_G\|_\infty < 1 \right\}, \tag{7.2}$$

in which $\mathcal{RH}_\infty^{p\times q}$ denotes the space of proper and real rational stable transfer function matrices of size $p \times q$. The measured output $y(t) \in \mathbb{R}$ is fed back to a

(non)linear single-input single-output (SISO) feedback controller K that generates the control signal $v(t) \in \mathbb{R}$. The generalized plant G in Figure 7.1 contains a nominal model of the plant to be controlled, scaling filters that normalize the uncertainty, and performance weighting filters (Glover and McFarlane, 1989; Skogestad and Postlethwaite, 2010). The latter filters are added for the purpose of including problem-specific input knowledge into the system description, and trade-off performance objectives between different input-output channels. In an LTI context, these filters can be used for specifying magnitude bounds on closed-loop transfer functions (Ortega et al., 2006; van de Wal et al., 2002).

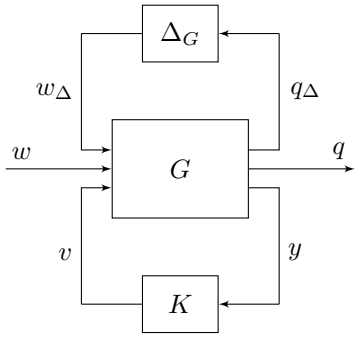

Figure 7.1. Generalized feedback configuration with plant uncertainty.

7.2.2 Problem formulation

The feedback controller K aims at stabilizing the closed-loop system, and achieving a certain level of system performance by minimizing (in some sense) the closed-loop mapping from exogenous inputs w to performance variables q. All of this must be achieved in the face of plant uncertainties. Formally, the design of a (non)linear SISO feedback controller K can be formulated as the following constraint optimization problem:

$$\begin{aligned} \underset{K}{\text{minimize}} \quad & J(K) \\ \text{subject to} \quad & \|T_{w\to q}(K, \Delta_G)\|_\infty \leq \gamma, \\ & K \text{ stabilizes } G_\Delta, \\ & K \in \mathcal{K}, \end{aligned} \tag{7.3}$$

in which $T_{w\to q}(K, \Delta_G) : \mathbb{R}^n \to \mathbb{R}^m$ is the closed-loop mapping from inputs w to the performance channel q, for given K and $\Delta_G \in \bar{\Delta}$, which is desired to have an H_∞-norm of at most γ with $\gamma > 0$. The H_∞-norm of a system is defined in

terms of the $\mathcal{L}_2$-gain (see also Chapter 5 for a formal definition):

$$\|T_{w\to q}\|_\infty = \sup_{\substack{w\in\mathcal{L}_2\setminus\{0\}\\ \text{dom } q\neq\{0\}}} \frac{\|q\|_2}{\|w\|_2}. \tag{7.4}$$

For LTI systems one finds the equivalence $\|T_{w\to q}\|_\infty = \sup_\omega \bar{\sigma}(T_{w\to q}(j\omega))$ where $\bar{\sigma}$ denotes the maximum singular value of a transfer function matrix, which, in the SISO case corresponds to the peak value of $\|T(j\omega)\|$. In (7.3), G_Δ represents the interconnection of the generalized plant G in (7.1) and the uncertainty Δ_G, $J(K)$ is an objective function that resembles certain control system requirements (*e.g.*, defined in terms of γ), and $K \in \mathcal{K}$ represents a structural constraint on the controller. In particular, the set $\mathcal{K}$ specifies the structure of the controller, as well as constraints on the associated tuning parameters. Structural constraints are added for accommodating practical situations, where it may be desired to find low-order controllers with a given structure, such as PID-based controllers, see, *e.g.*, Apkarian and Noll, 2006.

7.2.3 Toward HIGS-based controller design

In an LTI context, two main directions can be found in the literature for solving the controller design problem (7.3): state-space methods and frequency-domain methods. In a state-space approach, it is customary to solve (7.3) using linear matrix inequalities (LMIs) (Apkarian and Noll, 2006; Apkarian et al., 2015; Doyle et al., 1989; Gahinet and Apkarian, 1994; Packard and Doyle, 1993; Zhou et al., 1996). The main advantage of these methods is that the structure of the controller is completely left to the optimization routine, and the resulting controller is guaranteed to be the optimal one (with respect to the performance objective). However, these approaches all require a state-space realization of the plant and controller. In a frequency-domain approach, (7.3) is solved via frequency-domain loop-shaping, done either manually (Glover and McFarlane, 1989; Steinbuch and Norg, 1998), or guided by an autotuner (Bruijnen et al., 2006; Åström et al., 1992). Although a loop-shaping approach not necessarily leads to an optimal controller, and the structure of the controller should be determined beforehand by the control engineer, the main advantages over numerical state-space methods are the possibility to directly use non-parametric models of the plant in the procedure, and the possibility for an intuitive/direct assessment of the effects from adjusting the controller parameters on the performance requirements. For these reasons, frequency-domain loop-shaping to this day remains the most popular method for LTI controller design in practice (Samad, 2017; Samad et al., 2020).

The objective in this chapter is to formulate a procedure for effectively solving (7.3), in which $K = K(C_i, \mathcal{H})$ is a HIGS-based controller that is constructed by interconnecting HIGS $\mathcal{H}$ with several LTI filter elements $C_i(s)$, $i = 1, \ldots, m$.

Note that the set $\mathcal{K}$ in (7.3) includes all controllers of this form. Inspired by the various directions for LTI controller design available in the literature, two approaches for solving (7.3) with K being a HIGS-based controller are pursued in this chapter. The first approach is based on matrix inequalities, and provides a synthesis procedure that leads to a closed-loop controller design with guaranteed robust stability and performance properties. It closely links to state-space methods for LTI design. The second approach exploits the describing function within a robust frequency-domain loop-shaping framework. It can be seen as a tuning procedure and connects to frequency-domain loop-shaping methods that are widely adopted in industry. Both approaches are discussed in detail in the next two sections.

7.3 Synthesis using matrix inequalities

7.3.1 System setting

In this section, a rigorous approach toward synthesis of HIGS-based controllers for the purpose of input disturbance rejection within the setting depicted in Figure 7.2 is considered. In this figure, P is the LTI plant, C_1, C_2 are the LTI parts of the controller K, $\mathcal{H}$ represents HIGS, $d(t)$ is a scalar-valued input disturbance signal, $y(t)$ is the scalar-valued measured output signal used for feedback control, and $q(t)$ is the scalar-valued performance output signal. The (strictly) proper and stable SISO LTI weighting filters W and W_Δ are, respectively, used to include knowledge of the input disturbance and plant uncertainty. Note that input multiplicative uncertainty is considered here, but, given the SISO LTI characteristics of the SISO plant and uncertainty, output multiplicative uncertainty can be considered as well.

It is assumed that the plant P in Figure 7.2 has a relative degree of at least two, such that, conform Assumption 2.3.1, the external inputs v, w, w_Δ as well as their time-derivatives do not appear directly as an input to HIGS.

The SISO LTI filters in K are initially fixed to $C_2(s) = 1$ and $C_1(s) = C(s)$ with C described in state-space by

$$C : \begin{cases} \dot{x}_c(t) &= A_c x_c(t) + B_c u(t), \\ v(t) &= C_c x_c(t) + D_c u(t), \end{cases} \tag{7.5}$$

with $x_c(t) \in \mathbb{R}^s$, $u(t) \in \mathbb{R}$ and $v(t) \in \mathbb{R}$ the filter state, input, and output, respectively, at time $t \in \mathbb{R}_{\geq 0}$, and A_c, B_c, C_c, D_c matrices of consistent dimensions. This specific choice for $C_1(s)$ and $C_2(s)$ is useful for deriving synthesis conditions, and will be reconsidered later.

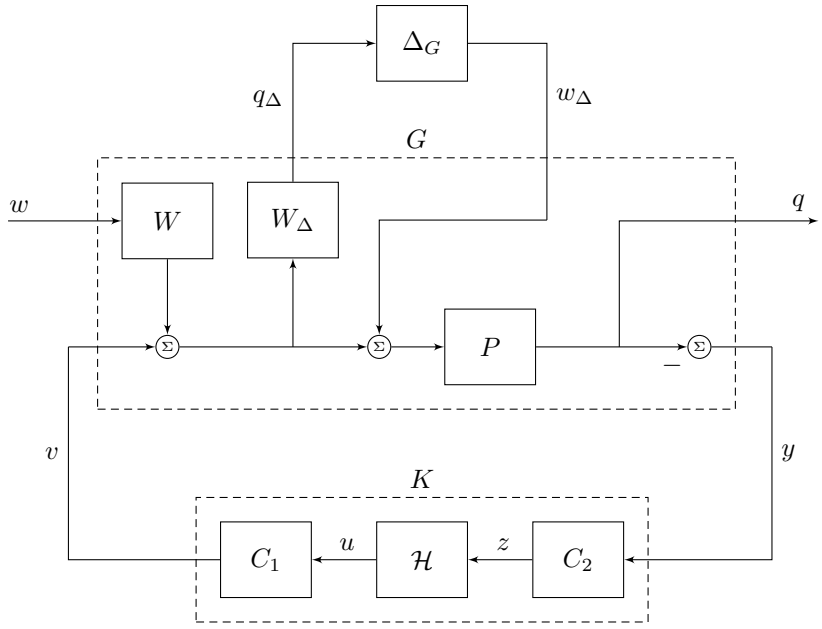

Figure 7.2. Input disturbance rejection within the generalized plant set-up.

Recall from Chapter 2 that HIGS is formulated as

$$\mathcal{H}: \begin{cases} \dot{x}_h(t) &= \omega_h z(t), \quad \text{if } (z(t), u(t), \dot{z}(t)) \in \mathcal{F}_1, \\ x_h(t) &= k_h z(t), \quad \text{if } (z(t), u(t), \dot{z}(t)) \in \mathcal{F}_2, \\ u(t) &= x_h(t), \end{cases} \tag{7.6}$$

where $x_h(t) \in \mathbb{R}$ is the integrator state, $z(t) \in \mathbb{R}$ is the input, $\dot{z}(t)$ is the corresponding time-derivative, $u(t) \in \mathbb{R}$ is the output at time $t \in \mathbb{R}_{\geq 0}$, and the sets $\mathcal{F}_1$ and $\mathcal{F}_2$ are given by

$$\mathcal{F}_1 = \left\{ (z, u, \dot{z}) \in \mathbb{R}^3 \mid k_h z u \geq u^2 \wedge (z, u, \dot{z}) \notin \mathcal{F}_2 \right\}, \tag{7.7a}$$

$$\mathcal{F}_2 = \left\{ (z, u, \dot{z}) \in \mathbb{R}^3 \mid u = k_h z \wedge \omega_h z^2 > k_h \dot{z} z \right\}. \tag{7.7b}$$

The design parameters of HIGS are given by the integrator frequency $\omega_h \in (0, \infty)$ and the gain $k_h \in (0, \infty)$. Closer inspection reveals that within the specific configuration of Figure 7.2 the gain k_h is redundant when used in conjunction with additional filters, as its effect can always be achieved by appropriate scaling of the output u, and integrator parameter ω_h. This effect can thus be encapsulated in the proportional gain of $C_1 = C$. In the remainder of this section, this parameter is therefore fixed at $k_h = 1$.

Interconnecting (7.1)–(7.6) in the manner as shown in Figure 7.2, and treating q_Δ, w_Δ as additional input-output channels results in the standard closed-loop system description

$$\Sigma : \begin{cases} \dot{x}(t) & = A_i x(t) + Bw(t) + B_\Delta w_\Delta(t), \quad \text{if } x(t) \in \mathcal{X}_i,\ i \in \{1,2\} \\ q(t) & = Cx(t), \\ q_\Delta(t) & = C_\Delta x(t) + D_\Delta w(t), \end{cases} \tag{7.8}$$

with states $x(t) = \left[x_g(t)^\top,\, x_h(t),\, x_c(t)^\top\right]^\top \in \mathbb{R}^{n+1}$, $n = m + s$. The sets $\mathcal{X}_i$, $i = \{1, 2\}$, are given by

$$\mathcal{X}_i = \{x \in \mathbb{R}^n \mid Ex \in \mathcal{F}_i\}, \tag{7.9}$$

where the matrix E is given by

$$E = \begin{bmatrix} C_z^\top & C_u^\top & (C_z A_1)^\top \end{bmatrix}^\top, \tag{7.10}$$

with $C_z = [C_p\ 0\ 0]$ and $C_u = [0\ 1\ 0]$. The system matrices are written as

$$A_1 = \begin{bmatrix} A_g & B_g D_c & B_g C_c \\ \omega_h C_p & 0 & 0 \\ 0 & B_c & A_c \end{bmatrix}, \quad A_2 = \begin{bmatrix} A_g & B_g D_c & B_g C_c \\ k_h C_p A_g & 0 & 0 \\ 0 & B_c & A_c \end{bmatrix}, \tag{7.11a}$$

whereas the input matrices are given by

$$B = \begin{bmatrix} B_w^\top & 0 & 0 \end{bmatrix}^\top, \quad B_\Delta = \begin{bmatrix} B_{w_\Delta}^\top & 0 & 0 \end{bmatrix}^\top, \tag{7.11b}$$

and the output matrices are

$$C = \begin{bmatrix} \bar{C}_q & 0 & 0 \end{bmatrix}, \quad C_\Delta = \begin{bmatrix} \hat{C}_q & \hat{D}_q D_c & \hat{D}_q C_c \end{bmatrix}, \quad D_\Delta = \hat{D}_w. \tag{7.11c}$$

7.3.2 From analysis to synthesis

Input-to-state stability (ISS) of the *nominal* closed-loop system in Figure 7.2 (with $\Delta_G = 0$) can be assessed via Theorem 4.3.3, where the existence of a quadratic ISS-Lyapunov function was guaranteed via the frequency-domain inequality

$$1 + \operatorname{Re}\left\{ \left(\lambda k C_u + F + \left(\lambda + k \frac{\omega_h}{k_h} \right) H \right) (j\omega I - \mathcal{A}_2)^{-1} b \right\} > 0, \tag{7.12}$$

with $\lambda \geq 0$, $k \geq 1$, and where the corresponding system matrices are given by $b = C_u^\top$, $H = k_h C_z - C_u$, $F = C_z(k_h A_1 - \omega_h I)$, and $\mathcal{A}_2 = A_2 + k\frac{\omega_h}{k_h} bH$. From the

Kalman-Yakubovich-Popov (KYP) lemma (see also Chapter 4) it readily follows that (7.12) is equivalent to the set of matrix inequalities

$$M = M^\top \succ 0, \tag{7.13a}$$

$$\begin{bmatrix} \left(A_2 + k\frac{\omega_h}{k_h} bH\right)^\top M + M\left(A_2 + k\frac{\omega_h}{k_h} bH\right) & Mb - c^\top \\ b^\top M - c & -2 \end{bmatrix} \prec 0. \tag{7.13b}$$

in which $c = \lambda k C_u + F + (\lambda + k\frac{\omega_h}{k_h})H$. Recall from Theorem 4.3.3 in Chapter 4 that (7.13) are sufficient conditions for guaranteeing feasibility of the set of inequalities in (4.10) with $\tau_1, \tau_2 \geq 0$ and $\tau_3 = 0$, *i.e.*, the existence of a common quadratic Lyapunov function (including S-procedure terms) for the closed-loop system in (7.8). Different from the set of "direct" inequalities in (4.10), however, the set of inequalities in (7.13) can also be used in an LTI context. In this regard, typical machinery used for synthesizing LTI controllers via matrix inequalities comparable with (7.13) can conveniently be exploited for synthesizing HIGS-based controllers. Before discussing this in more detail, the inequalities in (7.13) are extended toward conditions for robust performance of the closed-loop system in (7.8). Hereto, a small-gain theorem from the input channel w_Δ to the output q_Δ is essentially exploited.

Proposition 7.3.1. *Consider the closed-loop system in* (7.8) *with* $w_\Delta = \Delta_G q_\Delta$. *Suppose there exist a symmetric matrix* $M = M^\top \succ 0$ *and numbers* $\lambda \geq 0$, $k \geq 1$, *and* $\gamma > 0$ *that satisfy the inequality*

$$\begin{bmatrix} \left(A_2 + k\frac{\omega_h}{k_h} bH\right)^\top M + M\left(A_2 + k\frac{\omega_h}{k_h} bH\right) & Mb - c^\top & M\bar{B} & \bar{C}^\top \\ b^\top M - c & -2 & 0 & 0 \\ \bar{B}^\top M & 0 & -\Gamma & \bar{D}^\top \\ \bar{C} & 0 & \bar{D} & -\Gamma \end{bmatrix} \prec 0, \tag{7.14}$$

in which $\bar{B} = [B \ B_\Delta]$, $\bar{C} = [C^\top \ C_\Delta^\top]^\top$, $\bar{D} = \mathrm{diag}(0, D_\Delta)$, *and* $\Gamma = \mathrm{diag}(\gamma, 1)$. *Then for all* $\Delta_G \in \bar{\Delta}$ *the closed-loop system in* (7.8) *is input-to-state stable (ISS) and has a finite* $\mathcal{L}_2$*-gain from* w *to* q *as in* (7.4) *smaller than or equal to* γ.

Proof. By virtue of the Schur complement, (7.14) is equivalent to

$$\begin{bmatrix} \mathcal{A}_2^\top M + M\mathcal{A}_2 + Q & M\bar{B} \\ \bar{B}^\top M & -\Gamma \end{bmatrix} + \begin{bmatrix} \bar{C}^\top \\ \bar{D}^\top \end{bmatrix} \Gamma^{-1} \begin{bmatrix} \bar{C} & \bar{D} \end{bmatrix} \prec 0, \tag{7.15}$$

with $\mathcal{A}_2 = \left(A_2 + k\frac{\omega_h}{k_h} bH\right)$ and $Q = \frac{1}{2}\left(Mb - c^\top\right)\left(Mb - c^\top\right)^\top \succeq 0$. Pre- and post multiplying (7.15) with $(x, \bar{w}) = (x, w, w_\Delta)$ yields

$$x^\top \left(\mathcal{A}_2^\top M + M\mathcal{A}_2 + Q\right) x + 2x^\top M\bar{B}\bar{w} + \frac{1}{\gamma} q^2 - \gamma w^2 + q_\Delta^2 - w_\Delta^2 < 0. \tag{7.16}$$

Define $V(x) = x^\top P x$ with

$$P = M + \lambda H^\top H + \lambda k(C_u^\top H + H^\top C_u), \tag{7.17}$$

and observe that due to the assumption on the relative degree, one finds $P\bar{B} = M\bar{B}$. Then, using the result in Theorem 4.3.3 it follows that $t \mapsto V(x(t))$ satisfies for almost all times and all $x \in \mathcal{X}_i$

$$\dot{V} \leq -\epsilon V + \gamma w^2 - \frac{1}{\gamma} q^2 + w_\Delta^2 - q_\Delta^2, \tag{7.18}$$

with $\epsilon > 0$ sufficiently small. By virtue of the bounded real lemma (Khalil, 2002) it follows that for all $\Delta_G \in \bar{\Delta}$ there exists a $V_\Delta(x_\Delta) > 0$ with $x_\Delta \in \mathbb{R}^s$ the (internal) states pertaining Δ_G that satisfies $\dot{V}_\Delta \leq -\mu V_\Delta + q_\Delta^2 - w_\Delta^2$. Hence, for the interconnection of the nominal system with the uncertainty Δ_G one finds $U(x, x_\Delta) = V(x) + V_\Delta(x_\Delta) > 0$ for all $(x, x_\Delta) \in \mathcal{X}_i \cup \mathbb{R}^s$, and

$$\dot{U} \leq -\tau U - \frac{1}{\gamma} q^2 + \gamma w^2, \tag{7.19}$$

for all $(x, x_\Delta) \in \mathcal{X}_i \cup \mathbb{R}^s$, and where $\tau = \min\{\epsilon, \mu\}$. The proof is then completed using standard arguments. □

The matrix inequality in (7.14) is instrumental in synthesizing robust HIGS-based controllers with guaranteed performance properties. In reformulating (7.14) into appropriate synthesis conditions, note that the parameters associated with the LTI part of the controller only appear in the matrices A_2 and $\bar{C}$. By gathering all LTI controller parameters into the single variable

$$K_c = \begin{bmatrix} A_c & B_c \\ C_c & D_c \end{bmatrix}, \tag{7.20}$$

and introducing the notation

$$A = \left[\begin{array}{cc:c} A_g & 0 & 0 \\ k_h C_p A_g & 0 & 0 \\ \hdashline 0 & 0 & 0 \end{array}\right] = \left[\begin{array}{c:c} A_0 & 0 \\ \hdashline 0 & 0 \end{array}\right], \quad \bar{C}_0 = \begin{bmatrix} \bar{C}_q & 0 & 0 \\ \hat{C}_q & 0 & 0 \end{bmatrix}, \tag{7.21}$$

and

$$\mathcal{B} = \begin{bmatrix} 0 & B_g \\ 0 & 0 \\ I & 0 \end{bmatrix}, \quad \mathcal{C} = \begin{bmatrix} 0 & 0 & I \\ 0 & I & 0 \end{bmatrix}, \quad \mathcal{D} = \begin{bmatrix} 0 & 0 \\ 0 & \hat{D}_q \end{bmatrix} \tag{7.22}$$

the matrix A_2 can be written more compactly as $A_2 = A + \mathcal{B}K_c\mathcal{C}$, whereas the matrix $\bar{C}$ is written as $\bar{C} = \bar{C}_0 + \mathcal{D}K_c\mathcal{C}$. As such, one can write the corresponding

inequality in (7.14) in the form

$$\begin{bmatrix} \mathcal{A}^\top M + M\mathcal{A} & Mb - c^\top & M\bar{B} & \bar{C}_0^\top \\ b^\top M - c & -2 & 0 & 0 \\ \bar{B}^\top M & 0 & -\Gamma & \bar{D}^\top \\ \bar{C}_0 & 0 & \bar{D} & -\Gamma \end{bmatrix} + \mathrm{He}\left\{ \begin{bmatrix} M\mathcal{B} \\ 0 \\ \mathcal{D} \end{bmatrix} K_c \begin{bmatrix} \mathcal{C} & 0 & 0 \end{bmatrix} \right\} \prec 0, \tag{7.23}$$

in which $\mathcal{A} = A + k\frac{\omega_h}{k_h} bH$, with A given in (7.21). The inequality in (7.23) is not an LMI and cannot be used directly for synthesis. However, it is in a standard form that allows for direct application of the elimination lemma (Boyd et al., 1994). Following the steps in Gahinet and Apkarian, 1994, Theorem 4.2 and Theorem 4.3, it is possible to show that the conditions in Proposition 7.3.1 are equivalent to the following set of inequalities:

$$\begin{bmatrix} W_{\mathcal{B}_0} & 0 \\ 0 & I \\ I & 0 \end{bmatrix}^\top \begin{bmatrix} \mathcal{A}_0 R + R\mathcal{A}_0^\top & b_0 - Rc_0^\top & B_0 & RC_0^\top \\ b_0^\top - c_0^\top R & -2 & 0 & 0 \\ B_0^\top & 0 & -\Gamma & D_0^\top \\ C_0 R & 0 & D_0 & -\Gamma \end{bmatrix} \begin{bmatrix} W_{\mathcal{B}_0} & 0 \\ 0 & I \\ I & 0 \end{bmatrix} \prec 0, \tag{7.24a}$$

$$\begin{bmatrix} W_{\mathcal{C}_0} & 0 \\ 0 & I \\ I & 0 \end{bmatrix}^\top \begin{bmatrix} S\mathcal{A}_0 + \mathcal{A}_0^\top S & Sb_0 - c_0^\top & SB_0 & C_0^\top \\ b_0^\top S - c_0 & -2 & 0 & 0 \\ B_0^\top S & 0 & -\Gamma & D_0^\top \\ C_0 & 0 & D_0 & -\Gamma \end{bmatrix} \begin{bmatrix} W_{\mathcal{C}_0} & 0 \\ 0 & I \\ I & 0 \end{bmatrix} \prec 0, \tag{7.24b}$$

$$\begin{bmatrix} R & I \\ I & S \end{bmatrix} \succ 0, \tag{7.24c}$$

in which $\mathcal{A}_0 = A_0 + k\frac{\omega_h}{k_h} b_0 H_0$ with A_0 given in (7.21),

$$B_0 = \begin{bmatrix} B_w & B_{w_\Delta} \\ 0 & 0 \end{bmatrix}, \quad C_0 = \begin{bmatrix} \bar{C}_q & 0 \\ \hat{C}_q & 0 \end{bmatrix}, \quad D_0 = \bar{D}, \tag{7.25}$$

and $b_0 = [0, 1]^\top$, $H_0 = [k_h C_p, -1]$, $c_0 = \lambda k b_0^\top + F_0 + (\lambda + k\frac{\omega_h}{k_h})H_0$ with $F_0 = [C_p(k_h A_g - \omega_h I), 0]$. Furthermore, the matrices $W_{\mathcal{B}_0}$ and $W_{\mathcal{C}_0}$ satisfy

$$\mathrm{Im}(W_{\mathcal{B}_0}) = \ker([B_g^\top, \hat{D}_q]), \quad \text{and} \quad \mathrm{Im}(W_{\mathcal{C}_0}) = \ker([0, I]). \tag{7.26}$$

Note that the above inequalities result from assuming the following structure on the matrix M:

$$M = \begin{bmatrix} R & X \\ X^\top & \star \end{bmatrix}, \quad \text{and} \quad M^{-1} = \begin{bmatrix} S & Y \\ Y^\top & \star \end{bmatrix}, \tag{7.27}$$

where $R, S \in \mathbb{R}^{(m+1)\times(m+1)}$ and $X, Y \in \mathbb{R}^{s\times s}$. For details regarding the structure in (7.27) and the explicit steps taken in reformulating the inequalities, see Gahinet and Apkarian, 1994.

7.3.3 Controller synthesis algorithm

Based on the conditions derived above and under the assumption $k_h = 1$, the controller synthesis problem can be formulated as follows:

$$\begin{aligned} \underset{R,S,k,\lambda,\omega_h}{\text{minimize}} \quad & \gamma \\ \text{subject to} \quad & (7.24) \\ & \lambda \geq 0,\ k \geq 1,\ \omega_h > 0. \end{aligned} \tag{7.28}$$

The inequalities in (7.24) are not LMIs due to products of the variables R, S with λ, k, ω_h, such that (7.28) is a non-convex optimization problem potentially with multiple local minima. Clearly, one could perform an exhaustive search over the parameters λ, k, and ω_h to find a (local) minimum to (7.28). Such approach, however, may be computationally intensive. To potentially improve the computational efficiency, one could exploit additional structure in (7.24). Namely, from the observation that $b_0^\top W_{\mathcal{C}_0} = 0$ the inequality in (7.24b) appears to be quasi-convex, in the sense that the inequality is convex (in the variables S, λ, ω_h, and γ) for fixed $\tau := k\omega_h$. This allows for a simple and intuitive two-step approach for finding a solution to the inequalities in (7.24), which is summarized as follows:

- **Step 1:** Fix τ, and minimize γ subject to the LMIs (7.24b), $S \succ 0$, $\lambda \geq 0$, and $\tau \geq \omega_h > 0$ in which the free variables are S, λ, and ω_h.

- **Step 2:** With the obtained values for S, λ, ω_h, and $k = \tau/\omega_h$, minimize γ subject to the LMIs (7.24a), and (7.24c).

If feasible, the resulting controller has guaranteed robust performance indicated by the maximum γ obtained in the above two steps and with respect to all uncertainties $\Delta_G \in \bar{\Delta}$. Although numerically efficient, the solution of this approach is not guaranteed to be a (local) minimum to (7.28). In order to refine the result, one can perform a bisection over the performance variable γ, or resort to more sophisticated (iterative) schemes such as, *e.g.*, branch-and-bound algorithms (Goh et al., 1994), path-following, and linearization approaches (Hassibi et al., 1999; Tran Dinh et al., 2012).

When a feasible solution is found, the LTI controller parameters K_c in (7.20) can be retrieved from the obtained matrices R and S by reconstructing M in (7.27). Hereto, the equality $XY^\top = I - RS$ should be solved first, *e.g.*, by using a singular value decomposition of $I - RS$, to obtain X and Y. Then, M can be

retrieved as (see Gahinet and Apkarian, 1994, Section 7)

$$M = \begin{bmatrix} S & I \\ Y^\top & 0 \end{bmatrix} \begin{bmatrix} I & R \\ 0 & X^\top \end{bmatrix}^{-1}. \tag{7.29}$$

The obtained matrix M, parameters λ, k, ω_h and performance level γ can then be used in (7.23) to compute K_c. Note that a solution to (7.23) is guaranteed to exist when (7.24) is feasible.

The resulting LTI part of the controller can be written as $C(s) = C_c(sI - A_c)^{-1}B_c + D_c$. Referring to Figure 7.2, the a priori choice $C_1(s) = C(s)$ and $C_2(s) = 1$ will yield a robustly stable closed-loop system with guaranteed performance indicated by γ. However, note that any (strictly) proper and stable $C_1(s)$ and $C_2(s)$ satisfying $C_1(s)C_2(s) = C(s)$ will yield a robust input-to-state stable closed-loop system, since the transfer function from u to z does not change. However, an $\mathcal{L}_2$-gain smaller than γ may not be guaranteed. In principle, one can set $C_1(s) = C(s)F^{-1}(s)$ and $C_2(s) = F(s)$ with $F(s)$ a (strictly) proper and stable filter. Clearly, the choice for $F(s)$ has an effect on switching properties of HIGS, and may benefit performance (recall the results in Chapter 3). At this point it is not clear what an appropriate choice for $F(s)$ would be in general, but this is expected to be highly dependent on the performance objective, as well as the nature of the external input signals.

7.3.4 Example

To demonstrate the merit of the above synthesis procedure, consider the second-order system

$$P(s) = \frac{1}{s^2 + 0.18s + 1} \tag{7.30}$$

for which a robustly stabilizing HIGS-based controller must be designed. For taking into account unmodelled dynamics at high frequencies, the uncertainty is characterized through the weighting filter

$$W_\Delta(s) = \frac{0.045s + 0.2}{0.02s + 1}. \tag{7.31}$$

To enforce integral action in the controller and obtain a gain of at least 20 dB at lower frequencies, the performance weighting filter W is set to $W(s) = 10^{-3}/(s + \epsilon)$ with $\epsilon = 10^{-5}$. Interconnecting the plant and weighting filters results in the generalized plant description

$$G : \begin{cases} \dot{x}_g &= A_g x_g + B_g v + B_w w + B_{w_\Delta} w_\Delta, \\ y &= C_g x_g, \\ q &= C_q x_g, \\ q_\Delta &= \hat{C}_q x_g + \hat{D}_q v, \end{cases} \tag{7.32}$$

with plant and filter states $x_g^\top = [x_p^\top, x_w, x_{w_\Delta}]^\top \in \mathbb{R}^4$, system matrices

$$\left[\begin{array}{c|c} A_g & B_g \\ \hline C_g & D_g \end{array}\right] = \left[\begin{array}{cccc|c} 0 & 1 & 0 & 0 & 0 \\ -1 & -0.18 & 1 & 0 & 1 \\ 0 & 0 & -10^{-5} & 0 & 0 \\ 0 & 0 & 1 & -50 & 1 \\ \hline -1 & 0 & 0 & 0 & 0 \end{array}\right],$$

and input-output matrices $B_w = [0\ 0\ 10^{-3}\ 0]^\top$, $B_{w_\Delta} = [0\ 1\ 0\ 0]^\top$, $C_q = -C_g$, $\hat{C}_q = [0\ 0\ 2.25\ \ -102.5]$, and $\hat{D}_q = 2.25$. A controller is synthesized by solving the conditions in (7.24) through the proposed two-step approach. The obtained controller is given by

$$\begin{aligned} A_c &= \begin{bmatrix} -73.03 & 8.59 & -5.91 & -21.57 & -2.27 \cdot 10^3 \\ 6.69 \cdot 10^{-2} & 110.58 & 6.88 & 600.47 & -3.41 \cdot 10^4 \\ -2.71 \cdot 10^{-2} & -68.02 & -10.33 & -3.06 \cdot 10^2 & 2.06 \cdot 10^4 \\ 4.22 \cdot 10^{-4} & 1.10 & 9.75 \cdot 10^{-2} & 4.65 & -3.37 \cdot 10^2 \\ 3.45 \cdot 10^{-2} & 0.95 & 4.70 \cdot 10^{-2} & 5.25 & -2.93 \cdot 10^2 \end{bmatrix}, \\ B_c &= \begin{bmatrix} -4.48 \cdot 10^5 & -1.54 \cdot 10^5 & 7.72 \cdot 10^4 & -724.28 & 1.35 \cdot 10^3 \end{bmatrix}^\top, \\ C_c &= \begin{bmatrix} -1.99 \cdot 10^{-2} & -6.15 \cdot 10^{-2} & 6.10 \cdot 10^{-3} & -0.48 & 19.86 \end{bmatrix}, \\ D_c &= 9.51, \end{aligned}$$

with $k_h = 1$, $\omega_h = 0.25$ rad/s, and is guaranteed to achieve an $\mathcal{L}_2$-gain smaller than $\gamma = 4.18$. Note that this can be a conservative estimate as the conditions in (7.24) are only sufficient. The frequency-domain characteristics of the LTI part of the HIGS-based controller are shown in Figure 7.3 in solid black.

Interestingly, the LTI part by itself demonstrates PID-like characteristics having high gain at high-frequencies. However, from a describing function perspective, HIGS acts as low-pass filter and provides desired roll-off at high-frequencies while inducing less phase lag as compared to a linear low-pass filter. The frequency-domain condition in (7.12) with $\lambda = 0.03$ and $k = 2.6$ is shown in Figure 7.4, and is seen to be satisfied with a certain margin, indeed indicating some room for uncertainty in the plant.

7.4 Robust loop-shaping design

In this section, an approach toward the design of HIGS-based controllers is presented that exploits a frequency-domain approximation of HIGS within a robust loop-shaping design framework. Key in the approach is to regard the modelling

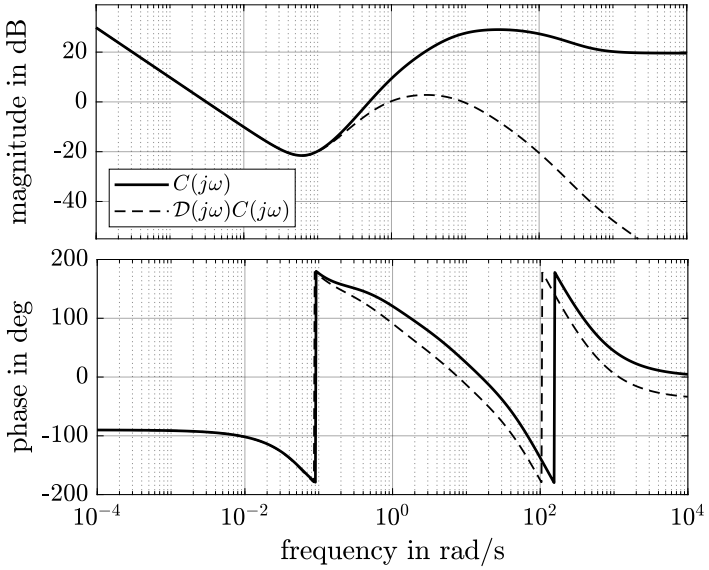

Figure 7.3. Frequency-domain characteristics of $C(j\omega) = C_c(j\omega I - A_c)^{-1}B_c + D_c$ (solid) and describing function of the HIGS-based controller (dashed).

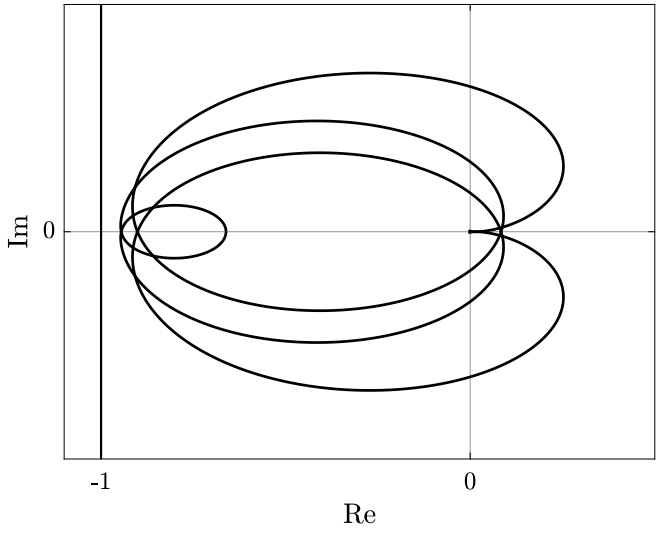

Figure 7.4. Frequency-domain check in (7.12) with $\lambda = 0.03$ and $k = 2.6$.

error induced by the controller approximation as an additional uncertainty in the system, next to possible uncertainties in the plant. Before presenting the approach in detail, it is stressed that the aim is not to provide a rigorous, but rather a practically helpful design procedure.

7.4.1 A conceptual loop-shaping idea

Consider the generalized plant set-up as depicted in Figure 7.1 in which $K = K(C_i, \mathcal{H})$ represents a HIGS-based controller, being the interconnection of HIGS $\mathcal{H}$ with additional LTI filters C_i, $i = 1, \ldots, m$. By separating HIGS from the LTI filters and embedding the latter into the generalized plant G, which results in the LTI interconnection $L = L(C_i, G)$, $i = 1, \ldots, m$ the original plant description can be rearranged into an equivalent Lur'e form as depicted in Figure 7.5a.

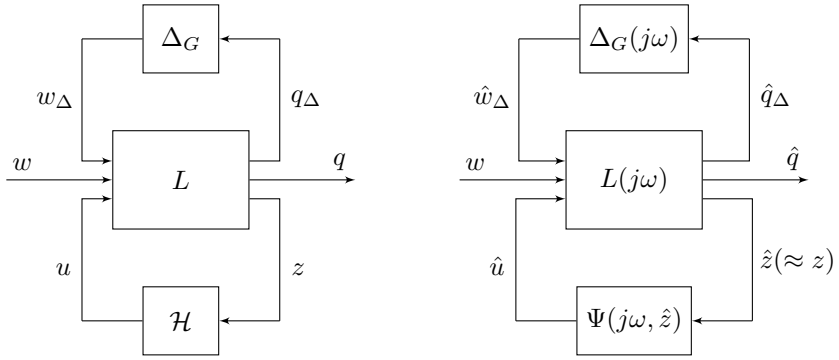

(a) Lur'e representation. **(b)** Quasi-linear approximation.

Figure 7.5. Lur'e representation (left), and quasi-linear approximation (right).

A classical way for design and analysis of a nonlinear system as in Figure 7.5a is to replace the corresponding nonlinearity by a describing function approximation (Atherton, 1982; Gelb and Vander Velde, 1968). In general, a describing function can be defined for each harmonic input component of the nonlinearity to the component of the same frequency at the output of the nonlinearity. For example, for an input to HIGS of the form

$$z(t) = \sum_{i=1}^{n} A_i \sin(\omega_i t + \varphi_i) \tag{7.33}$$

with $n \in \mathbb{N}_{\geq 1}$, frequencies $\omega_i \in \mathbb{R}_{\geq 0}$, amplitudes $A_i \in \mathbb{R}$, and phase $\varphi \in [0, 2\pi)$ the output u of HIGS will contain, among components at many frequencies, components at frequencies ω_i, $i = 1, \ldots, n$. Let the complex Fourier coefficient of these components be denoted by $U_i(j\omega_i) \in \mathbb{C}$. Then, the general describing

function for each component is defined as (Gelb and Vander Velde, 1968)

$$\Psi(j\omega_i, z) = \frac{U_i(j\omega_i)}{A_i e^{j\varphi_i}}. \tag{7.34}$$

For $n = 1$, (7.34) will coincide with the sinusoidal input describing function, which for HIGS has been explicitly derived in Chapter 2, and is given by

$$\mathcal{D}(j\omega) = \frac{\omega_h}{j\omega}\left(\frac{\gamma}{\pi} + j\frac{e^{-2j\gamma} - 4e^{-j\gamma} + 3}{2\pi}\right) + k_h\left(\frac{\pi - \gamma}{\pi} + j\frac{e^{-2j\gamma} - 1}{2\pi}\right), \tag{7.35}$$

with $\gamma(\omega) = 2\arctan(k_h\omega/\omega_h)$. When an explicit expression for (7.34) is available, it can aid the design and analysis of the nonlinear system using (approximate) frequency-domain loop-shaping techniques. This setting is depicted in Figure 7.5b, where $\hat{q}$, $\hat{u}$, $\hat{z}$, $\hat{w}_\Delta$, and $\hat{q}_\Delta$ are approximations of the corresponding nonlinear closed-loop signals in Figure 7.5a in steady-state. For a single sinusoidal input to the nonlinearty, loop-shaping based on sinusoidal input describing functions has been considered in the literature for the design of nonlinear systems, see, *e.g.*, Colgren and Jonckheere, 1997; Gelb and Vander Velde, 1968; Saikumar et al., 2019. For such approach to be meaningful, the input to the nonlinearity must be nearly sinusoidal. In practice, this is often not the case, for example when the external input w in Figure 7.5 contains multiple harmonic components. In case of multi-harmonic input signals to the nonlinearity, however, an exact analytical expression for $\Psi(j\omega, \hat{z})$ in (7.34) may be difficult (or even impossible) to obtain, because in general it not only depends on the input frequencies, but also on the amplitude distribution of harmonic components in the input, as well as the phase. As such, direct use of multiple-harmonic describing functions may be of limited value in practice.

In order to still exploit frequency-domain reasoning for HIGS-based controller design, it is proposed to approximate (7.34) by the sinusoidal input describing function in (7.35), and lump the modelling error induced by this approximation in an additive uncertainty in the controller. This uncertainty is characterized as

$$\Delta_\Psi(j\omega, \hat{z}) = \Psi(j\omega, \hat{z}) - \mathcal{D}(j\omega), \tag{7.36}$$

where $\hat{z}$ provides an approximation of the closed-loop signal z to HIGS in Figure 7.5a. This idea is depicted in Figure 7.6, in which $\mathcal{N}$ represents the nominal model resulting from the interconnection of $L(C_i, G)$, $i = 1, \ldots, m$ and $\mathcal{D}$. Controller design now entails loop-shaping with the describing function to obtain robustness of the *nominal* closed-loop system $\mathcal{N}$ against both uncertainty in the plant as well as uncertainty in the controller. One may argue that the difficulty in finding an appropriate expression for Ψ is now only shifted toward the characterization of Δ_Ψ. But, within a robust control design framework there is no need to find Δ_Ψ exactly, as one can exploit an estimate for the characteristics of Δ_Ψ (*e.g.*, in terms of an upper-bound on its magnitude), which may be easier to obtain. Interesting work related to this approch can be found in Taylor, 1970.

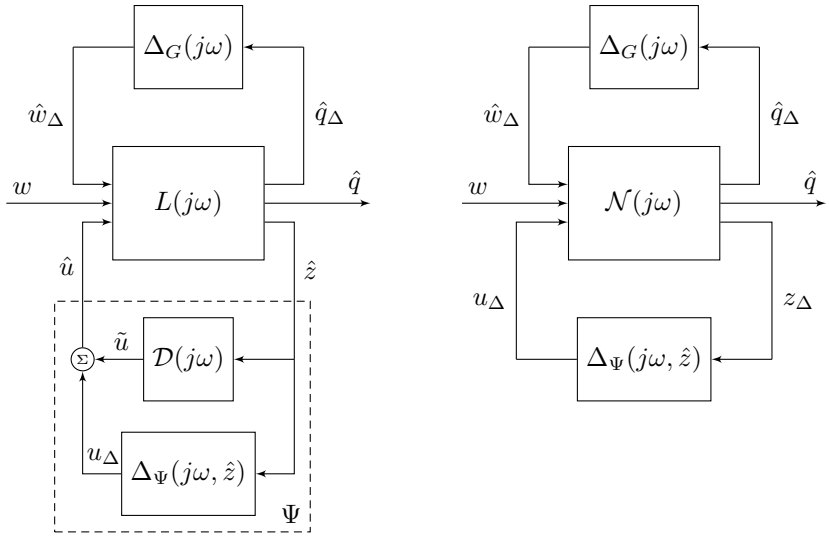

(a) Controller uncertainty. **(b)** Quasi-linear system.

Figure 7.6. Approximation with controller uncertainty (left), and quasi-linear system representation with uncertainties (right).

Approximating the multi-harmonic describing function Ψ in (7.34) by the sinusoidal input describing function $\mathcal{D}$ in (7.35) seems rather naive given the absence of superposition in HIGS. However, there are good reasons for doing this. First of all, $\mathcal{D}$ in (7.35) closely relates to standard frequency-response functions for LTI systems. It can be easily embedded into existing and intuitive frequency-domain loop-shaping tools which are well understood by practising control engineers. Second, as observed in previous chapters, the describing function in (7.35) provides a surprisingly accurate prediction for stability of a motion system in feedback with a HIGS-based controller. This heuristic observation suggests the possibility for separating design aspects for robust stability from design aspects for robust performance. Namely, design for robust stability involves only $\mathcal{N}$ and Δ_G, whereas design for performance involves $\mathcal{N}$, Δ_G, and Δ_Ψ. As such, Δ_Ψ is considered relevant only for performance-based controller design.

7.4.2 Characterizing $\boldsymbol{\Delta_\Psi}$

For developing insights into properties of the modelling error Δ_Ψ it is instructive to consider an input signal to HIGS of the form

$$\hat{z}(t) = A_1 \sin(\omega_1 t) + A_2 \sin(\omega_2 t + \varphi), \tag{7.37}$$

with frequencies $\omega_1, \omega_2 \in \mathbb{R}_{\geq 0}$, amplitudes $A_1, A_2 \in \mathbb{R}$, and phase $\varphi \in [0, 2\pi)$. For such inputs, $\Psi(j\omega, \hat{z})$ in (7.34) corresponds to the two-sinusoidal input describing function (Gelb and Vander Velde, 1968, Chapter 5). Although an explicit expression for this describing function cannot be derived, assuming $\omega_1 < \omega_2$, some practically useful insights can be obtained from considering two cases: i) the low-frequency component at ω_1 rad/s dominates in the input to HIGS, *i.e.*, $A_1/A_2 >> 1$, and ii) the high-frequency component at ω_2 rad/s dominates in the input to HIGS, *i.e.*, $A_1/A_2 << 1$. Input-output characteristics typical for these two situations are depicted in Figure 7.7.

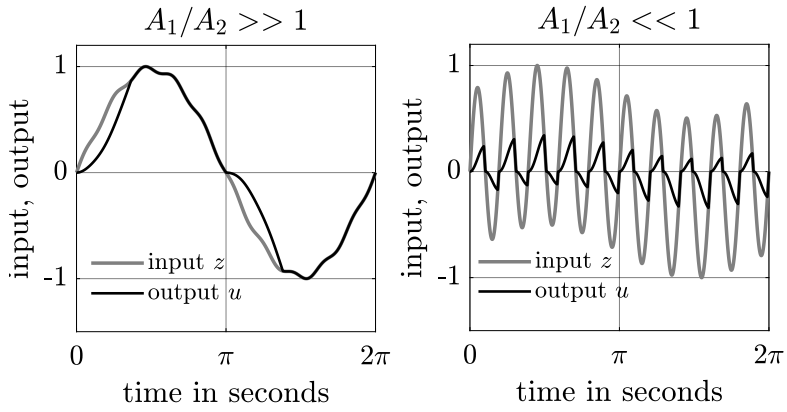

Figure 7.7. Input-output characteristics of HIGS for an input of the form $\hat{z}(t) = A_1 \sin(2\pi t) + A_2 \sin(20\pi t)$ with $A_1/A_2 = \{0.33, 33\}$, $k_h = 1$, and $\omega_h = 3\pi$ rad/s. In case the low-frequency content dominates in the input to HIGS ($A_1/A_2 = 33 >> 1$, in the left part) switching is mainly triggered by the low-frequency component. The presence of a dominating high-frequency term ($A_1/A_2 = 0.33 << 1$, in the right part) triggers high-frequency switching.

From Figure 7.7 it can be seen that the dominating harmonic in the input to HIGS triggers the switching mechanism of HIGS, thereby largely determining its response. This is a direct consequence of the loss of superposition. Regarding the modelling error in (7.36), two worst-case situations can be recognized. First, for $A_1/A_2 >> 1$ and $\omega_1 \to 0$ one finds $u(t) \approx k_h \hat{z}(t)$ in which case HIGS essentially behaves as a linear gain, and $\Psi(j\omega_1, \hat{z}) \approx \Psi(j\omega_2, \hat{z}) \approx k_h$, leading to

$$\Delta_\Psi(j\omega_i, \hat{z}) \approx k_h - \mathcal{D}(j\omega_i), \quad i = \{1, 2\}\,. \tag{7.38}$$

Second, for $A_1/A_2 << 1$ and $\omega_2 \to \infty$ one finds $u(t) \approx 0$ such that $\Psi(j\omega_1, \hat{z}) \approx \Psi(j\omega_2, \hat{z}) \approx 0$, and

$$\Delta_\Psi(j\omega_i, \hat{z}) \approx 0 - \mathcal{D}(j\omega_i), \quad i = \{1, 2\}\,. \tag{7.39}$$

Although discussed for a two sinusoidal input, the above rationale holds true for an input with an arbitrary number of harmonics, where the dominating harmonic in the input to HIGS largely determines its response. Note that (7.38) is typical for HIGS and results from the presence of the static gain-mode, whereas (7.39) results from the dynamic integrator-mode and can also be found to occur in other type of hybrid/switching nonlinearities such as reset integrators (Clegg, 1958; Horowitz and Rosenbaum, 1975; Zaccarian et al., 2005) or split-path integrators (Sharif et al., 2021b; van Loon et al., 2016). From the above rationale, it is possible to estimate an upper-bound on the magnitude of the modelling error Δ_Ψ in (7.36) for any input $\hat{z}$ consisting of multiple harmonics, namely

$$\|\Delta_\Psi(j\omega, \hat{z})\|_\infty \leq \max\{\|k_h - \mathcal{D}(j\omega)\|, \|0 - \mathcal{D}(j\omega)\|\} \tag{7.40}$$

for all $\omega \in \mathbb{R}_{\geq 0}$. However, the upper-bound in (7.40) may be restrictive since it assumes the presence of harmonics at $\omega = 0$ and $\omega = \infty$. In practice, the frequencies of the present harmonics are restricted to a finite range. Also, the upper-bound on Δ_Ψ to some extent should reflect the nature of $\hat{z}$. For example, for an input $\hat{z}(t) = \sin(\omega t)$ one finds $\Delta_\Psi(j\omega, \hat{z}) = 0$. Noting that $\lim_{\omega\to 0} \mathcal{D}(j\omega) = k_h$ and $\lim_{\omega\to\infty} \mathcal{D}(j\omega) = 0$, and from the observation that the dominant harmonic largely dictates properties of the response of HIGS, an alternative, potentially less conservative estimate for Δ_Ψ is conjectured as follows.

Conjecture 7.4.1. *For an input signal of the form $\hat{z}(t) = \sum_{i=1}^{n} A_i \sin(\omega_i t + \varphi_i)$ with amplitude $A_i \in \mathbb{R}$, phase $\varphi_i \in [0, 2\pi)$, and non-harmonically related input frequencies $\omega_i \in \mathbb{R}_{\geq 0}$, the approximation error Δ_Ψ in (7.36) satisfies for all $\omega = \omega_i$, $i = 1, \ldots, n$*

$$\|\Delta_\Psi(j\omega, \hat{z})\|_\infty \leq \max\{\|\mathcal{D}(j\underline{\omega}) - \mathcal{D}(j\omega)\|, \|\mathcal{D}(j\overline{\omega}) - \mathcal{D}(j\omega)\|\}, \tag{7.41}$$

where $\underline{\omega}, \overline{\omega} \in \mathbb{R}_{\geq 0}$ denote the smallest and largest frequencies present in $\hat{z}$.

For a sinusoidal input $\hat{z}(t) = A\sin(\omega t)$ one has $\underline{\omega} = \omega = \overline{\omega}$ such that the upper-bound in (7.41) reduces to zero, whereas for a two-sinusoidal input as in (7.37) one has $\underline{\omega} = \omega_1$ and $\overline{\omega} = \omega_2$, leading to $\|\mathcal{D}(j\omega_2) - \mathcal{D}(j\omega_1)\|$ when considering $\omega = \omega_1$, and $\omega = \omega_2$. Though the estimation in (7.41) is based on heuristics, and a formal justification is lacking, the practical value of this bound is supported by the numerical results presented in Figure 7.8.

Figure 7.8 depicts the modelling error $\Delta_\Psi(j\omega, \hat{z})$ for the component at a frequency $\omega = \omega_1$ of a two-sinusoidal input $\hat{z}(t) = A_1 \sin(\omega_1 t) + A_2 \sin(\omega_2 t + \varphi)$ to HIGS, with a fixed frequency $\omega_2 = \{0.2\pi, 2\pi, 20\pi, 200\pi\}$ rad/s, for different amplitude ratios $A_1/A_2 = \{0.1, 1, 10\}$, and with $\varphi = 0$. The upper-bound given in (7.41) is depicted in black in Figure 7.8. It can be seen that in all cases considered, the inequality in (7.41) is satisfied, and the largest values are indeed obtained for smaller values of the ratio A_1/A_2, *i.e.*, when the harmonic at ω_2 dominates the input. The contribution of a non-zero phase φ is not depicted in

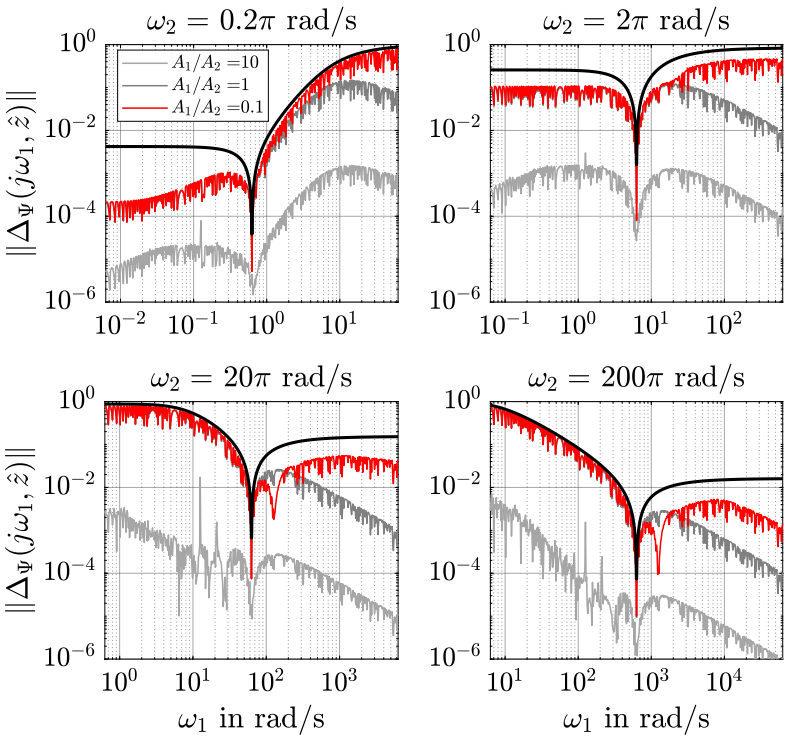

Figure 7.8. Numerically obtained modelling error $\|\Delta_\Psi(j\omega_1, \hat{z})\| = \|\Psi(j\omega_1, \hat{z}) - \mathcal{D}(j\omega_1)\|$ as a function of ω_1 for an input of the form $\hat{z}(t) = A_1 \sin(\omega_1 t) + A_2 \sin(\omega_2 t + \varphi)$, with a fixed frequency $\omega_2 = \{0.2\pi, 2\pi, 20\pi, 200\pi\}$ rad/s, various amplitude ratios $A_1/A_2 = \{0.1, 1, 10\}$, and phase $\varphi = 0$. The estimated upper bound $\|\Delta_\Psi(j\omega_1, \hat{z})\|_\infty \leq \|\mathcal{D}(j\omega_1) - \mathcal{D}(j\omega_2)\|$ is shown in solid black. The parameters of HIGS are set to $k_h = 1$ and $\omega_h = 2\pi$ rad/s.

Figure 7.8 as this parameter is observed to have little effect on the results. These observations are in line with Gelb and Vander Velde, 1968, Chapter 5 where it is argued that for non-harmonically related input sinusoids the phase φ can be seen as a random variable, making the describing function independent of φ.

Remark 7.4.2. *For harmonically related input frequencies, Conjecture 7.4.1 may be false. Namely, given* $\Psi(j\omega_i, \hat{z}) = U_i(j\omega_i)/A_i e^{j\varphi_i}$, *for* $A_i \to 0$, U_i *may be non-zero when related to higher-harmonics generated by input components at frequencies lower than* ω_i. *In that case* $\Psi(j\omega_i, \hat{z}) \to \infty$, *such that* (7.41) *is violated. Note that Figure 7.8 depicts numerical results for both harmonically and non-harmonically related input components. As in all cases considered the upper-bound is satisfied, these results indicate that, at least to some extent,* (7.41)

can be of use for harmonically related input components.

The following example illustrates several phenomena that can occur in a closed-loop system with HIGS, and which are captured effectively through the modelling error Δ_Ψ.

Example 7.4.3. *Consider the system in Figure 7.9, where the LTI plant P and LTI part of the controller C are given by*

$$P(s) = \frac{1}{s^2 + 0.18s + 1}, \quad \text{and} \quad C(s) = \frac{\omega_i}{s} \cdot \frac{\omega_{lp}}{(s + \omega_{lp})}. \tag{7.42}$$

The closed-loop system is subject to an input of the form $r(t) = r_1 \sin(\omega_1 t) + r_2 \sin(\omega_2 t)$, with amplitudes $r_1, r_2 \in \mathbb{R}$, and frequencies $\omega_1, \omega_2 \in [0.01, 2]$ rad/s.

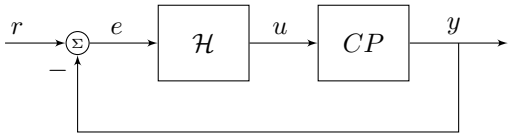

Figure 7.9. Nonlinear system configuration with multi-sine input r.

A nominal controller is designed using the describing function within a standard loop-shaping setting, resulting in $\omega_i = 0.24$ rad/s, $\omega_{lp} = 1.25$ rad/s, $k_h = 1$, and $\omega_h = 0.2$ rad/s. The nominal quasi-linear sensitivity characteristics

$$\mathcal{S}(j\omega) = \frac{1}{1 + \mathcal{D}(j\omega)C(j\omega)P(j\omega)} \tag{7.43}$$

are shown in Figure 7.10 by the bold black curve. From the nature of the external input r, it is reasonable to approximate the input to HIGS by $e(t) \approx \hat{z}(t) = A_1 \sin(\omega_1 t + \varphi_1) + A_2 \sin(\omega_2 t + \varphi_2)$. Based on this approximation, one finds $\Delta_\Psi(j\omega, \hat{z}) = W_\Delta(j\omega, \hat{z})\Delta_{\psi_0}(j\omega, \hat{z})$, with $\|\Delta_{\Psi_0}(j\omega, \hat{z})\| \leq 1$, and

$$W_\Delta(j\omega, \hat{z}) = \max\left\{\|\mathcal{D}(0.01j) - \mathcal{D}(j\omega)\|, \|\mathcal{D}(j\omega) - \mathcal{D}(2j)\|\right\}. \tag{7.44}$$

The worst-case sensitivity magnitude characteristics are given by

$$\|\mathcal{S}_\Delta(j\omega, \hat{z})\| = \frac{1}{\|1 + \mathcal{D}(j\omega)C(j\omega)P(j\omega)\| - \|W_\Delta(j\omega, \hat{z})C(j\omega)P(j\omega)\|}, \tag{7.45}$$

and are depicted in Figure 7.10 by the thin black curve.

Figure 7.10 predicts a significant variation in both low-frequency disturbance attenuation as well as sensitivity to high-frequencies. The steady-state error $e = r - y$ resulting from a two-sinusoidal input r can be written as

$$e(t) = e_1 \sin(\omega_1 t + \varphi_1) + e_2 \sin(\omega_2 t + \varphi_2) + e^*(t),$$

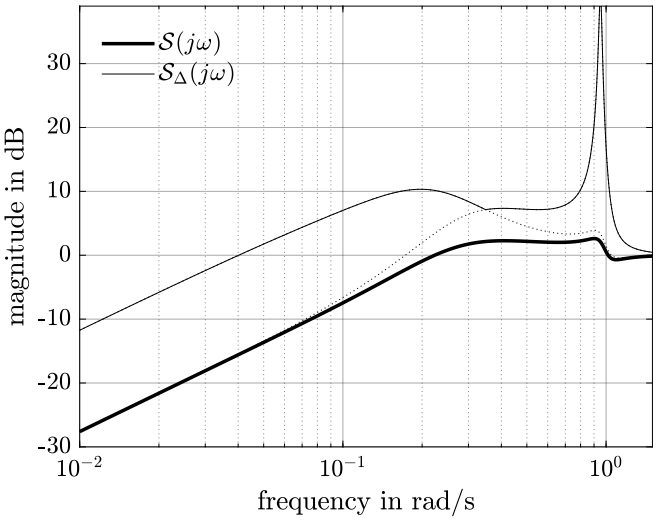

Figure 7.10. Nominal sensitivity characteristics (bold black) and predicted worst-case characteristics (thin black).

where e^* contains the harmonics at frequencies different from those in the input. Note that Figure 7.10 predicts $\|\mathcal{S}(j\omega_i)\| \leq |e_i/r_i| \leq \|\mathcal{S}_\Delta(j\omega_i)\|$, $i = \{1, 2\}$. The numerically obtained amplification ratios $|e_1/r_1|$ and $|e_2/r_2|$ with their predicted minimum and maximum, as well as the relative contribution of higher harmonics to the total energy in the error response for an input with $\omega_1 = 0.03$ rad/s, $\omega_2 = 0.94$ rad/s, and various amplitude ratios r_1/r_2 are reported in Table 7.1. The numerical values in Table 7.1 are in accordance with the predictions based on the sensitivity characteristics in Figure 7.10. Note, however, that the predicted worst-case amplifications appear conservative.

Table 7.1. Predicted and numerically obtained error characteristics of the nominal design with $\omega_1 = 0.03$ rad/s, $\omega_2 = 0.94$ rad/s, and $r_1/r_2 = \{10^4, 10^2, 1\}$.

		$\lvert e_1/r_1\rvert$ in dB	$\lvert e_2/r_2\rvert$ in dB	$\lVert e^*\rVert_2/\lVert e\rVert_2$ in %
prediction	nominal	−18.10	2.41	–
	worst-case	−2.39	33.89	–
simulation	$r_1/r_2 = 10^4$	−18.03	20.61	2.51
	$r_1/r_2 = 10^2$	−17.66	10.21	10.27
	$r_1/r_2 = 1$	−10.13	2.43	5.22

The numerical results in Table 7.1 demonstrate a large dependency on the input amplitude ratio r_1/r_2. For decreasing values of r_1/r_2, the high-frequency content in the input r is becoming more dominant, which results in the input to HIGS to have an increasingly dominating component at 0.94 *rad/s. As a consequence, switching of HIGS is mainly triggered by this high-frequency component, leading to a decrease of low-frequency suppression properties at* 0.03 *rad/s. On the other hand, for increasing values of r_1/r_2, the low-frequency component at* 0.03 *rad/s is dominantly present in the input to HIGS, resulting in significant amplification of high-frequency content at* 0.94 *rad/s. In all cases considered, the relative contribution of higher-harmonics in the error remains contained.*

7.4.3 Design procedure

From the results in Example 7.4.3 it is clear that performance of a closed-loop system with HIGS largely depends on the distribution of input amplitudes. This amplitude dependency is an immediate consequence of the loss of superposition in HIGS, and may compromise low-frequency tracking properties or high-frequency sensitivity. Two complementary design solutions for effectively dealing with these potential issues are discussed next. In particular, a solution for the reduced low-frequency disturbance suppression is explicitly considered in time-domain, whereas a solution for the increased sensitivity at high frequencies is proposed in terms of a design constraint in the frequency-domain.

Pre- and post-filtering strategy

Deteriorated suppression properties of the closed-loop system at low-frequencies stem from the fact that for $A_1/A_2 << 1$ the high-frequency component at ω_2 rad/s in the input to HIGS acts as a carrier wave for the low-frequency component at ω_1 rad/s. As a consequence of high-frequency switching, the output of HIGS is significantly smaller than what is required for achieving the anticipated low-frequency suppression properties, recall Figure 7.7 (right). This situation is comparable to a low-gain feedback control design.

An intuitive solution to the problem of "gain-loss" at low-frequencies may be found in a pre- and post-filtering strategy as depicted in Figure 7.11. Such strategy has already been applied effectively within the context of audio applications and variable-gain control (Heertjes et al., 2009; Oppenheim et al., 1968).

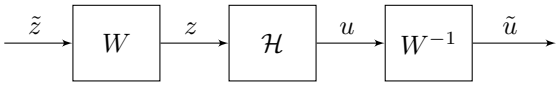

Figure 7.11. Pre- and post-filtering strategy.

The LTI weighting filter $W(s), s \in \mathbb{C}$ in Figure 7.11 should be chosen such

that it lifts the relevant frequency content in the input to HIGS, and switching is triggered in an appropriate manner. With such approach, one effectively enforces the situation $A_1/A_2 >> 1$. Possible design choices for W include (skew) notch filters, low-pass filters, and bandpass filters. In any case, the use of weighting filters that sustain a constant (DC) output, like an integrator, should generally be avoided. The reason for this being that input signals having an offset can cause undesired (asymmetric) switching of HIGS, or in the absence of any zero-crossings may prevent switching at all.

The inverse operation W^{-1} in Figure 7.11 is included to compensate for the additional gain and phase introduced by W, so that the overall describing function characteristics are preserved. Furthermore, in a closed-loop setting it assures that the loop transfer connecting the output u to the input z (see also Figure 7.5a) remains unaffected, so that closed-loop stability properties remain unaffected as well. The justification for applying the inverse operation W^{-1} on the output u, which could lead to the amplification of higher-harmonics, should be in accordance with the usual low-pass filter hypothesis (Gelb and Vander Velde, 1968, Chapter 3). This renders a well-balanced choice for pre- and post-filters dependent on the interconnected system, and exogenous inputs. It is important to realize that the weighting filter W will not play a role in the frequency-domain loop-shaping procedure discussed in the previous section due to its cancellation by the exact inverse W^{-1} in the chain of filters. This makes these filters susceptible to time-domain tuning only. It is argued that this weighting filter strategy is not only effective for HIGS, but is sufficiently generic to allow for extension to various other types of nonlinear integrators, including reset and split-path integrators.

Sensitivity constraints

As mentioned before, applying a pre- and post-filter strategy essentially enforces the situation $A_1/A_2 >> 1$, in which case the only relevant component in (7.41) to consider is

$$\|\Delta_\Psi(j\omega, \hat{z})\|_\infty \leq \|\mathcal{D}(j\underline{\omega}) - \mathcal{D}(j\omega)\|, \tag{7.46}$$

which implies small modelling error at low frequencies, and larger error at high-frequencies. In limiting the sensitivity peaking associated with such modelling error (see Figure 7.10), one may consider $\Delta_\Psi(j\omega, \hat{z}) = W_\Delta(j\omega, \hat{z})\Delta_{\Psi_0}(j\omega, \hat{z})$, with normalized uncertainty $\|\Delta_{\Psi_0}(j\omega, \hat{z})\|_\infty \leq 1$ for all $\omega \in \mathbb{R}_{\geq 0} \cup \{\infty\}$, and

$$W_\Delta(j\omega, \hat{z}) = \mathcal{D}(j\underline{\omega}) - \mathcal{D}(j\omega), \tag{7.47}$$

where the latter filter can be used as a robust performance weighting filter to be included in the plant $\mathcal{N}$ in Figure 7.6b. Design of a HIGS-based controller can

then be formulated as a quasi-linear loop-shaping procedure as:

$$\begin{aligned} \underset{K(C_i,\mathcal{D})}{\text{minimize}} \quad & J(K(C_i,\mathcal{D})) \\ \text{subject to} \quad & \|\mathcal{M}(j\omega,\hat{z})\|_\infty \leq 1, \quad \text{for all } \omega \in \mathbb{R}\cup\{\infty\}, \\ & K(C_i,\mathcal{D}) \text{ stabilizes } G, \\ & K(C_i,\mathcal{D}) \in \mathcal{K}, \end{aligned} \tag{7.48}$$

in which $K(C_i,\mathcal{D})$ denotes the quasi-linear controller description (where HIGS is replaced by $\mathcal{D}$), and $\mathcal{M}$ represents the nominal system $\mathcal{N}$ augmented with the weighting filter W_Δ in (7.47). As in the LTI case, (7.48) can be solved by a standard manual/automated loop-shaping approach.

Remark 7.4.4. *By the approach in* (7.48) *no formal guarantees are given for the resulting nonlinear system in terms of robust closed-loop stability and performance. To deal with this shortcoming, the results from Proposition 7.3.1 can be applied. In fact, by the KYP-lemma the matrix inequality in* (7.14) *admits an equivalent frequency-domain interpretation that can be embedded in the quasi-linear optimization procedure* (7.48)*. Specifically, the quasi-linear constraint "$K(C_i,\mathcal{D})$ stabilizes G" can be replaced with this sufficient frequency-domain condition. The latter can be integrated effectively in the design procedure* (7.48) *without the need for a parametric model. In this way, robust stability with respect to plant uncertainties $\Delta_G \in \bar{\Delta}$ is guaranteed for the true nonlinear system, and the worst-case $\mathcal{L}_2$-gain is given by γ. Additional performance criteria are enforced through describing function characteristics. Hence, such approach combines the rigorous design procedure in Section 7.3 with describing function-based reasoning. The main difference with the approach in Section 7.3, however, is that the structure of the controller should be selected a priori. Also, including the rigorous frequency-domain constraints in* (7.48) *may lead to a conservative design that limites the potential of HIGS. An interesting direction to explore further in this regard is to translate the matrix inequalities in Chapter 5 into frequency-domain conditions, potentially reducing this conservatism.*

Summarizing, design of a HIGS-based (motion) controller may proceed according to the following steps:

- **Step 1:** Robust frequency-domain design based on the quasi-linear loop-shaping procedure outlined in (7.48), in which high-frequency modelling error is accounted for by the weighting filter in (7.47).
- **Step 2:** Augment the controller with pre- and post weighting filters that are designed as to enforce switching of HIGS within the relevant frequency range (for instance, a range below the bandwidth).

Example 7.4.5 (Example 7.4.3 revisited)**.** *Returning to the previous example in Figure 7.9 with P given in* (7.42)*, the controller is redesigned on the basis of*

the above design procedure with $W_\Delta(j\omega, \hat{z}) = \mathcal{D}(0.01j) - \mathcal{D}(j\omega)$*, resulting in*

$$C(s) = \frac{0.22}{s} \cdot \frac{0.53}{(s + 0.53)}, \tag{7.49}$$

with $k_h = 1$*, and* $\omega_h = 0.25$ *rad/s. The resulting sensitivity characteristics are shown in Figure 7.12 and demonstrate a significant reduction of high frequency sensitivity as compared to the initial design in Figure 7.10. Key in this example for achieving reduced sensitivity is sufficient rotation of the resonance of the plant in the open-loop toward the complex right-half plane in the Nyquist plot by reducing the cut-off frequency of the low-pass filter in* (7.49)*.*

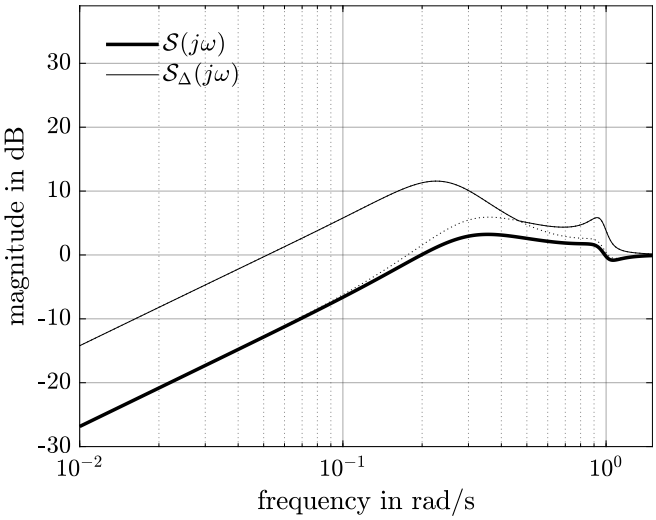

Figure 7.12. Nominal sensitivity characteristics (bold black) for the system with redesigned controller, and predicted worst-case characteristics (thin black).

The numerical results presented in Table 7.2 for $\omega_1 = 0.03$ *rad/s,* $\omega_2 = 0.94$ *rad/s, and various* r_1/r_2 *support the effectiveness of the robust loop-shaping design approach, as for all* r_1/r_2 *the amplification factor* $|e_2/r_2|$ *at* 0.94 *rad/s remains significantly more contained as compared to the initial design in Table 7.1. However, low-frequency suppression properties are still compromised for an increasingly dominant high-frequency component in the input, i.e., for decreasing values of* r_1/r_2*. To account for this, a pre-filter is chosen as*

$$W(s) = \frac{s^2 + 2\beta_z\omega_z s + \omega_z}{s^2 + 2\beta_p\omega_p s + \omega_p^2}, \tag{7.50}$$

with $\omega_z = \omega_p = \omega_2 = 0.94$ *rad/s,* $\beta_z = 0.005$*, and* $\beta_p = 0.1$*. This filter suppresses content at* 0.94 *rad/s in the input to HIGS, thereby enforcing the*

switching mechanism to be primarily triggered by the component at 0.03 *rad/s. Effectiveness of the filtering strategy for improving low-frequency rejection properties is demonstrated by the numerical results in Table 7.2. Compared to the previous designs, dependency on the amplitude distribution of the input signal is reduced, and low-frequency disturbance rejection is achieved without significant high-frequency amplification. Note that, compared to the results in Table 7.1, the robust redesign provides some additional robustness against the effects of higher-harmonics. An industrial example illustrating the effectiveness of the design approach for a broader input spectrum of input frequencies is discussed in detail in Chapter 8.*

Table 7.2. Predicted and numerically obtained error characteristics of the robust redesign with $\omega_1 = 0.03$ rad/s, $\omega_2 = 0.94$ rad/s, and $r_1/r_2 = \{10^4, 10^2, 1\}$.

		$\lvert e_1/r_1\rvert$ in dB	$\lvert e_2/r_2\rvert$ in dB	$\lVert e^*\rVert_2/\lVert e\rVert_2$ in %
prediction	nominal	-17.20	1.10	–
	worst-case	-3.25	6.01	–
without pre- and post-filtering strategy				
simulation	$r_1/r_2 = 10^4$	-17.19	4.72	2.21
	$r_1/r_2 = 10^2$	-17.18	4.47	2.49
	$r_1/r_2 = 1$	-10.85	1.14	2.01
with pre- and post-filtering strategy				
simulation	$r_1/r_2 = 10^4$	-17.19	4.40	2.63
	$r_1/r_2 = 10^2$	-17.19	4.22	3.13
	$r_1/r_2 = 1$	-16.10	3.39	2.39

7.5 Summary

In this chapter, two methods for HIGS-based controller design are presented. The first method provides a rigorous way for controller synthesis. In particular, the frequency-domain stability conditions as derived in Chapter 4 are reformulated into matrix inequalities which allow for a direct translation toward appropriate synthesis conditions. The latter conditions show a strong resemblance with synthesis conditions typically used in an LTI setting. The presented approach returns a robustly stabilizing HIGS-based controller with guaranteed $\mathcal{L}_2$-performance properties. The approach, however, requires the use of a parametric model and provides limited insight in parameter tuning and robust redesign, which in an industrial setting is sometimes considered to be a drawback.

As an alternative, a practical tuning approach is presented that hinges on the use of the describing function within a robust loop-shaping framework. Key in the approach is to approximate the closed-loop system by a quasi-linear system, and capture the modelling error induced by the describing function approximation as an uncertainty in the controller, for which a heuristic bound on the magnitude characteristics is derived. Through this bound, relevant performance issues are revealed for which effective solutions are proposed in the form of both time- and frequency-domain design guidelines. The approach strongly connects to the industrial practice where frequency-domain loop-shaping design with non-parametric models typically sets the standard.

Given the practical applicability of the loop-shaping design approach guided by describing functions, in the next chapter this approach is used for the design of a HIGS-based PID controller for a scanning stage system of an industrial wafer scanner. Performance of the resulting nonlinear feedback design is compared to that of a baseline linear strategy.

Chapter 8

Case-Study on an Industrial Wafer Scanner

8.1 Introduction

Wafer scanners employ a crucial step during the manufacturing process of integrated circuits (IC's), namely, transferring the circuit topology obtained from a reticle onto the photosensitive layers of a silicon wafer. Both reticle and wafer are part of separate high-precision positioning systems: the reticle-stage and the wafer-stage. The dynamical behaviour of these stages can be accurately modelled according to the linear paradigm, allowing for the application of well-developed linear feedforward and feedback control methods (Butler, 2011; Martinez and Edgar, 2006). In fact, most of the feedback control loops in wafer scanners originate from a decoupling design in combination with proportional-integral-derivative (PID) control (Heertjes et al., 2020; Oomen et al., 2014). Despite the clear advantages of PID control in terms of simplicity and predictability, servo performance is usually compromised as a result of inherent design trade-offs. The fact that modern linear techniques such as H_∞ control cannot overcome these trade-offs poses a serious challenge for meeting the ever growing demands on scanning accuracy and throughput in wafer scanners.

As a potential means to alleviate the problem, this chapter considers the use of multiple HIGS-based filters within an otherwise linear PID configuration that is commonly used for feedback control of the reticle- and wafer-stages. From a describing function perspective, the HIGS-based filters demonstrate similar magnitude characteristics as their linear counterparts, but with preferable phase properties that can be tuned independently of the magnitude. This extra design freedom facilitates increased controller bandwidths, giving rise to improved

disturbance rejection and transient properties of the closed-loop system. Performance is evaluated through measurement results obtained from a wafer stage system of an industrial wafer scanner. In order to show the relative improvements in both time- and frequency-domain, a comparison is made with a baseline linear PID design. Besides demonstrating the potential benefits of HIGS-based control in practice, the experiments are valuable for identifying practically relevant factors that may affect controller performance within an industrial setting, and, therefore, require specific attention in the early phases of the design process.

This chapter is organized as follows. To develop some intuition for the wafer scanning application at hand, Section 8.2 introduces relevant scanning principles and performance measures. The wafer stage dynamics and current feedforward and feedback control methods are discussed in Section 8.3, whereas the HIGS-based feedback control strategy is presented in Section 8.4. Practically relevant design aspects are considered in Section 8.5, and measurement results are presented in Section 8.6. Section 8.7 summarizes the main findings of this chapter.

8.2 Wafer scanning principles

8.2.1 Scanning procedure and setpoint definition

The case-study considered in this chapter is an industrial wafer scanner, of which an artist impression and schematics are provided in Figure 8.1.

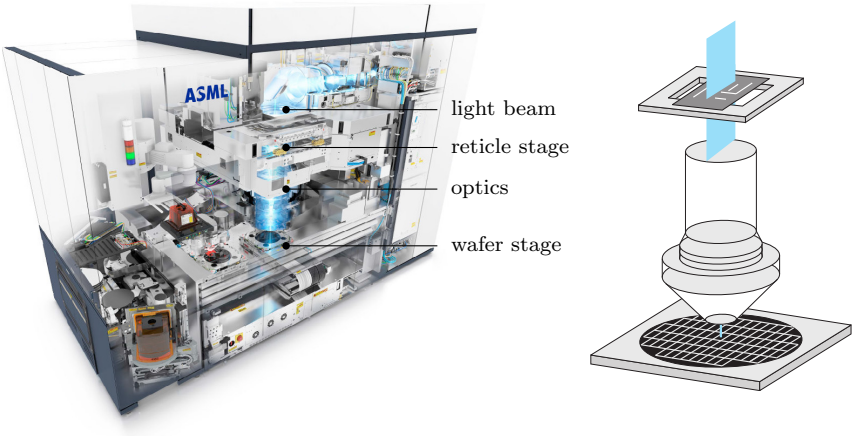

Figure 8.1. Left: artist impression of an industrial wafer scanner. Right: simplified visualization of an exposure process showing from top to bottom a reticle atop a reticle stage, an optics column, and a wafer atop a wafer stage (images acquired from https://www.asml.com and Oomen et al., 2012).

Many wafer scanners exploit the lithographic principle in which deep or extreme ultraviolet (DUV/EUV) light emitted by a source falls onto a reticle (or mask), being a quartz plate which contains a blueprint of the integrated circuit to be processed. After passing through the reticle, the light travels through an optical column which scales down the image of the circuit topology by a factor of four, and projects it onto the photosensitive layers of a silicon wafer. A schematic illustration of the exposure process is shown in Figure 8.1. Both reticle and wafer are part of separate motion systems: the reticle stage and the wafer stage. Each of these stages employs a dual-stroke strategy. A long-stroke stage is used for coarse positioning with accuracy at the micrometer level, whereas a short-stroke stage is used for fine positioning with accuracy at the nanometer level. For realizing accurate and fast projection of the circuit topology onto the wafer, both reticle- and wafer stage perform a synchronized meandering motion in which exposure by the light beam takes place during repeated intervals of zero and constant velocity in x- and y-direction, respectively. A typical meandering profile for the wafer stage is shown in Figure 8.2. The scanning phases, indicated in the figure by the solid arrows, are alternated with preparation phases: intervals with non-zero acceleration in both directions, allowing the system to reach the next exposure area, the latter also referred to as die. In order for setpoint-induced transients to sufficiently die out before starting a new scan, an additional (zero-acceleration) settling phase can be introduced. In the z-direction, the wafer-stage generally tracks a non-zero reference, reflecting the measured wafer topology.

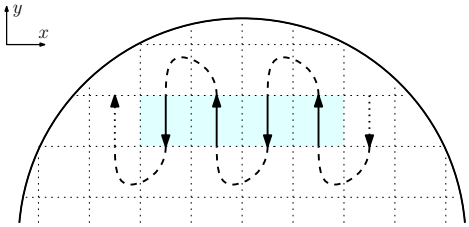

Figure 8.2. Top view of a meandering profile for the wafer stage system. The scanning phases, indicated by the solid arrows, are alternated with preparation phases, indicated by the dashed lines (Butler, 2011).

For the wafer stage application considered in this chapter, a third-order motion profile is considered in x- and y-direction. Third order refers to the fact that the position, velocity, and acceleration profiles are smooth, and only the jerk profile (third derivative) is non-smooth and contains discontinuities. This results in generation of less high-frequency input content as compared to lower-order setpoints. Since the setpoint/reference profile can be seen as a key deterministic input affecting the closed-loop system, this results in a tracking error that is generally less affected by high-frequency signals, and thus benefits scanning

performance. Some representative parameters used for generating the third-order setpoint profile in scanning y-direction are listed in Table 8.1, and the corresponding time-domain profiles are depicted in Figure 8.3. For this setpoint profile the settling time is set to zero seconds such that exposure starts directly after the acceleration phase. It should be mentioned that for the application considered, this setpoint profile is considered rather aggressive (high jerk), but allows for a significant increase in wafer throughput.

Table 8.1. Third-order setpoint parameters.

Limit	Value	
Maximum scanning velocity	0.8	m/s
Maximum acceleration	30	$\mathrm{m/s^2}$
Maximum jerk	6600	$\mathrm{m/s^3}$
Acceleration/velocity ratio	37.5	Hz
Jerk/acceleration ratio	220	Hz
Settling time	0	s

The acceleration/velocity and jerk/acceleration ratios listed in Table 8.1 are of special interest for the true system, as these determine the location of zeros in the frequency spectrum of the setpoint profile. This is immediate by studying the Fourier transform of the reference position $r(t)$, which, given the typical block-shaped profile of the jerk signal as depicted in the lower plot in Figure 8.3, can be derived analytically as (see Butler, 2011 for further details)

$$\mathcal{F}\{r(t)\} = 4 \cdot \frac{j_{\max}}{\omega^4} \cdot e^{-j\frac{\omega\tau_v}{2}} \cdot \sin\left(\frac{\omega\tau_a}{2}\right) \sin\left(\frac{\omega\tau_j}{2}\right), \tag{8.1}$$

with time-constants $\tau_a = v_{\max}/j_{\max}$, $\tau_j = a_{\max}/j_{\max}$ and $\tau_v = \tau_a + \tau_j$. By appropriate tuning of the acceleration/velocity and acceleration/jerk ratios, the zeros in the input spectrum can be set to match the frequencies where in the physical plant a saddle and/or torsion mode are present, as to minimize excitation of these modes. Moreover, in the HIGS-based feedback control context as considered in this chapter, different setpoint characteristics may affect switching of the HIGS elements, and thus effectiveness of the overall controller. The frequency spectrum of the considered setpoint profile in scanning y-direction is depicted in Figure 8.4. Note the 80 dB amplitude decrease per decade at higher frequencies, which is a typical feature for the third-order setpoint profile that readily follows from (8.1).

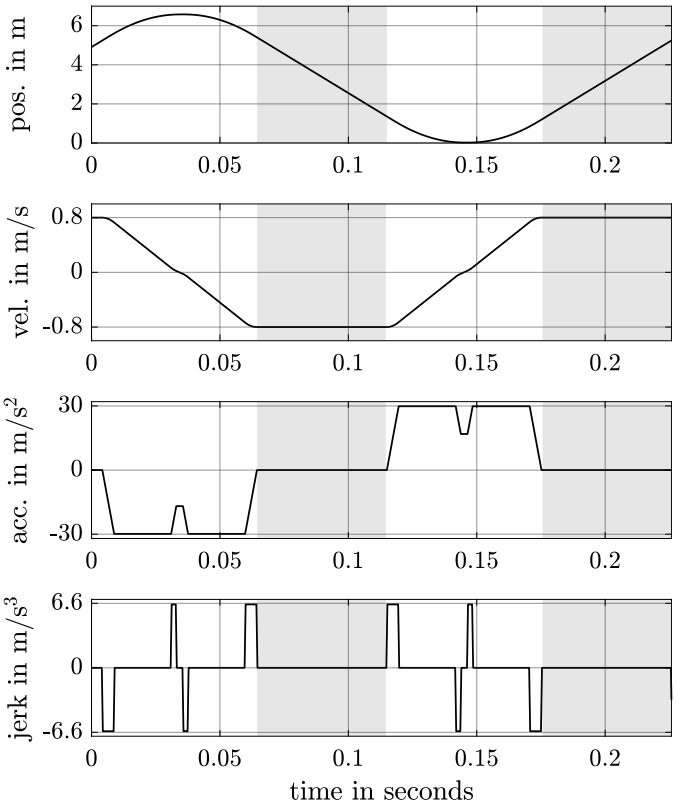

Figure 8.3. Time-domain characteristics of the third-order setpoint in scanning y-direction. From top to bottom: position, velocity, acceleration, and jerk. The scanning intervals are indicated in grey.

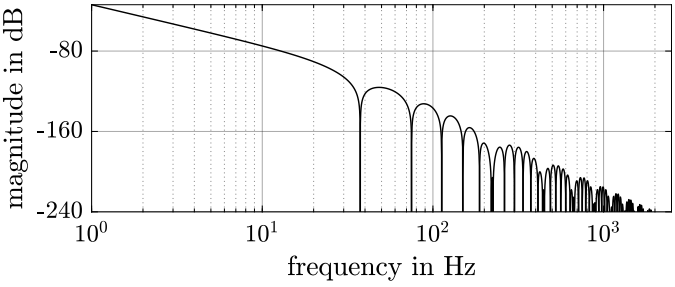

Figure 8.4. Amplitude spectrum of the third-order position setpoint profile in scanning y-direction, as provided in (8.1).

8.2.2 Scanning performance measures

Performance of wafer scanners is driven by three measures: overlay, imaging, and throughput. Overlay refers to the ability to expose two layers on top of each other, imaging generally refers to image quality in terms of uniformity, and throughput refers to the number of processed wafers per hour. Throughput is mainly related to the settling phase prior to scanning, whereas overlay and imaging relate to the scanning interval in which exposure takes place, and translate into measurable (servo specific) functions as follows.

The actual position of the stage during exposure determines the location to which the circuit topology is transferred onto the wafer, and thus is critical for overlay, *i.e.*, layer-to-layer accuracy. This low-frequency effect directly translates to the moving average (MA) of the positioning error $e(t) = r(t) - y(t)$, being the difference between the reference r and the actual position y, which is defined as

$$\mathrm{MA}(t) := \frac{1}{T_e} \int_{t-T_e/2}^{t+T_e/2} e(\tau) d\tau. \tag{8.2}$$

Here, T_e is the exposure time, *i.e.*, the time it takes for a single point on the wafer to receive a full dose of the DUV/EUV light emitted by the source. The quality of a single layer, on the other hand, is affected by stage-positioning accuracy, since positioning errors reduce contrast (Butler, 2011). Even when the average position is correct, high-frequency vibrations of the stage result in the projection of a blurry image onto the wafer, and thus deteriorate the imaging quality. This high-frequency effect is quantified through the moving standard deviation (MSD) of the positioning error $e(t)$, which is computed by

$$\mathrm{MSD}(t) := \sqrt{\frac{1}{T_e} \int_{t-T_e/2}^{t+T_e/2} \left(e(\tau) - \mathrm{MA}(t)\right)^2 d\tau}. \tag{8.3}$$

Note that the MA and MSD values in (8.2) and (8.3) are computed over an exposure window of length T_e seconds. Hence, the computation of MA and MSD values requires the positioning error in the exposure window to be known upfront, which makes (8.2) and (8.3) non-causal operations that can only be performed off-line (after exposure has taken place).

8.3 Wafer-stage dynamics and control

The process of wafer scanning requires accurate and fast positioning of the wafer-stage system in six degrees-of-freedom (DOF): three planar DOF's (x, y, z), and three rotational DOF's (r_x, r_y, r_z). Through an appropriate (position-dependent) decoupling strategy, the to-be-controlled system becomes diagonally dominant such that multivariable control design aspects are reduced to a multi-loop single-input single-output (SISO) design. This section reviews SISO strategies that are currently used for wafer-stage control.

8.3.1 Control problem formulation

For stage control, one basically distinguishes between two problems: i) the servo (tracking) problem in which the output y of the stage should track the set-point profile r, and ii) the disturbance rejection (regulator) problem in which the tracking error $e = r - y$ should be brought close to zero in the presence of external disturbances d, the latter which are assumed to be uncorrelated with r (Trentelman et al., 2001). The servo problem can largely be solved by an LTI feedforward controller $F(s)$, whereas the remaining disturbance rejection problem is dealt with by an LTI feedback controller $C(s)$ as illustrated in Figure 8.5.

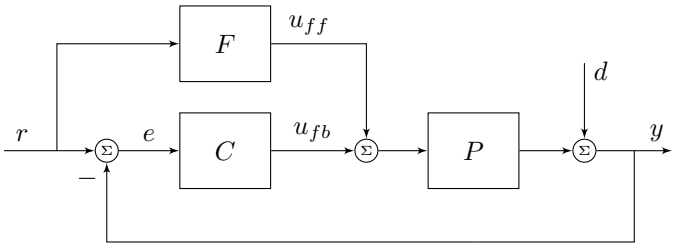

Figure 8.5. Simplified wafer stage control architecture.

In this figure, P represents the wafer stage dynamics in one DOF. Typical frequency-response function (FRF) characteristics of the stage in scanning y-direction, measured at different positions on the wafer are shown in Figure 8.6.

Figure 8.6 indicates that up to a frequency of 500 Hz, the stage mainly behaves as a floating mass system, *i.e.*, a double integrator characterized by a 40 dB/decade amplitude decay combined with 180 degrees phase lag. Beyond 500 Hz, the rigid body assumption is no longer valid as several resonances appear that associate with non-rigid body dynamics of the stage. Notice the additional phase lag due to the sampling rate of 5 kHz which is observed at higher frequencies. To provide some further intuition for the system dynamics at hand, a parametric model of the plant with delay is given by

$$P(s) = \frac{bs + k}{m_1 m_2 s^4 + (m_1 + m_2) b s^3 + (m_1 + m_2) k s^2} \cdot e^{-T_s s}. \tag{8.4}$$

Here, $m_1 = 5$ kg represents the mass of the motor yoke driving the stage, $m_2 = 17.7$ kg represents mainly the mass of the mirror block carrying the wafer, and $m = m_1 + m_2$ is the total mass. The stiffness coefficient $k = 1.186 \cdot 10^8$ N/m and damping coefficient $b = 193.6$ Nm/s represent properties of the coupling interface between motor and stage, whereas $T_s = 2 \cdot 10^{-4}$ seconds is the sampling time. The model characteristics are depicted in Figure 8.6 in black.

Given the LTI context of Figure 8.5, the servo error signal $e := r - (y + d)$ satisfies (in the Laplace domain)

$$e(s) = S(s)(1 - P(s)F(s))r(s) - S(s)d(s), \tag{8.5}$$

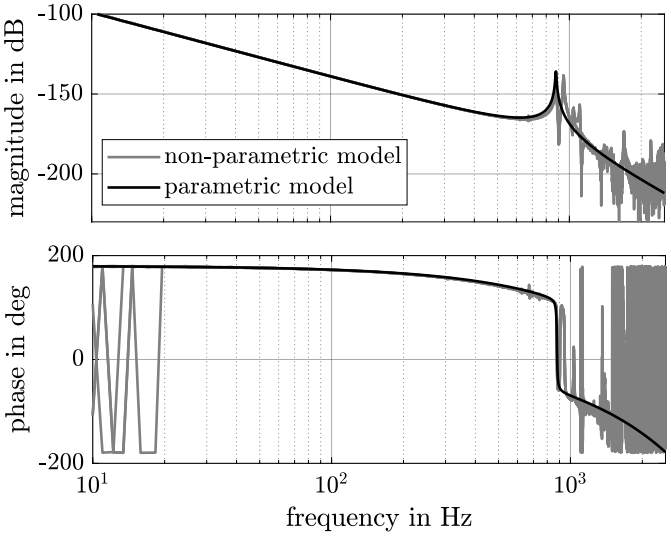

Figure 8.6. Measured FRF characteristics of the wafer-stage in scanning y-direction (grey) and parametric model (black).

where $S(s) = (1 + P(s)C(s))^{-1}$ is the closed-loop sensitivity function. In view of minimizing the error contribution in (8.5), three main directions are taken: i) input shaping in which the setpoint r is designed to minimize the excitation of higher-order dynamics (recall Section 8.2.1, and see, *e.g.*, Boettcher et al., 2012; Cutforth and Pao, 2004), ii) feedforward control design as to achieve $F = P^{-1}$, and iii) feedback control design to minimize S. Wafer stage feedforward and feedback control design is discussed in more detail next.

8.3.2 Feedforward control

As mentioned before, for solving the servo problem, it readily follows from (8.5) that F ideally should match the inverse of the plant, *i.e.*, $F = P^{-1}$. However, in practice there are numerous reasons for why an exact inverse cannot be fully realized, thereby implying that P^{-1} may only be approximated. In this regard, the dominant double integrator characteristics appearing in Figure 8.6 and (8.4) motivate the use of acceleration feedforward control (Boerlage et al., 2004; Butler, 2011), resulting in

$$F(s) = ms^2. \tag{8.6}$$

Atop the feedforward structure in (8.6) typical advancements found in wafer scanners include jerk derivative (snap) feedforward control (Boerlage et al.,

2004), finite impulse response (FIR) feedforward control (Heertjes et al., 2010; Potsaid and Wen, 2004), adaptive feedforward control (Butler, 2013), and compliance compensation techniques (Kontaras et al., 2016).

It is interesting to observe that during the acceleration phase, at least 99.9% of the performance is achieved through acceleration feedforward control. To give an example, for the performance in scanning y-direction, a mass of around $m = 20$ kg is accelerated with a maximum acceleration of 30 m/s^2, which accounts for an actuator force of 600 N. The error is typically in the order of $e \approx 10$ nm, and the feedback controller gains are in the order of $2 \cdot 10^7$ N/m, leading to a feedback actuator force of 0.2 N. In comparison to the feedforward force of 600 N, this provides only 0.033% of the total control output. Note that while feedforward control is crucial during the acceleration phase for tracking the setpoint profiles, during the scanning phase feedback control becomes essential for suppressing unknown disturbances that cannot be compensated for by feedforward control, as well as uncertainty in the plant that through a mismatch in feedforward signals results in an error residue that is left to the feedback controller. In the remainder of this chapter, availability of a well-designed (advanced) feedforward controller is assumed.

8.3.3 Feedback control

Concerning (8.5), the LTI feedback controller C should be designed so that the magnitude of the sensitivity function S is as small as possible, at least in a frequency range of interest. For achieving this, the structure that is commonly used in wafer-stage control is a PID-based feedback controller of the form:

$$C(s) = C_{pid}(s)C_{lp}(s)\prod_{i=1}^{n} C_{n,i}(s), \tag{8.7}$$

in which

$$C_{pid}(s) = k_p\left(1 + \frac{\omega_i}{s} + \frac{s}{\omega_d}\right), \tag{8.8a}$$

is a PID filter with proportional gain $k_p \in \mathbb{R}_{>0}$, integrator frequency $\omega_i \in \mathbb{R}_{>0}$, and differentiator frquency $\omega_d \in \mathbb{R}_{>0}$,

$$C_{lp}(s) = \frac{\omega_{lp}^2}{s^2 + 2\beta_{lp}\omega_{lp} + \omega_{lp}^2}, \tag{8.8b}$$

is a second-order low-pass filter with cut-off frequency $\omega_{lp} \in \mathbb{R}_{>0}$ and dimensionless damping coefficient $\beta_{lp} \in \mathbb{R}$, and where

$$C_{n,i}(s) = \frac{s^2 + 2\beta_{z,i}\omega_{z,i} + \omega_{z,i}^2}{s^2 + 2\beta_{p,i}\omega_{p,i} + \omega_{p,i}^2}, \tag{8.8c}$$

is a notch filter with zero and pole frequencies $\omega_{z,i}, \omega_{p,i} \in \mathbb{R}_{>0}$, and dimensionless damping coefficients $\beta_{z,i}, \beta_{p,i} \in \mathbb{R}$. The PID filter C_{pid} aims at low frequency/constant disturbance suppression coming from the integrator, and robust stability provided by the differentiator. The second-order low-pass filter C_{lp} is used to avoid high-frequency noise amplification. Several notch filters $C_{n,i}$ are added to account for performance limiting resonances in the plant.

In tuning the controller in (8.7), it is strived to maximize the controller bandwidth, defined as the frequency where the open-loop system $L(s) = P(s)C(s)$ crosses zero dB for the first time, while simultaneously satisfying a peaking constraint on the closed-loop sensitivity function $S(s)$. In this way, the region where low-frequency disturbance suppression is achieved is maximized, while the high-frequency noise response is kept small. Recall from Section 8.2 that low-frequency error content directly affects MA values and thus overlay, hence the need for good low-frequency disturbance suppression. High-frequency content affects MSD values and the related imaging quality, thereby requiring limited noise amplification. Although crucial in the controller design, the use of an integrator as well as a low-pass filter in (8.7) leads to the introduction of phase lag in the feedback loop as an inevitable consequence of Bode's gain-phase relationship (Seron et al., 1997; Skogestad and Postlethwaite, 2010). This leads to inherent trade-offs between, *e.g.*, i) enhanced low-frequency disturbance rejection by increasing the bandwidth, ii) robust stability properties, and ii) transient response such as overshoot and settling time.

8.4 HIGS in a PID architecture

To allow more design freedom, and potentially balance between the aforementioned trade-offs in a more desirable manner, this section discusses the use of integrators and low-pass filters along with their HIGS-based counterparts into the PID structure of (8.7).

8.4.1 HIGS-based integrator and low-pass filter design

Consider the generic interconnection as depicted in Figure 8.7 where HIGS is augmented with LTI filters $W(s), V(s), s \in \mathbb{C}$.

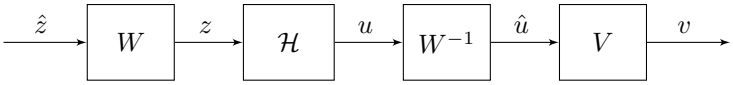

Figure 8.7. Generic HIGS-based filter design with weighting filter $W(s)$ and loop-shaping filter $V(s)$.

In Figure 8.7, one may recognize the pre- and post-filtering strategy as discussed in Chapter 7 for modulating the switching characteristics of HIGS. The

LTI filter V is added for the specific purpose of shaping the overall describing function of the interconnection to achieve desirable magnitude and phase characteristics. In this context, this filter can be regarded as a "loop-shaping" filter. Through linear reasoning, the describing function characteristics of the nonlinear filter in Figure 8.7 read

$$\mathcal{D}^*(j\omega) = \mathcal{D}(j\omega)V(j\omega), \tag{8.9}$$

where $\mathcal{D}(j\omega)$ is the describing function of HIGS, derived in Chapter 2 as

$$\mathcal{D}(j\omega) = \frac{\omega_h}{j\omega}\left(\frac{\gamma}{\pi} + j\frac{e^{-2j\gamma} - 4e^{-j\gamma} + 3}{2\pi}\right) + k_h\left(\frac{\pi - \gamma}{\pi} + j\frac{e^{-2j\gamma} - 1}{2\pi}\right), \tag{8.10}$$

with $\gamma(\omega) = 2\arctan(k_h\omega/\omega_h)$, and V is chosen as

$$V(s) = H^{-1}(s)C^*(s), \quad \text{with} \quad H(s) = k_h\left(\frac{\omega_c}{s + \omega_c}\right), \tag{8.11}$$

where $\omega_c = \frac{\omega_h}{k_h}|1 + \frac{4j}{\pi}|$ rad/s, and in which $C^*(s) \in \mathbb{C}$ is an arbitrary LTI filter. Recall that the describing function $\mathcal{D}(j\omega)$ in (8.10) resembles first-order low-pass characteristics with low-frequency (DC) gain k_h, cross-over frequency ω_c rad/s, and a phase lag that does not exceed 38.15 degrees. The filter $H(s)$ in (8.11) then provides an approximation of $\mathcal{D}(j\omega)$ in terms of its magnitude. As such, the non-realizable filter $H^{-1}(s)$ "inverts" the magnitude characteristics of $\mathcal{D}(j\omega)$, and provides additional phase lead up to 90 degrees. Hence, for all $\omega \in \mathbb{R}$ one achieves

$$\|\mathcal{D}^*(j\omega)\| \approx \|C^*(j\omega)\|, \quad \text{and} \quad \arg(\mathcal{D}^*(j\omega)) = \arg(C^*(j\omega)) + \varphi(\omega),$$

with $\varphi(\omega) = \arg(H^{-1}(j\omega)) + \arg(\mathcal{D}(j\omega)) \in (0, 58.85)$ degrees. In other words, the describing function $\mathcal{D}^*(j\omega)$ in (8.9) possesses similar magnitude characteristics as the LTI filter $C^*(s)$, but with a phase lag reduction up to 58.85 degrees. Comparable strategies that combine linear and nonlinear filters into linear-like elements with improved phase properties as observed from their describing function can be found in, *e.g.*, Cai et al., 2020; Guo et al., 2009; Karybakas, 1977; Li et al., 2011; Saikumar et al., 2019. By selecting $C^*(s) = C_i(s) = \omega_i/s$ or $C^*(s) = C_{lp}(s)$ with C_{lp} in (8.8b) one obtains, respectively, a HIGS-based integrator or HIGS-based low-pass filter for which the describing function characteristics are depicted in Figure 8.8 in black. Note that the filter $C^*(s)H^{-1}(s)$ is realizable. The characteristics of the corresponding linear filters are shown in grey. It can be seen that the nonlinear filters demonstrate a significant phase advantage over their linear counterparts.

Remark 8.4.1. *Regarding the above design philosophy, it is important to point out that the freedom in designing the magnitude characteristics of $\mathcal{D}^*(j\omega)$ is completely determined by the parameters associated with $C^*(s)$, whereas the freedom*

in designing the phase is determined by both the parameters of $C^*(s)$ and those related to $\varphi(\omega)$. As the only parameters that appear in $\varphi(\omega)$ are ω_h and k_h associated with HIGS, magnitude and phase are no longer uniquely related, but, to some extent, can be designed separately.

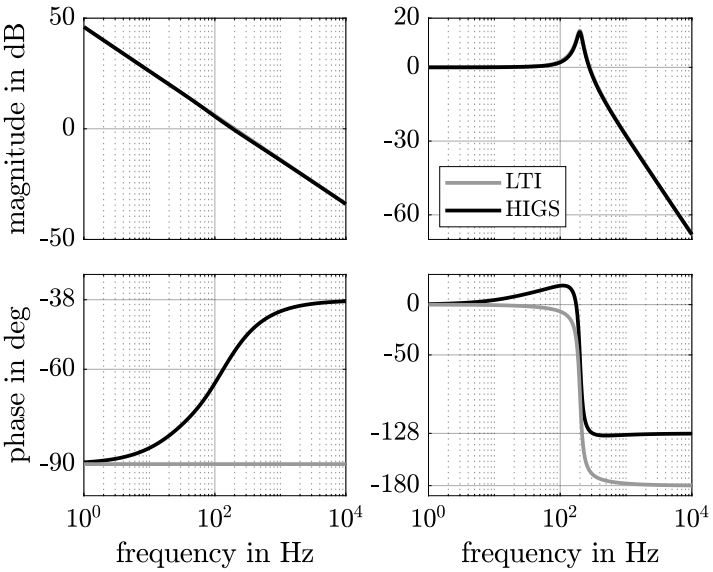

Figure 8.8. Describing function of an LTI integrator and its HIGS-equivalent design (left), and an LTI low-pass filter and its HIGS-equivalent design (right).

Remark 8.4.2. *It should be mentioned that in practice both time- and frequency-domain properties of the linear equivalent filter C^* can be recovered by selecting $\omega_h \to \infty$. Indeed, in frequency-domain this choice yields $H^{-1}(j\omega)\mathcal{D}(j\omega) \to 1$ such that $\mathcal{D}^*(j\omega) \to C^*(j\omega)$ for all $\omega \in \mathbb{R}$. In time-domain, it can be argued that for $\omega_h \to \infty$ the integrator-mode in HIGS is simply too fast, such that HIGS effectively reduces to a linear gain k_h. Together with the previous observations this implies that the input-output signals of the filter in Figure 8.7 satisfy $v \to C^*\hat{z}$, i.e., the linear filter operation is approximated.*

8.4.2 HIGS-based PID scheme

A configuration that adopts both a HIGS-based integrator, denoted by $C_i\{\mathcal{H}\}$, and a HIGS-based low-pass filter, denoted by $C_{lp}\{\mathcal{H}\}$ within the PID structure of (8.7) is depicted in Figure 8.9.

Different from the LTI setting, the sequence in which linear and nonlinear filters appear with respect to each other affects the input-output characteristics

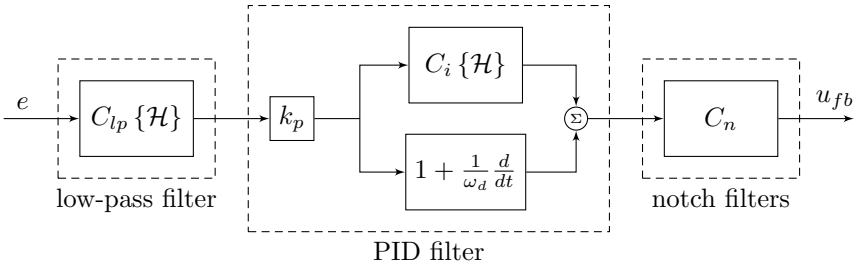

Figure 8.9. Structure of a HIGS-based PID controller $C\{\mathcal{H}\}$ with HIGS-based integrator $C_i\{\mathcal{H}\}$ and HIGS-based low-pass filter $C_{lp}\{\mathcal{H}\}$.

of the controller, see also Chapter 3 and Chapter 7. The specific choice for placing the integrator branch $C_i\{\mathcal{H}\}$ after the low-pass filter $C_{lp}\{\mathcal{H}\}$ in Figure 8.9 is motivated by the consideration that filters sustaining a constant output should be placed after HIGS as to avoid asymmetric switching or no switching at all due to an input signal with an offset. It is furthermore required that the linear characteristics $W_{lp}^{-1}V_{lp}W_i$ separating each HIGS element have a relative degree of at least one for ensuring the input signal to HIGS associated with $C_i\{\mathcal{H}\}$ to be C^1-differentiable. This can be realized by choosing $V_{lp}(s) = H_{lp}^{-1}(s)C_{lp}(s)$ and restricting the weighting filters W_{lp} and W_i to be proper filters.

Remark 8.4.3. *Currently, well-posedness of generic interconnections containing multiple HIGS elements is still an open issue. For guaranteeing global existence of solutions for the interconnection in Figure 8.5, in which $C = C\{\mathcal{H}\}$ is a HIGS-based PID controller as depicted in Figure 8.9, however, the results in Deenen et al., 2021; Sharif et al., 2019 can directly be extended provided the inputs belong to the class of piecewise Bohl functions, and the HIGS elements are separated by an LTI filter having a relative degree of at least one.*

The engineering heuristic underlying the use of two HIGS-based filters in the configuration of Figure 8.9 is explained as follows. As argued in Chapter 7, HIGS relies on the spectral content of its input for generating effective outputs with anticipated gain and phase characteristics. Phase advantages for an integrator should be accessed in the low-frequency range, thereby allowing for larger integrator gains and increased low-frequency disturbance rejection. The functionality of HIGS in the integrator is therefore purely performance based. On the other hand, for the low-pass filter phase advantages are to be accessed around the system bandwidth to increase robust stability margins. A clear distinction can be made in frequency content on the basis of which HIGS should primarily switch. Due to the lack of superposition, however, HIGS can only generate outputs that are effective in one region, thereby compromising properties in the other region. For example, choosing $\omega_{h,lp}$ associated with HIGS in $C_{lp}\{\mathcal{H}\}$ small yields broad-banded phase advantages, but at the same time can result in low-

frequency gain-loss (recall Chapter 7). Using both $C_i\{\mathcal{H}\}$ as well as $C_{lp}\{\mathcal{H}\}$ allows for separating the switching objectives such that HIGS associated with each filter can be made effective in its respective frequency region by selecting appropriate weighting filters.

8.4.3 Frequency-domain approximation

For tuning purposes, it is useful to have a describing function characterization of the controller in Figure 8.9. The use of multiple nonlinearities, however, complicates an analytical derivation. In Gelb and Vander Velde, 1968, Chapter 3, Section 3.6, it is argued that replacing the nonlinearities with their respective individual describing function is permitted if the LTI filters separating them have sufficient low-pass filter characteristics, thereby filtering higher-order harmonics generated by the preceding nonlinear element. In that case, one finds the approximation

$$\mathcal{C}(j\omega) \approx \mathcal{D}_{pid}(j\omega)\mathcal{D}_{lp}(j\omega) = k_p\left(1 + \mathcal{D}_i(j\omega) + \frac{j\omega}{\omega_d}\right)\mathcal{D}_{lp}(j\omega), \tag{8.12}$$

in which $\mathcal{D}_i(j\omega)$ and $\mathcal{D}_{lp}(j\omega)$ denote the describing function of $C_i\{\mathcal{H}\}$ and $C_{lp}\{\mathcal{H}\}$, respectively. However, this filtering assumption may be limiting or partially invalid. An alternative route for justifying the approximation in (8.12) exploits the following frequency-domain separation principle:

- In PID tuning it approximately holds true that $\gamma\omega_i < \omega_b < \omega_{lp}/\gamma$, with ω_b the system bandwidth and $\gamma > 1$ (Steinbuch and Norg, 1998). Phase benefits with $C_{lp}\{\mathcal{H}\}$ are to be obtained around the bandwidth, such that an appropriate tuning for the parameter $\omega_{h,lp}$ associated with HIGS in $C_{lp}\{\mathcal{H}\}$ should roughly satisfy $\omega_{h,lp} \geq \omega_b$.

- For sinusoidal inputs satisfying $\omega < \omega_b$, HIGS associated with $C_{lp}\{\mathcal{H}\}$ is dominantly in gain-mode such that the input to $C_i\{\mathcal{H}\}$ is (nearly) sinusoidal, *i.e.*, the nonlinear effect of $C_{lp}\{\mathcal{H}\}$ is sufficiently contained for low-frequency inputs as to avoid interference with $C_i\{\mathcal{H}\}$. Hence, $\mathcal{D}_i(j\omega)$ plays the main role in the describing function of the controller.

- For inputs satisfying $\omega \geq \omega_b$, the proportional-derivative branch of the PID part in Figure 8.9 largely dominates over the fundamental harmonic in the response of $C_i\{\mathcal{H}\}$, such that $\mathcal{D}_{lp}(j\omega)$ plays the main role in the describing function of the controller.

Typical frequency-domain characteristics for both linear and HIGS-based PID controllers are shown in Figure 8.10. The parameters are chosen to match the magnitude characteristics of both designs. To indicate those regions where phase benefits are to be expected from $C_i\{\mathcal{H}\}$ and $C_{lp}\{\mathcal{H}\}$, the asymptotic phase

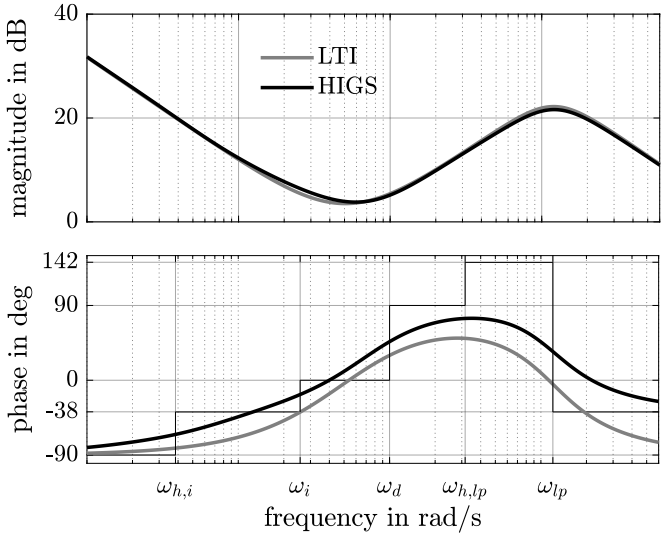

Figure 8.10. Frequency-domain characteristics of the linear and HIGS-based PID controllers in (8.7) and (8.12), respectively. Asymptotic behaviour of the latter is indicated by the thin grey lines. Phase benefits due to $C_i\{\mathcal{H}\}$ are mainly obtained for all $\omega \in [\omega_{h,i}, \omega_i]$, whereas benefits due to $C_{lp}\{\mathcal{H}\}$ are obtained for $\omega \geq \omega_{h,lp}$. Note that both regions are sufficiently separated.

behaviour of $\mathcal{C}(j\omega)$ is shown by the thin dotted lines. Note the clear separation of both regions for which phase advantages are obtained by the integrator and low-pass filter, which results from the fact that $\omega_{h,lp}$ is chosen sufficiently large.

8.5 Closed-loop design aspects

In this section, practically relevant aspects for tuning a HIGS-based PID controller for an industrial wafer stage system are discussed in detail. The procedure is based on the quasi-linear loop-shaping approach outlined in Chapter 7 and involves modelling uncertainty and tuning of the weighting filters.

8.5.1 Modelling uncertainty

Characterizing modelling uncertainty in the describing function approximation (8.12) requires approximate knowledge of the servo errors in terms of harmonic content. Representative characteristics of a servo error signal e in scanning y-direction when applying acceleration feedforward control and linear feedback control are shown in Figure 8.11.

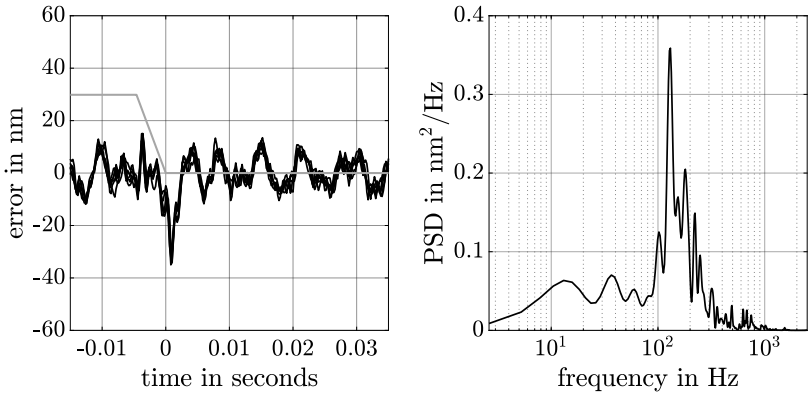

Figure 8.11. Representative characteristics of a servo error signal e in both time- and frequency-domain when applying linear PID control.

The main parts of the frequency content in the servo errors e are due to the setpoint profile, despite the use of an appropriate feedforward controller. It can be seen that harmonic content in the region $100 - 250$ Hz dominates the frequency spectrum, which can be linked to the 235 Hz bandwidth of the closed-loop system. Also, in the range $600 - 800$ Hz harmonic contributions are present that result from structural dynamics of the plant. Given the high reproducibility of the setpoint profiles, it is reasonable to expect that these frequencies dominantly persist in the servo error when applying a HIGS-based PID controller as well.

Remark 8.5.1. *By virtue of the separation principle discussed in the previous section, the main source of modelling error at high-frequencies may be identified to result from the HIGS-based low-pass filter $C_{lp}\{\mathcal{H}\}$. Namely, as for higher frequencies the output of the integrator is largely dominated by the proportional-derivative branch in Figure 8.9, modelling uncertainty in the frequency-domain approximation of $C_i\{\mathcal{H}\}$ at high frequencies is found to become insignificant as compared to modelling uncertainty in $C_{lp}\{\mathcal{H}\}$. Although both uncertainties can be taken into account, the latter will be of primary interest for subsequent robust controller design and is therefore discussed next.*

Based on the above observations, a meaningful test signal to approximate the input to HIGS associated with $C_{lp}\{\mathcal{H}\}$ may be of the form

$$\hat{z}(t) = \sin(2\pi f_1 t) + \alpha \sin(2\pi f_2 t),$$

where $f_1 \in [100, 250]$ Hz, $f_2 \in [600, 800]$ Hz, and $\alpha \in (0, 1)$. Assuming f_1 and f_2 to be incommensurate, modelling uncertainty in the describing function approximation of the HIGS-based low-pass filter can be characterized by $\Delta_\Psi(j\omega, \hat{z}) =$

$\Delta_{\Psi 0}(j\omega, \hat{z})W_\Delta(j\omega)$ with $\|\Delta_{\Psi 0}(j\omega, \hat{z})\|_\infty \leq 1$, and $W_\Delta(j\omega) = \mathcal{D}(j\omega_{\min}) - \mathcal{D}(j\omega)$ for all $\omega \geq 600 \cdot 2\pi$ rad/s, and zero otherwise, and $\omega_{\min} = 100 \cdot 2\pi$ rad/s. Further specifics regarding this characterization can be found in Chapter 7.

To demonstrate the relevance of accounting for this modelling uncertainty in the wafer stage control context, three HIGS-based PID controllers are designed by solving the following optimization problem:

$$\begin{aligned} \underset{\mathcal{C}}{\text{maximize}} \quad & \omega_b, \\ \text{subject to} \quad & \|W_{\mathcal{S}}(j\omega)\mathcal{S}(j\omega)\|_\infty + \lambda \|W_a(j\omega)\mathcal{S}(j\omega)P(j\omega)\|_\infty \leq 1, \\ & \mathcal{C} \text{ stabilizes } P, \end{aligned} \tag{8.13}$$

where $\mathcal{C}$ is given in (8.12) and denotes the describing function approximation of the HIGS-based PID controller in Figure 8.9, ω_b denotes the open-loop bandwidth, *i.e.*, the frequency at which $\mathcal{L}(j\omega) = P(j\omega)\mathcal{C}(j\omega)$ crosses the zero dB line for the first time, $\mathcal{S}(j\omega) = (1 + \mathcal{L}(j\omega))^{-1}$ is the quasi-linear sensitivity function, $W_a(j\omega) = W_\Delta(j\omega)\mathcal{D}_{pid}(j\omega)V_{lp}(j\omega)$ represents the additive modelling uncertainty in the controller due to the HIGS-based low-pass filter, and $W_{\mathcal{S}}(j\omega) = 1/\sqrt{10}$ defines a 10 dB peaking constraint on the sensitivity. The additional factor $\lambda \in [0, 1]$ is used as a means to determine the degree to which modelling uncertainty is taken into account. It is found in practice that the choice $\lambda = 1$ often leads to overly restrictive designs. A balanced choice is left to the control engineer and typically depends on the system and disturbances at hand. Remark that for $\lambda = 1$ the constraint in (8.13) implies that the magnitude of the worst-case sensitivity $|\mathcal{S}_\Delta| = |\mathcal{S}|/(1 - |W_a\mathcal{S}P|)$ does not exceed 10 dB. Note that $P(j\omega)$ in (8.13) is the *measured* frequency-response-function (FRF) of the stage, and the stability constraint can be verified on the basis of a Nyquist-like test on the open-loop characteristics $\mathcal{L}(j\omega)$. The resulting nominal and worst-case sensitivity characteristics for designs with $\lambda = \{0, 0.3, 0.6\}$ are shown in Figure 8.12, along with a linear design that is considered for reference. Measurement results obtained from a wafer-stage are presented in Figure 8.13.

From the figures, a clear correlation can be seen between the worst-case predictions and the actual measurements in terms of increased error content around 700 Hz which translates to a deterioration of the MSD-values in Figure 8.13, especially in the scanning interval. By partly taking into account the modelling uncertainty, this content can be significantly reduced, thereby demonstrating the merit of the proposed approach. In fact, the design with $\lambda = 0.6$ is already able to bring this content and the MSD values to about the same level as for the linear case, despite 12 dB peaking of the worst-case quasi-linear sensitivity. In addition to comparable MSD-values, the cumulative error representation in Figure 8.13 demonstrates improved low-frequency disturbance rejection properties (translating to improved MA-values) as compared to the linear design. In the comparison, the setpoint signal is highly reproducible and constitutes the main part of the frequency contents in e. This is different for the exogenous input

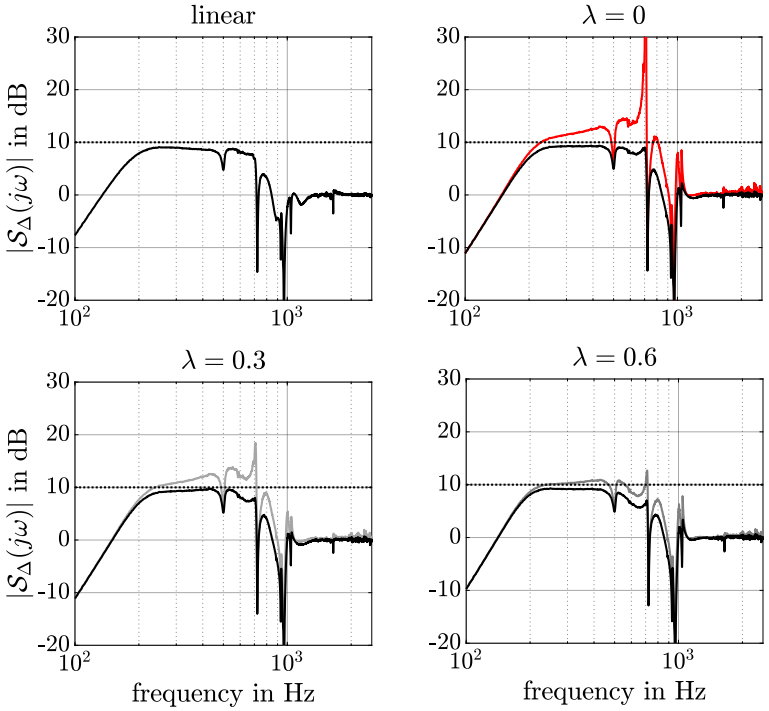

Figure 8.12. Nominal (black) and worst-case (red, grey) quasi-linear sensitivities for three HIGS-PID designs with different levels of robustness ($\lambda = \{0, 0.3, 0.6\}$). A nominal linear design (top left) is considered for reference.

that stems from multiple noise sources and that is generally non-reproducible. Its contribution, however, constitutes a minor part of the frequency contents in e. In this regard, taking into account the uncertainty with $\lambda = 1$ may be too restrictive for the disturbances at hand.

8.5.2 Design and tuning of the pre- and post-filters

As shown in Chapter 7, high-frequency signal content may compromise anticipated gain and phase properties of the HIGS-based controller at low-frequencies. Considering the content in Figure 8.11, the use of pre- and post-filters (recall the structure in Figure 8.7) becomes particularly relevant for the HIGS-based integrator $C_i\{\mathcal{H}\}$. That is, as $C_i\{\mathcal{H}\}$ is intended to be effective at low frequencies, typically below 100 Hz, dominating content beyond this frequency may compromise switching of HIGS. Note that for the low-pass filter $C_{lp}\{\mathcal{H}\}$, HIGS should typically switch at frequencies around the bandwidth, such that the use

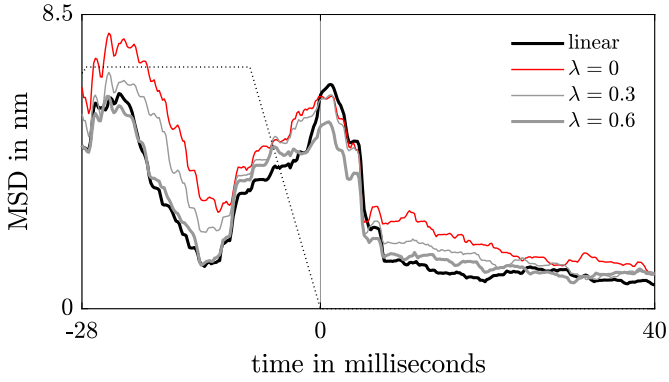

(a) Time-series measurements of the MSD-filtered servo errors.

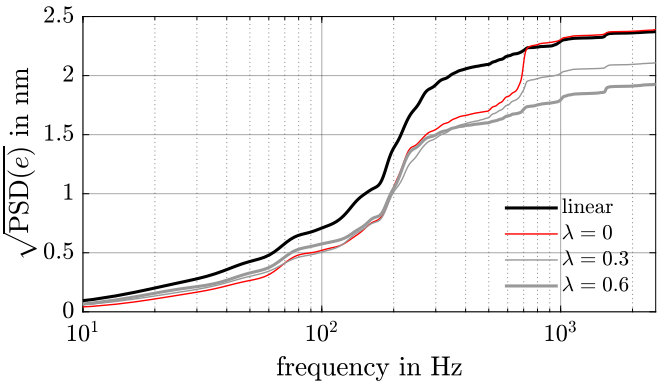

(b) Cumulative root-mean-square representation of the servo errors.

Figure 8.13. Time- and frequency-domain representation of the measured servo errors for three HIGS-based PID designs with $\lambda = \{0, 0.3, 0.6\}$. Measurements with a linear design (black) are provided for reference.

of weighting filters in that case is of less significance.

To illustrate the need for a weighting filter design in the context of wafer-stage feedback control, consider a HIGS-based PID controller that is tuned by solving the same optimization problem as in (8.13). The resulting describing function-based sensitivity characteristics are depicted in Figure 8.14 in grey. For reference, a baseline linear design is provided in black.

When using no weighting filter in the integrator, *i.e.*, $W_i(s) = 1$, the measurement results in Figure 8.15 show inferior low-frequency disturbance rejection properties for the current HIGS-based design (red curve) as compared to the baseline linear design (black curve). This is not in accordance with the predic-

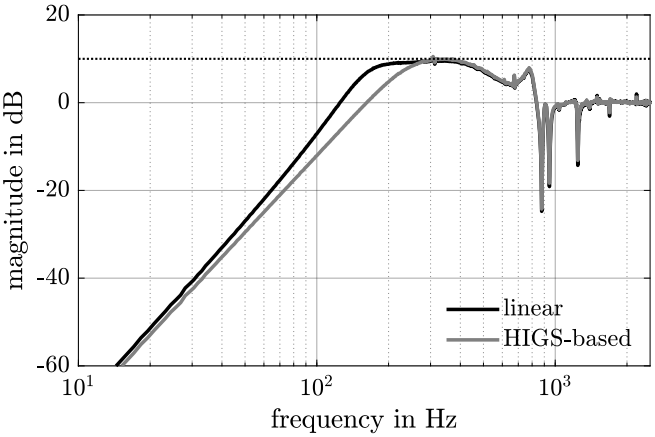

Figure 8.14. Bode magnitude characteristics of the closed-loop sensitivity functions with linear PID control (black) and HIGS-based PID control (grey).

tions in Figure 8.14. The discrepancy between linear PID and HIGS-based PID performance without filtering is particularly visible for low frequencies. Note for example the dominant 40 Hz component in the MA filtered error with HIGS-based control, which for the linear design appears to be largely suppressed. From the cumulative power spectrum significant gain-loss is found in the frequency range below 100 Hz which is the result of frequency contributions above 100 Hz that induce too-frequent switching of HIGS to gain-mode.

As a solution to performance loss in terms of deteriorated low-frequency disturbance rejection, consider the HIGS-based integrator $C_i\{\mathcal{H}\}$ in which the weighting filter $W_i(s)$ is chosen as a skew notch filter of the form

$$W_i(s) = \left(\frac{\omega_{pi}^2}{\omega_{zi}^2}\right) \cdot \frac{s^2 + 2\beta_{zi}\omega_{zi}s + \omega_{zi}^2}{s^2 + 2\beta_{pi}\omega_{pi}s + \omega_{pi}^2}, \tag{8.14}$$

with $\omega_{pi} = 100 \cdot 2\pi$ rad/s, $\omega_{zi} = 1000 \cdot 2\pi$, $\beta_{zi} = \beta_{pi} = 1$. Note that (8.14) is proper, and its exact inverse is realizable. The choice for (8.14) along with the tuning of its parameters is motivated by the design argument to let $C_i\{\mathcal{H}\}$ operate (and thus switch) on frequency content below 200 Hz. Of course, mitigation of the problem with $W_i(s)$ is less effective should either the exogenous inputs have more high-frequency components or the existing high-frequency components become more dominant. Hence, the choice for $W_i(s)$ depends on the application at hand.

In Figure 8.15, also the measurement result of the HIGS-based PID controller with weighting filter design as in (8.14) is shown through the grey curve. It can be seen that the result is well in line with the expectations raised from the sensi-

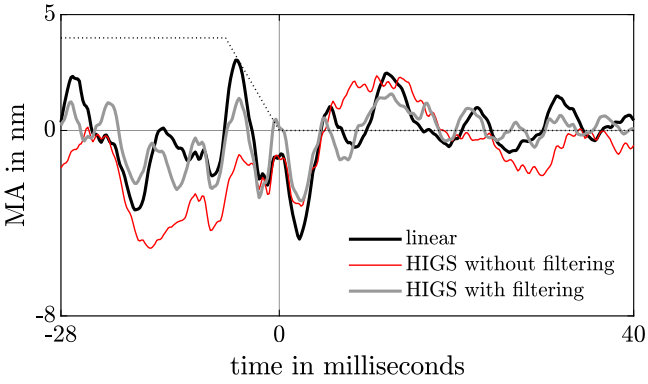

(a) Time-series measurements of the MA-filtered servo errors.

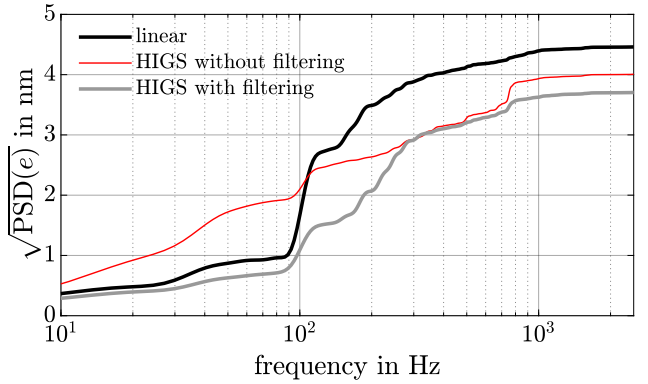

(b) Cumulative root-mean-square representation of the servo errors.

Figure 8.15. Time- and frequency-domain representation of the measured servo errors with (grey) and without (red) weighting filter strategies. Measurements with a linear design (black) are provided for reference.

tivity predictions in Figure 8.14, thereby demonstrating effectiveness of the pre- and post-filtering approach. The describing function-based sensitivity function for the considered wafer stage example appears to only provide a meaningful frequency-domain reflection of performance for the design with weighting filters.

For a final observation, remark that the case without filtering also induces increased sensitivity to frequencies around 800 Hz, which also affects the MA-filtered response. This increased sensitivity is a consequence from the fact that frequencies below the bandwidth (around 40 Hz) are significantly present in the error, and thus also in the input to HIGS associated with $C_{lp}\{\mathcal{H}\}$, thereby affecting switching in an undesirable manner.

Remark 8.5.2. *In the examples above, an approximate Nyquist-like check on the quasi-linear open-loop characteristics $\mathcal{L}(j\omega) = P(j\omega)\mathcal{C}(j\omega)$ is found to be particularly useful for guiding a stable closed-loop controller design. Still, there remains a need for a formal assessement of closed-loop stability. In principle, the tools presented in Chapters 4 and 5 can be extended toward interconnections of multiple HIGS elements. Preliminary results in this direction are presented in van den Eijnden et al., 2020b. Note, however, that the complexity of the conditions significantly increases with an increasing number of piecewise linear subsystems. In this regard, a compositional approach as presented in Arcak et al., 2016 may appear useful in order to derive more tractable conditions.*

8.6 Comparative design and performance evaluation

In this section, the obtained insights are combined into a HIGS-based PID design that aims at performance improvements of the wafer stage system in scanning y-direction. Performance is evaluated on the basis of measurement results, and is compared to a baseline linear design that is tuned under identical constraints.

8.6.1 Design for performance

Consider a HIGS-based PID controller as depicted in Figure 8.9 that contains three notch filters. Tuning for maximum bandwidth is done through an automated loop-shaping procedure formulated as the optimization problem in (8.13) with $\lambda = 0.4$, and where $W_{\mathcal{S}}(j\omega)$ defines a piecewise linear peaking constraint on the quasi-linear sensitivity function. Note that in defining this constraint, explicit knowledge regarding machine-to-machine variations is exploited. To account for position-dependent behaviour of the stage, five FRF's, measured at different (x, y)-locations on the wafer (see Figure 8.6) are used in the tuning procedure. A linear PID controller with four notch filters is tuned under equivalent design constraints.

The resulting set of controller parameters along with the obtained bandwidths are listed in Table 8.2. A Nyquist plot of the (quasi-)linear open-loop characteristics and the corresponding closed-loop sensitivity characteristics are shown in Figure 8.16. Table 8.2 shows a substantial increase in proportional gain k_p for the quasi-linear design as compared to the linear design. This increase in gain translates into a 25% increase in bandwidth, and a $4-6$ dB improvement in low-frequency disturbance suppression as seen in the sensitivity characteristics in Figure 8.16b.

Table 8.2. Parameter values for the controllers in scanning y-direction.

		linear design	HIGS design	
PID filter	k_p	$2.67 \cdot 10^7$	$3.38 \cdot 10^7$	N/m
	ω_i	$100 \cdot 2\pi$	$106 \cdot 2\pi$	rad/s
	ω_d	$127.5 \cdot 2\pi$	$169.7 \cdot 2\pi$	rad/s
HIGS (integrator)	k_h	-	1	-
	ω_h	-	$146 \cdot 2\pi$	rad/s
weighting filter (integrator)	ω_z	-	$104 \cdot 2\pi$	rad/s
	β_z	-	1	-
	ω_p	-	$2000 \cdot 2\pi$	rad/s
	β_p	-	1	-
low-pass filter	ω_{lp}	$850.2 \cdot 2\pi$	$907 \cdot 2\pi$	rad/s
	β	0.17	0.33	-
HIGS (low-pass filter)	k_h	-	1	-
	ω_h	-	$544.2 \cdot 2\pi$	rad/s
notch filter	ω_z	$1034.63 \cdot 2\pi$	$717 \cdot 2\pi$	rad/s
	β_z	0.0092	0.119	-
	ω_p	$1027.83 \cdot 2\pi$	$766.6 \cdot 2\pi$	rad/s
	β_z	0.0089	0.184	-
notch filter	ω_z	$1109.43 \cdot 2\pi$	$1020 \cdot 2\pi$	rad/s
	β_z	0.0061	0.0053	-
	ω_p	$1243.75 \cdot 2\pi$	$1606.4 \cdot 2\pi$	rad/s
	β_z	0.0028	0.1308	-
notch filter	ω_z	$1005.6 \cdot 2\pi$	$1745.2 \cdot 2\pi$	rad/s
	β_z	0.068	0.1874	-
	ω_p	$979.57 \cdot 2\pi$	$1701 \cdot 2\pi$	rad/s
	β_z	0.467	0.3696	-
notch filter	ω_z	$709.91 \cdot 2\pi$	-	rad/s
	β_z	0.131	-	-
	ω_p	$840 \cdot 2\pi$	-	rad/s
	β_z	0.333	-	-
bandwidth	ω_b	$235 \cdot 2\pi$	$293 \cdot 2\pi$	rad/s

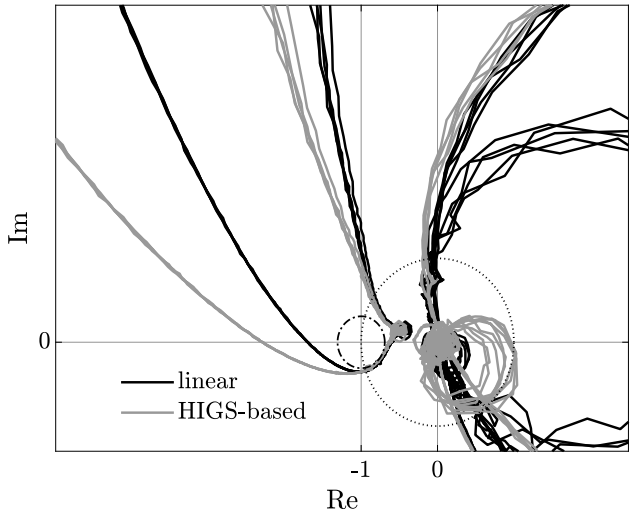

(a) Nyquist plots of the open-loop characteristics.

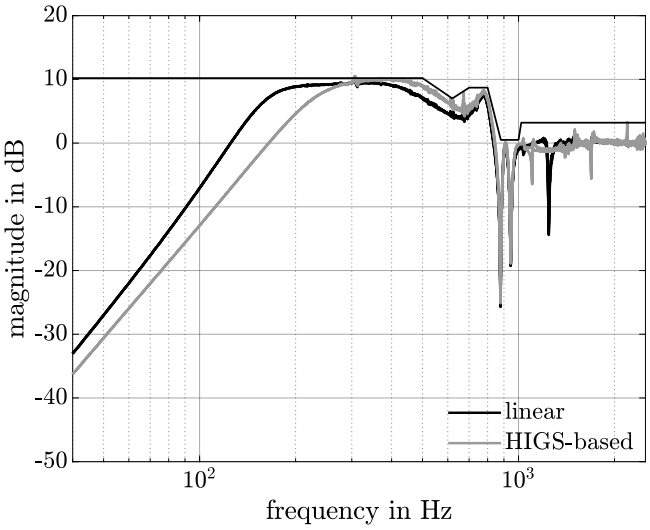

(b) Closed-loop sensitivity characteristics.

Figure 8.16. Describing function-based Nyquist curves (top) and sensitivity characteristics (bottom) for the wafer-stage system with linear PID control (black) and HIGS-based PID control (grey). In the latter figure, the performance constraint defined by $W_{\mathcal{S}}$ is shown by the thin black curve.

8.6.2 Time-domain measurement results

The linear and HIGS controllers are applied for feedback control of the wafer-stage in scanning y-direction. In the actual implementation, discrete-time versions of the controllers are used on the basis of a sampling frequency of 5 kHz. In both configurations, the wafer stage is subject to the setpoint signals as depicted in Figure 8.3, and an identical feedforward controller is applied.

The MA- and MSD-filtered servo errors measured at the center point of the wafer (die one) and the top right corner of the wafer (die three) during four consecutive scanning motions are shown in Figure 8.17. The first point on a die is exposed in the interval from $t = 0$ seconds to $t = T_e$ seconds, with T_e the exposure time, meaning that the computation of MA- and MSD-values relevant for scanning performance starts at $\frac{1}{2}T_e = 3.8$ milliseconds after the start of the scan. This is indicated in Figure 8.17 by the dotted vertical line. The results in Figure 8.17 show improvements in terms of MA- and MSD-values during the relevant scanning interval. In particular, the peak values of the MA-filtered error at die one and die three, occurring at $t = 3.8$ milliseconds decrease from respectively 3.59 nm and 4.05 nm in the linear case to 1.56 nm and 2.37 nm in the HIGS controlled case, thereby demonstrating a significant $40-55\%$ improvement. Note that there is a large transient effect present at the start of the scan which results from a non-ideal feedforward controller in the absence of a settling phase. It can be seen that the HIGS-based controller is able to better deal with these transient effects in terms of reduced overshoot and settling times.

Improvements are also observed for the MSD-filtered error as the peak values at die one and die three reduce from 8.05 nm, and 8.45 nm in the linear case to 5.66 nm and 5.41 nm in the HIGS controlled case. Note that simultaneous improvements in both MA and MSD is generally not trivial due to *i*) the waterbed effect, and *ii*) the generation of non-smooth control signals which potentially induce more high-frequency distortion.

The observed improvements in scanning performance are effectuated by well-balanced switching between integrator-mode and gain-mode of both HIGS elements, which for one particular measurement is illustrated in Figure 8.18. The switching sequences are depicted in grey: non-zero values correspond to HIGS operating in gain-mode, whereas zero values correspond to HIGS operating in integrator-mode. It can be seen that HIGS associated with $C_i\{\mathcal{H}\}$ roughly switches on the basis of a dominating 100 Hz component, whereas HIGS associated with $C_{lp}\{\mathcal{H}\}$ roughly switches between $500 - 600$ Hz, thereby indicating both elements to operate on the basis of appropriate spectral content in sufficiently separated frequency intervals.

8.6.3 Frequency-domain measurement results

Harmonic contributions in the error response are studied in more detail through a cumulative root-mean-square (RMS) representation of the measured servo error

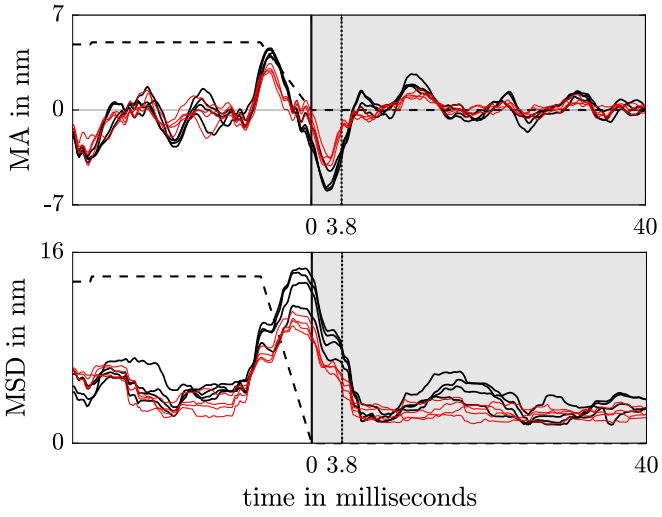

(a) Measurements at die one (center die).

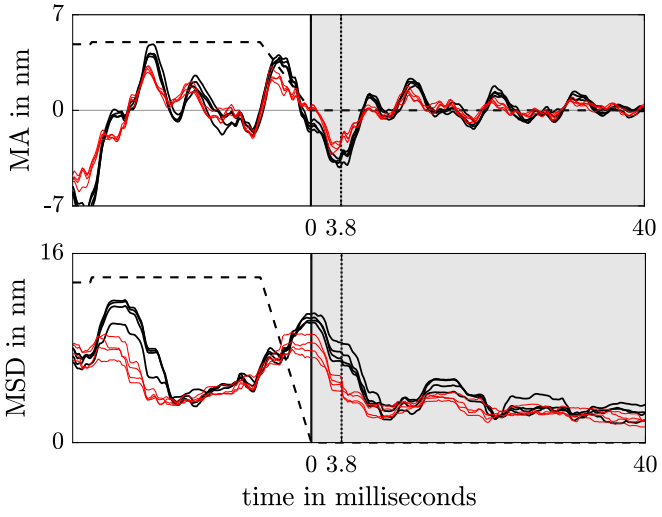

(b) Measurements at die three (top right die).

Figure 8.17. Four consecutive time-series measurements of the MA- and MSD-filtered servo errors in scanning y-direction at die one and die three obtained with linear control (black) and HIGS-based control (red). The scanning phase is indicated by the grey interval, and the acceleration profile (scaled) is shown by the dashed black line. The start of relevant computations for scanning performance is indicated by the dotted line.

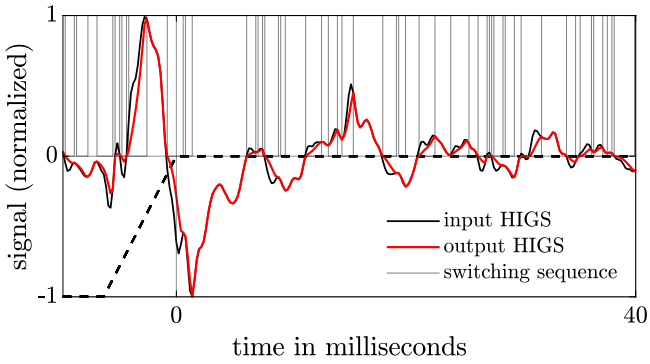

(a) Switching of HIGS in the integrator $C_i\{\mathcal{H}\}$.

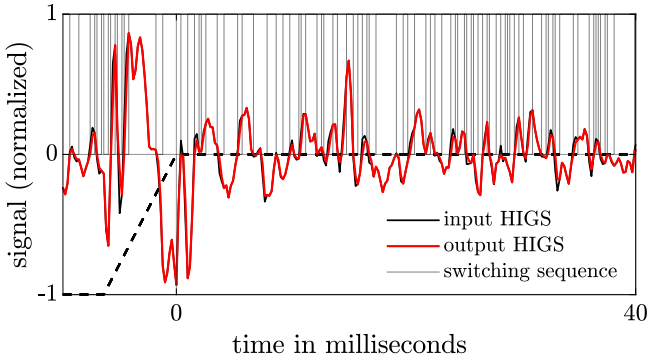

(b) Switching of HIGS in the low-pass filter $C_{lp}\{\mathcal{H}\}$.

Figure 8.18. Switching characteristics of HIGS associated with the integrator $C_i\{\mathcal{H}\}$ (top figure) and low-pass filter $C_{lp}\{\mathcal{H}\}$ (bottom figure). The switching sequences are indicated in grey: non-zero values correspond to the gain-mode, and zero values correspond to the integrator-mode.

signals as presented in Figure 8.19.

In Figure 8.19, the values of 3.2 nm and 4.2 nm provide a measure for the total energy of the servo error signals in the scanning interval. The particular values of 1.4 nm and 2.8 nm are associated with the critical frequency $f_c = 148$ Hz, which is interpreted as the maximum frequency below which the *linear* closed-loop system may benefit from feedback control, *i.e.*, the point at which disturbance suppression is obtained without inducing any amplifications. Since the linear controller is designed for maximizing this point (through maximizing the bandwidth ω_b), it provides an objective measure for quantifying improvements in low-frequency disturbance suppression with HIGS. It can be seen that HIGS-based control is able to reduce the RMS value at the critical frequency by

a factor of two, thereby demonstrating better low-frequency disturbance rejection properties. This factor is well in accordance with the expectations raised by the sensitivity characteristics in Figure 8.16b. Note that more frequency contributions are present in the nonlinear system for the range $400 - 900$ Hz as compared to the linear system. Within the range $400 - 700$ Hz this is in line with the expectations raised by the describing function-based sensitivity characteristics in Figure 8.16b. For the range $700 - 900$ Hz, an increased content may be the result from the generation of higher harmonics, as well as an increased sensitivity to high frequencies that does not appear from the describing function characteristics, but results from the switching behaviour of HIGS as discussed previously in Section 8.5 (see also Chapter 7). Such increased sensitivity is emphasized by resonance frequencies in the plant, which for the stage in y-direction occur around $700 - 900$ Hz (recall the FRFs in Figure 8.6). The design is chosen to be sufficiently robust against these effects in the sense that the influence on performance (in terms of MA- and MSD-values) remains fairly small.

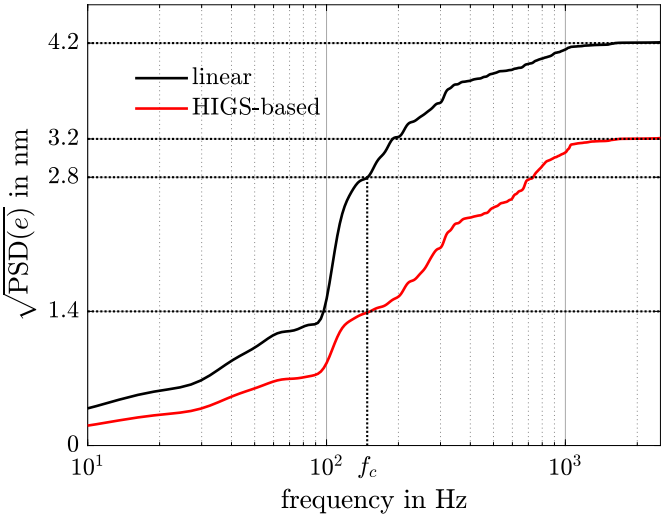

Figure 8.19. Cumulative root-mean-square (RMS) representation of the measured servo error. The critical frequency f_c indicates the point below which the linear system benefits from feedback control.

8.7 Summary

In this chapter, the performance improving potential of HIGS-based PID control is demonstrated on a wafer stage system of a state-of-practice industrial wafer

scanner. The reduced phase characteristics associated with this specific controller structure are exploited in a robust quasi-linear loop-shaping procedure to achieve increased bandwidths, enabling improved low-frequency disturbance rejection properties when compared to a linear equivalent design. The procedure is complemented with knowledge of relevant signal content that may affect switching of HIGS, thereby leading to an effective closed-loop controller design in practice. Measurement results with the HIGS-based controller obtained from a wafer stage show a factor two improvement in disturbance rejection properties of the system as compared to the baseline linear design, without excessive transmission of high-frequency content. These results support the potential of HIGS-based control for high-precision motion systems.

Part IV

Closing

Chapter 9

Conclusions and Recommendations

9.1 Conclusions

In this thesis, the so-called *hybrid integrator-gain system* (HIGS) has been considered as a possible means for dealing with the fundamental performance limitations of linear time-invariant (LTI) control for LTI (motion) systems. In terms of performance, HIGS can offer comparable benefits as other hybrid control concepts such as reset controllers that originate from the Clegg integrator, however, with the additional advantage of HIGS avoiding the need for hard state resets and exploiting continuous control. The latter opens up new opportunities in both application-based as well as system-theoretic directions. In view of the above, the following research objective as stated in Section 1.4 has been addressed in this thesis:

Explore the possibilities of HIGS as a viable hybrid control strategy for enabling performance improvements for continuous-time LTI motion systems, and develop comprehensive and innovative tools for the design and analysis of HIGS-controlled systems.

The results presented in this thesis, addressing the above objective, can be categorized into three main parts. In the first part, the potential of HIGS for overcoming fundamental performance limitations of LTI control for LTI plants is considered. In the second part, novel tools for analysing stability and performance of HIGS-controlled systems are developed. The third part addresses the practical aspects of HIGS-based control in terms of performance-based design and experimental validation on industrial benchmark systems. The main conclusions for each of these parts are presented below.

9.1.1 Overcoming fundamental limitations of LTI control

The question whether nonlinear/hybrid control concepts can overcome fundamental limitations of LTI control for LTI plants is an essential one. In the first part of this thesis this question was answered positively for HIGS. By means of a numerical example it was shown in Chapter 3 that unavoidable overshoot in the step-response of a closed-loop controlled single-input single-output (SISO) LTI plant having a real unstable open-loop pole can be completely avoided with a well-designed HIGS-based controller. Key in this design is the sequence in which the linear filters appear with respect to HIGS. The results obtained in Chapter 3 provided valuable directions for controller design with HIGS and demonstrated the possibility for enabling genuine performance advantages over LTI control.

9.1.2 Stability and performance analysis

In the second part of this thesis, continuous-time tools for stability and performance analysis of HIGS-controlled systems are developed. Regarding tools for stability analysis, two main directions are pursued. The first direction is pursued in Chapter 4 and results in frequency-domain tools for stability analysis. These tools allow for graphical verification of input-to-state stability (ISS) by means of non-parametric models, and can be used for direct evaluation of robust stability in the presence of plant uncertainty. The conditions strongly connect to the industrial state-of-practice where non-parametric models are often easily obtained with high-accuracy, and plant uncertainty resulting from machine-to-machine variation is highly relevant. While the presented frequency-domain conditions are less conservative than existing ones found in the literature, these still introduce a certain amount of conservatism in the analysis which is mainly attributed to the underlying use of a common quadratic Lyapunov function for an essentially piecewise linear system.

To further reduce conservatism in the analysis, a second approach is pursued in Chapter 5 that exploits piecewise quadratic (PWQ) functions to formulate sufficient conditions for ISS in the form of linear matrix inequalities (LMIs). The conditions are shown to successfully reduce conservatism in the analysis as compared to, *e.g.*, the frequency-domain conditions in Chapter 4. In fact, for certain examples the conditions closely resemble what would be expected from a necessary condition for closed-loop stability. Reduced conservatism, however, may come at the cost of increased computational burden. The LMI conditions are additionally extended toward performance analysis in terms of the $\mathcal{L}_2$-gain and $\mathcal{H}_2$-norm, providing measures for both steady-state and transient performance. To highlight the indispensable flexibility offered by PWQ functions and guide further function refinements, necessary conditions for feasibility of the LMIs have been provided.

The performance measures discussed in Chapter 5 are generic in the sense that they quantify performance for a broad class of input signals, but may not

always reflect the actual performance objective of the system under study, concerning, *e.g.*, specific (steady-state) response characteristics in the presence of specific inputs. To accommodate performance analysis in such situations, in Chapter 6 the notion of convergent systems is exploited, *i.e.*, systems enjoying the property of having for each bounded (time-varying) input, a unique and bounded steady-state response. While convergence is not easy to establish for switched/hybrid systems in general, by partitioning the incremental input-output space of HIGS, regional incremental passivity properties are identified that can conveniently be exploited for deriving conditions for convergence. These conditions are presented in terms of both LMIs and frequency-domain inequalities, and are shown to be useful also for estimating steady-state performance on the basis of the describing function with guaranteed error margins. It must be mentioned, however, that at this point the presented conditions for convergence are only applicable to "modified" HIGS elements for which the underlying (integrator) dynamics possess strict passivity properties.

9.1.3 Design and experimental validation

In the third part of this thesis, in Chapter 7, two approaches toward closed-loop controller design with HIGS are presented. The first approach presents a method for robust controller synthesis by exploiting matrix inequalities that are derived from the frequency-domain tools presented in Chapter 4. The corresponding matrix inequalities allow for a direct translation toward appropriate synthesis conditions that show a strong resemblance with conditions typically used in an LTI setting. Although the approach returns a HIGS-based controller with rigorous robust stability and performance guarantees, there is a lack of clear physical insight regarding parameter tuning and robust controller re-design, something which in an industrial setting may be experienced as less desirable.

As an alternative, an approach is presented that exploits the describing function of HIGS within a robust loop-shaping framework. Key in the approach is to express the modelling error induced by the describing function as an uncertainty in the controller, through which possible performance issues with a HIGS-based controller design are revealed. In dealing with these issues, effective solutions are proposed in the form of both time- and frequency-domain design guidelines. Although the approach does not come with rigorous guarantees for stability and performance, it still provides a practically useful and insightful design method that interfaces well with the industrial (motion) control design practice.

In Chapter 8, a HIGS-based PID control strategy exploiting multiple HIGS elements is applied for feedback control of a state-of-the-art industrial wafer-stage system. Through several case studies it is shown that appropriate design of a HIGS-based controller requires carefully addressing the interaction between (the switching mechanism of) HIGS and the LTI parts of the system. This interaction is shown to be sufficiently addressed in practice by following the describ-

ing function-based design guidelines presented in Chapter 7. Compared to the state-of-practice linear PID control solution, the HIGS-based PID design enables a substantial increase in bandwidth which is attributed to the "phase" advantages offered by HIGS. Wafer stage measurement results demonstrate a factor of two improvement in low-frequency disturbance rejection properties without compromising high-frequency noise amplification, thereby supporting also the potential of HIGS-based control for industrial high-precision systems.

9.2 Recommendations

The concept of hybrid integrator-gain systems (HIGS) is relatively new, and there is still a broad range of interesting and important challenges to be addressed. Based on the results and conclusions presented in this thesis, several recommendations for future research directions are formulated:

- As discussed in Chapter 2, HIGS exploits projection of the vector field to keep its input-output trajectory within a sector, and can be represented within the framework of extended projected dynamical systems (ePDS) as introduced in Sharif et al., 2019. The framework of ePDS may allow for generalizing the "projection-based" philosophy of HIGS to include higher-order (non)linear dynamics. It is interesting to further explore the performance potential of projection-based control strategies.

- At this point, the question regarding existence and uniquess of solutions is still widely open, except for the restricted set of piecewise Bohl inputs and LTI plants for which the existence property was shown in Deenen et al., 2021. The uniqueness question, however, is unanswered at present, and also the use of more natural input functions, *e.g.*, Lebesgue measurable functions is open. Moreover, interconnections with multiple HIGS elements and nonlinear plants is completely untouched.

- The new frequency-domain conditions for stability as presented in Chapter 4 have so far been shown to be sufficient conditions for feasibility of the set of LMIs in (4.10). It would be interesting to study whether these conditions are also necessary, as suggested by the numerical example in Chapter 4. One possible starting point in this direction is to explore the approach undertaken in King et al., 2011 that proves the equivalence between specific LMIs and frequency-domain inequalities. In turn, this may provide a way for unifying the now seemingly different frequency conditions presented in Theorem 4.3.1–4.3.3 into a single condition.

- Compared to the conditions in Chapter 4, the LMI conditions presented in Chapter 5 provide less conservative conditions for stability. Two suggestions regarding these conditions are given now. First, it would be in-

teresting to study how restrictive this approach is, compared to the use of arbitrary continuous Lyapunov functions. That is, it would be useful to provide a converse result showing that, whenever a Lyapunov function exists, it can be approximated arbitrarily close by a PWQ function and thus a solution to the LMIs exists. Such a result is known to hold for smooth nonlinear systems (Rantzer and Johansson, 2000, Theorem 5), and is also suggested by the numerical examples presented in Chapter 5. Second, in view of the practical benefits associated with frequency-domain conditions for stability as advocated in Chapter 4, and the potential for extending the conditions toward controller synthesis as exploited in Chapter 7, it may be useful to translate the LMI conditions in Chapter 5 into frequency-domain conditions. A key step for obtaining such a translation may come from combining the results in Chapter 4 with the results and ideas from Skorodinskii, 1981, Theorem 1 in order to reduce a number of LMIs into a single LMI. The latter may be transformed into an equivalent frequency-domain inequality by means of the Kalman-Yakubovich-Popov lemma (Khalil, 2002). Besides, in view of the PID design in Chapter 8 it is of interest to extend the time- and frequency-domain tools for stability and performance toward systems containing multiple HIGS elements. In this regard, the multi-input multi-output (MIMO) circle criterion (Lipkovich and Fradkov, 2016) and a compositional approach (Arcak et al., 2016) may appear useful.

- Besides the Lyapunov-based approaches as considered in Chapters 4 and 5, it is expected that alternative, input-output concepts such as integral quadratic constraints (IQCs) (Megretski and Rantzer, 1997) and scaled relative graphs (SRGs) (Chaffey et al., 2021) can provide useful and interesting new directions for robust stability analysis of HIGS-controlled systems that may aid further development of easy-to-use (graphical) tools. In the same spirit, rigorously studying applicability of the describing function as a tool for stability analysis is believed to be a highly beneficial direction for further research, because it has been observed to provide surprisingly accurate predictions in practice. The line of work in Bergen et al., 1982; Mees, 1984 might be helpful in setting up such study.

- Besides the $\mathcal{H}_2$-norm studied in Chapter 5, another relevant measure for transient performance is given by the $\mathcal{L}_\infty$-norm (Scherer et al., 1997), which can be used for quantifying, *e.g.*, overshoot in a step-response. Extending the LMI conditions presented in Chapter 5 toward computation of the $\mathcal{L}_\infty$-norm may be particularly useful in the context of HIGS-controlled systems. To potentially reduce conservatism, one can apply the ideas presented in Thibodeau et al., 2009, where additional relaxation terms exploiting knowledge of local extrema in the response are included.

- The conditions for incremental stability and convergence as presented in

Chapter 6 may be conservative. Part of this conservatism possibly comes from the fact that some of the conditions only exploit static input-output properties of HIGS, rather than taking into account the full incremental closed-loop system dynamics. To improve upon this aspect, it may be fruitful to combine the approach pursued in Chapter 6 with the ideas and results outlined in Waitman et al., 2016 and Waitman et al., 2019. Note that incremental stability/convergence analysis of switched/hybrid systems in general is a relevant and challenging topic that received only limited attention in the literature, but deserves further exploration.

- Regarding the matrix inequality-based synthesis approach discussed in Chapter 7, some recommendations are given. First, it would be useful to extend the matrix inequality-based synthesis procedure toward more general settings, and avoid the need for partly fixing the linear portion of the controller a priori. In this way, the additional design freedom coming from the sequence of linear and nonlinear filters with respect to each other is directly taken into account in the synthesis procedure. Second, it would be useful to reduce conservatism in the conditions coming from the use of a quadratic Lyapunov function by considering the use of piecewise quadratic functions, see, *e.g.*, the approach in Ban and Kim, 2019.

- A recommendation regarding the performance-based loop-shaping design approach considered in Chapter 7 is to further (rigorously) characterize the modelling error Δ_Ψ, for example for periodic signals in which content is present at harmonically related input frequencies. In addition, it would be useful to extend the frequency-domain design approach with time-domain performance objectives, for instance, maximizing the bandwidth while minimizing overshoot and settling-time.

- In Chapter 8, a continuous-time multi-loop SISO approach was pursued for the design of a HIGS-based controller for a wafer stage system. Although this approach was motivated by the high sampling rate and largely decoupled wafer stage dynamics, discrete-time and multivariable design aspects of HIGS-based control systems are important and largely untouched so far. Particularly for high-precision applications these aspects will be essential, and therefore provide relevant directions for future research.

9.3 Final thoughts

The development of hybrid control strategies is largely driven by the needs from industry to realize performance beyond what is possible with linear control. Despite their promising potential, it is surprising to see that hybrid controllers are still far from being completely adopted in industrial applications. This seems

attributed to the fact that hybrid controllers are generally more difficult to analyse and design for stability and performance than their linear counterparts, and require advanced training of control engineers. Broader acceptance in industry can be accelerated by focusing on the development of accessible, intuitive, and systematic tools for analysis and design, and by providing experimental proof-of-concepts. This thesis contributed to these important areas for a hybrid control strategy known as HIGS. With a suitable design, HIGS-based controllers have the ability to outperform linear controllers, thereby opening up new possibilities to further push the performance of linear systems. It was shown that such possibilities not only exist on paper, but can be realized in practical applications as well. This thesis closes with the hope that its findings merit further developments in the appealing and challenging area of nonlinear and hybrid control.

Bibliography

Aangenent, W., Witvoet, G., Heemels, W. M., Molengraft, M., and Steinbuch, M. (2010). Performance analysis of reset control systems. *International Journal of Robust and Nonlinear Control*, 20:1213 –1233.

Aangenent, W., van de Molengraft, R., and Steinbuch, M. (2005). Nonlinear Contol of a Linear Motion System. *IFAC Proceedings Volumes* (16th IFAC World Congress), 38(1):446–451.

Abbott, B., Abbott, R., Abbott, T., Abernathy, M., Acernese, F., Ackley, K., Adams, C., Adams, T., Addesso, P., Adya, V., Affeldt, C., Agathos, M., Agatsuma, K., Aggarwal, N., Aguiar, O., Ain, A., Ajith, P., and Zweizig, J. (2016). Observation of Gravitational Waves from a Binary Black Hole Merger. *Physical Review Letters*, 116(6):1–16.

Abidi, K. and Sabanovic, A. (2007). Sliding-Mode Control for High-Precision Motion of a Piezostage. *IEEE Transactions on Industrial Electronics*, 54:629 –637.

Alcorta Garcia, E., Rodriguez-Alfaro, L. H., Diaz-Romero, D., and Posadas-Castillo, C. (2010). Characterization of frequency response functions for nonlinear convergent systems. In *Conference on Control and Fault-Tolerant Systems*, pages 630 –635.

Ambrosino, R. and Garone, E. (2015). Piecewise quadratic Lyapunov functions over conical partitions for robust stability analysis. *International Journal of Robust and Nonlinear Control*, 25(14):2348–2361.

Andersen, E., Roos, C., and Terlaky, T. (2003). On implementing a primal-dual interior-point method for conic quadratic programming. *Mathematical Programming*, 95:249–277.

Angeli, D. (2002). A Lyapunov approach to incremental stability properties. *IEEE Transactions on Automatic Control*, 47:410 –421.

Apkarian, P. and Noll, D. (2006). Nonsmooth H_∞ Synthesis. *IEEE Transactions on Automatic Control*, 51(1):71–86.

Apkarian, P., Dao, M. N., and Noll, D. (2015). Parametric Robust Structured Control Design. *IEEE Transactions on Automatic Control*, 60(7):1857–1869.

Arcak, M., Larsen, M., and Kokotović, P. (2003). Circle and Popov criteria as tools for nonlinear feedback design. *Automatica*, 39(4):643–650.

Arcak, M., Meissen, C., and Packard, A. (2016). *Networks of Dissipative Systems*. Springer International Publishing.

Armstrong, B., McPherson, J., and Li, Y. (1996). A Lyapunov stability proof for nonlinear-stiffness PD control. In *Proceedings of IEEE International Conference on Robotics and Automation*. Volume 1, pages 945–950.

Armstrong, B., Gutierrez, J., Wade, B., and Joseph, R. (2006). Stability of Phase-Based Gain Modulation with Designer-Chosen Switch Functions. *International Journal of Robotics Research*, 25:781–796.

Ascher, U., Mattheij, R., and Russell, R. (1988). *Numerical solution of boundary value problems for ordinary differential equations*. English. 1st ed. edition. Prentice-Hall series in computational mathematics. Prentice-Hall.

Åström, K. (2000). Limitations on Control System Performance. *European Journal of Control*, 6(1):2–20.

Åström, K. and Hägglund, T. (2001). The future of PID control. *Control Engineering Practice*, 9(11):1163–1175.

Atherton, D. (1982). *Nonlinear Control Engineering*. Van Nostrand Reinhold.

Aubin, J.-P. and Cellina, A. (1984). *Differential Inclusions*. Springer Berlin Heidelberg.

Bailey, A. (1963). Stabilization of Contol Systems by the Use of Driven Limiters. *Proceedings of IEE*, 113(1):169–174.

Ban, J. and Kim, S. W. (2019). Design of Reset Control for SISO Linear Systems using PWQ Lyapunov functions. In *2019 IEEE 15th International Conference on Control and Automation (ICCA)*, pages 1253–1257.

Baños, A. and Barreiro, A. (2012). *Reset Control Systems*. Springer London.

Beerens, R., Bisoffi, A., Zaccarian, L., Heemels, W., Nijmeijer, H., and van de Wouw, N. (2019). Reset integral control for improved settling of PID-based motion systems with friction. *Automatica*, 107:483–492.

Beerens, R., Bisoffi, A., Zaccarian, L., Nijmeijer, H., Heemels, M., and van de Wouw, N. (2022). Reset PID Design for Motion Systems With Stribeck Friction. *IEEE Transactions on Control Systems Technology*, 30(1):294–310.

Beker, O., Hollot, C., and Chait, Y. (2001). Plant with integrator: An example of reset control overcoming limitations of linear feedback. *IEEE Transactions on Automatic Control*, 46:1797 –1799.

Beker, O., Hollot, C., Chait, Y., and Han, H. (2004). Fundamental properties of reset control systems. *Automatica*, 40(6):905–915.

Bergen, A., Chua, L., Mees, A., and Szeto, E. (1982). Error Bounds for General Describing Function Problems. *IEEE Transactions on Circuits and Systems*, 29(6):345–354.

Biemond, J. J. B., Postoyan, R., Heemels, W. P. M. H., and Wouw, N. van de (2018). Incremental Stability of Hybrid Dynamical Systems. *IEEE Transactions on Automatic Control*, 63(12):4094–4109.

Boerlage, M., Tousain, R., and Steinbuch, M. (2004). Jerk derivative feedforward control for motion systems. In *Proceedings of the 2004 American Control Conference*. Volume 5, pages 4843–4848.

Boettcher, U., Fetzer, D., Li, H., Callafon, R. A. de, and Talke, F. E. (2012). Reference Signal Shaping for Closed-Loop Systems With Application to Seeking in Hard Disk Drives. *IEEE Transactions on Control Systems Technology*, 20(2):335–345.

Boyd, S., El Ghaoui, L., Feron, E., and Balakrishnan, V. (1994). *Linear Matrix Inequalities in System and Control Theory*. Volume 15. Studies in Applied Mathematics. Philadelphia, PA: SIAM.

Branicky, M. (1998). Multiple Lyapunov Functions and Other Analysis Tools for Switched and Hybrid Systems. *IEEE Transactions on Automatic Control*, 43:475 –482.

Brogliato, B. and Tanwani, A. (2019). Dynamical Systems Coupled with Monotone Set-Valued Operators: Formalisms, Applications, Well-Posedness, and Stability. *SIAM Review*, 62.

Bruijnen, D., Molengraft, R. van de, and Steinbuch, M. (2006). Optimization aided loop shaping for motion systems. In *2006 IEEE Conference on Computer Aided Control System Design, 2006 IEEE International Conference on Control Applications, 2006 IEEE International Symposium on Intelligent Control*, pages 255–260.

Butler, H. (2011). Position Control in Lithographic Equipment. *Control Systems, IEEE*, 31:28 –47.

Butler, H. (2013). Adaptive Feedforward for a Wafer Stage in a Lithographic Tool. *IEEE Transactions on Control Systems Technology*, 21(3):875–881.

Cai, C., Dastjerdi, A. A., Saikumar, N., and HosseinNia, S. (2020). The optimal sequence for reset controllers. In *2020 European Control Conference (ECC)*, pages 1826–1833.

Callaway, E. (2015). The revolution will not be crystallized: A new method sweeps through structural biology. *Nature*, 525:172–174.

Camlibel, M., Heemels, W., and Schumacher, J. (2003). Stability and controllability of planar bimodal linear complementarity systems. In *42nd IEEE International Conference on Decision and Control*. Volume 2, pages 1651–1656.

Carrasco, J., Baños, A., and Schaft, A. (2010). A passivity-based approach to reset control systems stability. *Systems & Control Letters*, 59:18–24.

Chaffey, T., Forni, F., and Sepulchre, R. (2021). Graphical Nonlinear System Analysis.

Chait, Y. and Hollot, C. V. (2002). On Horowitz's contributions to reset control. *International Journal of Robust and Nonlinear Control*, 12(4):335–355.

Chesi, G. (2010). LMI Techniques for Optimization Over Polynomials in Control: A Survey. *IEEE Transactions on Automatic Control*, 55(11):2500–2510.

Clarke, F. H. (1983). *Optimization and nonsmooth analysis*. Wiley.

Clegg, J. C. (1958). A nonlinear integrator for servomechanisms. *Transactions of the American Institute of Electrical Engineers, Part II: Applications and Industry*, 77(1):41–42.

Coccia, M. (2019). Why do nations produce science advances and new technology? *Technology in Society*, 59:1–9.

Colgren, R. and Jonckheere, E. (1997). H_∞ control of a class of nonlinear systems using describing functions and simplicial algorithms. *IEEE Transactions on Automatic Control*, 42(5):707–712.

Concini, C. D. and Procesi, C. (2010). *Topics in Hyperplane Arrangements, Polytopes and Box-Splines*. Springer New York.

Coogan, S. D. and Margaliot, M. (2019). Approximating the Steady-State Periodic Solutions of Contractive Systems. *IEEE Transactions on Automatic Control*, 64:847–853.

Cortes, J. (2008). Discontinuous dynamical systems. *IEEE Control Systems Magazine*, 28(3):36–73.

Cutforth, C. F. and Pao, L. Y. (2004). Adaptive input shaping for maneuvering flexible structures. *Automatica*, 40(4):685–693.

Dastjerdi, A. A., Astolfi, A., and HosseinNia, S. H. (2020). A Frequency-Domain Stability Method for Reset Systems. In *2020 59th IEEE Conference on Decision and Control (CDC'20)*, pages 5785–5791.

Deenen, D. A., Heertjes, M. F., Heemels, W. P. M. H., and Nijmeijer, H. (2017). Hybrid integrator design for enhanced tracking in motion control. In *Proceedings of the American Control Conference (ACC'17)*, pages 2863–2868.

Deenen, D. A., Sharif, B., van den Eijnden, S., Nijmeijer, H., Heemels, M., and Heertjes, M. (2021). Projection-based integrators for improved motion control: Formalization, well-posedness and stability of hybrid integrator-gain systems. *Automatica*, 133:109830.

Demidovich, B. P. (1967). *Lectures on Stability Theory*. Moscow.

Dinther, D., Sharif, B., Eijnden, S. van den, Nijmeijer, H., Heertjes, M., and Heemels, M. (2021). Overcoming Performance Limitations of Linear Control

with Hybrid Integrator-Gain Systems. In *IFAC Conference on Analysis and Design of Hybrid Systems (ADHS) 2021*.

Doyle, J., Glover, K., Khargonekar, P., and Francis, B. (1989). State Space Solution to Standard H2 and H_∞ Control Problem. *IEEE Transactions on Automatic Control*, 34:831 –847.

Dupuis, P. and Nagurney, A. (1993). Dynamical systems and variational inequalities. *Annals of Operations Research*, 44(1):7–42.

Ferreres, G. and Fromion, V. (1998). Nonlinear analysis in the presence of parametric uncertainties. *International Journal of Control*, 69:695–716.

Feuer, A., Goodwin, G. C., and Salgado, M. (1997). Potential benefits of hybrid control for linear time invariant plants. In *Proceedings of the 1997 American Control Conference (ACC'97)*. Volume 5, pages 2790–2794.

Fong, M. and Szeto, W. (1980). Application of a nonlinear filter to a conditionally stable system. *International Journal of Control*, 32(6):963–981.

Forni, F. and Sepulchre, R. (2012). A Differential Lyapunov Framework for Contraction Analysis. *IEEE Transactions on Automatic Control*, 59(3):614–628.

Foster, W., Gieseking, D., and Waymayer, W. (1966). A Nonlinear Filter for Independent Gain and Phase (With Applications). *Transactions of ASME Journal of Basic Engineering*, 88:457–462.

Franklin, G., Powell, J., and Emami-Naeini, A. (2005). *Feedback control of dynamic systems (5th ed.)* Prentice Hall.

Freudenberg, J. and Looze, D. (1985). Right half plane poles and zeros and design tradeoffs in feedback systems. *IEEE Transactions on Automatic Control*, 30(6):555–565.

Freudenberg, J., Middleton, R., and Stefanpoulou, A. (2000). A survey of inherent design limitations. In *Proceedings of the 2000 American Control Conference (ACC)*. Volume 5, pages 2987–3001.

Fromion, V., Monaco, S., and Normand-Cyrot, D. (1996). Asymptotic properties of incrementally stable systems. *IEEE Transactions on Automatic Control*, 41(5):721–723.

Gahinet, P. and Apkarian, P. (1994). A Linear Matrix Inequality Approach to H_∞ Control. *International Journal of Robust & Nonlinear Control*, 4(4):421–448.

Garulli, A., Masi, A., Valmorbida, G., and Zaccarian, L. (2013). Global Stability and Finite L2m-Gain of Saturated Uncertain Systems via Piecewise Polynomial Lyapunov Functions. *IEEE Transactions on Automatic Control*, 58(1):242–246.

Gelb, A. and Vander Velde, W. (1968). *Multiple-input Describing Functions and Nonlinear Systems Design*. McGraw Hill, New York.

Ghodrat, M. and Marquez, H. (2021). L 2 -incremental gain stability of linear systems with nonlinear Lipschitz actuator. *Systems & Control Letters*, 147:104846.

Glover, K. and McFarlane, D. (1989). Robust stabilization of normalized coprime factor plant descriptions with H_∞-bounded uncertainty. *IEEE Transactions on Automatic Control*, 34(8):821–830.

Goebel, R., Sanfelice, R., and Teel, A. (2009). Hybrid Dynamical Systems. *IEEE Control Systems*, 29:28 –93.

Goh, K., Turan, L., Safonov, M., Papavassilopoulos, G., and Ly, J. (1994). Biaffine matrix inequality properties and computational methods. In *Proceedings of 1994 American Control Conference*. Volume 1, 850–855 vol.1.

Griggs, W. M., King, C. K., Shorten, R. N., Mason, O., and Wulff, K. (2010). Quadratic Lyapunov functions for systems with state-dependent switching. *Linear Algebra and its Applications*, 433(1):52–63.

Gruntjens, K., Heertjes, M., Van Loon, S., Van De Wouw, N., and Heemels, W. (2019). Hybrid Integral Reset Control with Application to a Lens Motion System. In *2019 American Control Conference (ACC)*, pages 2408–2413.

Guo, Y., Wang, Y., and Xie, L. (2009). Frequency-Domain Properties of Reset Systems With Application in Hard-Disk-Drive Systems. *IEEE Transactions on Control Systems Technology*, 17(6):1446–1453.

Hassibi, A. and Boyd, S. (1998). Quadratic stabilization and control of piecewise-linear systems. In *Proceedings of the 1998 American Control Conference.* Volume 6, pages 3659–3664.

Hassibi, A., How, J., and Boyd, S. (1999). A path-following method for solving BMI problems in control. In *Proceedings of the 1999 American Control Conference*. Volume 2, pages 1385–1389.

Hazeleger, L., Heertjes, M., and Nijmeijer, H. (2016). Second-order reset elements for stage control design. In pages 2643–2648.

Heemels, W. P. M. H., Camlibel, M. K., and Heertjes, M. F. (2020). Oblique Projected Dynamical Systems and Incremental Stability Under State Constraints. *IEEE Control Systems Letters*, 4(4):1060–1065.

Heemels, W., Camlibel, M., and Schumacher, J. (2002). On the dynamic analysis of piecewise-linear networks. *IEEE Transactions on Circuits and Systems I: Fundamental Theory and Applications*, 49(3):315–327.

Heemels, W., Schumacher, J., and Weiland, S. (2000). Projected dynamical systems in a complementarity formalism. *Operations Research Letters*, 27(2):83–91.

Heemels, W. and Weiland, S. (2008). Input-to-state stability and interconnections of discontinuous dynamical systems. English. *Automatica*, 44(12):3079–3086.

Heertjes, M., Schuurbiers, X., and Nijmeijer, H. (2009). Performance-Improved Design of N-PID Controlled Motion Systems With Applications to Wafer Stages. *IEEE Transactions on Industrial Electronics*, 56:1347 –1355.

Heertjes, M. and Steinbuch, M. (2004). Stability and performance of a variable gain controller with application to a dvd storage drive. *Automatica*, 40(4):591–602.

Heertjes, M., van den Eijnden, S., Sharif, B., Heemels, M., and Nijmeijer, H. (2019). Hybrid Integrator-Gain System for Active Vibration Isolation with Improved Transient Response. *IFAC-PapersOnLine* (8th IFAC Symposium on Mechatronic Systems MECHATRONICS 2019), 52(15):454–459.

Heertjes, M. and Verstappen, R. (2014). Self-tuning in integral sliding mode control with a Levenberg–Marquardt algorithm. *Mechatronics*, 24(4):385–393.

Heertjes, M. F., Sahin, I. H., Wouw, N. van de, and Heemels, W. P. M. H. (2013). Switching Control in Vibration Isolation Systems. *IEEE Transactions on Control Systems Technology*, 21(3):626–635.

Heertjes, M., Butler, H., Dirkx, N., Meulen, S. van der, Ahlawat, R., O'Brien, K., Simonelli, J., Teng, K.-T., and Zhao, Y. (2020). Control of Wafer Scanners: Methods and Developments. In *2020 American Control Conference (ACC)*, pages 3686–3703.

Heertjes, M., Van Den Eijnden, S., Heemels, W., and Nijmeijer, H. (2021). A solution to gain loss in hybrid integrator-gain systems. In *2021 IEEE Conference on Control Technology and Applications (CCTA)*, pages 1179–1184.

Heertjes, M. M., Hennekens, D. D., and Steinbuch, M. (2010). MIMO feedforward design in wafer scanners using a gradient approximation-based algorithm. *Control Engineering Practice*, 18:495–506.

Henry, C. (1973). An existence theorem for a class of differential equations with multivalued right-hand side. *Journal of Mathematical Analysis and Applications*, 41(1):179–186.

Hespanha, J. P. and Morse, A. (2002). Switching between stabilizing controllers. *Automatica*, 38(11):1905–1917.

Horowitz, I. and Rosenbaum, P. (1975). Non-linear design for cost of feedback reduction in systems with large parameter uncertainty. *International Journal of Control*, 21(6):977–1001.

HosseinNia, S., Tejado, I., and Vinagre, B. (2014). A method for the design of robust controllers ensuring the quadratic stability for switching systems. *Journal of Vibration and Control*, 20:1085 –1098.

HosseinNia, S. H., Tejado, I., and Vinagre, B. M. (2013). Fractional-order reset control: Application to a servomotor. *Mechatronics*, 23(7):781–788.

Hu, G.-D. (2006). Observers for one-sided Lipschitz non-linear systems. *IMA Journal of Mathematical Control and Information*, 23(4):395–401.

Huang, H.-H. and Wey, J. (2010). Research on the high-speed pick and place device for die bonders. In *IEEE ICCA 2010*, pages 1683–1687.

Hunnekens, B., van de Wouw, N., and Nešić, D. (2016). Overcoming a fundamental time-domain performance limitation by nonlinear control. *Automatica*, 67:277–281.

Iervolino, R., Vasca, F., and Iannelli, L. (2015). Cone-Copositive Piecewise Quadratic Lyapunov Functions for Conewise Linear Systems. *IEEE Transactions on Automatic Control*, 60(11):3077–3082.

Impram, S. and Munro, N. (2001). Describing functions in non-linear systems with structured and unstructured uncertainties. *International Journal of Control*, 74:600–608.

Impram, S. T. and Munro, N. (2001). A note on absolute stability of uncertain systems. *Automatica*, 37(4):605–610.

Jiang, Z., Teel, A., and Praly, L. (1994). Small-gain theorem for ISS systems and applications. *Mathematics of Control, Signals and Systems*, 7:95–120.

Johansson, M. and Rantzer, A. (1998). Computation of piecewise quadratic Lyapunov functions for hybrid systems. *IEEE Transactions on Automatic Control*, 43(4):555–559.

Johansson, M. (2002). Piecewise Linear Control Systems - A Computational Approach. *Lecture Notes in Control and Information Sciences*, 284.

Kamenetskiy, V. (2017). Frequency-domain stability conditions for hybrid systems. *Automation and Remote Control*, 78:2101–2119.

Kamenetskiy, V. (2019). Switched Systems, Lur'e Systems, Absolute Stability, Aizerman Problem. *Automation and Remote Control*, 80:1375–1389.

Karybakas, C. A. (1977). Nonlinear Integrator With Zero Phase Shift. *IEEE Transactions on Industrial Electronics and Control Instrumentation*, IECI-24(2):150–152.

Katebi, M. and Zhang, Y. (1995). H_∞ control analysis and design for nonlinear systems. *International Journal of Control*, 61(2):459–474.

Khalil, H. K. (2002). *Nonlinear Systems*. 3rd edition. Upper Saddle River, New Jersey: Prentice-Hall.

King, C., Griggs, W., and Shorten, R. (2011). A Kalman-Yakubovich-Popov-type lemma for systems with certain state-dependent constraints. *Automatica*, 47:2107–2111.

Kontaras, N., Heertjes, M., and Zwart, H. (2016). Continuous compliance compensation of position-dependent flexible structures. *IFAC-PapersOnLine* (12th IFAC Workshop on Adaptation and Learning in Control and Signal Processing ALCOSP 2016), 49(13):76–81.

Krasovskii, N. and Subbotin, A. I. (1988). *Game-Theoretical Control Problems*. Springer-Verlag.

Kunze, M., Karimi, A., and Longchamp, R. (2008). Frequency domain controller design by linear programming guaranteeing quadratic stability. In *2008 47th IEEE Conference on Decision and Control (CDC'08)*, pages 345–350.

Lamnabhi-Lagarrigue, F., Annaswamy, A., Engell, S., Isaksson, A., Khargonekar, P., Murray, R. M., Nijmeijer, H., Samad, T., Tilbury, D., and Van den Hof, P. (2017). Systems & Control for the future of humanity, research agenda: Current and future roles, impact and grand challenges. *Annual Reviews in Control*, 43:1–64.

Lau, K. and Middleton, R. (2003). Switched Integrator Control Schemes for Integrating Plants. *European Journal of Control*, 9:539–559.

Laub, A., Heath, M., Paige, C., and Ward, R. (1987). Computation of system balancing transformations and other applications of simultaneous diagonalization algorithms. *IEEE Transactions on Automatic Control*, 32(2):115–122.

Le, J. H. and Teel, A. R. (2021). Passive soft-reset control for nonlinear systems. In *60th IEEE Conference on Decision and Control (CDC)*, pages 5320 –5325.

Leonov, G. A., Ponomarenko, D. V., and Smirnova, V. B. (1996). *Frequency-Domain Methods for Nonlinear Analysis: Theory and Applications*. WORLD SCIENTIFIC.

Li, Y., Guo, G., and Wang, Y. (2011). Reset Control for Midfrequency Narrowband Disturbance Rejection With an Application in Hard Disk Drives. *IEEE Transactions on Control Systems Technology*, 19(6):1339–1348.

Li, Y., Phillips, S., and Sanfelice, R. (2014). Results on incremental stability for a class of hybrid systems. In *53rd IEEE Conference on Decision and Control*, pages 3089–3094.

Liberzon, D. (2003). *Switching in Systems and Control*. Birkhauser, Boston.

Lipkovich, M. and Fradkov, A. (2016). Equivalence of MIMO Circle Criterion to Existence of Quadratic Lyapunov Function. *IEEE Transactions on Automatic Control*, 61(7):1895–1899.

Löfberg, J. (2004). YALMIP : a toolbox for modeling and optimization in MATLAB. In *2004 IEEE International Conference on Robotics and Automation*, pages 284–289.

Lohmiller, W. and Slotine, J.-J. E. (1998). On Contraction Analysis for Nonlinear Systems. *Automatica*, 34(6):683–696.

Loquen, T., Nešić, D., Prieur, C., Tarbouriech, S., Teel, A., and Zaccarian, L. (2010). Piecewise quadratic Lyapunov functions for linear control systems with First Order Reset Elements. *IFAC Proceedings Volumes*, 43:807–812.

Martinez, V. and Edgar, T. F. (2006). Control of lithography in semiconductor manufacturing. *IEEE Control Systems Magazine*, 26(6):46–55.

Maslen, E. H., Montie, D. T., and Iwasaki, T. (2005). Robustness Limitations in Self-Sensing Magnetic Bearings. *Journal of Dynamic Systems, Measurement, and Control*, 128(2):197–203.

Mees, A. I. (1984). Describing Functions: Ten Years On. *IMA Journal of Applied Mathematics*, 32(1-3):221–233.

Megretski, A. and Rantzer, A. (1997). System analysis via integral quadratic constraints. *IEEE Transactions on Automatic Control*, 42(6):819–830.

Mercader, P., Davo, M., and Baños, A. (2013). H_∞ / H_2 analysis for time-delay reset control systems. In *2013 3rd International Conference on Systems and Control, ICSC 2013*, pages 518–523.

Middleton, R. (1991). Trade-offs in linear control system design. *Automatica*, 27(2):281–292.

Mokyr, J. (2018). The past and the future of innovation: Some lessons from economic history. *Explorations in Economic History*, 69:13–26.

Moore, B. (1981). Principal component analysis in linear systems: Controllability, observability, and model reduction. *IEEE Transactions on Automatic Control*, 26(1):17–32.

Moore, G. (1998). Cramming More Components Onto Integrated Circuits. *Proceedings of the IEEE*, 86(1):82–85.

Morinaga, E., Hirata, K., and Ohta, Y. (2004). Performance analysis of control systems with input constraints via piecewise quadratic storage functions. *Asian Journal of Control*, 6:34 –45.

Munnig Schmidt, R., Schitter, G, Rankers, A, and van Eijk, J (2014). *The design of high performance mechatronics: high-tech functionality by multidisciplinary system integration (2nd revised edition)*. English. IOS Press.

Nagurney, A. and Zhang, D. (1996). Projected Dynamical Systems. In *Projected Dynamical Systems and Variational Inequalities with Applications*. Boston, MA: Springer US, pages 9–43.

Narendra, K. and Taylor, J. (1973). *Frequency Domain Criteria for Absolute Stability*. Academic Press.

Nešić, D., Zaccarian, L., and Teel, A. (2008). Stability properties of reset systems. *Automatica*, 44(8):2019–2026.

Nešić, D., Teel, A. R., and Zaccarian, L. (2011). Stability and Performance of SISO Control Systems With First-Order Reset Elements. *IEEE Transactions on Automatic Control*, 56(11):2567–2582.

Oehlerking, J. (2011). Decomposition of stability proofs for hybrid systems. PhD thesis, Carl von Ossietzky Universitat.

Oomen, T., Herpen, R. van, Quist, S., Wal, M. van de, Bosgra, O., and Steinbuch, M. (2014). Connecting System Identification and Robust Control for Next-

Generation Motion Control of a Wafer Stage. *IEEE Transactions on Control Systems Technology*, 22(1):102–118.

Oomen, T., Herpen, R. van, Quist, S., Wal, M. M. J. van de, Bosgra, O. H., and Steinbuch, M. (2012). Next-generation wafer stage motion control: Connecting system identification and robust control. *2012 American Control Conference (ACC)*:2455–2460.

Oppenheim, A., Schafer, R., and Stockham, T. (1968). Nonlinear filtering of multiplied and convolved signals. *Proceedings of the IEEE*, 56(8):1264–1291.

Ortega, M., Vargas, M., Castaño, F., and Rubio, F. (2006). Improved design of the weighting matrices for the S/KS/T mixed sensitivity problem - Application to a multivariable thermodynamic system. *IEEE Transactions on Control Systems Technology*, 14:82 –90.

Packard, A. and Doyle, J. (1993). The complex structured singular value. *Automatica*, 29(1):71–109.

Palanikumar, A., Saikumar, N., and HosseinNia, S. H. (2018). No More Differentiator in PID: Development of Nonlinear Lead for Precision Mechatronics. In *2018 European Control Conference (ECC)*, pages 991–996.

Panni, F. S., Waschl, H., Alberer, D., and Zaccarian, L. (2014). Position Regulation of an EGR Valve Using Reset Control With Adaptive Feedforward. *IEEE Transactions on Control Systems Technology*, 22(6):2424–2431.

Pavlov, A., Hunnekens, B., Wouw, N., and Nijmeijer, H. (2013). Steady-state performance optimization for nonlinear control systems of Lur'e type. *Automatica*, 49(7):2087–2097.

Pavlov, A., Wouw, van de, N., and Nijmeijer, H. (2006a). *Uniform output regulation of nonlinear systems : a convergent dynamics approach*. English. Systems and control : foundations and applications. Switzerland: Birkhäuser Verlag.

Pavlov, A., Pogromsky, A., Wouw, N., Nijmeijer, H., and Rooda, K. (2006b). Convergent piecewise affine systems: Analysis and design Part II: discontinuous case. In volume 2005, pages 5397 –5402.

Pavlov, A., Wouw, N., Pogromsky, A., Heertjes, M., and Nijmeijer, H. (2008). Frequency domain performance analysis of nonlinearly controlled motion systems. In *Proceedings of the IEEE Conference on Decision and Control*, pages 1621 –1627.

Pavlov, A., Wouw, N. van de, and Nijmeijer, H. (2007). Frequency Response Functions for Nonlinear Convergent Systems. *IEEE Transactions on Automatic Control*, 52(6):1159–1165.

Pettersson, S. and Lennartson, B. (1996). Stability and robustness for hybrid systems. In *Proceedings of 35th IEEE Conference on Decision and Control*. Volume 2, pages 1202–1207.

Pliss, V. A. (1964). *Non-Local Problems of the Theory of Oscillations*. Nauka, Moscow 1964; Academic Press, London 1966.

Pogromsky, A. and van den Berg, R. (2014). Frequency Domain Performance Analysis of Lur'e Systems. *IEEE Transactions on Control Systems Technology*, 22(5):1949–1955.

Potsaid, B. and Wen, J. (2004). High performance motion tracking control. In *Proceedings of the 2004 IEEE International Conference on Control Applications, 2004.* Volume 1, pages 718–723.

Preumont, A. (1997). Collocated versus non-collocated control. In *Vibration Control of Active Structures: An Introduction*. Dordrecht: Springer Netherlands, pages 60–74.

Rantzer, A. and Johansson, M. (2000). Piecewise linear quadratic optimal control. *IEEE Transactions on Automatic Control*, 45(4):629–637.

Rantzer, A. (1996). On the Kalman—Yakubovich—Popov lemma. *Systems & Control Letters*, 28(1):7–10.

Romanchuk, B. G. and Smith, M. C. (1999). Incremental gain analysis of piecewise linear systems and application to the antiwindup problem. *Automatica*, 35(7):1275–1283.

Ruffer, B. S., van de Wouw, N., and Mueller, M. (2013). Convergent systems vs. incremental stability. *Systems & Control Letters*, 62(3):277–285.

Russo, G., Di Bernardo, M., and Sontag, E. (2010). Global Entrainment of Transcriptional Systems to Periodic Inputs. *PLoS computational biology*, 6:1000739.

Saikumar, N., Sinha, R. K., and HosseinNia, S. H. (2019). "Constant in Gain Lead in Phase" Element– Application in Precision Motion Control. *IEEE/ASME Transactions on Mechatronics*, 24(3):1176–1185.

Sam, Y. M., Osman, J. H., and Ghani, M. A. (2004). A class of proportional-integral sliding mode control with application to active suspension system. *Systems & Control Letters*, 51(3):217–223.

Samad, T. (2017). A Survey on Industry Impact and Challenges Thereof. *IEEE Control Systems Magazine*, 37(1):17–18.

Samad, T., Bauer, M., Bortoff, S., Di Cairano, S., Fagiano, L., Odgaard, P. F., Rhinehart, R. R., Sánchez-Peña, R., Serbezov, A., Ankersen, F., Goupil, P., Grosman, B., Heertjes, M., Mareels, I., and Sosseh, R. (2020). Industry engagement with control research: Perspective and messages. *Annual Reviews in Control*, 49:1–14.

Sanfelice, R. G., Goebel, R., and Teel, A. R. (2008). Generalized solutions to hybrid dynamical systems. *ESAIM: Control, Optimisation and Calculus of Variations*, 14(4):699–724.

Scherer, C., Gahinet, P., and Chilali, M. (1997). Multiobjective output-feedback control via LMI optimization. *IEEE Transactions on Automatic Control*, 42(7):896–911.

Sciavicco, L. and Siciliano, B. (2000). *Modelling and Control of Robot Manipulators*. Springer, London.

Seron, M. M., Braslavsky, J. H., and Goodwin, G. C. (1997). *Fundamental Limitations in Filtering and Control*. Springer, Berlin.

Sharif, B., Heertjes, M., Nijmeijer, H., and Heemels, W. (2021a). On the Equivalence of Extended and Oblique Projected Dynamics with Applications to Hybrid Integrator-Gain Systems. In *American Control Conference (ACC) 2021, New Orleans, USA*.

Sharif, B., Heertjes, M. F., and Heemels, W. P. M. H. (2019). Extended Projected Dynamical Systems with Applications to Hybrid Integrator-Gain Systems. In *IEEE 58th Conference on Decision and Control (CDC'19)*, pages 5773–5778.

Sharif, B., van der Maas, A., Wouw, N. van de, and Heemels, W. P. M. H. (2021b). Filtered Split-Path Nonlinear Integrator: A Hybrid Controller for Transient Performance Improvement. *IEEE Transactions on Control Systems Technology*:1–13.

Shevitz, D. and Paden, B. (1994). Lyapunov stability theory of nonsmooth systems. *IEEE Transactions on Automatic Control*, 39(9):1910–1914.

Shorten, R., Corless, M., Wulff, K., Klinge, S., and Middleton, R. (2009). Quadratic Stability and Singular SISO Switching Systems. *IEEE Transactions on Automatic Control*, 54(11):2714–2718.

Skogestad, S. and Postlethwaite, I. (2010). *Multivariable Feedback Control: Analysis and Design (2nd ed.)* Wiley and Sons.

Skorodinskii, V. I. (1981). Absolute stability and absolute instability of control systems with two nonlinear nonstationary elements. *Automation and Remote Control*, 42(9):1149–1157.

Solarin, S. and Yuen, Y. (2016). A global analysis of the impact of research output on economic growth. *Scientometrics*, 108:855–874.

Sontag, E. D. and Wang, Y. (1995). On characterizations of the input-to-state stability property. *Systems & Control Letters*, 24(5):351–359.

Steinbuch, M. and Norg, M. (1998). Advanced Motion Control: An Industrial Perspective. *European Journal of Control*, 4(4):278–293.

Stoorvogel, A. (1995). Nonlinear L_1 optimal controllers for linear systems. *IEEE Transactions on Automatic Control*, 40(4):694–696.

Åström, K., Hägglund, T., Hang, C., and Ho, W. (1992). Automatic Tuning and Adaptation for PID Controllers - A Survey. *IFAC Proceedings Volumes* (4th IFAC Symposium on Adaptive Systems in Control and Signal Processing 1992, Grenoble, France, 1-3 July), 25(14):371–376.

Taylor, L. O. (1970). Error bounds for the dual input describing function technique. PhD thesis, Purdue university.

Teel, A. R. (2022). Continuous-Time Implementation of Reset Control Systems. In *Trends in Nonlinear and Adaptive Control: A Tribute to Laurent Praly for his 65th Birthday*. Edited by Z.-P. Jiang, C. Prieur, and A. Astolfi. Cham: Springer International Publishing, pages 27–41.

Thenozhi, S. and Tang, Y. (2016). Frequency Response Function modeling of nonlinear convergent systems. In *2016 IEEE 13th International Conference on Networking, Sensing, and Control (ICNSC)*, pages 1–6.

Thibeault, N. M. and Smith, R. S. (2002). Magnetic Bearing Measurement Configurations and Associated Robustness and Performance Limitations. *Journal of Dynamic Systems, Measurement, and Control*, 124(4):589–598.

Thibodeau, T., Tong, W., and Hu, T. (2009). Set invariance and performance analysis of linear systems via truncated ellipsoids. *Automatica*, 45(9):2046–2051.

Tran Dinh, Q., Gumussoy, S., Michiels, W., and Diehl, M. (2012). Combining Convex–Concave Decompositions and Linearization Approaches for Solving BMIs, With Application to Static Output Feedback. *IEEE Transactions on Automatic Control*, 57(6):1377–1390.

Trentelman, H. L., Stoorvogel, A. A., and Hautus, M. (2001). *Control Theory for Linear Systems*. Springer London.

Tsypkin, Y. Z. and Polyak, B. T. (1992). Robust Absolute Stability of Continuous Systems. In *Robustness of Dynamic Systems with Parameter Uncertainties*. Edited by M. Mansour, S. Balemi, and W. Truöl, pages 113–121. Basel: Birkhäuser Basel.

Utkin, V. (1993). Sliding mode control design principles and applications to electric drives. *IEEE Transactions on Industrial Electronics*, 40(1):23–36.

van de Wal, M., Baars, G., Sperling, F., and Bosgra, O. (2002). Multivariable H_∞/μ feedback control design for high-precision wafer stage motion. *Control Engineering Practice*, 10:739–755.

van den Berg, R., Pogromsky, A., and Rooda, K. (2008). Well-posedness and accuracy of harmonic linearization for Lur'e systems. In *In Proceedings of the 2008 IEEE COnference of Decision and Control (CDC'08)*, pages 3841–3846.

van den Eijnden, S. J. A. M., Heertjes, M. F., Heemels, W. P. M. H., and Nijmeijer, H. (2020a). Hybrid Integrator-Gain Systems: A Remedy for Overshoot Limitations in Linear Control? *IEEE Control Systems Letters*, 4(4):1042–1047.

van den Eijnden, S. J. A. M., Heertjes, M. F., Heemels, W. P. M. H., and Nijmeijer, H. (2021). Frequency-Domain Tools for Stability Analysis of Hy-

brid Integrator-Gain Systems. In *2021 European Control Conference (ECC)*, pages 1895–1900.

van den Eijnden, S., Francke, M., Nijmeijer, H., and Heertjes, M. (2020b). Improving Wafer Stage Performance With Multiple Hybrid Integrator-Gain Systems. *IFAC-PapersOnLine* (21st IFAC World Congress), 53(2):8321–8326.

van den Eijnden, S., Heemels, W., Heertjes, M., and Nijmeijer, H. (2022a). Incremental Stability and Convergence of Systems with Sector-Bounded Hybrid Integrators. In preparation.

van den Eijnden, S., Heemels, W., Nijmeijer, H., and Heertjes, M. (2022b). Stability and Performance Analysis of Hybrid Integrator-Gain Systems: A Linear Matrix Inequality Approach. *Nonlinear Analysis: Hybrid Systems*, 45:101192.

Van den Eijnden, S., Heertjes, M., and Nijmeijer, H. (2019). Robust Stability and Nonlinear Loop-Shaping Design for Hybrid Integrator-Gain-Based Control Systems. In *2019 American Control Conference (ACC)*, pages 3063–3068.

van den Eijnden, S., Heertjes, M., and Nijmeijer, H. (2020c). Experimental Demonstration of a Nonlinear PID-Based Control Design Using Multiple Hybrid Integrator-Gain Elements. In *2020 American Control Conference (ACC)*, pages 4307–4312.

van den Eijnden, S., Knops, Y., and Heertjes, M. (2018). A Hybrid Integrator-Gain Based Low-Pass Filter for Nonlinear Motion Control. In *2018 IEEE Conference on Control Technology and Applications (CCTA)*, pages 1108–1113.

van der Maas, A., Wouw, N. van de, and Heemels, W. (2017). Filtered Split-Path Nonlinear Integrator (F-SPANI) for improved transient performance. In *2017 American Control Conference (ACC)*, pages 3500–3505.

van der Schaft, A. (2017). *L_2-Gain and Passivity Techniques in Nonlinear Control*. Springer International Publishing.

Van Loon, S., Gruntjens, K., Heertjes, M., Wouw, N., and Heemels, W. M. (2017). Frequency-domain tools for stability analysis of reset control systems. *Automatica*, 82:101–108.

van Loon, S., Hunnekens, B., Heemels, W., van de Wouw, N., and Nijmeijer, H. (2016). Split-path nonlinear integral control for transient performance improvement. *Automatica*, 66:262–270.

van Schoot, J., Troost, K., Bornebroek, F., Ballegoij, R. van, Lok, S., Krabbendam, P., Stoeldraijer, J., Loopstra, E., Benschop, J. P., Finders, J., et al. (2017). High-NA EUV lithography enabling Moore's law in the next decade. In *International Conference on Extreme Ultraviolet Lithography 2017*. International Society for Optics and Photonics, page 10450.

Waitman, S., Massioni, P., Bako, L., Scorletti, G., and Fromion, V. (2016). Incremental L_2-gain analysis of piecewise-affine systems using piecewise quadratic

storage functions. In *2016 IEEE 55th Conference on Decision and Control (CDC)*, pages 1334–1339.

Waitman, S., Massioni, P., Bako, L., and Scorletti, G. (2019). Incremental L2-gain stability of piecewise-affine systems with piecewise-polynomial storage functions. *Automatica*, 107:224–230.

Willems, J. C. (2007). Dissipative Dynamical Systems. *European Journal of Control*, 13(2):134–151.

Xie, L., Shishkin, S., and Fu, M. (1997). Piecewise Lyapunov functions for robust stability of linear time-varying systems. *Systems & Control Letters*, 31(3):165–171.

Yakubovich, V. (1962). Solution of certain matrix inequalities in the stability theory of nonlinear control systems (in Russian). *Dokl. Akad. Nauk. SSSR*, 143:1304–1307.

Yakubovich, V. A. (1964). Method of matrix inequalities in stability theory for nonlinear control systems: I. Absolute stability of forced vibrations. *Automation and Remote Control*, 25:1017 –1029.

Yfoulis, C. A. and Shorten, R. (2004). A numerical technique for the stability analysis of linear switched systems. *International Journal of Control*, 77(11):1019–1039.

Zaccarian, L., Nešić, D., and Teel, A. (2005). First order reset elements and the Clegg integrator revisited. In *Proceedings of the 2005, American Control Conference, 2005.* Volume 1, pages 563–568.

Zaccarian, L., Nešić, D., and Teel, A. R. (2011). Analytical and numerical Lyapunov functions for SISO linear control systems with first-order reset elements. *International Journal of Robust and Nonlinear Control*, 21:1134–1158.

Zhao, G., Nešić, D., Tan, Y., and Hua, C. (2019). Overcoming overshoot performance limitations of linear systems with reset control. *Automatica*, 101:27–35.

Zhao, G., Nešić, D., Tan, Y., and Wang, J. (2013). Open problems in reset control. In *52nd IEEE Conference on Decision and Control*, pages 3326–3331.

Zhao, G. and Wang, J. (2016). On L_2 gain performance improvement of linear systems with Lyapunov-based reset control. *Nonlinear Analysis: Hybrid Systems*, 21:105–117.

Zheng, Y., Chait, Y., Hollot, C., Steinbuch, M., and Norg, M. (2000). Experimental demonstration of reset control design. *Control Engineering Practice*, 8:113–120.

Zhou, K., Doyle, J. C., and Glover, K. (1996). *Robust and Optimal Control*. USA: Prentice-Hall, Inc.

List of publications

Peer-reviewed journal articles

- S.J.A.M. van den Eijnden, W.P.M.H. Heemels, M.F. Heertjes, and H. Nijmeijer, "Incremental Stability and Convergence of Systems with Sector-Bounded Hybrid Integrators", 2022, in preparation.
- B. Sharif, S.J.A.M. van den Eijnden, M. Beijen, S. Achten, H. Nijmeijer, W.P.M.H. Heemels, and M.F. Heertjes, "Hybrid Integrator-Gain Based Bandpass Filter for Active Vibration Isolation with Improved Skyhook Damping", 2022, in preparation.
- S.J.A.M. van den Eijnden, W.P.M.H. Heemels, H. Nijmeijer, and M.F. Heertjes, "Stability and Performance Analysis of Hybrid Integrator-Gain Systems: A Linear Matrix Inequality Approach", *Nonlinear Analysis: Hybrid Systems*, vol. 45, 2022.
- D.A. Deenen, B. Sharif, S.J.A.M. van den Eijnden, H. Nijmeijer, W.P.M.H. Heemels, and M.F. Heertjes, "Projection-Based Integrators for Improved Motion Control: Formalization, Well-Posedness and Stability of Hybrid Integrator-Gain Systems", *Automatica*, vol. 133, 2021.
- S.J.A.M. van den Eijnden, M.F. Heertjes, W.P.M.H. Heemels, and H. Nijmeijer, "Hybrid Integrator-Gain Systems: A Remedy for Overshoot Limitations in Linear Control?", *IEEE Control Systems Letters*, vol. 4, no. 4, pp. 1042-1047, 2020.

Peer-reviewed articles in conference proceedings

- S.J.A.M. van den Eijnden, M.F. Heertjes, W.P.M.H. Heemels, and H. Nijmeijer, "Frequency-Domain Tools for Stability Analysis of Hybrid

Integrator-Gain Systems", in *Proceedings of the European Control Conference (ECC)*, pp. 1895-1900, Rotterdam, The Netherlands, 2021.

- M.F. Heertjes, S.J.A.M. van den Eijnden, W.P.M.H. Heemels, and H. Nijmeijer, "A Solution to Gain-Loss in Hybrid Integrator-Gain Systems", in *Proceedings of the IEEE Conference on Technology and Applications (CCTA)*, pp. 1179-1184, San Diego, California, USA, 2021.

- D. van Dinther, B. Sharif, S.J.A.M. van den Eijnden, H. Nijmeijer, M.F. Heertjes, and W.P.M.H. Heemels, "Overcoming Performance Limitations of Linear Control with Hybrid Integrator-Gain Systems", in *Proceedings of the 7th IFAC Conference on Analysis and Design of Hybrid Systems (ADHS)*, pp. 289-294, Brussels, Belgium, 2021.

- S.J.A.M. van den Eijnden, M.F. Heertjes, W.P.M.H. Heemels, and H. Nijmeijer, "Hybrid Integrator-Gain Systems: A Remedy for Overshoot Limitations in Linear Control?", in *Proceedings of the 59th IEEE Conference on Decision and Control (CDC)*, pp. 5779-5784, Jeju Island, Republic of Korea, 2020.

- S.J.A.M. van den Eijnden, M.F. Heertjes, and H. Nijmeijer, "Experimental Demonstration of a Nonlinear PID-Based Control Design Using Multiple Hybrid Integrator-Gain Elements" in *Proceedings of the 2020 American Control Conference (ACC)*, pp. 4307-4312, Denver, Colorado, USA, 2020.

- S.J.A.M. van den Eijnden, H.M. Francke, H. Nijmeijer, and M.F. Heertjes, "Improving Wafer Stage Performance with Multiple Hybrid Integrator-Gain Systems", in *Proceedings of the 21st IFAC World Congress*, pp. 8321-8326, Berlin, Germany, 2020.

- M.F. Heertjes, S.J.A.M. van den Eijnden, B. Sharif, W.P.M.H. Heemels, and H. Nijmeijer, "Hybrid Integrator-Gain System for Active Vibration Isolation with Improved Transient Response", in *Proceedings of the 8th IFAC Symposium on Mechatronic Systems*, pp. 454-459, Vienna, Austria, 2019.

- S.J.A.M. van den Eijnden, M.F. Heertjes, and H. Nijmeijer, "Robust Stability and Nonlinear Loop-Shaping Design for Hybrid Integrator-Gain-Based Control Systems", in *Proceedings of the 2019 American Control Conference (ACC)*, pp. 3063-3068, Philadelphia, Pennsylvania, USA, 2019.

- S.J.A.M. van den Eijnden, Y, Knops, and M.F. Heertjes, "A Hybrid Integrator-Gain Based Low-Pass Filter for Nonlinear Motion Control", in *Proceedings of the IEEE Conference on Technology and Applications (CCTA)*, pp.1108-1113, Copenhagen, Denmark, 2018.

- E. Lefeber, S.J.A.M. van den Eijnden, and H. Nijmeijer, "Almost Global Tracking Control of a Quadrotor UAV on $SE(3)$", in *Proceedings of the 56th Annual Conference on Decision and Control (CDC)*, pp. 1175-1180, Melbourne, Australia, 2017.

Dankwoord

Op deze plaats wil ik iedereen die, op welke manier dan ook, een bijdrage heeft geleverd aan de totstandkoming van dit proefschrift hartelijk bedanken. Een aantal van jullie benoem ik graag in het bijzonder.

Henk, ik ben je zeer dankbaar voor je vertrouwen in mij als onderzoeker en de mogelijkheid om binnen jouw groep dit promotieonderzoek uit te voeren. Al tijdens mijn masteropleiding heb je me als mentor altijd met raad en daad bijgestaan wat zowel op wetenschappelijk als persoonlijk vlak veel voor me heeft betekend. Daarnaast heb ik je kritische input en gevoel voor humor tijdens onze meetings altijd erg gewaardeerd. Bedankt voor dit alles.

Marcel, jouw ongeremde enthousiasme, positieve instelling, en unieke gave om theorie en praktijk perfect met elkaar in balans te brengen zijn inspirerend en ongeëvenaard. Ik wil je graag bedanken voor de uiterst prettige samenwerking van de afgelopen jaren en voor de vele plezierige discussies waar ik technisch inhoudelijk, maar ook persoonlijk ontzettend veel van heb geleerd.

Maurice, jouw oprechte interesse in mijn onderzoek alsmede in mij als persoon heb ik altijd bijzonder gewaardeerd. Ik wil je dan ook graag bedanken voor je betrokkenheid bij dit project, de prettige omgang, en de waardevolle feedback die niet alleen dit proefschrift, maar ook ook mijn wiskundige vaardigheden en onderzoekend vermogen naar een hoger niveau heeft weten te tillen.

I would like to express my gratitude toward Roland Tóth, Jim Freudenberg, Kanat Camlibel, and Luca Zaccarian for their time and effort spent reading my dissertation and participating in my defense committee.

Ook wil ik op deze plaats de afdelingen Research Mechatronics en Mechatronic Systems Development van ASML bedanken voor de financiële ondersteuning van dit onderzoek, de behulpzaamheid en de open discussies. Het was enorm motiverend om de verschillende ideeën te mogen testen op de machine. In het bijzonder wil ik graag Roel, Michiel, Jeroen, Anish, Burak en Rob bedanken voor hun onmisbare hulp bij het schrijven en testen van de software, en bij het voorbereiden en uitvoeren van experimenten. Ruud, ook jou wil ik graag

bedanken voor de goede gesprekken en inspirerende samenwerking zowel op de TU/e als bij ASML.

Next, I would like to thank all (former) D&C and CST colleagues for the pleasant work atmosphere and memorable times at conferences, Benelux meetings, and group outings. A special thanks goes to my (former) office mates Mark, Chyannie, Tomas and Bardia. Mark, bedankt voor alle leerzame discussies op het gebied van stabiliteit, en voor het delen van je passie om aan oude motorvoertuigen te sleutelen. Ik hoop dat je je oude Volkswagen ondertussen aan de praat hebt gekregen. Chyannie, thank you for the many serious and not so serious conversations we had. I have learned a lot from you and it was truly a joy having you in the office. Tomas, hoewel onze pogingen om verschillende problemen (lees LMIs) te vereenvoudigen soms tevergeefs waren, heb ik wel enorm genoten van alle leuke discussies en creatieve ideeën die daaruit voortkwamen. Bedankt hiervoor, en ik hoop dat we onze ideeën in de toekomst nog vaker zullen uitwisselen. Last, but certainly not least, I would like to thank my fellow HIGS companion, Bardia, for being an outstanding sparring partner, and for the many fruitful discussions that have been indispensable for the results in this thesis. I will cherish the good times we shared in and outside the office, particularly our extraordinary trip to L'Aquila. Thank you for this.

Daniel, als een van de grondleggers van HIGS mag ook jij zeker niet ontbreken in dit dankwoord. Bedankt voor het leggen van een basis waarop ik mijn onderzoek heb kunnen voortbouwen, en voor de scherpe discussies die me vaak tot nieuwe inzichten en ideeën hebben gebracht.

Geertje en Nancy, bedankt voor alle onmisbare hulp die ik van jullie heb ontvangen de afgelopen jaren. Jullie inzet voor het creëren van een fijne werksfeer binnen zowel de D&C groep als de CST groep wordt buitengewoon gewaardeerd.

Het is fijn (en wellicht noodzakelijk) om zo nu en dan te horen dat er ook nog iets anders in het leven is dan HIGS. De volgende woorden van dank zijn dan ook voor mijn vrienden die de afgelopen jaren voor de essentiële combinatie van rust, afleiding, en avontuur hebben gezorgd.

Allereerst wil ik jullie, Robin, Mike, Brandon en Marcella, Chris, Jurie en Alizée, en Diederik, bedanken voor de hechte vriendschap die we al meer dan 18 jaar met elkaar hebben, en voor alle mooie tijden die we daarin hebben beleefd. Ondanks dat we elkaar de laatste tijd wat minder vaak zien, voelt het als we afspreken toch altijd als vanouds, en ik hoop dat dat nog lang voort mag duren.

Bram en Irina, Robin en Vesna, Robin en Britt, Boyd en Annabelle, Joost, Tim, en Michiel, bedankt voor alle mooie momenten die we met elkaar delen. Robin, Tim, Michiel, Joost, Boyd, en Bram, jullie in het bijzonder bedankt voor de vele uren die we met elkaar in de gym hebben versleten. Laus, jij 'bedankt' voor het me veelvuldig herinneren aan alle deadlines.

Als volgende wil ik Wil en Yolanda, en Rick en Tari bedanken voor de warme ontvangst binnen jullie gezin, voor alle gezellige momenten samen, voor de betrokkenheid, en voor de altijd aanwezige interesse in mij en mijn onderzoek.

De laatste woorden van dank zijn voor mijn familie. Adriaan en Elena, bedankt dat ik altijd op jullie kan bouwen en voor het banen van de weg. Ik ben ontzettend trots op alles wat jullie doen en bereiken met jullie beestenboel thuis. Lieve pa en ma, zonder jullie aanmoediging, adviezen, onvoorwaardelijke steun en liefde had ik nooit kunnen zijn wie ik nu ben. Jullie hebben me de vrijheid gegeven om mijn eigen weg te vinden in het leven, en bieden me te allen tijde een veilige thuishaven waar ik op kan terugvallen als dat nodig is. Jullie zijn mijn rots in de branding. Ik ben jullie enorm dankbaar voor alles.

Tot slot, lieve Simone, bedankt voor je eindeloze geduld en begrip als ik weer eens in mijn eigen wereld zat of iets moest 'afmaken'. Bedankt dat je er altijd voor me bent en me leert genieten van de kleine dingen in het leven. En bovenal, bedankt voor je liefde. Dit proefschrift maakt me trots, jij maakt me gelukkig.

Sebastiaan van den Eijnden
Eindhoven, April 2022

About the author

Sebastiaan van den Eijnden was born on December 15, 1991 in Eindhoven, The Netherlands. After finishing secondary education at the Stedelijk College in Eindhoven, the Netherlands, he studied Mechanical Engineering at the Eindhoven University of Technology, Eindhoven, The Netherlands. He received the Bachelor of Science and Master of Science degree in 2013 and 2017, respectively. As part of his curriculum he performed an internship at the Norwegian University of Science and Technology (NTNU) in Trondheim, Norway. His master's thesis focused on nonlinear feedback control of quadrotors, and was carried out at the Eindhoven University of Technology within the Dynamics and Control group under the supervision of Erjen Lefeber and Henk Nijmeijer.

In December 2017, Sebastiaan started his Ph.D. research in the Dynamics and Control group at the department of Mechanical Engineering at the Eindhoven University of Technology, under the supervision of Henk Nijmeijer, Marcel Heertjes, and Maurice Heemels. The main results of his research are included in this thesis, and are centered on hybrid controllers for linear motion systems. The research is carried out at the Eindhoven University of Technology, and is financially supported by ASML, Veldhoven, The Netherlands.

Stellingen behorende bij het proefschrift

Hybrid Integrator-Gain Systems

Analysis, Design, and Applications

1. Het feit dat sommige niet-lineaire regelaars prestatie beperkingen van lineaire regelaars kunnen omzeilen, toont slechts aan dat niet-lineaire regelaars een andere - mogelijk kleinere - set van prestatie beperkingen hebben (dit proefschrift).

2. Stabiliteitscriteria voor lineaire systemen op basis van tijddomein (matrix) ongelijkheden laten zich wiskundig vertalen naar frequentiedomein gebaseerde (matrix) ongelijkheden, maar numeriek zijn deze twee sets van ongelijkheden niet eenvoudig in elkaar om te zetten. Eenzelfde bewering is ook van toepassing op sommige lineaire systemen met een uitgangsgebaseerde niet-lineaire terugkoppeling (dit proefschrift).

3. Frequentie-domein technieken zijn waardevol voor de analyse en het ontwerp van niet-lineaire en hybride regelsystemen (dit proefschrift).

4. Veel schakelende regelaars zouden beter presteren wanneer de interactie tussen het schakelmechanisme en de overige systeemcomponenten tijdens de ontwerpfase expliciet meegenomen wordt (dit proefschrift).

5. Omdat de sampled-data implementatie van hybride regelaars een natuurlijke vorm van tijdsregularisatie bewerkstelligt, zal Zeno-achtig gedrag in een hybride regelsysteem nooit optreden in de praktijk.

6. Een regeltechnicus zou enige ervaring moeten hebben met het tunen van niet-lineaire regelaars voor lineaire systemen.

7. Regeltechniek is bedoeld om toegepast te worden in de praktijk.

8. Regeltechniek kan niet altijd toegepast worden in de praktijk.

9. In de huidige maakindustrie moet niet de vraag óf iets gemaakt kan worden, maar de vraag of iets klimaatneutraal gemaakt kan worden centraal staan.

10. Een overdaad aan wedstrijdcategorieën in powerlifting vergroot de kans op prestige-inflatie.

Propositions accompanying the thesis

Hybrid Integrator-Gain Systems

Analysis, Design, and Applications

1. The fact that some nonlinear controllers can circumvent performance limitations of linear controllers, only demonstrates that nonlinear controllers possess a different - possibly smaller - set of performance limitations (this thesis).

2. Stability criteria for linear systems based on time-domain (matrix) inequalities can be mathematically translated into frequency-domain based (matrix) inequalities, but numerically these sets can not easily be converted into each other. A similar statement applies to some linear systems with output-based nonlinear feedback (this thesis).

3. Frequency-domain techniques are valuable for the analysis and design of nonlinear and hybrid control systems (this thesis).

4. Many switching controllers would perform better if the interaction between the switching mechanism and the remaining system components is taken into account explicitly during the design phase (this thesis).

5. Since a sampled-data implementation of hybrid controllers naturally enforces some form of time-regularization, Zeno-like behaviour in hybrid control systems will never occur in practice.

6. A control engineer should have some experience in tuning nonlinear controllers for linear systems.

7. Control engineering is meant to be applied in practice.

8. Control engineering can not always be applied in practice.

9. In the current manufacturing industry not the question whether something can be made, but the question whether something can be made in a climate-neutral manner should be central.

10. An excess of categories in powerlifting competitions increases the risk of prestige-inflation.